OAK RIDGE NATIONAL LABORATORY
operated by
UNION CARBIDE CORPORATION
NUCLEAR DIVISION
for the
U.S. ATOMIC ENERGY COMMISSION

ORNL - TM - 1691 - Del.
NASA CR-72090

[redacted]

BRAYTON-CYCLE RADIOISOTOPE HEAT SOURCE DESIGN STUDY

PHASE 1 (CONCEPTUAL DESIGN) REPORT

ORNL-TM-1691
NASA CR-72090

Contract No. W-7405-eng-26

BRAYTON-CYCLE RADIOISOTOPE HEAT SOURCE DESIGN STUDY PHASE I (CONCEPTUAL DESIGN) REPORT

R. A. Robinson
R. J. Beaver
D. W. Burton
T. G. Chapman
C. W. Craven, Jr.
S. T. Ewing
A. J. Miller
J. P. Nichols
R. L. Stephenson

These evaluation studies at ORNL were supported by the National Aeronautics and Space Administration, Lewis Research Center, under an Interagency Agreement with the Atomic Energy Commission — C-64217-A.

AUGUST 1967

OAK RIDGE NATIONAL LABORATORY
Oak Ridge, Tennessee
operated by
UNION CARBIDE CORPORATION
for the
U.S. ATOMIC ENERGY COMMISSION

CONTENTS

Page

Page

BRAYTON-CYCLE RADIOISOTOPE HEAT SOURCE DESIGN STUDY PHASE I (CONCEPTUAL DESIGN) REPORT

R. A. Robinson

R. J. Beaver
D. W. Burton*
T. G. Chapman
C. W. Craven, Jr.
S. T. Ewing
A. J. Miller
J. P. Nichols
R. L. Stephenson

Abstract

Conceptual designs were prepared for $^{238}PuO_2$, $^{244}Cm_2O_3$, and $^{147}Pm_2O_3$ radioisotope heat source systems that will provide 25 kw of thermal power to a Brayton-cycle power conversion system for space applications. The conceptual designs for all three fuels show primary containment provided by multilayered fuel capsules, with tantalum-based alloy T-222 as the principal stress-bearing layer and platinum as the outer corrosion-resistant layer. All the designs show the assembly of fuel capsules contained within a single reentry body for protection against reentry heating and subsequent impact in the event of a mission abort. The designs are based on containing the radioisotope fuel within the fuel capsules for a period of time equal to ten half-lives or longer of the radioisotope. Estimated system weights based on the conceptual designs range from approximately 3000 to 25,000 lb, depending on the fuel and design concept.

1. INTRODUCTION

In July 1965, the Oak Ridge National Laboratory started work on preliminary designs for a 25-kw radioisotope heat source that could be coupled to a Brayton-cycle power-generating system to provide electric power for use in space applications. The study is being done for the National Aeronautics and Space Administration, Lewis Research Center, under Interagency Agreement C-64217-A. Valuable assistance is being given for this study by the NASA-Lewis Research Center project manager, L. I. Shure, and by P. R. Bobbitt of the NASA-Langley Research Center.

The overall objectives of the study are to

1. provide the NASA-Lewis Research Center with preliminary designs of the radioisotope heat source, and

*On loan from Oak Ridge Gaseous Diffusion Plant.

2. define the research and development problems that require solutions prior to undertaking the detailed design of such a heat source.

The work has been divided into two phases: conceptual designs (phase I), which is the subject of this report, and preliminary designs (phase II). In phase I various heat source concepts were evolved, critical problems were identified, the feasibility of their solution was evaluated, and estimates were made of the physical dimensions and weights of the various concepts. It is planned in the phase II work to select the most promising of the phase I conceptual designs and prepare a more detailed preliminary design for a specific mission concept in order to minimize weight and volume, detail development problems, and assess the safety problems from the time of capsule fueling to postmission recovery.

A schematic diagram of a radioisotope-fueled Brayton-cycle power system is shown in Fig. 1.1, and the operating conditions supplied by NASA-Lewis Research Center for use in the phase I conceptual designs are given in Table 1.1.

Table 1.1. Brayton-Cycle Specifications

Working fluid	Argon
Shaft power, kw	5
Turbine inlet temperature, °R	1960
Turbine inlet pressure, psia	13.2
Compressor inlet temperature, °R	536
Compressor inlet pressure, psia	6.0
Pressure drop in heat source heat exchanger, %	3–7
Recuperator effectiveness	0.90
Weight flow, lb/sec	0.30
Thermal input (at end of one year), kw	25

Three radioisotopes, ^{238}Pu, ^{244}Cm, and ^{147}Pm, were considered as potential fuels for the heat source, and the primary concern in the conceptual designs was to insure that the radioisotope fuel would remain contained within the fuel capsules under all credible conditions. Weight and volume considerations were kept secondary to safety in evolving the

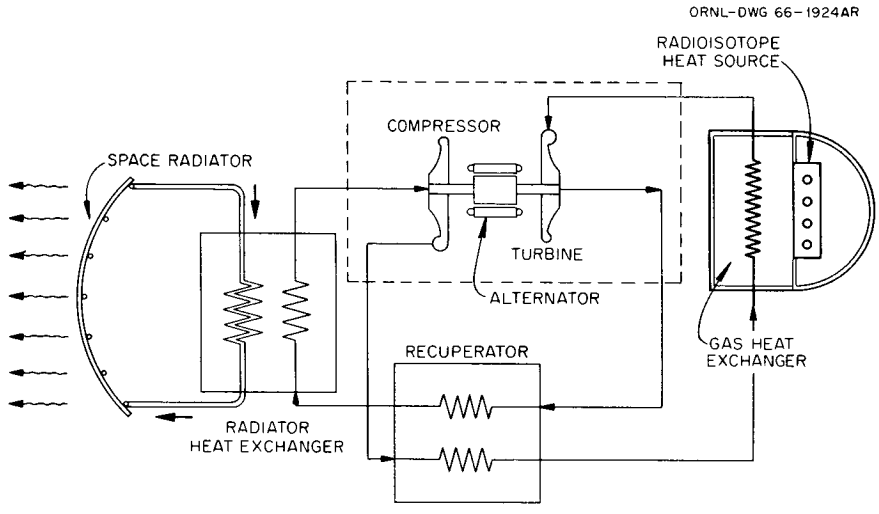

Fig. 1.1. Schematic Diagram of Radioisotope Brayton-Cycle Power Conversion System.

conceptual designs. The major safety guidelines used in the conceptual design studies were

1. The maximum surface temperature of the fuel capsules at any time during the prelaunch, launch, and orbital phases of the mission must not exceed 2000°F, even if the Brayton-cycle system is inoperative.
2. The system must be designed so that heat can be transferred to either of two completely independent Brayton-cycle systems, including two completely independent heat exchangers.
3. The system must be designed for containment of the radioisotope within the capsules for a period of time equal to ten half-lives or more of the radioisotope under all credible conditions.
4. The radioisotope fuel must remain contained within the fuel capsules in the event of a launch-pad fire or other emergencies during launch and orbital injection.
5. The radioisotope fuel must remain contained within the capsules during and after an uncontrolled reentry from space.
6. Burial with subsequent loss of containment must be avoided.
7. The assembly of a critical mass of the ^{238}Pu and ^{244}Cm fuel forms must be prevented under all credible conditions.

These goals can be approached in only a limited fashion in conceptual and preliminary design studies. Loss of containment due to sabotage or catastrophic explosions of fuels in orbit were not considered. Release mechanisms for the reentry body were not included in the phase I studies, and the results of release mechanism failure during some modes of uncontrolled reentry could conceivably cause burnup of containment and release of fuel. It is planned to treat these matters in more detail in the phase II work.

NASA-Lewis Research Center did not put any restrictions on the conceptual designs with respect to weight or volume, since it is recognized that safety, not size, is the paramount problem in the design of radioisotope heat sources. It is recognized, however, that if safety considerations are equal, light and compact heat source designs are preferable. NASA-Lewis Research Center did specify that the conceptual designs should adhere as closely as possible to current or expected near-future

technology with regard to materials and methods of fabrication and launch operation capabilities.

One of the most likely types of mission that will require multikilowatt levels of power will be the manned orbiting laboratory, and therefore the conceptual designs include radiation shielding. The shielding model (see Fig. 6.1) used for the phase I studies allows a dose rate of 3 mrem/hr at a 3-meter-diam circular dose plane located 3 meters from the heat source, 60 mrem/hr at any other point within the vehicle 3 meters from the source, and 600 mrem/hr at any point outside the spacecraft 3 meters from the source. This model was specified by NASA-Lewis Research Center only to provide a comparison of conceptual systems on a shielded basis, and it does not necessarily represent any particular mission requirement.

The radioisotope fuel requirements for the heat source are based on an operating life of one year, and the rate of heat output at the end of the one-year operational period is 25 kw. It is assumed that in a normal mission the radioisotope fuel will be returned to earth in a separate ferry vehicle or by a controlled deorbiting and impact in a selected area. However, since it is possible for an accident to occur during launch or after some period in orbit that results in a random reentry of the heat source, the conceptual designs are more strongly influenced by the abnormal mission conditions than the normal mission mode.

In addition to preliminary design work, the phase II study will include a more general investigation of weight and volume reduction. Estimates of heat source weight and volume will be obtained for systems in which the vehicle configuration, radiation tolerance limits, safety guidelines, and design stress limits are modifications of those used in the mainline study.

2. SUMMARY

All three radioisotope fuels considered in this study, ^{238}Pu, ^{244}Cm, and ^{147}Pm, could probably be made available in sufficient quantities for 25-kw heat sources by the mid seventies. Plutonium-238 has already been produced in kilogram quantities, and numerous studies suggest that it can be made available in the much larger quantities (hundreds of kilograms) needed for a large heat source program if the demand warrants the necessary plant investment. Recycling of power reactor fuels may also provide a significant amount of ^{238}Pu in the mid to late seventies. At the present time only a couple of hundred grams of ^{244}Cm has been separated; however, approximately 4.5 kg for experimental work is being processed at the Atomic Energy Commission's Savannah River Laboratory. Curium-244 could also be produced in much larger quantities in AEC production reactors if needed and, as is the case with ^{238}Pu, private power reactors may also be a source of ^{244}Cm. The Isochem plant located at AEC's Hanford Operations is presently scheduled to go on stream in late 1968 or 1969 and is expected to separate up to 30 to 50 megacuries of ^{147}Pm annually. While this is not a large enough production rate to make 25-kw sources, the techniques for processing large quantities of ^{147}Pm will be developed.

The oxides of each of the radioisotopes were chosen as the most favorable compound form for this application. The compound ^{238}PuN and ^{147}Pm metal were also considered, but they did not offer any significant advantages over the oxides and there is much less information on their properties. There are also numerous gaps in the property data for the oxides of the three radioisotopes, particularly in the area of long-term compatibility with potential refractory alloy encapsulating materials; however, calculated values were used where necessary in the conceptual design work.

As noted previously, safety was the major consideration in the conceptual designs, and the primary safety requirement was to keep the radioisotope fuel contained within the fuel capsules under all credible circumstances. No single encapsulating material could be suggested that had the necessary high-temperature strength properties in combination with acceptable corrosion and oxidation resistance, so a multicomponent capsule

design was necessary. The tantalum-based alloys T-111 or T-222 were considered the best choice for the inner-layer stress-bearing capsule material and platinum was chosen for the outer layer of the capsule because of its superior all-around corrosion and oxidation resistance. Available data suggested that platinum would probably diffuse into the tantalum-based alloy layer over a long period of time, so a thoria diffusion barrier was placed between them in the conceptual designs. Free-energy calculations indicated that there may be problems with the long-term compatibility of all three radioisotope fuel compounds, particularly $^{238}PuO_2$, with the hafnium in the T-111 or T-222 alloys. In the phase I conceptual capsule designs, the fuel is contained within a thin tungsten liner to provide more assurance of compatibility. Finally, the outer platinum layer is coated with iron titanate to improve its emissivity because all but one of the system design concepts employ radiant heat transfer to the Brayton-cycle gas heat exchanger.

Probably the most important problem with respect to the long-term containment of the two alpha-emitting fuels, ^{238}Pu and ^{244}Cm, is the internal capsule pressure resulting from the helium produced during decay. The problem involves predicting the effect of constantly varying stress and temperature on the long-term life of the encapsulating material with relatively short-term creep data that were obtained at nominally constant stress and temperature. A method of mathematically constructing temperature-compensated stress rate versus creep curves was developed that is more representative of the conditions existing during alpha decay than the conventional total stress versus creep curves usually found in the literature. With this method it was found that for a T-111 capsule having a start-of-life temperature of approximately 2000°F, creep would no longer be a dominant factor in stress-strain relationships at approximately 11 years in the case of $^{244}Cm_2O_3$ and 54 years for $^{238}PuO_2$. Beyond these times, the temperature would be lowered to the point where capsule strength would be described in terms of the elastic properties of the material. The maximum total stress in the capsule walls would occur later, at about one and one half times the half-life of the alpha-decaying fuel. In contrast, ^{147}Pm does not liberate a gas during decay, so the capsule design is not restricted by the need to leave a void volume to keep the internal

pressure within acceptable limits. The ^{147}Pm capsule diameter is limited, however, by center-line fuel temperature limitations.

All the system concepts developed in phase I have a single reentry body which, in the event of a mission abort and impact, would not bury itself but might rupture and release its capsules. Subsequent burial of an individual capsule in drifting sand was judged to be credible. The temperature that would be attained in an insulating medium such as sand is important in determining the proper wall thickness of the primary capsule. In the conceptual capsule designs for the ^{238}Pu and ^{244}Cm fuels, the capsule surface heat flux was limited to values that would give a capsule surface temperature of 2000°F or less in the event of burial. The computer studies used to determine both the minimum weight and minimum volume of capsules required for the Brayton-cycle heat source showed that a relatively minor weight penalty and a rather large volume penalty were incurred in designing to this burial temperature limitation. In the case of ^{147}Pm fuel capsules the burial temperature was allowed to go to 2500°F because there would be no internal pressure problem and the fuel would have a much shorter half-life. The power levels in the conceptual fuel capsule designs for the three fuels vary from 100 to 300 watts per capsule and the capsule diameters vary from approximately 1.0 to almost 4.5 in. The length-to-diameter ratio in all cases is 4.

All three fuels require radiation shields to meet the shielding-model requirements. Promethium-147 requires only gamma shielding; ^{238}Pu, only neutron shielding; and ^{244}Cm requires both gamma and neutron shielding. Lithium hydride is used in the conceptual designs for neutron shielding and tantalum for gamma shielding. Significant savings in shield weight can be made in the case of a pure ^{238}Pu fuel by using oxygen depleted by a factor of approximately 4 in ^{17}O and approximately 20 in ^{18}O content when preparing the $^{238}PuO_2$ fuel compound because most of the neutron radiation comes from (α,n) reactions with these two isotopes. Actually, the extent to which the depletion of ^{17}O and ^{18}O is worthwhile depends on the concentration of other contaminants in the fuel that produce neutrons by (α,n) reactions. Comparable shield-weight savings cannot be gained by doing the same thing when preparing the $^{244}Cm_2O_3$ fuel compound because of the much greater number of neutrons from spontaneous fission. When using

depleted oxygen for the $^{238}PuO_2$, a radiation shield is required only in the direction of the manned compartment.

An analysis of the criticality problem showed that even under the most idealized conditions of reflection and moderation, a critical mass of $^{244}Cm_2O_3$ would not be present in a 25-kw heat source. There would be more than a critical mass of ^{238}Pu; however, if it remained within the individual fuel capsules considered in this study, it would not be possible to get a critical array.

From the time of lift-off until the time the orbit has been established and the Brayton-cycle power system is activated, some means must be provided for preventing the heat source from rising to an excessive temperature. This can be done by incorporating in the device any one of several possible heat sink materials, such as silicon, BeO, or low-melting mixed oxides. A similar, though more severe, problem exists in the case of a launch-pad fire. Scaling up time-temperature data obtained during an Atlas-Centaur launch-pad fire indicated that a heat sink equivalent to approximately 100 lb of BeO in conjunction with the mass of the device would keep the capsule temperature well below failure temperature long enough to permit recovery. A substantially smaller weight of silicon would accomplish the same thing; however, compatibility problems make its use doubtful.

Some means must be provided for dumping the heat from the radioisotope fuel to space in the event the Brayton-cycle power conversion systems become inoperative. This would usually be done by having emergency cooling loops in the heat exchanger or by opening insulated doors or shutters to let the heat source radiate directly to space. In this study, the concept of separate emergency cooling loops was not used, not only because of space limitations in the heat exchanger, but also it was desired to avoid the use of separate pumping systems and a separate space radiator. Most of the system concepts require the opening of an insulated door and/or the mechanical movement of the heat source to dump the heat to space in the emergency mode. However, one concept was evolved that provides a completely passive heat-rejection system. This concept has a reservoir of molten metal covering the back side of the Brayton-cycle heat exchangers.

At normal operating temperature, the vapor pressure of the metal is very low, and therefore very little heat is removed by vaporization. If the Brayton cycle became inoperative, the temperature of the heat source would rise rapidly, and heat would be removed by vaporization of the fluid. The vapor would condense back into the reservoir and the liquid would return to the heated area by capillary forces. Lithium metal has about the right characteristics for this application. The volume required by this concept is somewhat larger than the volume for some of the other concepts, so its use does not provide the minimum-weight system. However, it may be the most reliable heat-dumping method.

The use of a single reentry body to house the radioisotope heat source offers the following important advantages from the standpoint of maximum reliability of containment over the emergency release of individual capsules: impact-velocity control, predictable impact orientation, capsule temperature control during reentry, means to prevent burial, and minimum area affected by the reentering heat source. Several of these advantages relate to means for providing some control over the environment to which a source capsule might be exposed, and by having this control there is some latitude in the design. For example, by varying the cross-sectional area of the reentry body, the ballistic coefficient is varied and therefore the velocity of impact and resulting stress on the capsule. Likewise, by varying the terminal velocity and shape of the body, it is possible to prevent burial on impact, which is an important point because of the effect earth burial would have on the temperature of the assembled heat source. In a normal mission, the heat source would not return to the earth in a random reentry fashion. If random reentry should occur as the result of some accident, it is highly desirable that the entire fuel source be in one small area rather than scattered over many square miles, as might occur in the case of many individual fuel capsules randomly reentering. There would be a much better chance of recovering all the fuel in the event of land impact of a single reentry body, and a minimum of land area would be affected.

The radiation shield is the major weight component in all the conceptual system designs. Therefore, for each of the system concepts, the lightest weight is obtained when using $^{238}PuO_2$ as the fuel because it

requires the least shielding; on the other hand, $^{244}Cm_2O_3$ fuel gives the largest weight because it requires the most shielding.

From the standpoint of long-term (ten half-life) containment reliability, $^{238}PuO_2$ is the least desirable fuel because of its long half-life and the helium pressure problem, whereas $^{147}Pm_2O_3$ is the best fuel for the opposite reasons. The total weights estimated for the various fuel block, reentry body, and shield system concepts vary considerably, with the lowest being approximately 3000 lb in the case of single-layer plane arrangement of fuel capsules containing $^{238}PuO_2$ fuel depleted by a factor of 20 in ^{18}O to a high of approximately 25,000 lb in the case of the passive emergency heat-rejection concept with $^{244}Cm_2O_3$ as the fuel. In most designs the weight of the system with $^{244}Cm_2O_3$ as the fuel is about twice that for $^{238}PuO_2$ as the fuel. The system weight for promethium ($^{147}Pm_2O_3$) fuel falls between that for ^{238}Pu fuel and that for ^{244}Cm fuel. If the allowable dose rate were increased by a factor of 4, $^{238}PuO_2$ depleted in ^{18}O would still give the lightest system weights; however, the difference between the weight with it and that with $^{244}Cm_2O_3$ would become much less pronounced.

From a heat transfer standpoint, all three fuels are capable of being assembled into a 25-kw heat source that would deliver the required amount of heat to the Brayton-cycle working fluid (argon) within the 2000°F capsule surface temperature limitation and without exceeding the allowable (3 to 7%) pressure drop in the heat exchanger. Relatively simple heat exchanger designs and presently available thermal insulations could be used. From a practical engineering standpoint, considerable development work is necessary, particularly in the area of fuel-compound stability and compatibility and in metals strength properties determination, before long-term containment integrity of the heat source can be assurred.

3. FUEL PROPERTIES AND AVAILABILITY

3.1 Fuel Properties

Three radioisotopes, ^{244}Cm, ^{238}Pu, and ^{147}Pm were considered as potential fuel materials for Brayton-cycle heat sources for space application. The compound forms of these radioisotopes of interest are

$^{238}PuO_2$, with both natural oxygen and oxygen depleted in ^{17}O and ^{18}O,

^{238}PuN,

$^{244}Cm_2O_3$ and $^{244}CmO_2$,

$^{147}Pm_2O_3$ and ^{147}Pm elemental metal.

During the course of the study ^{238}PuN, $^{244}CmO_2$, and ^{147}Pm metal were dropped from consideration for one or more of the following reasons:

1. There was little or no advantage over the retained compound.
2. There would be compatibility or stability problems.
3. There would probably be production difficulties.

The remaining compounds were carried through the entire conceptual design phase of the study.

The Division of Isotopes Development, AEC, is presently carrying out several properties determination programs on fuel forms at Oak Ridge National Laboratory, Battelle Northwest Laboratories, Mound Laboratory, and Savannah River. However, these programs are in their initial stages, and it was often necessary to estimate property values from preliminary experimental data, by analogy to chemically similar compounds, or with data obtained from different isotopes of the same element.

3.1.1 Plutonium-238

Plutonium-238 is produced in a reactor by neutron capture in a ^{237}Np target:

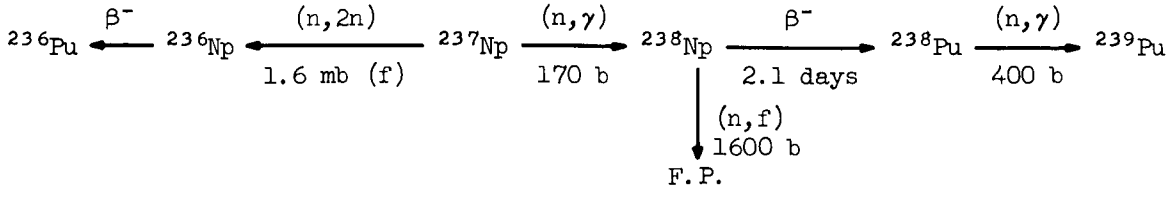

It is also formed by the alpha decay of ^{242}Cm, which gives a product free of ^{236}Pu and ^{239}Pu; however, this is not the usual method of obtaining the isotope. It has a half-life of 86.4 y, and its specific activity is 17.4 curies/g. A typical isotopic distribution of the reactor-product plutonium produced by irradiating ^{237}Np, as reported by Mound Laboratory,[1] is listed below:

Plutonium Isotope	Average Abundance (%)
238	80.0
239	16.5
240	2.5
241	0.8
242	0.08

In addition to these isotopes, reactor-produced ^{238}Pu contains a small amount of ^{236}Pu, which could have a significant effect on the shielding requirements, as discussed in Section 6. It is expected that ^{236}Pu contamination can be kept at less than 1 to 2 ppm.

Plutonium-238 nitride has a higher melting point, higher power density, and lower neutron output (Table 3.1, based on Refs. 1 and 2) than $^{238}PuO_2$; however, it reacts spontaneously with air, and therefore the fuel preparation and encapsulation operations are greatly complicated. In the case of an intact reentry application, ^{238}PuN is probably a greater safety hazard than $^{238}PuO_2$ because a capsule failure on the ground would result in a reaction of the fuel with air that would probably result in a very fine particulate smoke. In the Brayton-cycle application where the capsule temperatures are well below the melting point of both $^{238}PuO_2$ and ^{238}PuN and where the power density of a capsule is primarily controlled by the free volume required for long-term helium containment, there is no significant advantage to the use of ^{238}PuN. There is very little definitive compatibility information for either compound with potential encapsulating materials, and future tests may show ^{238}PuN to be superior to $^{238}PuO_2$ in this regard.

At the present time, the dioxide is the most commonly considered compound of ^{238}Pu for isotopic power applications. The compound is prepared

at Mound Laboratory both as pressed high-density pellets and plasma-spheroidized (microspheres) particles. The microsphere fuel form ranges in size from 37 to 250 μ with an average size of approximately 150 μ, and the best packing that can be expected is 80%. Even though this would

Table 3.1. Properties of Plutonium-238 Fuel Forms Based on Mixture of 80% ^{238}Pu–20% ^{239}Pu and Other Impurities

	$^{238}PuO_2$	^{238}PuN
Half-life, y	86.4	86.4
Specific activity of compound, curies/g	11.7	12.9
Specific power of compound, w/g	0.406	0.435
Power of compound, w/cm^3	3.7[a]	6.2
Chemical purity, %	~99	~99
Neutron activity, neutrons/sec·g	10^4 (b)	10^3
Density, g/cm^3	11.46	14.25
Melting point, °C	2280[c]	2627
Boiling point, °C	3550	
Specific heat at 25°C, cal/mole·°K	16.4	
Thermal expansion coefficient at 1000°C, °C^{-1}	14.4×10^{-6}	
Thermal conductivity, w/cm·°C	See Figs. 3.1 through 3.4	Fig. 3.1
Crushing strength, kg	>1	
Electrical resistivity, ohm-cm	800 at 1250°K	
Heat of formation, kcal/mole	−252.9 at 25°C −253.3 at 1200°C	
Free energy of formation, kcal/mole	−240.4 at 25°C −192.3 at 1200°C	
Absolute entropy, cal/°K·mole	19.7 at 298°K	

[a] Assumes 80% packing for microspheres.

[b] Naturally occurring ratio of oxygen isotopes assumed.

[c] Reported melting temperature is actually for $PuO_{1.62}$ due to dissociation of PuO_2 as it approaches this temperature. The melting point of PuO_2 is 2400°C.

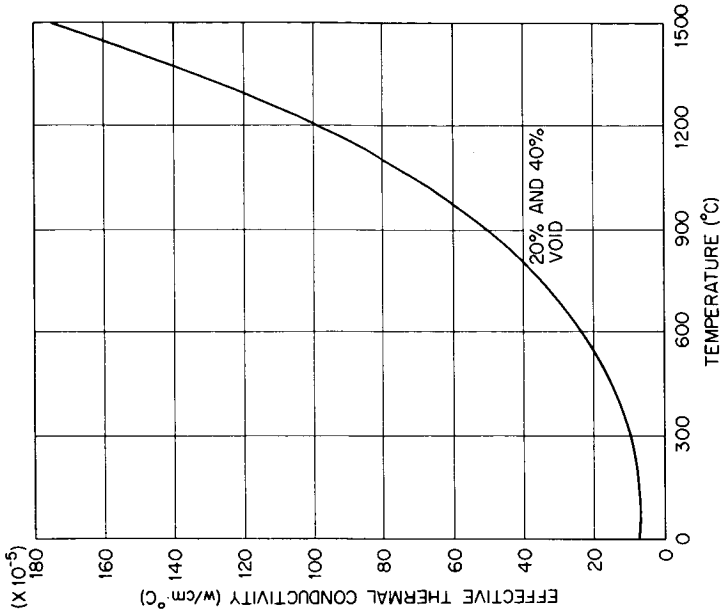

Fig. 3.2. Effective Thermal Conductivity of Packed PuO_2 Spheroids in Vacuum.

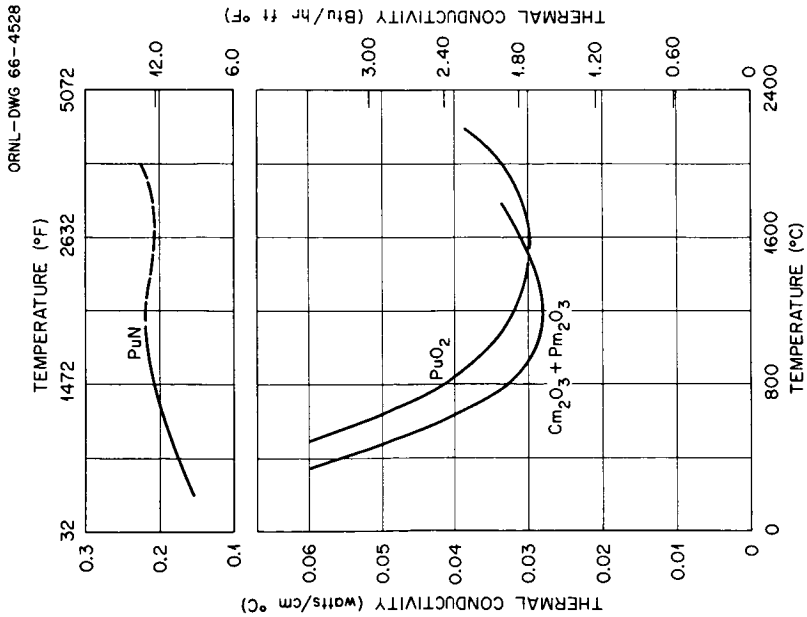

Fig. 3.1. Estimated Thermal Conductivity Values for Several $^{238}PuO_2$ and ^{238}PuN Pressed-and-Sintered Pellets.

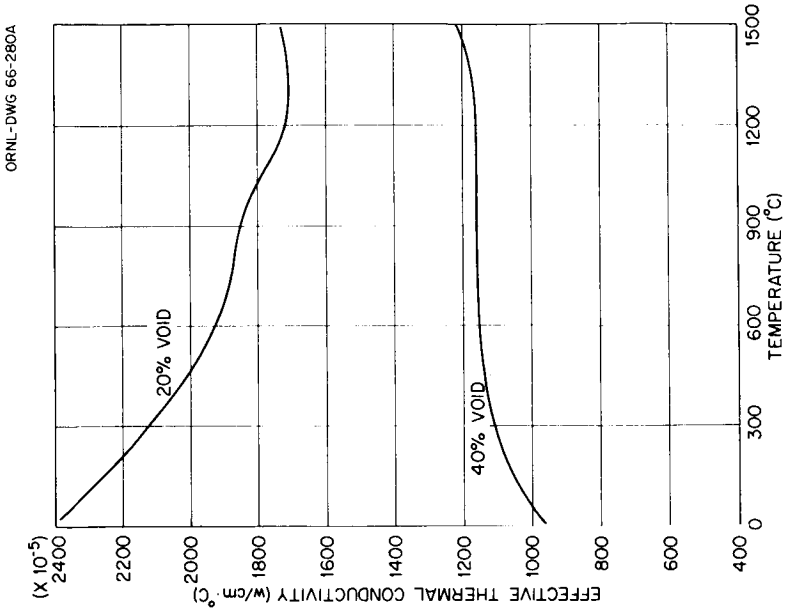

Fig. 3.4. Effective Thermal Conductivity of Packed PuO_2 Spheroids in 10 atm Helium Pressure.

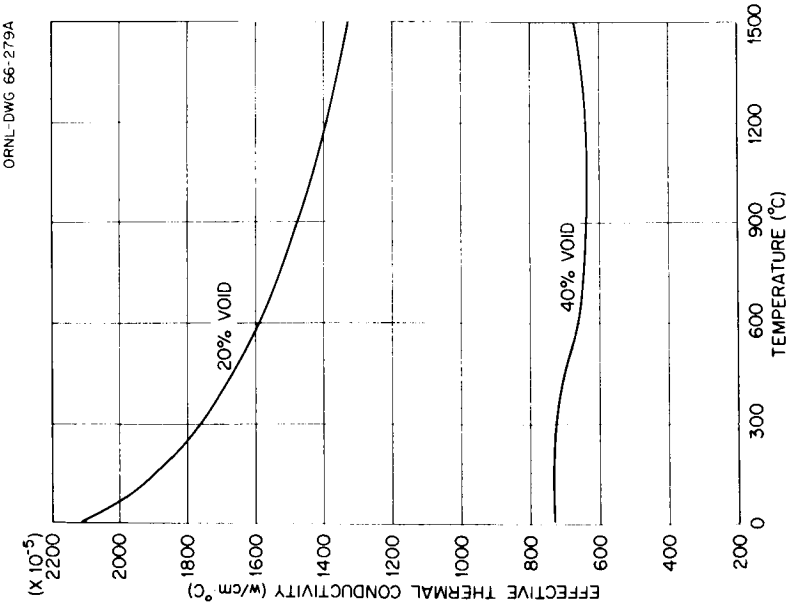

Fig. 3.3. Effective Thermal Conductivity of Packed PuO_2 Spheroids in 1 atm Helium Pressure.

result in a lower thermal conductivity value and would require more volume to hold the fuel, the low solubility of the microsphere form in seawater and its inertness to the atmosphere more than compensate for the higher density of the pressed-and-sintered pellet form. Thus the microsphere form of $^{238}PuO_2$ was selected. The composition of the plutonium dioxide microspheres formed by the plasma-torch technique was determined by crystallographic techniques to be $PuO_{1.98}$. There is some speculation that at the operating temperature of interest (~2000°F) the plutonium oxide fuel form might exist as a mixture of Pu_2O_3 and PuO_2 (Ref. 3). Properties related to its use as an isotopic power fuel are given in Table 3.1. Most physicochemical values for this table were determined by the measurements on compounds of the more stable ^{239}Pu isotope.

Since very little information on the thermal conductivities of the plutonium fuel forms is available, approximate thermal conductivity values were determined by utilizing the values reported for several chemically similar fuel forms. The estimated thermal conductivity values for pressed-and-sintered pellets of $^{238}PuO_2$ and ^{238}PuN are shown in Fig. 3.1. The estimated thermal conductivity of the plutonium dioxide pressed-and-sintered pellet was determined from data[4] obtained for UO_2. The estimated thermal conductivity of PuN was obtained by using data[5] for UN at lower temperatures and data[6] for TiN and ZrN at higher temperatures. The criteria used in estimating[7] the effective thermal conductivity (conductance) of PuO_2 packed microspheres were

Average particle size, μ	150
Packing density, %	80 and 60
Pressure between particles	Vacuum and 1 and 10 atm helium

The results are shown in Figs. 3.2, 3.3, and 3.4, where the effective thermal conductivity, K_{eff}, is plotted against temperature, and K_{eff} is defined as

$$K_{eff} = K_{sc} + K_{gsc} + K_{rad} + K_{nc} ,$$

where

K_{eff} = effective thermal conductivity of the fuel,

K_{sc} = thermal conductivity due to solid contact,
K_{gsc} = thermal conductivity due to gas-solid contact,
K_{rad} = thermal conductivity due to radiation,
K_{nc} = thermal conductivity due to natural convection.

3.1.2 Curium-244

Curium-244 is produced by multiple neutron captures in ^{239}Pu according to the following sequence:

$$^{239}Pu \xrightarrow[303\ b]{(n,\gamma)} {}^{240}Pu \xrightarrow[250\ b]{(n,\gamma)}$$

$$^{241}Pu \xrightarrow[390\ b]{(n,\gamma)} {}^{242}Pu \xrightarrow[52\ b]{(n,\gamma)} {}^{243}Pu$$

$$^{243}Pu \xrightarrow{4.98\ h,\ \beta} {}^{243}Am \xrightarrow[138\ h]{(n,\gamma)} {}^{244}Am \xrightarrow[26\ m]{\beta} {}^{244}Cm$$

The oxide form of ^{244}Cm is the only compound that has been investigated as an isotopic power fuel. Two stable oxides, Cm_2O_3 and CmO_2, are possible; however, the results of several thermogravimetric analyses[8,9] of milligram quantities of curium oxide show that CmO_2 will not exist above 1000 to 1100°C. The present production method for this material involves precipitation as an oxalate followed by calcination to the oxide at temperatures in excess of 1000°C; therefore, it is probable that the oxide will be largely in the Cm_2O_3 valence state, so this form was selected for this study.

Very little information is available on the various nuclear, thermophysical, and mechanical properties of this fuel, but work is in progress at both ORNL and Savannah River to determine these characteristics. The expected composition based on large-scale production of ^{244}Cm is given below:[10]

Nuclide	Mass Abundance* (wt %)
^{242}Cm	0.02
^{243}Cm	0.002
^{244}Cm	95.3
^{245}Cm	0.9
^{246}Cm	2.7
^{247}Cm	0.07
^{248}Cm	0.05
^{243}Am	0.5
^{252}Cf	$<4 \times 10^{-5}$

The property data available[10-12] for this product curium (~95% ^{244}Cm) are listed below; most values are estimates based on chemically similar stable materials whose properties are known:

Half-life, y	18.1
Specific activity of compound, curies/g	~70.5
Specific power of compound, w/g	2.43
Power of compound, w/cm^3	26.0
Chemical purity, %	~95
Neutron activity, neutrons/sec·g	4.2×10^5
Density, g/cm^3	10.7
Melting point, °C	1950
Thermal expansion coefficient, $°C^{-1}$	$<1 \times 10^{-5}$
Thermal conductivity, w/cm·°C	See Fig. 3.1
Modulus of rupture, kg/cm^2	170
Compressive strength, kg/cm^2	1900

Two physical forms of Cm_2O_3 were investigated — pressed-and-sintered pellets and packed powder. There has been some experimental work at ORNL directed at perfecting a method of preparing $^{244}Cm_2O_3$ microspheres, but this fuel form was not considered because it is still in the laboratory development stage. The thermal conductivity for pressed-and-sintered pellets (Fig. 3.1) was estimated[11] from known values for the chemically similar materials Y_2O_3, UO_2, and ThO_2. In this application, the conceptual capsules each have only a very small volume of $^{244}Cm_2O_3$ in relation to the total capsule volume, and a lightly packed powder form of the compound is satisfactory from the standpoint of temperature in the fuel. The lightly packed powder fuel was assumed to have only 50% packing, and the thermal

*One year after reactor irradiation, 97% of the ^{244}Cm product will be of this composition; 3% of the product will contain higher concentrations of ^{242}Cm and ^{243}Cm.

conductivity was estimated to be similar to that of PuO_2 microspheres with the same packing. With this approach, the estimated thermal conductivity of Cm_2O_3 packed powder (50% packing) at 1200°C is 0.0035 w/cm·°C.[7] This value was used in the capsule design program.

3.1.3 Promethium-147

Promethium-147 is a fission product that is separated from reactor fuel-reprocessing wastes. It can also be obtained by the irradiation of neodymium; however, the high target-fabrication and handling costs do not make this method an attractive alternative. The significant contaminants are ^{146}Pm and ^{148}Pm. The other rare earths can be separated and reduced to an insignificant level by ion exchange. Promethium-148, which has a half-life of 42 d, can be brought to an acceptably low level by aging the waste before processing. Promethium-146 has a half-life of 4.4 y and therefore cannot be removed adequately by aging. Promethium-146 is formed by the (n,2n) reaction on ^{147}Pm, and fortunately the cross section for this reaction at thermal fluxes is low. Promethium-147 obtained from highly thermalized production reactors[13] has approximately $5 \times 10^{-5}\%$ ^{146}Pm, while that obtained from typical power reactors is expected to have an order-of-magnitude larger quantity of ^{146}Pm (Table 3.2).

The two forms of ^{147}Pm considered for this study were ^{147}Pm metal and $^{147}Pm_2O_3$ pressed-and-sintered pellets. At the expected operating temperatures (~2000°F) the ^{147}Pm metal would be in a molten form, and it would require a special inner container to retain the fuel in the configuration required. The container would have to be compatible with the molten promethium metal. In the conceptual designs of the capsule for ^{147}Pm, the capsule is essentially completely filled with the fuel because there is no gas evolution during radioactive decay. Therefore, the slightly higher power density of the metal would offer a corresponding advantage of about 15% in weight of fuel. Because of the lack of information and lack of planned experimental programs to determine the compatibility of liquid and vapor-phase ^{147}Pm metal with potential encapsulating materials, as well as the potentially severe dispersal problem if the molten metal should come in contact with air, it was not carried through to a conceptual design.

Table 3.2. Promethium Isotopic Activity Ratios at Discharge from a Power Reactor[a]

Irradiation Time (years)	Activity Ratio of ^{148}Pm (Act ^{148}Pm/Act ^{147}Pm)	Promethium-146 Activity Ratios (Act ^{146}Pm/Act ^{147}Pm)						
		$\Phi_f/\Phi_{th} = 0.1$[b]	$\Phi_f/\Phi_{th} = 0.3$	$\Phi_f/\Phi_{th} = 0.5$	$\Phi_f/\Phi_{th} = 1.0$	$\Phi_f/\Phi_{th} = 3.0$	$\Phi_f/\Phi_{th} = 5.0$	$\Phi_f/\Phi_{th} = 10.0$
		$\times 10^{-6}$	$\times 10^{-6}$	$\times 10^{-6}$	$\times 10^{-6}$	$\times 10^{-6}$	$\times 10^{-6}$	$\times 10^{-6}$
0.33	0.112	0.417	0.502	0.588	0.802	1.659	2.515	4.657
0.66	0.125	0.287	0.415	0.543	0.861	2.138	3.414	6.601
1.0	0.129	0.234	0.382	0.529	0.898	2.375	3.852	7.544
1.25	0.130	0.211	0.368	0.524	0.915	2.479	4.044	7.951
1.5	0.131	0.196	0.359	0.521	0.927	2.550	4.175	8.230
1.75	0.132	0.186	0.352	0.519	0.935	2.599	4.266	8.427
2.0	0.132	0.178	0.347	0.517	0.941	2.638	4.335	8.574
2.167	0.133	0.173	0.345	0.516	0.944	2.657	4.369	8.652
2.33	0.133	0.170	0.343	0.515	0.947	2.673	4.401	8.716
2.50	0.133	0.167	0.341	0.515	0.950	2.690	4.430	8.777
2.66	0.133	0.164	0.339	0.514	0.952	2.700	4.452	8.825
2.83	0.133	0.162	0.338	0.514	0.953	2.712	4.471	8.867
3.0	0.133	0.160	0.337	0.513	0.955	2.721	4.485	8.902
3.167	0.133	0.159	0.336	0.512	0.956	2.728	4.500	8.931
3.33	0.134	0.157	0.335	0.512	0.957	2.735	4.514	8.959
3.50	0.134	0.156	0.334	0.512	0.959	2.742	4.526	8.984
3.66	0.134	0.155	0.334	0.512	0.959	2.748	4.535	9.004
3.83	0.134	0.154	0.333	0.510	0.960	2.753	4.543	9.025
4.0	0.134	0.153	0.332	0.512	0.961	2.754	4.550	9.037
4.25	0.134	0.152	0.332	0.512	0.962	2.761	4.560	9.058
4.5	0.134	0.151	0.331	0.512	0.962	2.766	4.568	9.073
4.75	0.134	0.150	0.331	0.512	0.963	2.770	4.577	9.094
5.0	0.134	0.150	0.331	0.512	0.964	2.772	4.580	9.099
5.25	0.134	0.150	0.331	0.512	0.964	2.775	4.584	9.108
5.5	0.134	0.149	0.331	0.512	0.964	2.774	4.586	9.113
5.75	0.134	0.149	0.330	0.511	0.964	2.776	4.588	9.117

[a]Oyster Creek Reactor parameters were used for the computations in this table. The thermal flux was taken to be 1.7×10^{13} neutrons/cm^2·sec.

[b]Ratio of fast flux to thermal flux.

The available properties of each of these fuel forms, as determined at Battelle-Northwest[13] and ORNL,[11,14] are listed in Table 3.3. Most values are estimated from neighboring rare-earth values.

Table 3.3. Properties of Promethium-147 Fuel Compounds

Properties	^{147}Pm Metal	$^{147}Pm_2O_3$
Half-life, y	2.62	2.62
Specific activity of compound, curies/g	928	798
Specific power of compound, w/g	0.333	0.286
Power of compound, w/cm^3	2.43	2.09
Chemical purity, %	>99	>99
Density, g/cm^3	7.3	7.3
Melting point, °C	1080	2270
Boiling point, °C	3300	
Thermal expansion coefficient at at 400°C, $°C^{-1}$	6.7×10^{-6}	9×10^{-6}
Thermal conductivity, w/cm·°C	Fig. 3.5	Fig. 3.1
Temperature of transition to body-centered cubic form, °C	890	
Heat of transition, kcal/mole	0.73	
Heat of sublimation at 960°C, kcal/mole	75	

The estimated thermal conductivity of $^{147}Pm_2O_3$ was assumed to be the same as that for $^{244}Cm_2O_3$ pressed-and-sintered pellets and is shown in Fig. 3.1. The calculated thermal conductivity for promethium metal,[14] both in solid and liquid form, is shown in Fig. 3.5.

3.1.4 Maximum Allowable Fuel Diameter

The maximum fuel center-line temperature for solid fuel forms as a function of fuel diameter was determined as shown in Fig. 3.6. In all cases the outer surface temperature of the fuel was assumed to be 2000°F and to simplify the calculation in a conservative manner, the end caps were considered as perfect insulators. The dashed lines represent points

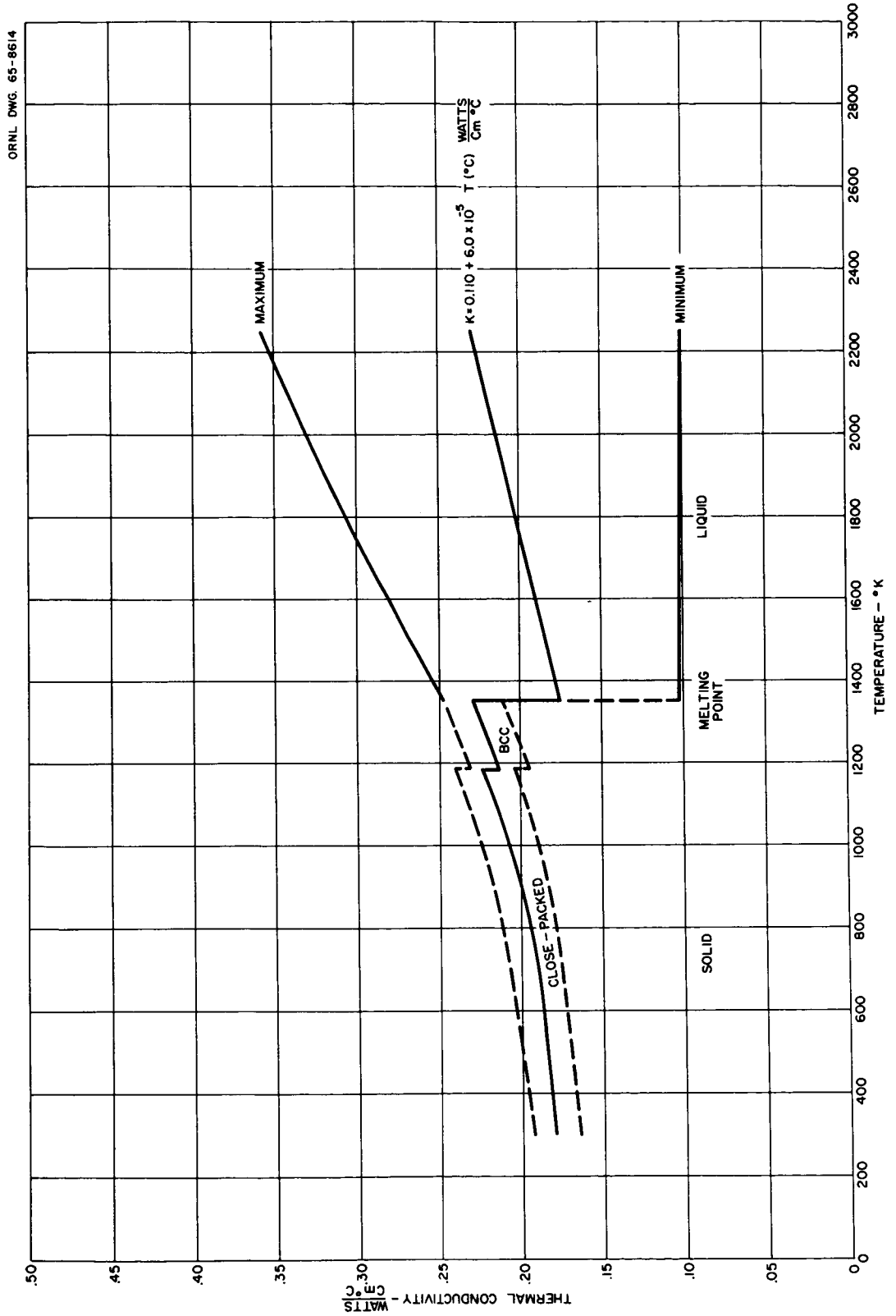

Fig. 3.5. Thermal Conductivity Estimate for Pure Elemental Promethium.

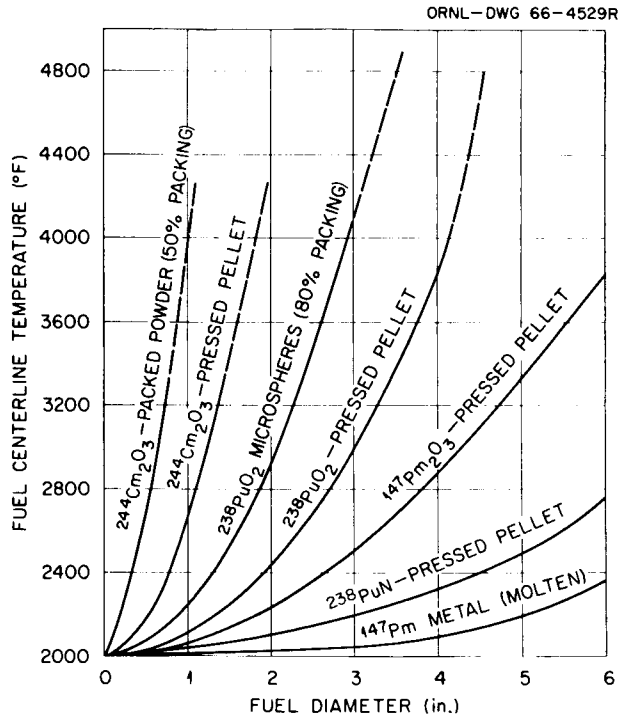

Fig. 3.6. Fuel Center-Line Temperature Versus Fuel Diameter for Fuel Forms Studied. Fuel outer surface temperature of 2000°F assumed.

where the maximum fuel temperature comes within 200°F of the fuel melting point. This criterion (200°F or more below the melting point) was used in the capsule design, and therefore the PuO_2 microsphere form was limited to a maximum diameter of approximately 3 in. and the PuO_2 pressed pellet to slightly over 4 in. The Cm_2O_3 pressed pellet was limited to diameters less then 1.5 in., while the Cm_2O_3 packed powder was the worst case and was limited to approximately 0.75 in. in diameter. Annular arrangement of the fuel in the capsule would permit much larger diameter capsules to be utilized if desired and still be within the design guidelines. As is shown in the capsule design study (Sect. 5), large void volume-to-fuel volume ratios are required to meet the stress limitations for ten half-life containment of the alpha-emitting fuels, and using an annular fuel arrangement would provide large volumes of free space at the center of each fuel capsule for the helium generated, as well as allow larger diameter capsules.

3.1.5 Fuel Property Summary

A summary of the property values used in this study for each of the three fuel compounds selected is given in Table 3.4. The values for the alpha emitters are based on 80% packing for the microsphere form of PuO_2 and 50% packing for the packed powder form of Cm_2O_3. The thermal conductivity values for each of the alpha emitters are based on assuming that helium occupies the void volumes in each of these fuels.

The total fuel requirements for a 25-kw Brayton-cycle heat source are listed in Table 3.5. The values for this table were based on assuming that the total wattage initially required would include allowing for fuel decay during the 1-year mission, 10% excess wattage for heat losses through the system insulation, and a two-month period for encapsulating fuel and loading it into the spacecraft prior to launch.

3.2. Fuel Availability

The Division of Isotopes Development, AEC, has estimated the quantities of ^{244}Cm, ^{238}Pu, and ^{147}Pm that may be available annually up to 1980, and their data[15] are listed in Table 3.6.

Table 3.4. Fuel Property Data Sheet for Brayton-Cycle Heat Source

General Properties	$^{238}PuO_2$[a]	$^{147}Pm_2O_3$	$^{244}Cm_2O_3$
Half-life, y	86.4	2.62	18.1
Density, g/cm^3	11.4	7.3	10.7
Specific power of compound, w/g	0.406	0.286	2.43
Power of compound, w/cm^3			
Maximum	4.63		26.0
Design	3.7[b]	2.09	13.0[c]
Melting point, °C	2280	2270	1950 in He
Thermal conductivity at 1200°C, w/cm·°C			
Maximum	0.0315		0.0280
Design	0.0135[b]	0.0280	0.0035[c]

[a]Based on 80% ^{238}Pu–20% ^{239}Pu and other impurities.

[b]Based on 80% packing.

[c]Based on 50% packing.

Table 3.5. Fuel Requirements for Brayton-Cycle Heat Source[a]

Requirements	$^{238}PuO_2$	$^{147}Pm_2O_3$	$^{244}Cm_2O_3$
Total power required to provide 25 kw(th) at end of 1-year mission, kw	27.9	39.75	29.25
Initial activity required, curies	842,000	111,000,000	850,000
Total weight required, lb	151	307	26.5
Total volume required, $in.^3$	460[b]	1160	138[c]

[a]Includes two-month lag between load and launch and 10% excess wattage for heat losses through insulation.

[b]Based on packing of 80%.

[c]Based on packing of 50%.

Table 3.6. Fuel Availability

Radioisotope	Product Compound	Availability [kw(th)/year]		
		1967	1970	1980
^{147}Pm	Pm_2O_3	1[a]	7.2[a]	33[b]
^{238}Pu	PuO_2	11.4[a]	15[a,c]	60[b]
^{244}Cm	Cm_2O_3	5[d]	100[e]	400

[a] Scheduled availability from AEC operations.

[b] Based on civilian nuclear power operations.

[c] Could be increased to 25 kw in 1970 and 180 kw in 1980 at a 50% increase in cost.

[d] Developmental

[e] In 1972.

It has been estimated[16] that if 25% of the commercial power reactors operating by the year 1980 recycle uranium and plutonium and separate the ^{243}Am and ^{237}Np for irradiation in high-flux ($>10^{14}$ neutrons/cm^2·sec) government reactors, the availability of ^{244}Cm could be increased to approximately 500 kw(th) per year and that of ^{238}Pu to approximately 200 kw(th) per year. The ^{147}Pm from a civilian power fuel economy of approximately 90,000 Mw(e) in 1980 would amount to approximately 40 kw(th) per year if the reprocessing waste were aged about two years to reduce the ^{148}Pm content to insignificant levels.[16]

Presently announced AEC plans for all three isotopes are not adequate to fuel even one 25-kw Brayton-cycle heat source in 1970, and only ^{238}Pu and ^{244}Cm would be available in sufficient quantity in the 1972 through 1980 time period.

4. MATERIALS

The general overall criterion that had the most influence on the studies leading to the selection of an encapsulating material for the isotopic heat source was the requirement for the containment of the fuel for ten half-lives. For ^{147}Pm this is 26 years; for ^{244}Cm, 181 years; and for ^{238}Pu, 864 years. There is no engineering precedent for designing even simple vessels for useful lives beyond about 30 years, and even in the 30-year cases it is assumed in the design that the vessel will be periodically inspected and maintained. In the case of the fuel capsules for this Brayton-cycle application, not only are the design life times very long, but also the capsules cannot be inspected and maintained. In addition, the fuel capsules may be at a high temperature (~2000°F) and, in the case of the ^{238}Pu and ^{244}Cm fuels, they will have a high internal pressure.

The conditions and properties that had to be determined in the selection of materials for the capsule were

1. expected worst temperature history throughout the design life,
2. structural properties of potential encapsulating materials in the temperature range and time of item 1,
3. expected worst stress history over the design life, and
4. chemical compatibility of the encapsulating materials with the fuel, potential external environments, and each other in the temperature range and time of item 1.

Since there are no experimental structural property data or compatibility data extending over periods of time that approach the times of interest in this application, it was necessary to take a cautious approach to the capsule conceptual design.

The initial capsule operating temperature will be approximately 2000°F and, although the temperature would decrease with time due to radioactive decay of the fuel, the capsule might be very hot for many years beyond the Brayton-cycle power system operating life. For example, in the event of a mission abort onto land and the subsequent burial by drifting sand or other medium of a capsule containing ^{238}Pu, more than 50 years would elapse before the capsule temperature would decrease to 1324°F (i.e.,

to three tenths its absolute melting temperature) if its initial burial temperature was 2000°F. Both curium and plutonium are alpha emitters, and therefore helium would be continuously generated and would create constantly changing internal pressures within the capsule. The creep resistance of the primary encapsulating material therefore becomes a most important factor in capsule design considerations. The operating temperature (2000°F) is beyond the range in which superalloys can be used, and thus a refractory metal is required. This, in turn, requires selection of corrosion-resistant metal to protect the container from oxidation, since during at least part of its life the capsule will be in air.

The worst long-term temperature condition to which a fuel capsule might be exposed in this application is considered to be the case of burial in a medium such as sand. As is discussed in Section 5, it is possible to design a capsule with a low enough surface heat flux to limit its maximum temperature under this condition to the same value (2000°F) as the normal operating temperature. The radioactive decay schemes of the radioisotope fuels are well known and it was therefore possible to determine quite accurately both the long-term temperature and internal pressure history for the burial case. The long-term structural and compatibility properties of encapsulating materials are now known, and it was necessary in determining the materials requirements to extrapolate in both time and temperature the relatively scanty and short-term data available. It is possible that the fuel capsules might be exposed to a short-term temperature environment higher than has been used in predicting the ten half-life containment requirement, such as in a launch-pad fire. The heat source must be designed to maintain containment of the radioisotope fuel under these conditions also; however, in this case the location of the fuel capsules is known and they can be recovered, and therefore containment for ten fuel half-lives is not required.

A schematic representation of a typical capsule for this application is presented as Fig. 4.1, which shows the multilayer design that is necessary to provide long-term containment of the fuel. Three of the materials, tungsten, platinum, and thoria, are used for compatibility and corrosion protection. The tantalum alloy T-222 is used to provide the necessary high-temperature strength, and the iron titanate coating[17] on the platinum

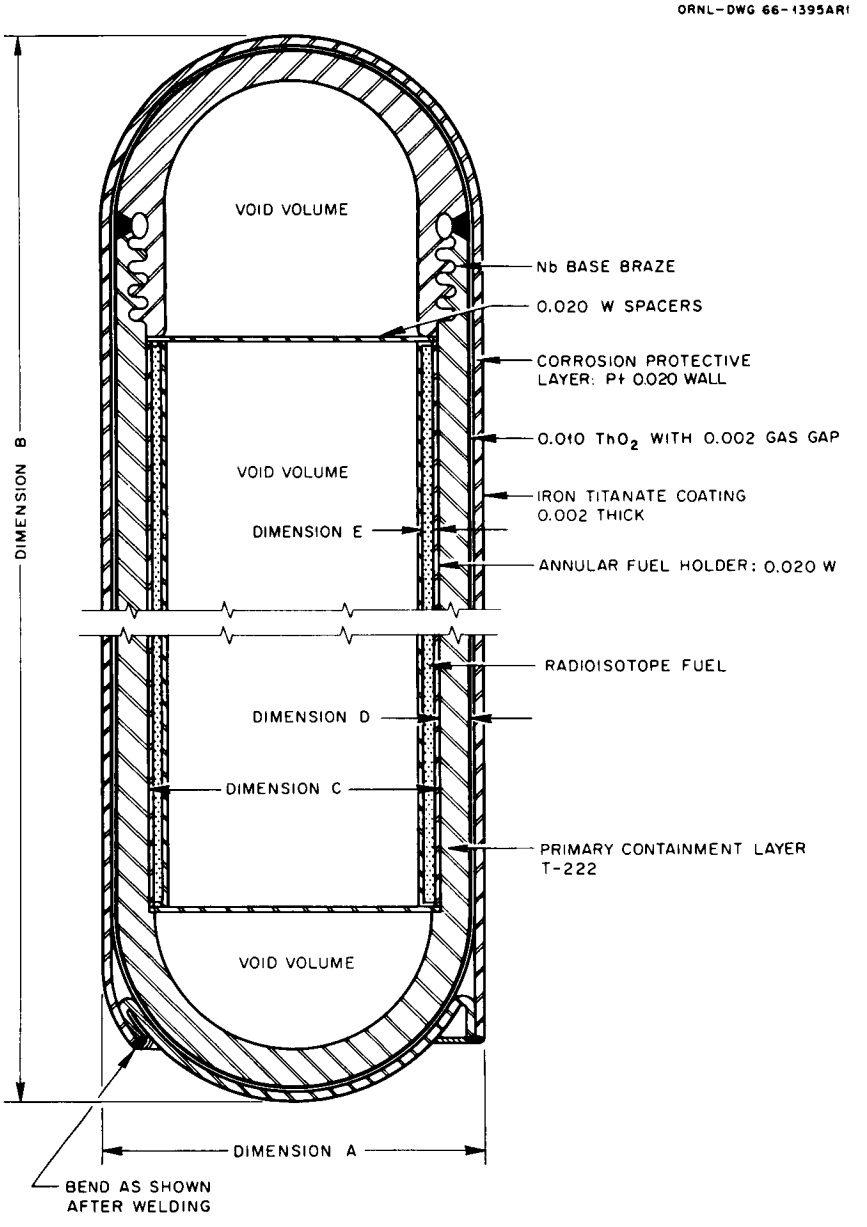

Fig. 4.1. Typical Fuel Capsule.

is needed to improve the emissivity of the capsule surface. In NASA experiments, iron titanate has maintained an emittance of 0.84 for 10,000 hr at 1700°F on Cb–1% Zr in a high-vacuum environment.

The determinations of the capsule dimensions and geometry for each of the fuels, $^{238}PuO_2$, $^{244}Cm_2O_3$, and $^{147}Pm_2O_3$, are described in Section 5. The remaining parts of this section discuss the reasons for the selection of the encapsulating materials shown in Fig. 4.1.

4.1 Selection of Protective Cladding

As noted previously, the expected fuel capsule temperatures (up to 2000°F) required that a refractor metal be used as the primary capsule and, because of the reactivity of refractory metals, that it be protected by a more inert cladding material. A literature search was made for information that would lead to the selection of a metal cladding that would offer the best potential for good resistance to both soil corrosion and air oxidation at temperatures up to 2000°F and sea-water corrosion at temperatures up to 200°F. These are the expected temperatures if a single capsule became buried in sand or immersed in the ocean (see Appendix A). Platinum, rhodium, or alloys of platinum with 10 to 30 wt % rhodium appear to offer this potential if it is assumed that oxidation will be the main corrosion mechanism when the capsules lie in soil. Figure 4.2 gives experimental data on the stability of platinum and rhodium in air. The chart combines the data of Hill and Albert[18] with the results of Krier and Jaffee[19] to cover the temperature range between 2000 to 3100°F. Platinum and rhodium lose weight at elevated temperatures by volatilization of their oxides to give the linear relationship shown; however, both rhodium and platinum show extremely low oxidation rates. A single point is included on Fig. 4.2 for Hastelloy X, an alloy considered to have good oxidation resistance, that clearly shows the superiority of platinum and rhodium. Rhodium exhibits a lower oxidation rate than platinum but the rates for both metals are in the same order of magnitude. A feature of rhodium that may significantly reduce its oxidation rate at temperatures below 1832°F is the formation of a "protective" oxide. Since there does not seem to be a large difference between platinum and rhodium

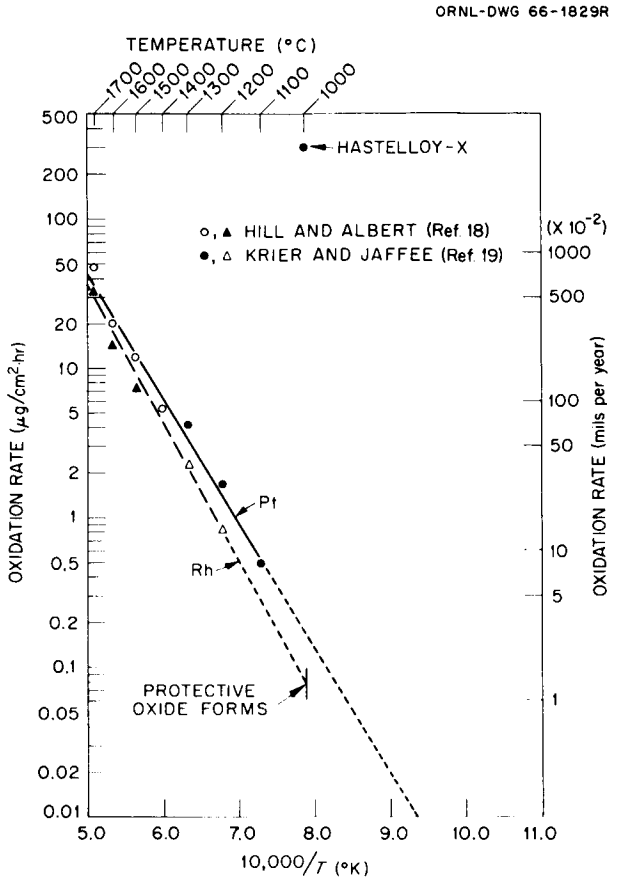

Fig. 4.2. Oxidation Rates of Platinum and Rhodium in Air.

and because platinum is considerably more abundant and less costly, pure rhodium was not considered any further in this study. Platinum-rhodium alloys may also exhibit the protective oxide formation and should be further evaluated.

Based on the corrosion rates shown in Fig. 4.2 and the temperature decay versus time relationship for ^{244}Cm and ^{238}Pu, the thickness of platinum required to protect the T-222 alloy from oxidation for ten fuel half-lives was calculated (Table 4.1). Because of the more rapid temperature decay of the ^{244}Cm fuel, the platinum thickness required is only 0.554 mil compared with a thickness of 2.026 mils for the ^{238}Pu fuel. After the temperature has declined to 1250°F, the effect of oxidation on platinum becomes insignificant.

The oxidation of platinum in air and the corrosion of platinum in soils at elevated temperature may not be equivalent. Zysk[20] reports that caustic, alkalis, nitrates, cyanides, alkaline earths, and the hydroxides of barium and lithium attack platinum at red heat. He also reports that phosphorus, arsenic, and sulfur cause embrittlement of platinum. Analyses of soils show that some of these elements exist in soluble form in soils in small percentages.[21] It is necessary, therefore, that the corrosion of platinum, and possibly platinum-rhodium alloys, in a variety of soils at elevated temperatures be studied to insure the reliability of these metals in this environment. In the absence of data on soil corrosion, we have allowed an order-of-magnitude safety factor that increases the platinum thickness to 20 mils.

As is discussed in Section 5, in the event of a mission abort and subsequent burial in soil of a capsule containing ^{147}Pm, the initial equilibrium temperature will be approximately 2500°F. Calculations indicate that the 20-mils-thick platinum cladding will be sufficient protection in this case too. Because of the shorter half-life of ^{147}Pm, the temperature decays more rapidly than for ^{244}Cm and ^{238}Pu sources, and its residence at the high temperatures is appreciably shorter.

Experimental data,[22] listed in Table 4.2, indicate that the resistance of platinum to seawater is excellent. The corrosion rate, which ranges between 0.001 and 0.005 mils penetration per year, indicates exceptional resistance. These experiments show that platinum is about two

Table 4.1. Anticipated Corrosion of Platinum for Brayton-Cycle Application When Exposed to Air at Elevated Temperatures

Temperature Decay (°F)	Service Years		Corrosion Rate (mils/year)	Total Penetration (mils)	
	^{244}Cm-Fueled Capsule	^{238}Pu-Fueled Capsule		^{244}Cm-Fueled Capsule	^{238}Pu-Fueled Capsule
2000 to 1830	5	10	8×10^{-2}	0.400	0.800
1830 to 1250	5	40	3×10^{-2}	0.150	1.200
1250 to 900	10	50	2×10^{-4}	0.002	0.010
900 to 500	30	100	2×10^{-5}	0.001	0.002
500 to 95	130	700	$<2 \times 10^{-5}$	0.001	0.014
Total	180	900		0.554	2.026

Table 4.2. Corrosion of Commercially Pure Platinum in Seawater Flowing at 2 fps

Specimen dimensions: 2 × 0.75 × 0.010 in.
Exposed area: 3 in.^{2}

Test Period (days)	Weight Loss (mg)	Corrosion Rate	
		mils/dm^2·day	mil/year
14	0.1	0.038	0.0025
31	0.4	0.068	0.0046
60	0.3	0.026	0.0017
179	2.2	0.065	0.0044
180	0.5	0.015	0.001

orders of magnitude more corrosion resistant than Hastelloy C,[23] an alloy frequently cited for its excellent corrosion resistance to seawater. No evidence of localized effects such as pitting were observed in these tests. The results are of limited value because of the relatively short duration of the tests and the fact that the tests were conducted at normal laboratory and seawater temperatures. In the event of an abort into the sea, capsules designed as shown in Section 5 (Figs. 5.1 and 5.2) would reach an equilibrium temperature of approximately 200°F. Although the existing data are encouraging, it is apparent that long-term elevated-temperature tests in seawater should be conducted to substantiate estimates based on existing data.

The possibility of galvanic corrosion in seawater also needs to be considered. Six-month tests to determine the anodic corrosion of platinum and its alloys in seawater did not show any disastrous effects.[24] The results of these tests are listed in Table 4.3. At a current density of 50 amp/ft^2 the corrosion rate was relatively unaffected. At 500 amp/ft^2 a significant increase in corrosion occurred, but the corrosion resistance could still be classified as excellent. The excellent corrosion resistance of Pt–20% Rh alloy in these tests indicates that this alloy is worth further study as a protective cladding.

Table 4.3. Anodic Corrosion of Platinum and Platinum Metal Alloys in Flowing Seawater

Exposed area of specimens: 3 in.^{2}
Duration of test: 6 months (179 days)

Anode Material	Density (g/cm^3)	Current Density (amp/ft^2)	Weight Loss (mg)	Consumption Rate (mg/amp·year)	Corrosion Rate (mil/year)
Platinum	21.4	50	4.5	9	0.009
		500	24.8	5	0.048
80% Pt-20% Pd	18.6	50	10.5	20	0.023
		500	70.7	14	0.157
80% Pt-20% Rh	18.7	50	6.5	13	0.015
		500	87.9	17	0.196
75% Pt-25% Ir	21.7	50	6.5	13	0.013
		500	55.0	11	0.105

4.1.1 Compatibility of the Platinum Cladding with the Primary Capsule Material

Recent studies by Seebold and Birks[25] on the niobium-platinum system revealed that after 188 hr at 2000°F, there was a 0.040-mil diffusion zone; the compounds Nb_3Pt, NbPt, $NbPt_2$, and $NbPt_3$ were identified in such zones. Since the niobium-platinum and tantalum-platinum phase systems are similar,[26] similar diffusion effects between platinum and tantalum would be expected. Passmore and his co-workers[27] examined the reaction of platinum with tantalum at 3100°F and found that after 1 hr there was a 0.040- to 0.100-mil-thick diffusion zone that had a maximum hardness of 1250 VHN. Although Passmore did not identify intermetallic compound formation, the high hardness value indicates the presence of a brittle intermetallic phase, probably Ta_3Pt. The penetration of this brittle compound is a serious matter because it would no doubt have a marked deleterious effect on the creep and yield properties of the T-222 alloy container. Although Passmore's data are limited, it is possible to estimate the time elapsed to form a 0.100-mil diffusion zone at 2000°F by using the relationship

$$\ln\left(\frac{D_{T_1}}{D_{T_2}}\right) = -\frac{Q}{R}\left(\frac{T_1 - T_2}{T_1 T_2}\right) , \qquad (1)$$

where

Q = activation energy = 60 kcal/mole,

R = gas constant,

D_{T_1} = diffusion coefficient at temperature T_1,

D_{T_2} = diffusion coefficient at temperature T_2.

On the basis that T_1 is 2000°F and T_2 is 3100°F, the ratio D_{T_1}/D_{T_2} equals 1.5×10^{-3}. From the relationship,

$$D_{T_1}/D_{T_2} = t_2/t_1 , \qquad (2)$$

where t_1 is the time to form a 0.100-mil diffusion zone and t_2 is the time to form a 0.100-mil diffusion zone at 3100°F ($t_2 = 3.6 \times 10^3$ sec), it is found that $t_1 = 2.4 \times 10^6$ sec (~1 month) and therefore one month at 2000°F is required to form a 0.100-mil-thick diffusion zone.

By utilizing the equation for volume diffusion, the diffusion coefficient at 2000°F can be estimated from the following relationship:

$$X = \sqrt{Dt} , \qquad (3)$$

where

X = thickness of diffusion zone,

t = time,

D = diffusion coefficient.

If we assume $X = 0.100$ mil and $t = 2.4 \times 10^6$ sec,

$$D = 4.2 \times 10^{-11} \text{ cm}^2/\text{sec} .$$

With this value we estimate that after ten years the penetration of the brittle intermetallic phase into the stress-bearing T-222 alloy will be 70 mils. This analysis only takes into account volume diffusion effects. Other considerations such as grain-boundary diffusion could increase penetration of the undesirable element by orders of magnitude. In order to circumvent this problem, a 10-mil plasma-sprayed coating of thoria

could be applied to the surface of the T-222 alloy primary capsule to act as a mechanical barrier to prevent the platinum from contacting the T-222. It would be necessary to do the plasma coating in a very high-purity inert-gas chamber to prevent damage to the refractory alloy and insure a high-purity coating. This approach is acceptable because, as is discussed in Section 5, the effect on the temperature drop across the capsule would not be significant.

4.2 Selection of Primary Capsule Material

Since ^{244}Cm and ^{238}Pu generate helium as they decay, a container for either of these isotopes is basically a pressure vessel. After reviewing the design requirements for this Brayton-cycle application, T-222, a tantalum-base alloy nominally containing 9.5 wt % tungsten, 2.5 wt % hafnium, and 100 ppm carbon, was selected as the stress-bearing material. T-222 alloy was considered the best commercially available refractory metal alloy to contain the helium gas pressure because in the operating temperature range of interest (2000°F maximum) the alloy combines good strength and ductility with weldability.[28,29] The mechanical strength limitations of this material when subjected to a constantly changing pressure, as is the case with ^{238}Pu and ^{244}Cm isotopic fuels, were obtained from a stress-rate theory developed by Kennedy.[30] Although there is not enough data on this refractory alloy to classify it as an engineering material in the sense that stainless steels are rated, it does have this potential. As a conservative measure, results[31] were used that were obtained from strength data on the T-111 alloy, which is very similar to the T-222 alloy but presumed to be somewhat weaker. For the purpose of this conceptual design, it was assumed that the creep strength properties of the T-111 alloy probably represent the lower side of the spread of creep strength properties of T-222 alloy.[32] It is expected that before a capsule is designed for fabrication, sufficient T-222 alloy strength data will have been obtained to refine the design. Stronger advanced tantalum-base alloys are being developed[33] that may, in the future, be substituted for T-111 or T-222 with a minimum of change in the basic capsule design.

4.2.1 Stress-Rate Analysis of Primary Capsule Life

Because of the radioactive decay characteristics of the alpha-emitting isotopes, the fuel capsule temperature would be a maximum and the pressure a minimum immediately after encapsulation. As time passed, the total number of moles of helium in the capsule would continuously increase; however, both the rate of increase and the temperature would decrease with time. After approximately 1.5 radioisotope fuel half-lives, the capsule internal pressure would pass through a maximum and then start decreasing for the rest of the life of the fuel because the rate at which helium was being generated would not be large enough to compensate for the rate at which the pressure was decreasing because of decreasing temperature. These relationships are shown schematically in Fig. 4.3 for a fuel capsule with a start-of-life temperature of 2000°F (1093°C), as do the fuel capsules for this study. The figure also shows that after a decay time of approximately 0.5 half-life, the temperature would decrease to about three-tenths the absolute melting temperature of the T-222 alloy being used for the primary fuel capsule.

The approach to predicting the required life expectancy for the T-222 alloy was based on the premise that when the wall temperature of the capsule declined to less than about three-tenths of the melting temperature (in degrees absolute), the creep strength of the material would no longer be an important factor. Below this temperature atom movements are sluggish and diffusion is not likely to produce creep and phase changes. Beyond this time, when the temperatures are lower, the prediction of failure should be considered an elastic problem. The tensile and yield (elastic) properties would assume more importance, but elastic failures would be very unlikely if the design stress were limited to 25% of the tensile strength and 33% of the yield strength when temperatures were below about three-tenths the absolute melting temperature of the T-222 alloy, which is 1324°F (718°C). A capsule containing ^{244}Cm would reach this temperature after approximately 11 years, and the internal helium pressure would reach a maximum after 28 years when the temperature had declined to approximately 750°F (400°C). In the case of a capsule containing ^{238}Pu, approximately 55 years would elapse before the temperature had declined

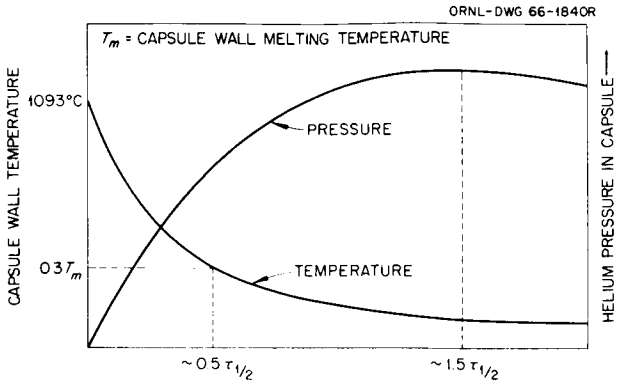

Fig. 4.3. Schematic Representation of Temperature-Time and Pressure-Time Relationships, with Time Indicated as Half-Lives of Isotopic Fuel.

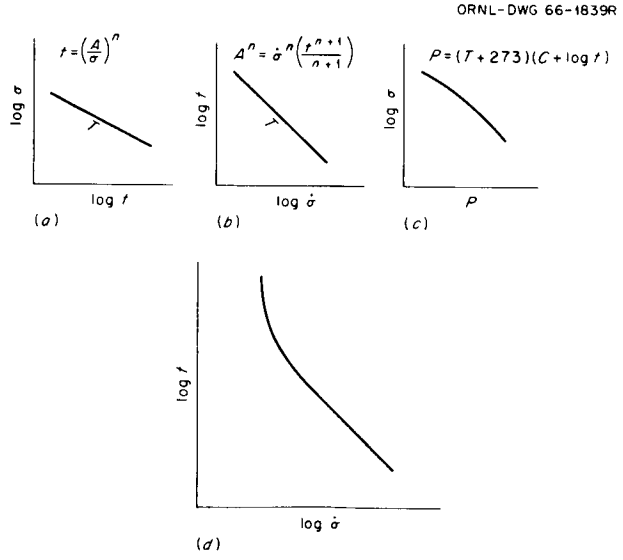

Fig. 4.4. Schematic Representation of (a) Stress-Strain Curve, (b) Log Strain-Time Versus Log Stress-Rate Curve, (c) Larson-Miller Curve, and (d) Temperature-Compensated Log Strain-Time Versus Log Stress-Rate Curve.

to 1324°F (718°C), and the pressure would not reach its maximum until 130 years had elapsed when the temperature of the capsule had decreased to approximately 750°F (400°C). An inspection of the elevated-temperature tensile and yield properties of the T-111 alloy indicates that these properties are not limiting and that this alloy has sufficient strength capability to resist the additional pressure generated after the temperature has declined to 1324°F (718°C).

It is concluded that ten half-life containment is feasible from a stress analysis standpoint if satisfactory creep behavior of a ^{244}Cm-bearing T-222 alloy capsule during a period of 11 years and a T-222 alloy capsule containing ^{238}Pu through a period of 54 years can be established with confidence. Conventional engineering practice would require that experimental creep test data be obtained for time periods up to at least one-fifth the time over which the life is to be predicted to obtain reliable results. Thus, in the case of the Brayton-cycle capsules, it would be desirable to have 2-year creep data in the 2000 to 1324°F (1093 to 718°C) temperature range when considering ^{244}Cm as the fuel and 10-year creep data in the case of the ^{238}Pu fuel. At the present time creep data for T-111 for times approaching those of interest in this study are not available, and it has been necessary to extrapolate in time.

Also, the creep experiments have been carried out in the conventional manner at constant temperature and constant nominal stress. In order to establish allowable design stress rates during the period in which the capsule is above three-tenths its melting point, a means of predicting the behavior of the encapsulating material under conditions of varying stress and temperature from conventional creep data is desirable. An approximate method for doing this was developed.

Important relationships in the development of this method are illustrated schematically in Fig. 4.4. A conventional stress-strain curve (determined at constant nominal stress and constant temperature) is illustrated in Fig. 4.4a. For most materials, this curve can be represented by the equation

$$t = (A/\sigma)^n , \qquad (4)$$

where t is time to strain, σ is stress, and A and n are constants.

Figure 4.4b shows a plot of the logarithm of time to strain versus the logarithm of stress rate ($\dot{\sigma}$) at constant temperature. This curve can be derived, as shown by Kennedy,[30] from conventional stress-strain data for a number of materials with the equation

$$A^n = \dot{\sigma}^n \frac{t^{(n+1)}}{n+1} , \tag{5}$$

where A and n are the constants in Eq. (4).

Figure 4.4c shows schematically a plot of log stress versus the Larson-Miller parameter,

$$\text{Log } \sigma = f(P) ,$$

$$P = (T + 273)(C + \log t) ,$$

where

P = Larson-Miller parameter,
C = Larson-Miller constant,
T = temperature,
t = time to rupture,

which provides the means of interpolating existing creep data in temperature and extrapolating in time.

For any radioactive isotope an equation can be written for the container temperature as a function of time:

$$T = (T_0 - T_a) \exp (-0.693t/\tau_{1/2}) + T_a , \tag{6}$$

where

T = temperature at time t,
T_0 = initial temperature,
T_a = ambient temperature,
t = time,
$\tau_{1/2}$ = half-life of the isotope.

By substituting an arbitrary value of time into Eq. (6), the temperature of the capsule (T) can be determined at that time. Substituting T and two arbitrarily chosen values of time (e.g., 10 and 1000 hr) into the

Larson-Miller equation gave the corresponding values of stress for constructing a stress-rupture curve for T. With this artificially constructed stress-rupture curve, the constants A and n of Eq. (4) were determined, and then by using Eq. (5) it was possible to calculate a point on a temperature-compensated plot of stress rate versus time for the particular combination of isotope and container material. By repeating this procedure at small time intervals, a complete curve can be calculated over any time range of interest. Such a curve is illustrated schematically in Fig. 4.4d. The curve can be generated on the basis of stress-to-rupture data or data for stress to any specified percent creep. In the calculation of each point on such a curve it is assumed that the stress is applied to the capsule at a single temperature, the low temperature corresponding to the stress-rate value. In the use of such curves it is assumed that the stress rate has a constant value, which is the initial high value that exists when the capsule becomes sealed. It is believed that the combined effects of the two assumptions tend to give low values for the time to rupture or time to reach the design strain. An example of the calculational procedure is given in Appendix B. In the temperature range of interest in this study this temperature-compensated curve will show a knee that identifies the stress rate and represents the design limit based on the creep data used. For achieving desired safety factors, a stress rate less than this can be selected.

A computer program was written for performing these calculations for this study. A Larson-Miller master rupture or creep function is first fitted to the data by a separately operable subroutine. The program then uses this plot to carry out the previously described calculations. The stress-rate curve for ^{244}Cm in a capsule initially at 2000°F based on stress-rupture data for T-111 alloy is shown in Fig. 4.5. The stress-rupture data used in constructing the curve are listed in Table 4.4.

It may be seen in Fig. 4.5 that the minimum stress rate that causes creep rupture or maximum stress rate that avoids creep rupture according to this temperature-compensated stress-rate versus rupture-time curve occurs at a stress rate of 0.8 psi/hr. As shown in Fig. 4.6 for ^{238}Pu, the maximum occurs at 0.15 psi/hr in a similar type of plot. The difference in

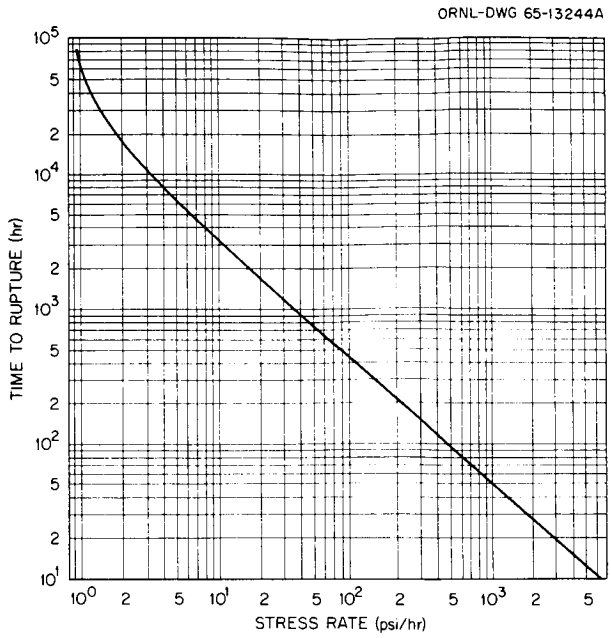

Fig. 4.5. Temperature-Compensated Stress-Rate Versus Rupture-Time Curve for ^{244}Cm-Containing T-111 Alloy Capsule Initially at 2000°F.

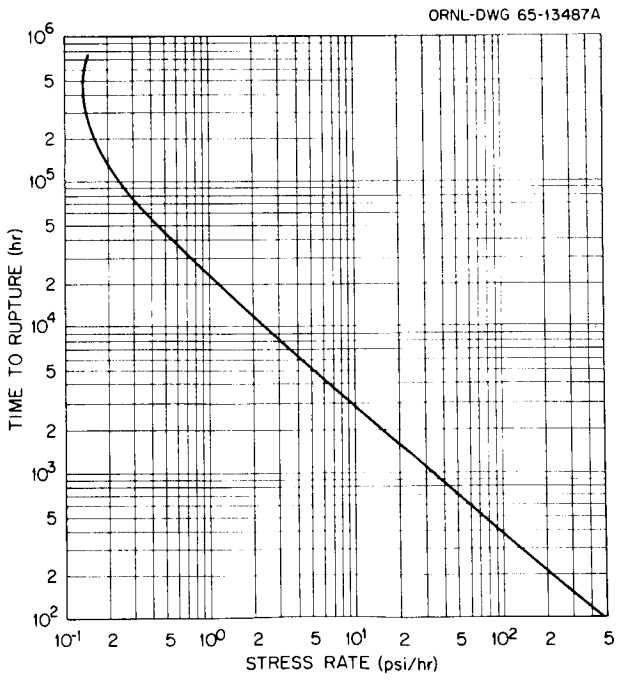

Fig. 4.6. Temperature-Compensated Stress-Rate Versus Rutpure-Time Curve for ^{238}Pu-Containing T-111 Alloy Capsule Initially at 2000°F.

Table 4.4. Stress-Rupture Data[31] for T-111 Alloy

Temperature		Stress (psi)	Time to Rupture (hr)
°C	°F		
1205	2200	35,000	8.60
		30,000	23.7
		25,000	65.6
		22,500	101.5
		20,000	485.0
		17,500	975.1
		15,000	1737.3
1425	2600	15,000	19.2
		12,500	25.1
		12,500	27.2
		10,000	168.5
		7,500	575.4
1650	3000	13,900	0.62
		10,000	2.90
		7,000	22.6
		4,500	177.0
		3,500	493.2

these stress-rate values is attributed directly to the longer half-life of the ^{238}Pu isotope, which accounts for its longer residence at temperatures higher than 1324°F (718°C) compared with the ^{244}Cm isotope. It is also worthy of note that the maximum stress rates that avoid creep rupture occur at time values on these curves at which the absolute temperature of the primary capsule material reaches approximately three-tenths its melting temperature. This will generally be the case if the creep rate of the material becomes very low at three-tenths its melting temperature and the design point temperature of the material is not appreciably higher than three-tenths the melting temperature so that the creep-temperature relationships are approximately linear. This maximum stress rate that avoids creep rupture represents compliance, insofar as creep is concerned, with the guideline of ten half-life containment. Appropriate safety factors were applied to such a stress rate to obtain the stress rates used for the design of the capsules described in Section 5.

Calculations were also made with a computer program to define the maximum stress rate that results in no more than 2% creep on a curve in which a temperature-compensated stress rate is plotted versus time to 2% elongation. The Larson-Miller plot for this is illustrated in Fig. 4.7, and the data from which the plot was derived are listed in Table 4.5. The results are illustrated in Figs. 4.8 and 4.9. In this case the maximum value according to the curve for the ^{244}Cm capsule occurs at a stress rate of 0.4 psi/hr. In the case of the capsule containing ^{238}Pu, it occurs at a stress rate of 0.065 psi/hr.

Table 4.5. Creep Data[31] for 2% Elongation of T-111 Alloy

Temperature		Stress (psi)	Time to 2% Creep (hr)
°C	°F		
1205	2200	35,000	1.20
		30,000	1.46
		25,000	5.50
		22,500	7.90
		20,000	21.0
		17,500	25.5
		15,000	43.8
1425	2600	15,000	0.90
		12,500	3.75
		12,500	4.70
		10,000	29.8
		7,500	64.7
1650	3000	13,900	0.05
		10,000	0.45
		7,000	2.67
		4,500	12.4
		3,500	22.7

Existing data on T-111 or T-222 alloys are not sufficient to design a capsule actually intended for operation. They have only been used in this study to estimate the potential offered by these alloys. The reliability of the tensile and creep properties of the T-222 alloy for these

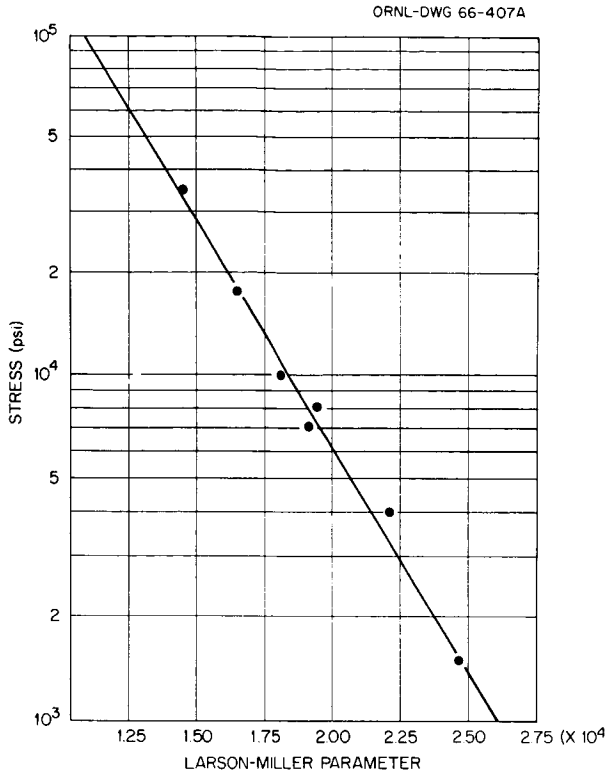

Fig. 4.7. Larson-Miller Plot for 2% Elongation of T-111 Alloy. (Data from Table 4.5.)

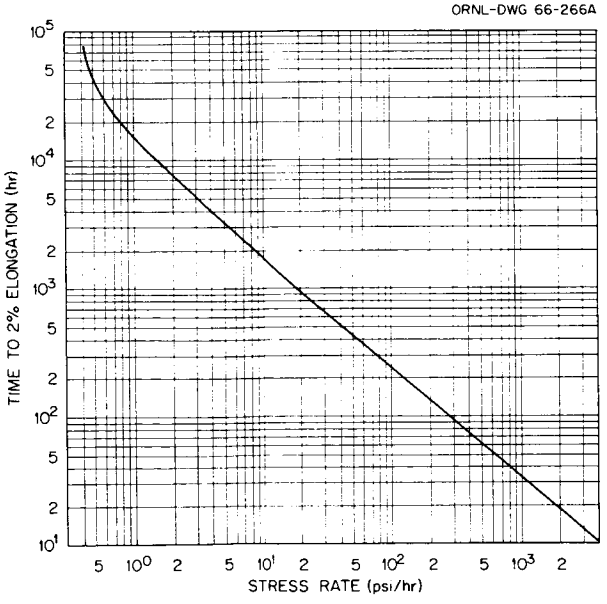

Fig. 4.8. Temperature-Compensated Stress Rate Versus Time to 2% Elongation for ^{244}Cm-Containing T-111 Alloy Capsule Initially at 2000°F.

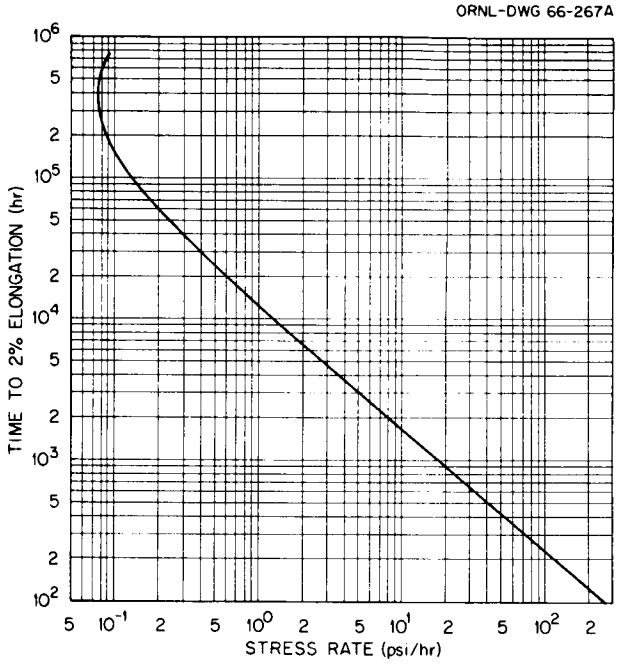

Fig. 4.9. Temperature-Compensated Stress Rate Versus Time to 2% Elongation for ^{238}Pu-Containing T-111 Alloy Capsule Initially at 2000°F.

long-time applications must be determined by testing and evaluation on a statistical basis. The areas of work include:

1. verification of the temperature-compensated stress-rate method of analysis by comparing experimental variable stress rate—variable temperature data with results calculated from experimental creep data,
2. determination of the effect of long-term high-temperature environment (equivalent to one-fifth the time involved in temperature decline to 1324°F) on the creep properties,
3. studies of the effect of the long times at elevated temperatures and stress on the tensile properties,
4. evaluation of the effect of long times at elevated temperatures on physical and metallurgical characteristics, such as grain size, etc., and
5. analyses of the effects of long times at elevated temperatures on weldments.

Collecting these data for a statistically meaningful number of heats of the T-222 alloy will be an arduous and expensive program. A possible alternate approach is to purchase, well in advance of the time it is to be used, a large heat of T-222 alloy so that the creep, tensile, and stress-rate data necessary to design fuel capsules for the intended application can be obtained from samples prepared from this heat and the remainder of the heat can be used for the fabrication of the actual capsules.

4.2.2 Compatibility of Fuel with Primary Capsule Material

It is important in isotopic power systems to ascertain that the isotope fuel, whether in the elemental or compound form, is compatible with the encapsulating material because of the effect an incompatibility might have on the long-term strength and integrity of the capsule. As mentioned before, the primary capsule material in this study is T-222 alloy, and the three fuel compounds being considered are $^{238}PuO_2$, $^{244}Cm_2O_3$, and $^{147}Pm_2O_3$. The common practice was followed for predicting whether two materials are compatible when experimental evidence is not available

of using an equation involving the reaction of the stoichiometric compounds and calculating the total free-energy change. No thermodynamic data were available for the curium and promethium oxides, so data for praseodymium oxide was used in the calculations. Data were available on PuO_2 and Pu_2O_3, and free-energy change calculations were made for both these oxides. The results of the thermodynamic calculations with each of the alloying elements in T-222, tantalum, tungsten, and hafnium, are listed in Table 4.6.

Table 4.6. Calculated Total Free-Energy Changes in Isotope Oxide-Metal Reactions

Reaction	Temperature (°K)	ΔF_{reac} (kcal)[a]	ΔF (kcal)[b]
$W + 4PuO_2 \rightleftharpoons 2Pu_2O_3 + WO_2$	1000	+68.6	+17.8
	2000	+48.0	
$2Ta + 10PuO_2 \rightleftharpoons 5Pu_2O_3 + Ta_2O_5$	1000	+27.0	−99.5
	2000	−27.5	
$Hf + 4PuO_2 \rightleftharpoons 2Pu_2O_3 + HfO_2$	1000	−55.2	−106.0
	2000	−73	
$2Pu_2O_3 + 3W \rightleftharpoons 4Pu + 3WO_2$	1000	+366.6	+444.6
$5Pu_2O_3 + 6Ta \rightleftharpoons 10Pu + 3Ta_2O_5$	1000	+484.5	+679.5
$2Pu_2O_3 + 3Hf \rightleftharpoons 4Pu + 3HfO_2$	1000	−4.8	+73.2
$3W + 2Pr_2O_3 \rightleftharpoons 4Pr + 3WO_2$	2000	+276	
$6Ta + 5Pr_2O_3 \rightleftharpoons 10Pr + 3Ta_2O_5$	2000	+990	
$3Hf + 2Pr_2O_3 \rightleftharpoons 4Pr + 3HfO_2$	2000	+89.0	

[a]Data from Refs. 34 and 35.

[b]Data from Ref. 36.

Two values of the free-energy change (ΔF) are given in the case of oxides of plutonium – the first, ΔF_{reac}, being based on thermodynamic values recommended by the Bureau of Mines[34] and data from Argonne National Laboratory[35] and the second, ΔF, based on Chikalla's values.[36] In both cases, there is an estimated uncertainty of ±50 kcal in the totals. It is shown in Table 4.6 that Pu_2O_3 should be more stable with tantalum and

tungsten than PuO_2 and that hafnium will very likely reduce PuO_2 as well as Pu_2O_3. If it is assumed that the free energy of Pr_2O_3 is equivalent to the free energies of Cm_2O_3 and Pm_2O_3, Cm_2O_3 and Pm_2O_3 should be stable with tantalum and tungsten. Although the ΔF of the reaction between hafnium and Pr_2O_3 is positive, some doubt exists regarding the stability of Cm_2O_3 and Pm_2O_3 with hafnium because the value (+89 kcal) is quite low. These thermodynamic calculations neglect the possibility of solubility between constituents. For example, there is a possibility of forming a compound of the type $Pu_xM_yO_3$, where M is the other metal and $x + y$ is 2. Russell and his co-workers[37] have already identified compounds of this type in which M has been barium, manganese, vanadium, chromium, and aluminum. In short, the phase diagrams of the constituents should be known before a large amount of dependence is placed in thermodynamic calculations based on stoichiometric compounds.

In addition to considering the compatibility of the initial fuel with the capsule, it is also necessary to consider the compatibility of the radioactive decay products with the capsule. This is particularly true in the case where long containment times, compared with the fuel half-life, are necessary during which a substantial part of the radioisotope fuel will decay to another chemical compound. In the case of ^{244}Cm the decay product is ^{240}Pu, which can be expected to have the same compatibility properties as ^{238}Pu. The half-life of ^{240}Pu is 6580 y, and it can therefore be considered stable insofar as ten half-life containment for ^{244}Cm (180 y) is concerned. The ^{238}Pu fuel form will decay to ^{234}U, which is, for this purpose, stable (half-life = 2.5×10^5 y). The compatibility of various uranium oxides with refractory metals has been investigated in connection with advanced reactor fuel concepts,[38] and it is expected to be quite similar to that of plutonium. The ^{147}Pm fuel form will decay to essentially stable ^{147}Sm which, being an adjoining rare earth, is expected to have about the same compatibility properties as the parent ^{147}Pm.

In considering the selection of the most favorable plutonium oxide, thermodynamics favor Pu_2O_3; however, at this time PuO_2 has been chosen primarily because the compound is readily made and retains its stability during handling, as mentioned in Section 3. Curium oxide (Cm_2O_3) and Pm_2O_3 are the choice forms for the ^{244}Cm and ^{147}Pm isotopes because the thermodynamics favor their stability with both tantalum and tungsten and possibly hafnium.

The thermodynamics indicate that there may be a compatibility problem with all these fuel oxides and hafnium and that the $^{238}PuO_2$ fuel form is worst in this respect. To circumvent this problem for the purpose of a conceptual capsule design, a tungsten-foil annular fuel holder is used to provide a wall between the T-222 alloy and the isotopic fuel. Its usefulness is based on the premise that diffusion of the hafnium from the T-222 alloy to the oxide fuel will be held in check by the tungsten. Quantitative diffusion tests are necessary to ascertain that tungsten will truly be an acceptable barrier between the hafnium and the fuel oxide.

4.2.3. Sealing the T-222 Alloy Container

Figure 4.1 (cited previously) illustrates the reference joint design suggested to effect a seal of the T-222 alloy container. The design is the result of a scheme for thicknening the wall of the capsule in the vicinity of the welded joint. In this manner the stress on the heat-affected zone in the welded region caused by the internal gas pressure can be greatly relieved. The operation involves electron-beam welding and backbrazing, and in order to be effective, the backbrazing must completely seal off the threads from the helium being generated by the fuel. Although several brazing alloys appear attractive,[40,41] and even though T-222 alloy appears to have good weldability, thorough testing and evaluation need to be conducted to establish reliability of this design. Further weld development work with the T-222 alloy may show that the creep and tensile properties are not seriously affected by welding and that there is no need to reduce the stresses in the vicinity of the weld; this would eliminate the need for the braze. If brazing were required, a test program would be needed to determine that over long periods of time the braze

does not gradually diffuse into the base metal and leave a void that would weaken the capsule. For conceptual design purposes, a niobium base braze has been specified.

An alternate design that essentially accomplishes the same purpose is shown schematically in Fig. 4.10. In this case, the increase in wall thickness in the vicinity of the weld is obtained by machining the capsule to the illustrated container design. Since in this design the opening in the top of the capsule is smaller than the inside diameter of the body of the capsule, the annular tungsten fuel holder will have to be made in the form of a ring that can be slightly compressed for insertion into the capsule.

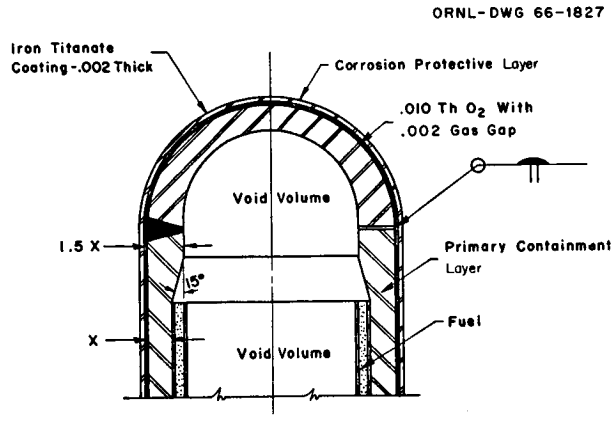

Fig. 4.10. Alternate Capsule Seal Design.

5. FUEL CAPSULE DESIGN

The design objective for the radioisotope fuel capsules is complete containment of the radioisotope fuel for ten fuel half-lives under all reasonable conditions. During this phase I analysis the main conditions that determined the fuel capsule conceptual designs were the abnormal situations in which the radioisotope fuel source might undergo random reentry into the earth's atmosphere and subsequent impact on the ground or into the water, where it might never be located for retrieval. The normal operating requirement of the fuel capsules (1 year at 2000°F) is relatively minor from a containment standpoint when compared with the abnormal mission abort conditions. The conceptual design approach has also been influenced by the desire to stay close to current or near-future technology in the areas of radioisotope fuel form and encapsulating materials manufacture and remote handling.

The reentry analysis (Sect. 8) showed that unprotected individual fuel capsules could not be expected to remain intact through a random reentry and impact from orbit. Shielding and armoring of the individual capsules could be used to avoid burnup during reentry and failure on impact; however, the possibility of earth burial or partial burial and subsequent meltdown would still exist. Also a wide dispersal of the capsules could occur that would complicate any attemps to find and recover the radioisotope fuel. Therefore, it was assumed in the capsule design that the capsules would be contained within a separate reentry body of low ballistic coefficient, which would provide the necessary protection from each of these eventualities.

Since two of the fuels considered, $^{238}PuO_2$ and $^{244}Cm_2O_3$, are alpha emitters, the main problem in the conceptual capsule design was to devise a method of coping with the internal pressure buildup resulting from the large quantity of helium that would be generated during the course of ten half-lives. Two approaches to this problem were considered:

1. a capsule that would allow the helium to vent, and
2. a capsule with sufficient void volume and wall thickness to contain the helium for a time equivalent to ten half-lives of the fuel.

The concept for venting helium was a capsule that contained a rupture disk and a porous plug in one end. The rupture disk would have sufficient strength to contain the helium for a period of approximately 5 years and then, if the source had not been recovered, the rupture disk would break and the accumulated helium would vent through the porous plug. The porous metal vent plug should have a filtration efficiency of 99.97% for 0.3-μ particles to be equivalent to the "absolute" air filters presently used in radioactive materials processing facilities in the United States. The choice of five years for the life of the rupture disk was made to allow ample time for search and recovery operations in the event the heat source was lost due to an aborted mission. The use of a vented capsule would permit much higher fuel loadings in each capsule than would be possible with a capsule designed for complete containment of the helium. However, as discussed in Section 5.2.2 and Appendix A, fuel loadings giving surface heat fluxes above 4000 Btu/hr·ft^2 would result in excessive temperatures if a capsule should become buried after reentry impact. Also, there would be the problem of oxidation of the primary capsule from the inside when the rupture disk broke and allowed air to diffuse into the capsule through the porous plug. In addition to these problems, the technology for fabricating and installing a suitable porous plug in a fuel capsule and insuring that it would maintain its integrity without cracking or plugging for very long periods of time is not yet available. For these reasons it was decided that a vented capsule design would not be used in the phase I conceptual studies and all the final conceptual designs would use fuel capsules designed for complete containment.

5.1 Capsule Geometry

Before the final encapsulating materials were chosen (Sect. 4), initial studies were made for each of the fuel forms to indicate practical individual capsule sizes to guide the initial thinking on the fuel block–heat exchanger concepts. It was assumed that the final conceptual design would be a multilayered capsule with a primary structure to withstand internal pressure buildup from the helium generation from the

alpha-emitting fuels and to withstand reentry impact, and an outer layer to withstand the corrosive effects of either seawater or land burial.

As a result of these initial considerations, the following capsule design boundary conditions were established:

Capsule surface temperature	
Normal operating life (10,000 hr)	2000°F or less
Earth burial	
$^{244}Cm_2O_3$ and $^{238}PuO_2$ fuel	2000°F or less
$^{147}Pm_2O_3$ fuel	2500°F or less
Maximum fuel compound temperatures	200°F or more below melting point
Primary structure wall thickness, t	0.060 in. $\leq$ t $\leq$ 0.250 in.
Primary structure inside diameter, d	0.5 in. $\leq$ d $\leq$ 4.0 in.
Primary structure length-to-diameter ratio	4 or less
Maximum allowable dimension change (creep) during operating life	3%

The normal operating temperature of the capsule surface (2000°F) was part of the original study criteria (Sect. 1). This same temperature restriction was held for the earth burial case for the ^{238}Pu and ^{244}Cm fuels. In the case of ^{147}Pm, there would be no internal pressure buildup during the decay of the radioisotope, and this coupled with the shorter half-life makes the containment problem much less severe. Therefore the temperature was allowed to go to 2500°F in the event of an accidental burial in sand. The limit on the maximum temperature in the fuel (200°F or more below melting point) was included to eliminate any liquid phase—solid phase solubility problems between fuel and capsule.

The limits on the diameter and wall thickness of the capsules were primarily determined by current hot-cell and remote-fabrication capabilities. A minimum acceptable wall thickness of 0.060 in. was selected to provide strength to the capsule for routine handling during fabrication, and the maximum thickness of 0.250 in. was selected because it was considered the maximum thickness for which a reliable weld could be made with current remote-welding techniques. To keep capsule sizes in a range that can be efficiently handled with remote manipulators, the maximum capsule inside diameter considered was 4 in. The minimum diameter (0.5 in.) was chosen because the analysis showed that an excessively large number of capsules would be required if smaller sizes were used.

The initial analysis showed that the capsule power density (w/lb) would increase as the length-to-diameter ratio increased. However, impact studies by the Sandia Corporation[42] indicated that to minimize columnar buckling effects in the case of an end-on impact at high velocity, the L/D ratio of a cylindrical capsule should not exceed approximately 4 or 5. A maximum L/D of 4 for the primary capsule was chosen for this study to avoid this problem.

The 3% dimensional change allowance during the one-year operating life was established to set tolerances on the capsule holder (fuel block) design. This did not turn out to be a limiting criterion because the capsule wall was made thick enough based on other considerations to reduce the first year creep to less than 1%.

Right cylinders, annular cylinders, and spheres were considered as possible fuel capsule shapes. Since relatively large void volumes are required for the helium generation from the alpha emitters, the annular-shaped capsules would not be utilizing the center of the capsule for this volume; therefore, there would be a much smaller amount of fuel for any selected diameter than for a corresponding right cylindrical capsule with an annular-shaped fuel matrix. The spherically shaped capsules give the lowest surface-area-to-volume ratio and lowest weight-to-volume ratio. However, since they could not be stacked as efficiently as cylinders, the total volume occupied by spherical capsules would be greater than for a source composed of cylindrical capsules. Also, the fabrication, fueling, and sealing of spherical capsules could be expected to be more difficult and time consuming than for the more conventional cylindrical capsules. Accordingly the right circular cylinder was used as the basic capsule shape for all three radioisotope fuels. In the case of the alpha emitters, hemispherical end caps were used and the fuel was arranged in an annular ring against the inside wall to aid heat transfer and leave the center of the capsule free to accommodate the helium given off during radioactive decay. The $^{147}Pm_2O_3$ fuel form does not have an internal gas pressure problem, so the cylindrical capsule has flat end caps; solid cylindrical fuel pellets fill essentially the entire internal volume.

Figures 5.1 and 5.2 show the final conceptual capsule designs. The results of the materials analysis, discussed in Section 4, led to the choice of the tantalum-based alloy T-222 for the primary pressure-bearing layer and platinum for the outer corrosion-resistant layer. The other layers shown in the figures are, as discussed in Section 4, a thoria diffusion barrier between the platinum and the T-222 alloy, an iron titanate coating on the platinum to improve its emissivity, and an inner tungsten liner for the fuel for compatibility assurance. The dimensions shown in Figs. 5.1 and 5.2 were determined by the capsule optimization procedures described in Sections 5.2 and 5.3.

5.2 Optimization of the $^{238}PuO_2$ and $^{244}Cm_2O_3$ Capsules

In this study the optimum capsule dimensions are those that will result in the minimum heat source system weight. In cases where little or no radiation shielding is required for the heat source system, the minimum system weight is obtained by using minimum weight capsules. However, where shielding becomes a significant part of the system weight, capsules having minimum volume or close to minimum volume may give the minimum total system weight.

5.2.1 $^{238}PuO_2$ and $^{244}Cm_2O_3$ Fuel Capsule Optimization for Minimum Weight of Unshielded Capsules and Fuel

The stepwise procedure used to arrive at optimum capsule designs for $^{238}PuO_2$ and $^{244}Cm_2O_3$ is described in Fig. 5.3. As indicated, it is necessary to determine both the capsule design that will give the minimum total weight of capsules without exceeding the 4-in.-OD and 0.250-in.-wall-thickness design limits and the design that will give the minimum total volume of capsules. A trade-off is then made between the two designs to arrive at the minimum system weight that is consistent with the capsule design boundary conditions given in Section 5.1. Figure 5.3 also shows that after determining the minimum weight and volume designs on the basis of normal operation, it is necessary to determine the equilibrium temperature the capsule would reach if it became buried and, if necessary, reduce the fuel loading in the capsule to a level that does not let the temperature exceed 2000°F.

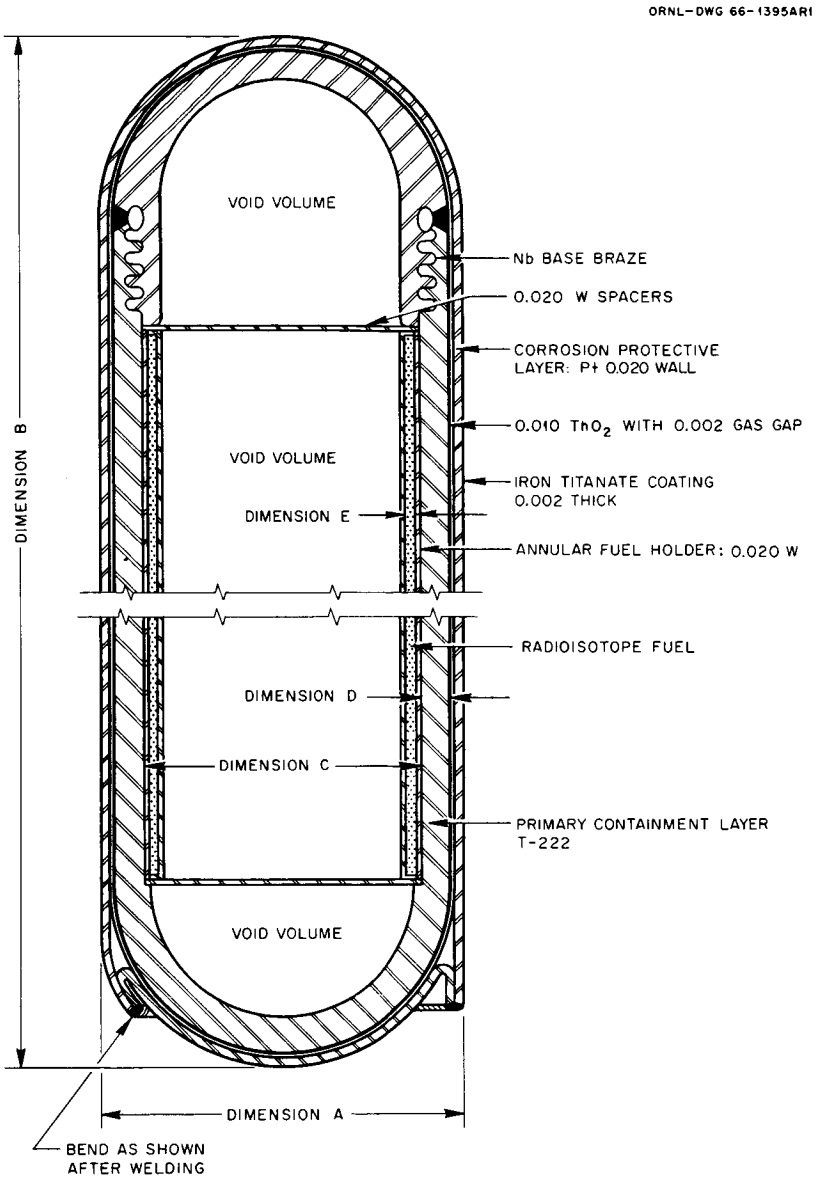

$^{238}PuO_2$ and $^{244}Cm_2O_3$ CAPSULE DATA

FUEL	STRESS RATE SAFETY FACTOR	NUMBER OF CAPSULES REQUIRED	CAPSULE AND FUEL DIMENSIONS (in.) A	B	C	D	E
$^{238}PuO_2$	2.5	108	2.580	10.13	2.062	0.227	0.090
	4	80	3.318	13.08	2.750	0.252*	0.075
	7	71	4.510	17.85	4.000	0.223	0.045
$^{244}Cm_2O_3$	2.5	274	1.022	3.90	0.750	0.104	0.090
	4	229	1.212	4.66	0.875	0.136	0.070
	7	172	1.598	6.20	1.250	0.142	0.050

*Slightly exceeds design guideline of 0.250 in. but was considered adequate

Conceptual Design of the $^{244}Cm_2O_3$ and $^{238}PuO_2$ Fueled Capsules

Fig. 5.1. Conceptual Design of $^{244}Cm_2O_3$ and $^{238}PuO_2$ Capsule.

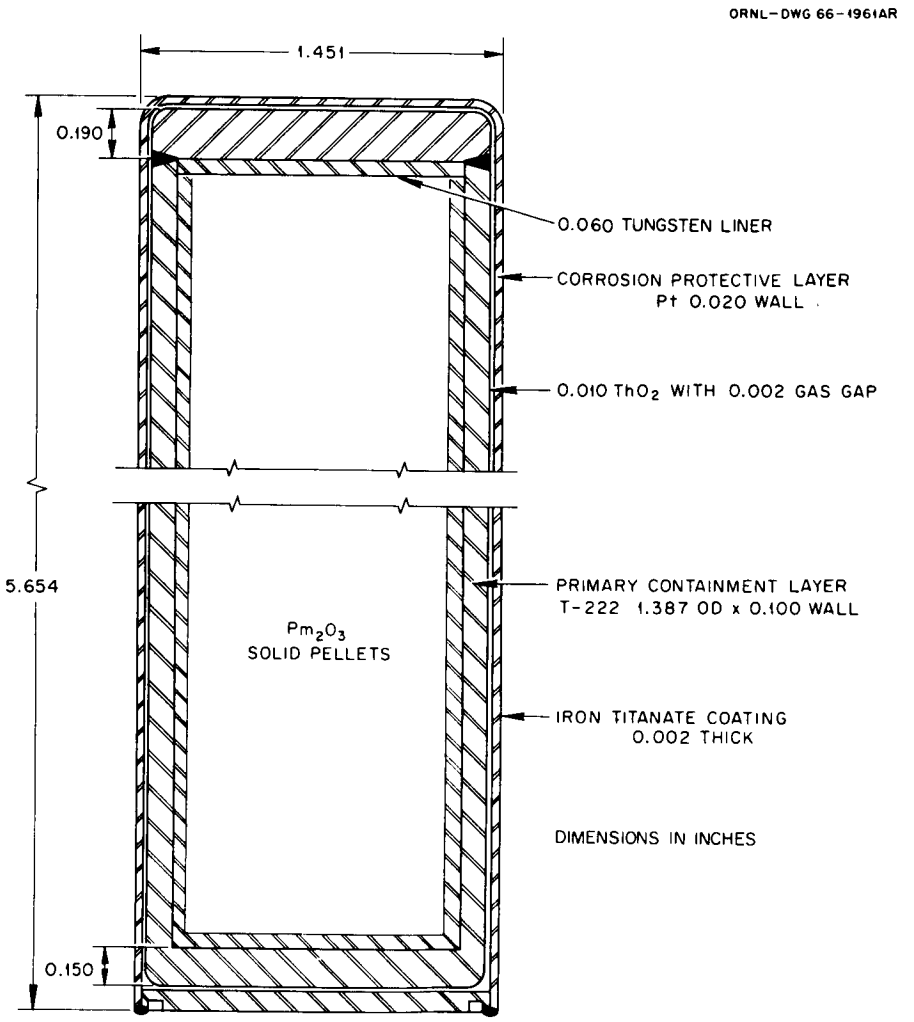

Fig. 5.2. Conceptual Design of the $^{147}Pm_2O_3$ Capsule; 204 Capsules Required.

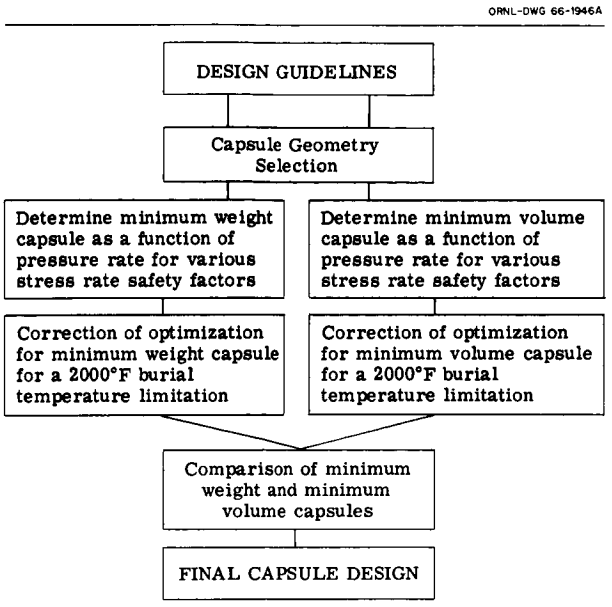

Fig. 5.3. Design Optimization Procedure for Capsules Containing Alpha Emitters.

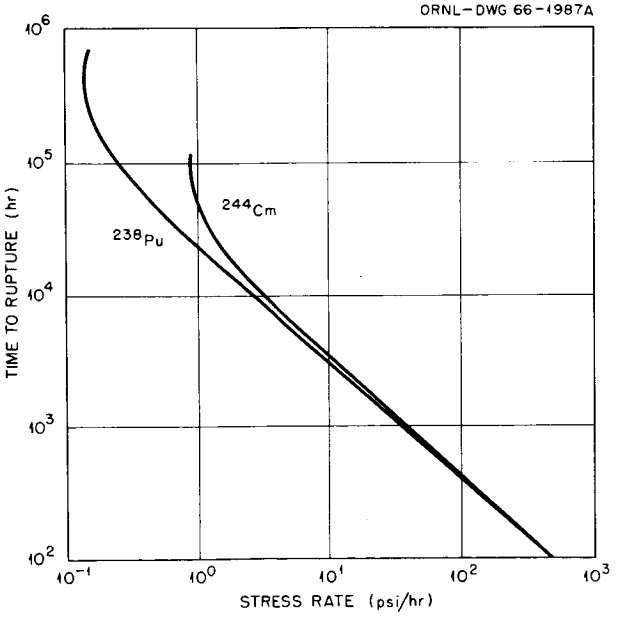

Fig. 5.4. Comparison of Maximum Allowable Stress-Rate Curves for T-111 Alloy Capsules Containing $^{238}PuO_2$ and $^{244}Cm_2O_3$.

The determination of the maximum allowable stress rate for the primary capsule material, T-222 alloy, was described in Section 4 and a comparison of the results for capsules containing $^{238}PuO_2$ and $^{244}Cm_2O_3$ is shown in Fig. 5.4. This figure illustrates the effect of the longer half-life for the ^{238}Pu on the maximum allowable stress rate. The maximum stress rate for the ^{238}Pu that will never result in a rupture due to creep is approximately 0.145 psi/hr, while for ^{244}Cm it is approximately 0.75 psi/hr. Since the ^{238}Pu has approximately 5 times as long a half-life as the ^{244}Cm, the difference in the maximum allowable stress rate is a factor of approximately 5. Also, the figure shows that the period required to reach the point on the curve that determines the maximum allowable stress rate for ^{238}Pu (54 years) is approximately 5 times as long as the corresponding time for ^{244}Cm (11 years).

As described in Section 4, the creep mode of failure for these capsules ceases to be a dominant factor at three-tenths the absolute melting temperature of the primary capsule material. However, the time required for the creep mode of failure to cease to be a dominant factor occurs at a point in time when the total capsule pressure is still increasing. The maximum capsule pressure for each fuel occurs at about 1.5 times the fuel half-life, while creep failure ceases to be dominant at slightly over 0.6 times the fuel half-life. As mentioned in Section 4, when the capsule age reaches 0.6 times the half-life of the fuel, the capsule would be expected to have adequate elastic strength, as well as creep strength, to withstand the continuing increase in helium pressure. For a conservative approach, the elastic strength was checked for each selected allowable stress rate by utilizing simultaneously the maximum pressure, which occurs at 1.5 times the half-life for each fuel, and the maximum temperature in the elastic range, which occurs at approximately 0.7 times the half-life. An example of this calculation is given in Appendix C. In all cases studied, the capsule strength in the elastic region meets or exceeds safety factors of 4 for tensile strength and 3 for yield strength. Thus when the capsule design is based on the maximum allowable stress rate for creep with appropriate safety factors, containment from a stress analysis standpoint can be shown for the complete ten half-life period for each fuel in this Brayton-cycle application.

The rate at which stress in the wall of the capsule increases with time can be changed by varying any one or all of the following factors: (1) amount of fuel in each capsule, (2) capsule wall thickness, and (3) capsule void volume. With the stress rates shown in Fig. 5.4 as the limitation for ten half-life containment, the capsule designs for both ^{238}Pu and ^{244}Cm were obtained by varying each of the variables listed above to find the combination that gave the minimum weight of fueled capsules for the 25-kw heat source. This process was repeated for each fuel and for stress-rate safety factors of 2.5, 4, and 7 so that the effect of the safety factor applied to the maximum allowable stress to obtain the design stress rate could also be determined. The computations were carried out on a CDC 1604-A computer in the following sequence.

For each design stress-rate value, the allowable pressure rate inside the capsule that would result in the design stress rate in the primary capsule wall was varied to determine the effect of varying fuel amounts, void volumes, and primary capsule wall thicknesses. This calculation was based on the hoop stress being the limiting stress and the ideal gas law, PV = NRT. This was done for different capsule inside diameters ranging from 0.5 to 4.0 in. For a particular allowable stress rate, allowable pressure rate, and capsule inside diameter and length, the maximum amount of fuel for that particular capsule was determined. After this was determined the total number of capsules for that particular capsule design was determined by dividing the amount of fuel in each capsule into the total amount of fuel required for the heat source. Then the total unshielded weight, including fuel and capsule material required for a particular capsule size, was determined and divided into the total power required to obtain the specific power of the fuel capsules in watts per pound. Finally, the capsule design that results in the highest specific power within limits of the design guidelines was determined for each fuel for each stress-rate safety factor studied. Details on the method of calculation for this program are in Appendix C.

Figures 5.5, 5.6, and 5.7 show the results of this weight minimizing program for $^{238}PuO_2$ for stress-rate safety factors of 2.5, 4, and 7. The effect of burial is not taken into account in these figures. The primary capsule inside diameters are plotted as the abscissa with the specific

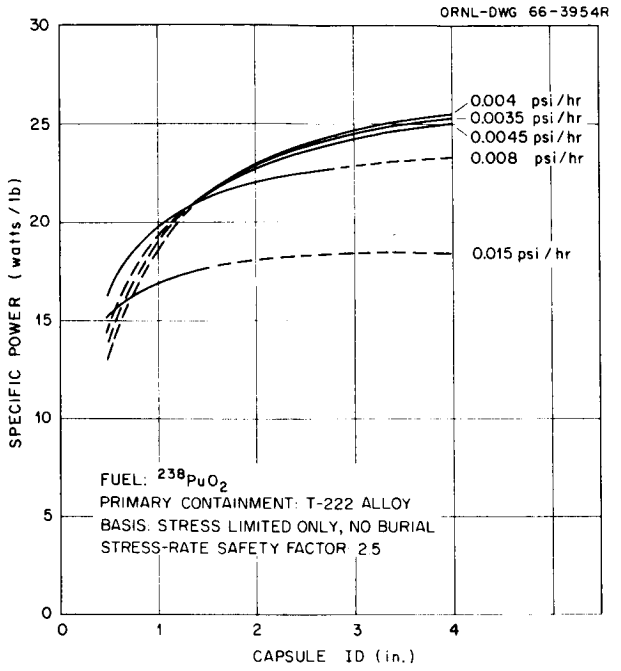

Fig. 5.5. $^{238}PuO_2$ Capsule Optimization for Minimum Unshielded Weight, No Burial Consideration, and a Stress-Rate Safety Factor of 2.5.

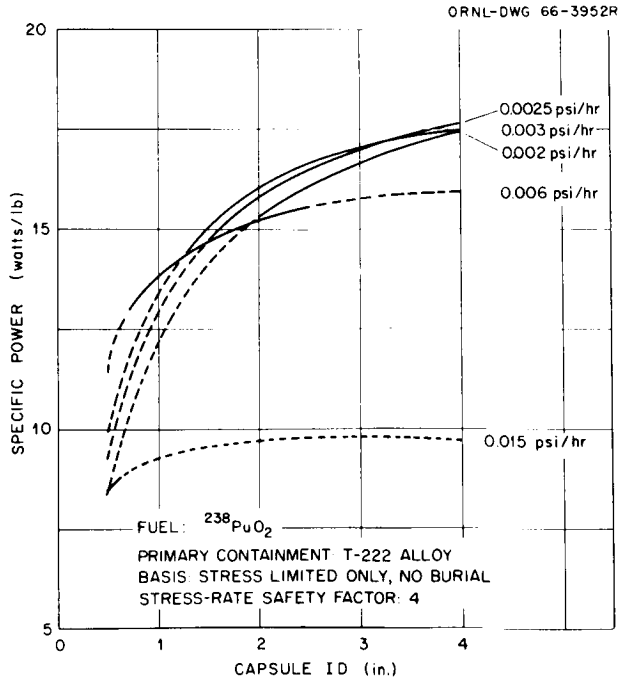

Fig. 5.6. $^{238}PuO_2$ Capsule Optimization for Minimum Unshielded Weight, No Burial Consideration, and a Stress-Rate Safety Factor of 4.

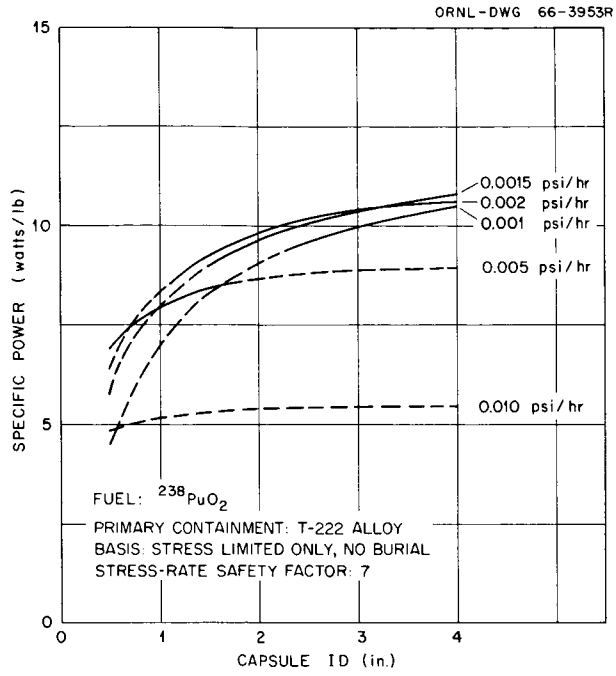

Fig. 3.7. $^{238}PuO_2$ Capsule Optimization for Minimum Unshielded Weight, No Burial Consideration, and a Stress-Rate Safety Factor of 7.

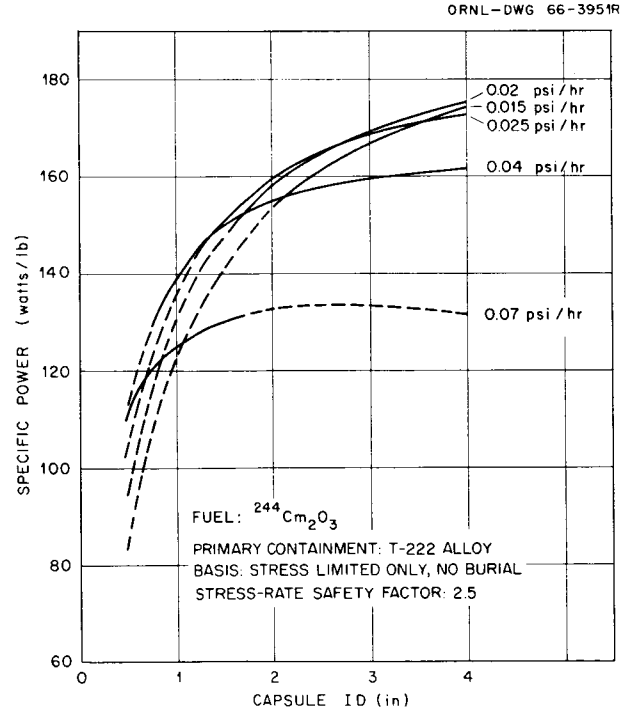

Fig. 5.8. $^{244}Cm_2O_3$ Capsule Optimization for Minimum Unshielded Weight, No Burial Consideration, and a Stress-Rate Safety Factor of 2.5.

power as the ordinate. For a given stress-rate safety factor the allowable pressure rate is varied as illustrated by the curves. The allowable pressure rate that results in the optimum combination of fuel, void volume, and primary capsule thickness is then determined. For example, in the case where the stress-rate safety factor is 2.5 (Fig. 5.5), the minimum-weight capsule design for a stress-limited condition only is a 4.0-in.-ID capsule with an allowable pressure rate of 0.004 psi/hr. The results for allowable pressure rates other than those shown in the figures were determined but were omitted for clarity. At pressure rates both above and below 0.004 psi/hr, the high points on the curves are at lower specific powers than the specific power for the 0.004-psi/hr case. The dashed-line portions of the curves indicate that capsules having inside diameters lying on that portion of the curve for that pressure rate have wall thicknesses that lie outside the capsule design boundary conditions of 0.060 to 0.250 in. The smaller diameter capsules with the lower allowable pressure rates generally result in required wall thicknesses less than 0.060 in., while the larger diameter capsules with the higher pressure rates generally exceed the 0.250-in. limitation. In all the $^{238}PuO_2$ cases studied, except for the higher allowable pressure rates, the maximum specific power is not obtained before the 4.0-in.-ID maximum allowable capsule diameter is exceeded. However, only a slight weight penalty is incurred since, as seen in the figures, the slopes of the curves are nearly zero at this point in all cases.

The results for the $^{244}Cm_2O_3$ fuel for the same stress-rate safety factors are shown in Figs. 5.8, 5.9, and 5.10. The maximum allowable stress rate was determined for each stress-rate safety factor, and the pressure rate that resulted in minimum unshielded capsule weight was determined for each case considered.

5.2.2 Effect of 2000°F Burial-Temperature Limitation on Capsule Optimization

As noted previously, the fuel capsules containing alpha emitters, in addition to having sufficient strength, must also be designed so that the temperature does not exceed 2000°F if an individual capsule becomes buried in an insulating medium such as dry sand. This is necessary because the

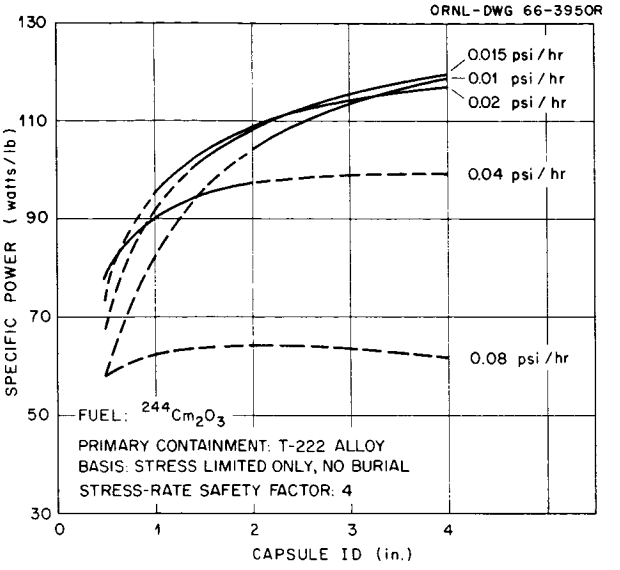

Fig. 5.9. $^{244}Cm_2O_3$ Capsule Optimization for Minimum Unshielded Weight, No Burial Consideration, and a Stress-Rate Safety Factor of 4.

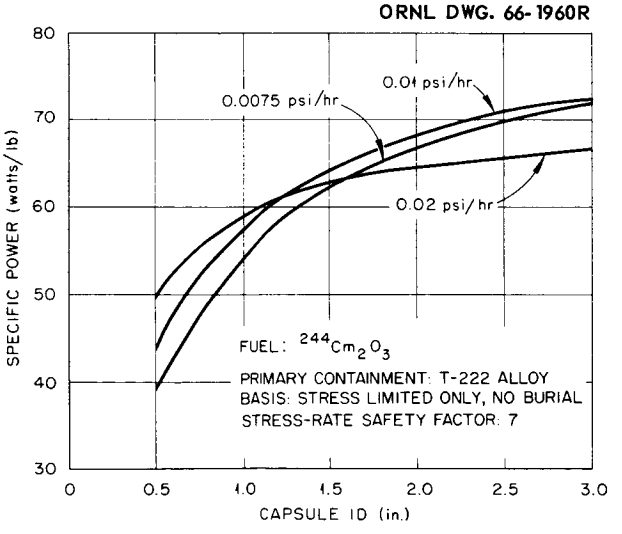

Fig. 5.10. $^{244}Cm_2O_3$ Capsule Optimization for Minimum Unshielded Weight, No Burial Consideration, and a Stress-Rate Safety Factor of 7.

capsule wall thickness for the long-term containment of the helium in the event of loss of the heat source after reentry was based on a maximum temperature of 2000°F. The reentry body, which would protect the fuel capsules in the event of a mission abort and random reentry from space, was designed to prevent the burial of the fuel capsules, as described in Section 8. However, if the individual capsules could also be designed not to exceed 2000°F if buried without imposing too big a weight penalty on the total system weight, it would be a desirable safety backup for the reentry body design.

The effect of the allowable temperature limitation and the capsule diameter on the maximum allowable power per capsule in case of earth burial of a single capsule is illustrated in Fig. 5.11. The method of calculation for this figure is given in Appendix A. As illustrated, the maximum allowable power per capsule would increase as the capsule diameter increased because of the increased area for heat transfer. Figure 5.12 is a typical example of the effect of the 2000°F burial-temperature limitation on the minimum weight capsule size for the alpha emitters. This figure shows a typical allowable pressure rate limitation curve obtained from the previously described unshielded weight minimizing procedure with a curve showing the effect on specific power of imposing a 2000°F burial-temperature limitation on the same range of capsule diameters. As illustrated, the smaller diameter capsules are not affected by the allowable burial temperature, while the specific powers of the larger diameter capsules are reduced by the burial-temperature limitation. This indicates that in large capsules there can be less fuel in each capsule if both the stress-rate and burial-temperature criteria are to be satisfied. This results in a corresponding increase in the number of capsules required for the total heat source for a given capsule diameter. The capsule design that has the greatest specific power and satisfies both criteria occurs at the point of intersection of the two curves.

The highest specific power for each design stress rate for each fuel was obtained by determining the intersection point between the two curves for each allowable pressure rate studied. The results of this analysis for each safety factor for ^{238}Pu, Figs. 5.13, 5.14, and 5.15, show that only the lower stress-rate safety factor values are affected by the 2000°F

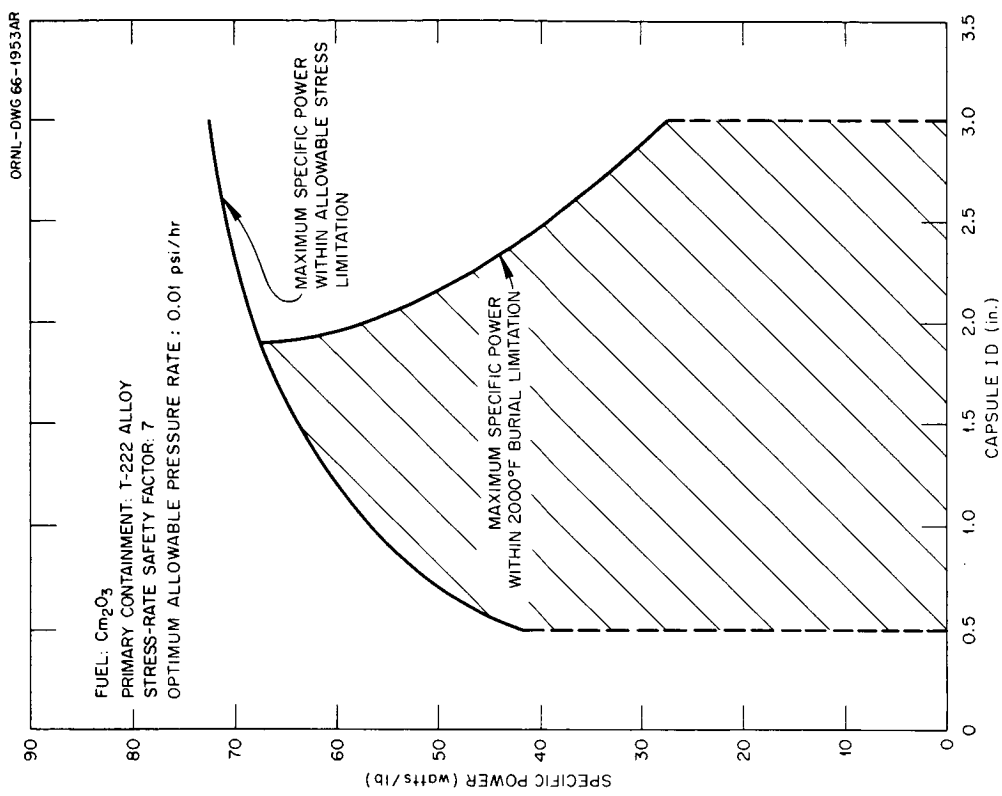

Fig. 5.12. Effect of Burial-Temperature Limitation on Capsule Optimization for Minimum Unshielded Weight.

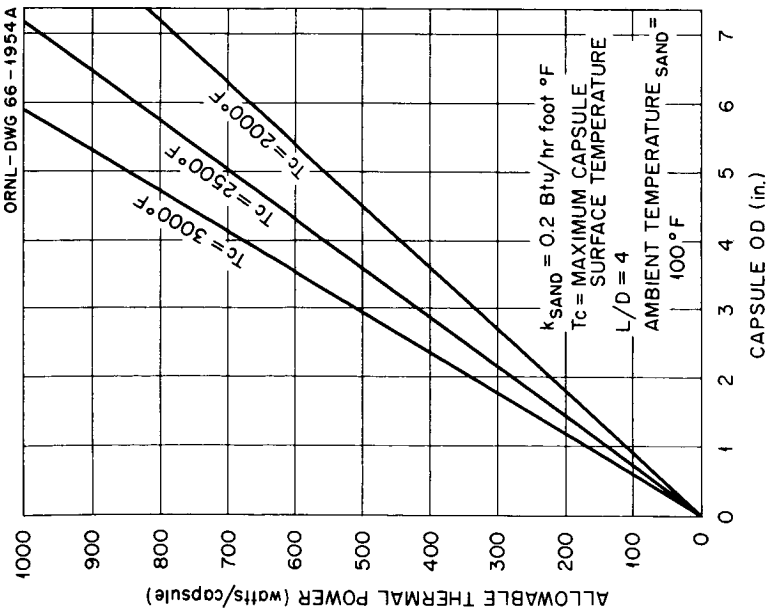

Fig. 5.11. Allowable Thermal Power of a Fuel Capsule Buried in Loose Sand as a Function of the Outside Diameter and Maximum Surface Temperature.

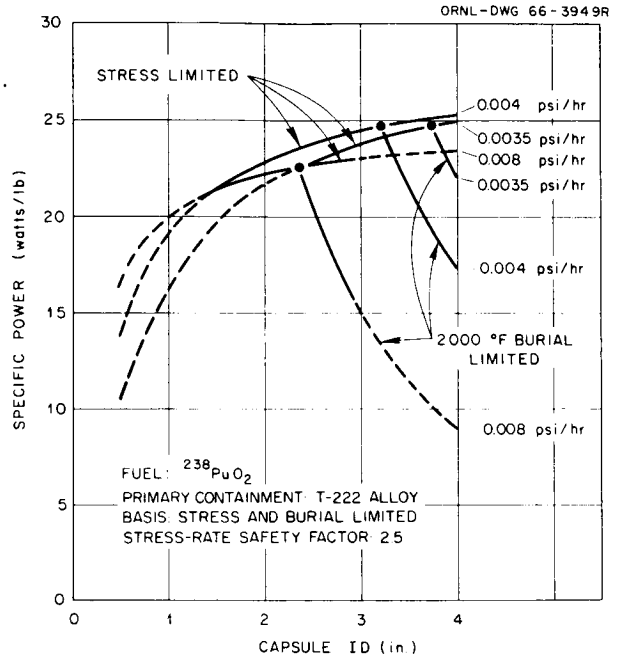

Fig. 5.13. Effect of Burial-Temperature Limitation on $^{238}PuO_2$ Capsule Optimization for Minimum Unshielded Weight and a Stress-Rate Safety Factor of 2.5.

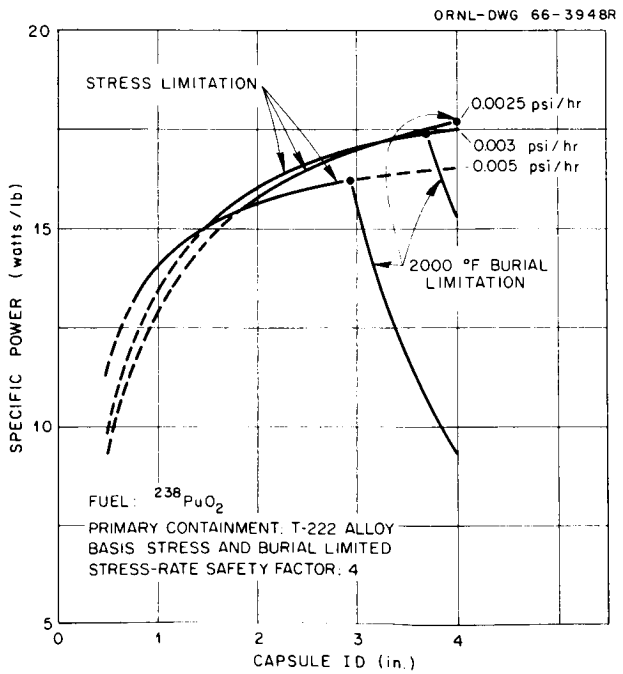

Fig. 5.14. Effect of Burial-Temperature Limitation on $^{238}PuO_2$ Capsule Optimization for Minimum Unshielded Weight and a Stress-Rate Safety Factor of 4.

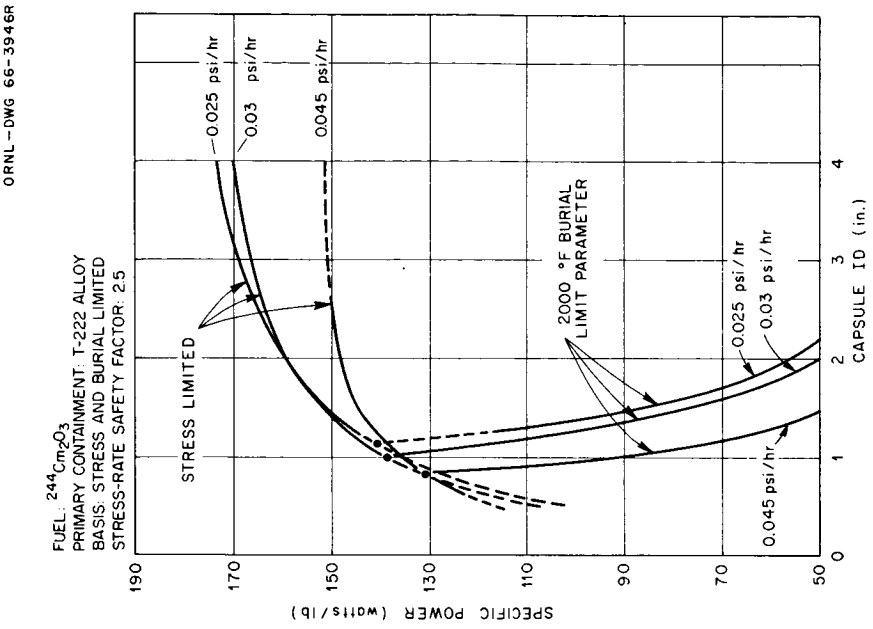

Fig. 5.16. Effects of Burial-Temperature Limitation on $^{244}Cm_2O_3$ Capsule Optimization for Minimum Unshielded Weight and a Stress-Rate Safety Factor of 2.5.

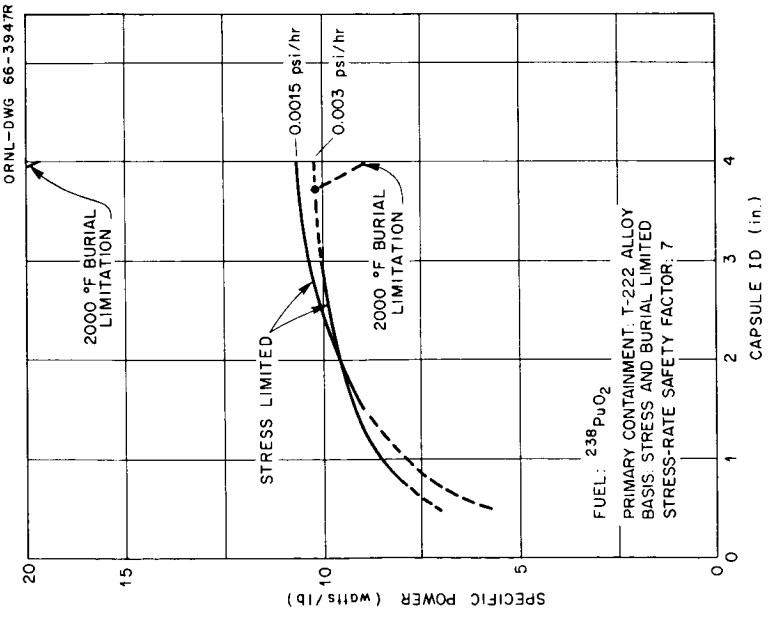

Fig. 5.15. Effect of Burial-Temperature Limitation on $^{238}PuO_2$ Capsule Optimization for Minimum Unshielded Weight and a Stress-Rate Safety Factor of 7.

burial-temperature limitation. Figure 5.13 shows three typical stress-limited curves with the corresponding 2000°F burial-temperature limitation curves. The peak specific power is obtained with a pressure rate of 0.004 psi/hr, while the other two intersection points occur below this point. Other pressure rate curves between and above and below these values were determined but were omitted from the figure for clarity. Figure 5.14 for $^{238}PuO_2$ with a stress-rate safety factor of 4 shows that the highest specific power is obtained with the the maximum-diameter capsule, 4 in., for a 0.0025-psi/hr pressure rate, and this capsule meets both the stress-rate and burial-temperature requirements for ten half-life containment. Other intersection points for different pressure rates occur below this point. The highest specific power for ^{238}Pu with a stress-rate safety factor of 7 (Fig. 5.15) is the optimum condition for the stress-rate limitation only. This is the peak specific power that can be obtained, and it is not affected by the burial-temperature limitation of 2000°F.

In the case of ^{244}Cm, the burial-temperature limitation affected the capsule optimization for all stress-rate safety factors considered. The results of this analysis are shown in Figs. 5.16, 5.17, and 5.18. Figure 5.16 for ^{244}Cm with a stress-rate safety factor of 2.5 shows that the optimum specific power which satisfies both criteria occurs with a 0.025-psi/hr pressure rate, but this capsule design does not meet the capsule design guidelines, since the primary capsule wall thickness is less than 0.060 in. The optimum capsule design that meets all requirements is the maximum allowable specific power point for the 0.030-psi/hr pressure rate. Figures 5.17 and 5.18 show the highest specific power for stress-rate safety factors of 4 and 7, respectively. In all cases for ^{244}Cm the 2000°F burial-temperature limitation limits the capsule design to smaller diameters that result in a large increase in the number of capsules required for the heat source and a larger percentage weight penalty than is the case for the ^{238}Pu.

Table 5.1 gives a summary for both fuels of the capsule optimizations for minimum unshielded weight with and without the 2000°F burial-temperature criterion imposed on the design. As shown by the table, a very small weight penalty compared with the total system weight is required to insure against accidental loss and burial of a single capsule for any case.

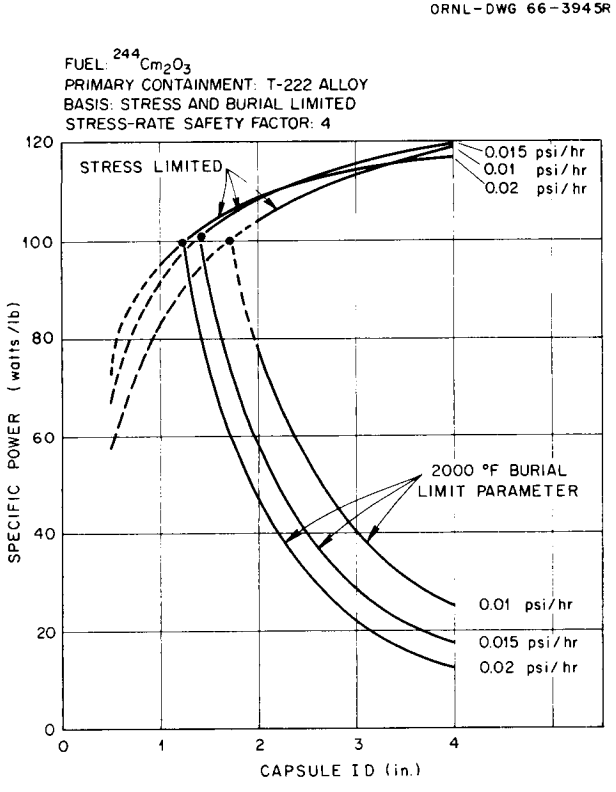

Fig. 5.17. Effects of Burial-Temperature Limitation on $^{244}Cm_2O_3$ Capsule Optimization for Minimum Unshielded Weight and a Stress-Rate Safety Factor of 4.

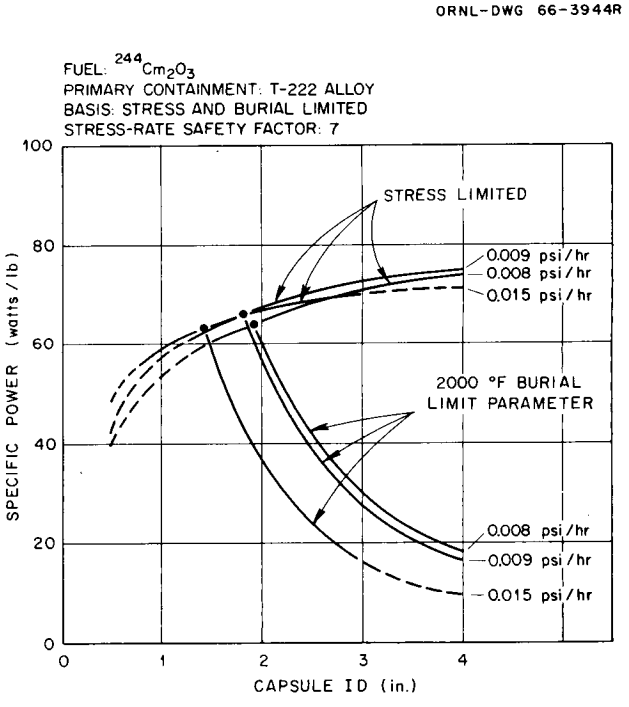

Fig. 5.18. Effects of Burial-Temperature Limitation on $^{244}Cm_2O_3$ Capsule Optimization for Minimum Unshielded Weight and a Stress-Rate Safety Factor of 7.

Table 5.1. Capsule Optimization for Minimum Unshielded Weight

Stress-Rate Safety Factor	Without 2000°F Burial-Temperature Limitation			With 2000°F Burial-Temperature Limitation		
	Capsules Required	Total Weight Required (lb)	Total Volume Required ($in.^3$)	Capsules Required	Total Weight Required (lb)	Total Volume Required ($in.^3$)
			Cm_2O_3 Fuel			
7	~15	429	3,750	134	484	3,525
4	~8	270	2,100	188	322	2,195
2.5	~6	184	1,550	250	236	1,250
1.5	~3	125	800	318	169	730
			PuO_2 Fuel			
7	96[a]	2849	25,300	96[a]	2849	25,300
4	59	1738	15,350	59	1738	15,350
2.5	38	1210	10,000	70	1243	10,000
1.5	27	785	6,850	92	836	6,700

[a]Not burial limited.

5.2.3 Optimization for Minimum Volume of Capsules and Comparison With Minimum Unshielded Weight Designs

The procedure just described for minimizing the weight of unshielded fuel capsules (Sect. 5.2.1) was repeated with modifications that gave the minimum volume of capsules for each stress-rate safety factor. Also, since neither the minimum unshielded weight capsule design nor the minimum volume design may, in the final analysis, be the best overall capsule design from the standpoint of total system weight, the designs for various allowable pressure rates between the ones that resulted in the minimum unshielded weight and volume designs were also determined.

Figures 5.19, 5.20, and 5.21 show the minimum unshielded weight and the minimum volume required for $^{238}PuO_2$ capsules in a 27.9-kw heat source, with stress-rate safety factors of 2.5, 4, and 7 for various allowable pressure rates. The designs satisfy both the stress limitations and the 2000°F burial-temperature limitation. The lines designate the minimum possible capsule volumes and weights, and the circles designate the design values that lead to the highest system weights as determined by iterative processes in Sections 9 and 10.

Figure 5.19 for ^{238}Pu with a stress-rate safety factor of 2.5 shows that the minimum unshielded weight capsule design results in an allowable pressure rate of 0.0025 psi/hr, as previously described in the minimum unshielded weight optimization section, but that the corresponding total volume required for this design is very high. The minimum volume design is obtained with an allowable pressure rate of 0.015 psi/hr with a correspondingly higher total capsule weight required. However, the dashed-line portion of the curve indicates the range where the design guideline maximum wall thickness of 0.250 in. was exceeded. The minimum volume design that does not exceed this design guideline occurs with an allowable pressure rate of approximately 0.01 psi/hr. As discussed in Section 9, the capsule designs that lead to minimum system weight for ^{238}Pu for all the stress-rate safety factors were those that resulted in a minimum volume of capsules within the maximum allowable wall thickness requirement. The approximately 17% increase in the total weight of the capsules in the case of a stress-rate safety factor of 2.5 was more than compensated by the shield weight saving obtained with the minimum system weight capsule

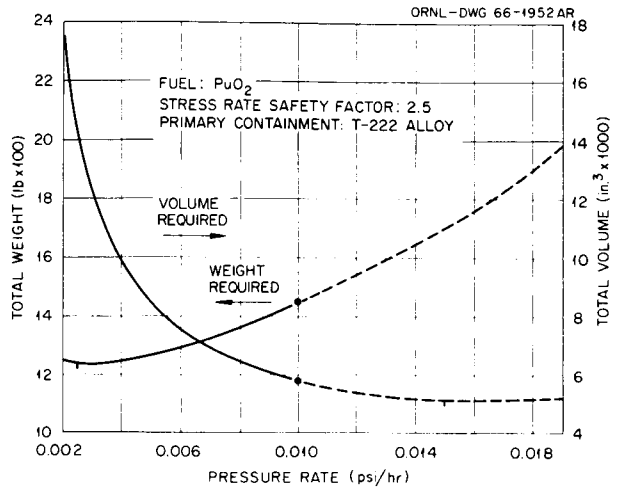

Fig. 5.19. Comparison of Weight and Volume Requirements for PuO_2 Capsules with a Stress-Rate Safety Factor of 2.5. (| Minimum, ● Design)

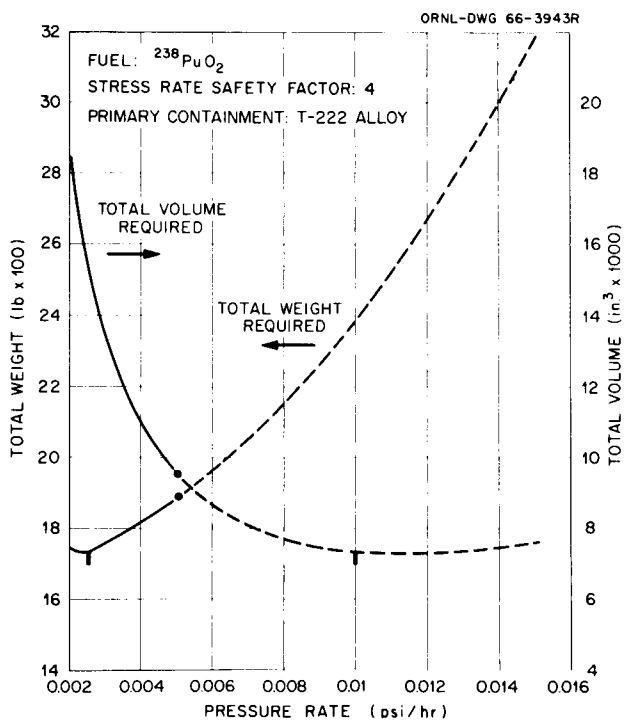

Fig. 5.20. Comparison of Weight and Volume Requirements for PuO_2 Capsules with a Stress-Rate Safety Factor of 4. (| Minimum, ● Design)

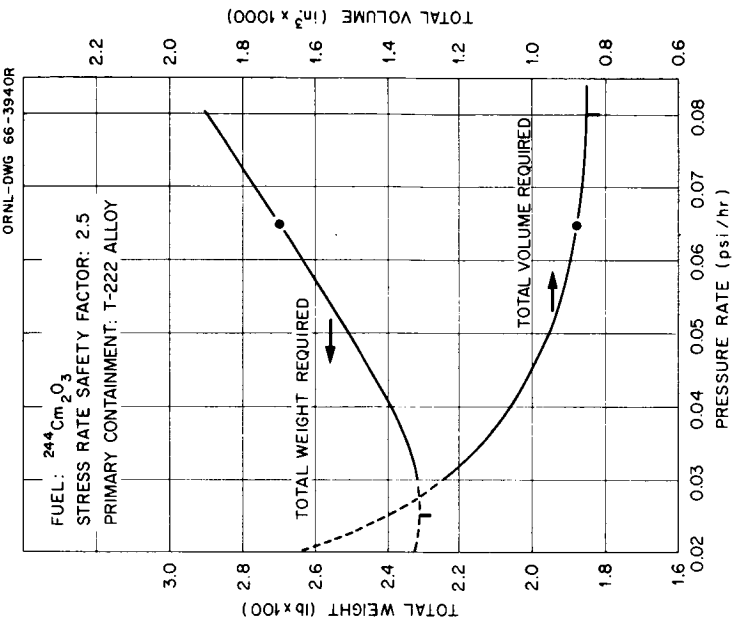

Fig. 5.22. Comparison of Weight and Volume Requirements Versus Allowable Pressure Rate for $^{244}Cm_2O_3$ with a Stress-Rate Safety Factor of 2.5. (| Minimum, ● Design)

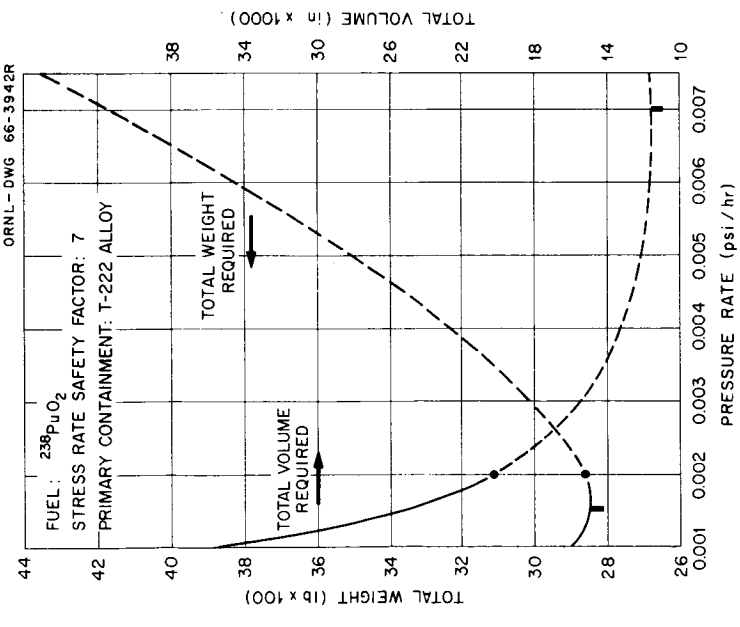

Fig. 5.21. Comparison of Weight and Volume Requirements for PuO_2 Capsules with a Stress-Rate Safety Factor of 7. (| Minimum, ● Design)

because of the smaller volume reentry body required to house the Brayton-cycle heat source.

This comparison of weight and volume requirements was repeated for ^{238}Pu for stress-rate safety factors of 4 and 7 with similar results, as shown in Figs. 5.20 and 5.21. However, it is evident that as the safety factor increases, the lowest volume acceptable to all design guidelines moves farther away from the true minimum volume design.

This program was repeated for ^{244}Cm for stress-rate safety factors of 2.5, 4, and 7, as shown in Figs. 5.22, 5.23, and 5.24. Figure 5.22 for ^{244}Cm with a stress-rate safety factor of 2.5 shows that the actual minimum unshielded weight design does not meet the minimum required wall thickness of 0.060 in., as discussed previously, while the minimum volume design is obtained with an allowable pressure rate of 0.08 psi/hr. As shown in Section 9 the best capsule design for a minimum system weight is a compromise between the minimum unshielded weight capsule and the minimum volume capsule and occurs with an allowable pressure rate of 0.065 psi/hr. For the other stress-rate safety factors considered (Figs. 5.23 and 5.24), the minimum system weight capsule design was also determined to be between the minimum unshielded weight and the minimum volume designs. In each case the capsule design for a minimum weight curium system was obtained by utilizing a design that resulted in only a slight penalty from the minimum capsule volume point while limiting the weight of the unshielded capsules to a 10 to 20% weight increase over the minimum capsule weight.

5.2.4 Conceptual Design of the ^{238}Pu and ^{244}Cm Capsule

Figure 5.1 (cited above) shows the phase I conceptual design selected for both the ^{238}Pu and ^{244}Cm fuel capsules for stress-rate safety factors of 2.5, 4, and 7. The choice of materials is discussed in Section 4. Typical examples of the expected thermal profiles of these designs are shown in Figs. 5.25 and 5.26. Figure 5.25 is the expected thermal profile for $^{238}PuO_2$ with a stress-rate safety factor of 2.5. The total temperature drop across the capsule is only 57°F, which is very low and is due primarily to the low individual capsule power when compared with a relatively large surface area of the capsule. The average helium temperature was

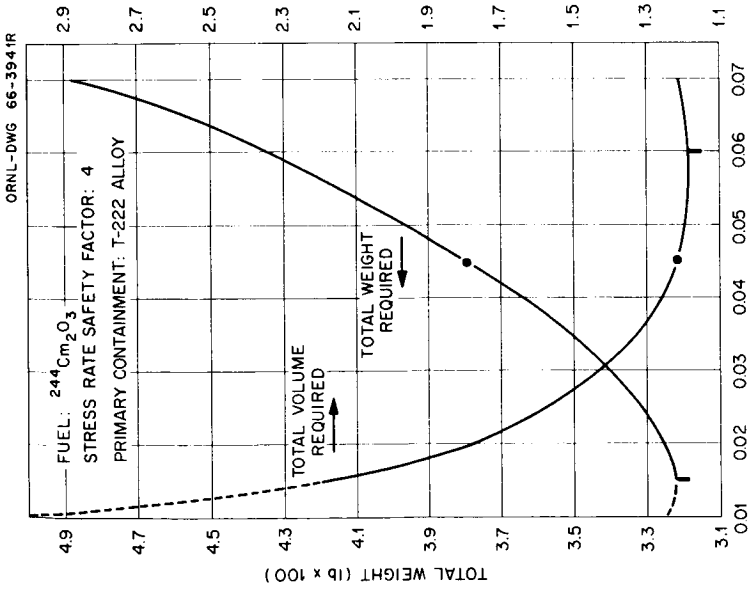

Fig. 5.23. Comparison of Weight and Volume Requirements Versus Allowable Pressure Rate for $^{244}Cm_2O_3$ with a Stress-Rate Safety Factor of 4. (| Minimum, ● Design)

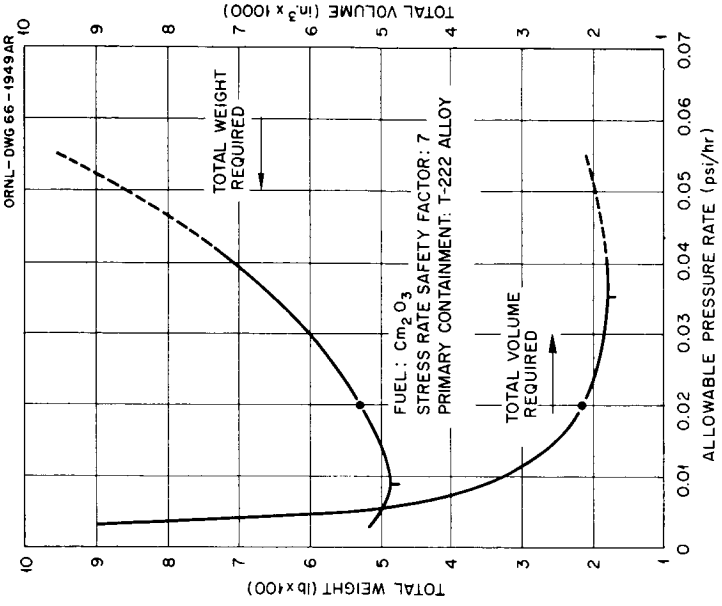

Fig. 5.24. Comparison of Weight and Volume Requirements Versus Allowable Pressure Rate for $^{244}Cm_2O_3$ with a Stress-Rate Safety Factor of 7. (| Minimum, ● Design)

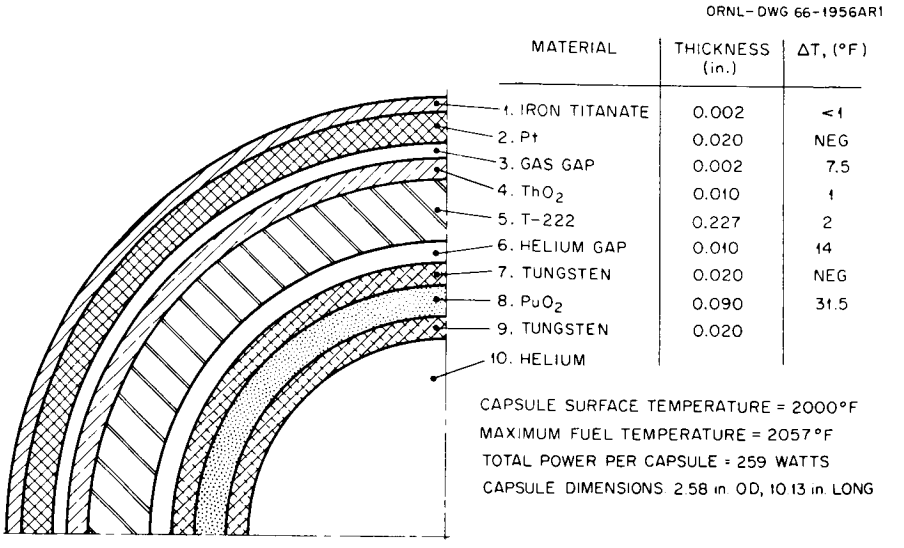

Fig. 5.25. Thermal Profile of PuO_2-Fueled Capsule.

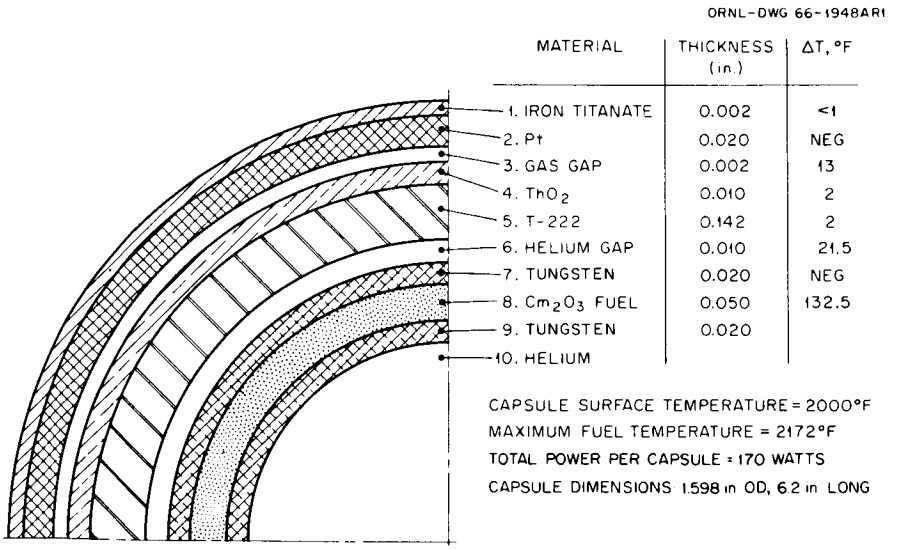

Fig. 5.26. Thermal Profile of Cm_2O_3-Fueled Capsule.

assumed to be the temperature at the outer surface of the fuel plus one-half the temperature drop across the fuel. It was also assumed that no heat was lost through either end cap and that the surface temperature was 2000°F.

Figure 5.26 shows the expected thermal profile for the $^{244}Cm_2O_3$ conceptual design with a stress-rate safety factor of 7. Even though the maximum fuel temperature is approximately 115°F higher than for the ^{238}Pu capsule, these temperatures are still well within the design guideline limitations. The comparatively large temperature drop across the fuel is due primarily to the 50% packing density expected for the loose powder with helium occupying the void volumes.

5.3 Optimization of the $^{147}Pm_2O_3$ Capsule

Since ^{147}Pm is a beta emitter with no resulting helium generation, the size of the ^{147}Pm capsules is limited only by (1) the allowable power to surface-area ratio required in order not to exceed the burial-temperature limitation, (2) the fuel center-line temperature, and (3) the primary capsule wall thickness sufficient to withstand a secondary impact when the reentry vehicle impacts with the earth. As discussed previously, the burial-temperature limitation for promethium was raised to 2500°F, since promethium has a relatively short half-life and therefore a shorter time at elevated temperatures. To obtain the best capsule design for this fuel form, the largest capsule with a primary capsule length-to-diameter ratio of 4 that could be effectively and completely filled with fuel and not exceed the 2500°F burial-temperature limit was selected.

Figure 5.2 (cited above) shows the conceptual design of the $^{147}Pm_2O_3$ capsule selected for the phase I studies. Basically the multilayered capsule principle for the alpha emitters is the same as that for ^{147}Pm. For this capsule, a minimum wall thickness of 0.100 in. was considered adequate to meet the expected secondary impact requirements. A flat-head design with rounded corners was provided, since no internal pressure problems are expected. A 0.010-in. tungsten liner was included to provide a barrier between the Pm_2O_3 and the T-222 alloy and to insure good full-strength welds.

The expected temperature profile for this conceptual design with a 2000°F normal-condition capsule surface temperature is shown in Fig. 5.27. Under burial conditions with a surface temperature of 2500°F, the expected temperature drop should be approximately 160°F, and thus the fuel would be well below its melting temperature.

5.4 Summary of Heat Source Capsule Design

To summarize the capsule design study, Table 5.2 compares the selected minimum system weight capsule designs for each fuel and for each selected stress-rate safety factor for the alpha emitters. The total unshielded weights and volumes required for each fuel show that on an unshielded basis the ^{238}Pu heat source is the heaviest, but, as shown in the systems section (Sect. 10), it is actually the lightest weight system because less shielding is required.

Table 5.2. Summary of Results of Capsule Optimization for Minimum System Weight

Fuel	Stress-Rate Safety Factor	Overall Total Capsule Size (in.)		Capsules Required	Total Weight (lb)	Total Volume ($in.^3$)
		Outside Diameter	Length			
$^{147}Pm_2O_3$		1.451	5.65	204	720	1,900
$^{244}Cm_2O_3$	2.5	1.022	3.90	274	265	875
	4	1.212	4.66	229	379	1,215
	7	1.598	6.20	172	534	2,150
$^{238}PuO_2$	2.5	2.580	10.13	108	1,450	5,750
	4	3.318	13.08	80	1,931	9,030
	7	4.510	17.85	71	2,860	20,250

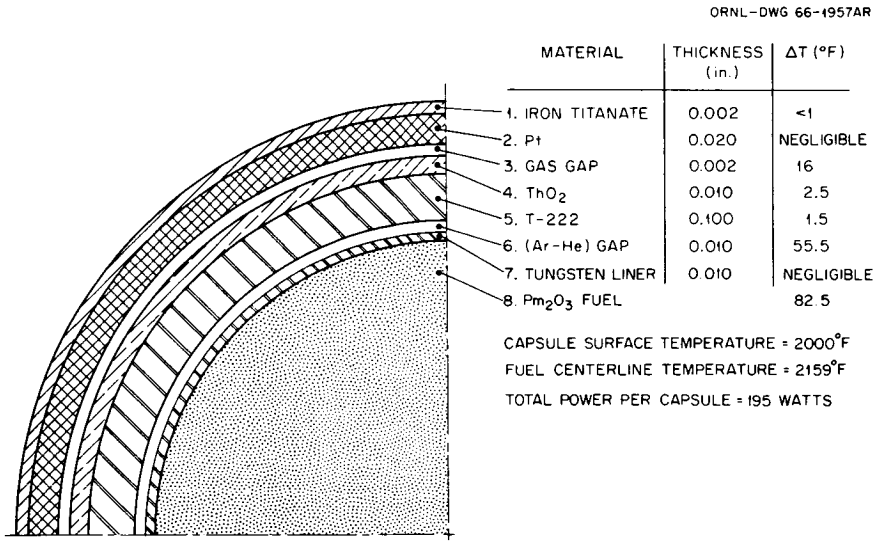

Fig. 5.27. Thermal Profile of Pm_2O_3 Capsule.

6. RADIATION SHIELDING

The basis developed for obtaining conceptual designs of shields for phase I $^{238}PuO_2$, and $^{244}Cm_2O_3$ heat sources is described below. These sources are characteristically large but relatively low in self-attenuation of penetrating radiation; consequently, the general approach in these studies was to develop point-attenuation kernels for sources of radiation and to select shields for actual sources by integrations over space. The following subsections give the dose criteria, assumed yield and energy distribution of radiation from the sources, calculated attenuation kernels, and phase I conceptual shield designs. The analysis of shield weights and results of studies to determine the effect of dose-rate criteria and separation distance are given in Section 10.

6.1 Shielding Model and Dose Criteria

The reference shield model and dose criteria used for phase I designs are summarized in Fig. 6.1, in which a panel is removed from the side of a vertically oriented vehicle or space station to show a typical shielded heat source and reentry body in an equipment compartment and its relationship to the manned compartment. The center of the source is located near one side of the vehicle, 3 meters below the manned compartment.

The allowable dose rates are based on radiation that originates in the Brayton-cycle isotope heat source and do not include contributions from natural radiation in the space environment or from other sources of radiation on the vehicle. The allowable dose rate at the floor of the manned compartment is 3 mrem/hr, which corresponds to an integrated dose of 26 rem for a one-year mission. In directions other than toward the manned compartment the allowable dose rate is no higher than 600 mrem/hr at a distance of 3 meters.

A low-radiation zone (60 mrem/hr) is provided on the side of the vehicle opposite the source to permit maintenance operations. This is not a determining criterion, however, because it is necessary to add more than enough shielding in that direction to prevent excessive scattering of radiation into the manned compartment by equipment in the equipment compartment.

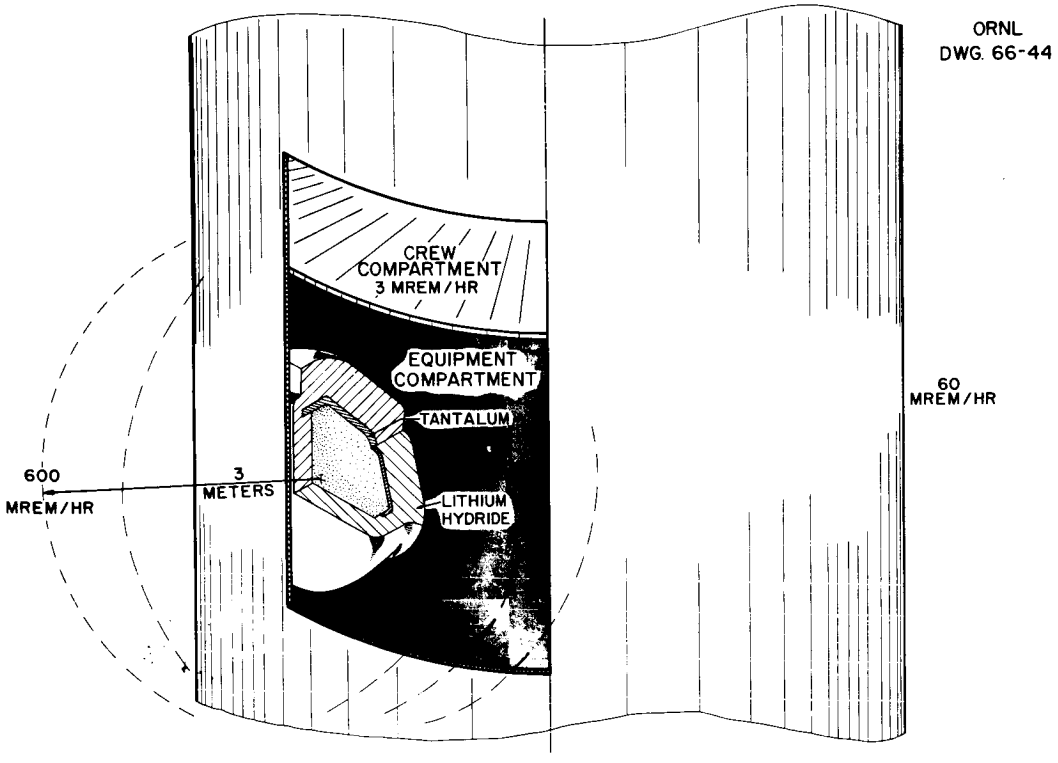

Fig. 6.1. Dose Rate Criteria.

Initially it was assumed that the radiation level in the vicinity of a reentry body following ground impact should be no greater than that directed toward space in the normal operating mode; that is, 600 mrem/hr at a distance of 3 meters. This criterion is accommodated for the $^{238}PuO_2$ and $^{147}Pm_2O_3$ fuels without weight penalty and without using a neutron shield in the reentry body. Several technical difficulties are encountered in providing an equivalent shield for the neutrons from $^{244}Cm_2O_3$. The shield, 9 in. of LiH on both sides of the source block, greatly increases the weight of the reentry body, introduces materials compatibility problems, and prohibits radiant heat transfer from the source block to the primary radiating surface. Also, it is probable that the LiH tank would be ruptured by ground impact, and molten LiH would flow out of the reentry body. The possibility of a shield of beryllium, 15 in. thick, operating at 2000°F was discarded on the basis of materials compatibility and its tremendous weight.

For phase I $^{244}Cm_2O_3$ designs, the neutron shield was omitted from the reentry body and reliance was placed on the effect of thermal radiation from the device to limit the residence time of people in dangerous radiation zones. Unless protective equipment is worn by persons closely approaching the device the thermal radiation will prevent neutron exposure rates in excess of 25 rem/hr. It has been reported[43] that the highest endurable intensity of long-wave-length heat rays on the skin is about 0.1 w/cm^2 or 300 $Btu/hr \cdot ft^2$. (Atmosphere-filtered solar-type radiation could be endured at factor-of-2 greater intensity.) Such heat rays are absorbed in the epidermal layer, and heat is conducted into the subcutaneous tissues. At 300 $Btu/hr \cdot ft^2$ the skin temperature approaches a steady-state value of approximately 115°F after 5 min. For a disk heat source with isotropic neutron emission and diffuse thermal radiation of 25 kw from one surface, the fast-neutron dose rate at points where the radiant heat flux is 300 $Btu\text{-}hr \cdot ft^2$ would be 25 rem/hr. If the disk were 5 ft in diameter, this dose rate and heat flux would occur at approximately 6 ft from the center of the disk.

6.2 Sources of Penetrating Radiation

The three isotope fuels considered in phase I studies, $^{238}PuO_2$, $^{147}Pm_2O_3$, and $^{244}Cm_2O_3$, emit penetrating radiation by several mechanisms. Table 6.1 shows the origin of the radiations that are dominant in shields that limit the radiation dose rate to 3 mrem/hr at a distance of 3 meters from a 25-kw heat source. Neutrons from subcritical multiplication in ^{238}Pu and ^{244}Cm were not considered to be significant and were omitted.

6.2.1 $^{238}PuO_2$

In this study it was assumed that the ^{238}Pu was the type made by irradiating ^{237}Np at Savannah River, which has an isotopic purity of approximately 80% (Sect. 3). The most important impurity from the standpoint of shielding considerations is ^{236}Pu. The ^{236}Pu is troublesome because one of the daughters in the decay chain, ^{208}Tl, decays with the emission of a 2.6-Mev gamma ray. The maximum intensity of this hard gamma radiation occurs about 18 years after purification of the plutonium, but the intensity is approximately 5% of the maximum after one year of aging.

The ^{236}Pu is formed by (n,2n) reactions on ^{237}Np. The concentration of ^{236}Pu in the ^{238}Pu product assumed for this study (1.2 ppm) is the average concentration in the present Savannah River product. It is also about the concentration that was predicted for a typical power reactor product.[44] If economics warrant it, the ^{236}Pu concentration could be decreased by a factor of 2 to 10 by selective irradiation schemes, but this is probably not necessary for the proposed application.

Photons from $^{238}PuO_2$ originate in decay processes, alpha interactions, spontaneous fission, fission products from spontaneous fission, and various neutron reactions, including capture and inelastic scattering. If the ^{238}Pu product (1.2 ppm ^{236}Pu) is aged no more than about two years, the predominant gamma ray is the 0.76-Mev photon that is emitted by decay of the ^{238}Pu isotope. For longer postseparation times the 2.62-Mev gamma from the ^{236}Pu decay chain is dominant.

About 10^8 neutrons/sec is emitted by the spontaneous fission process in a 25-kw heat source of ^{238}Pu. If the PuO_2 is made with natural oxygen, approximately 1.8×10^9 neutrons/sec originates from neutron reactions

Table 6.1. Dominant Radiation from 25-kw Isotopic Power Sources Shielded to a Level of 3 mrem/hr at 3 Meters

Fuel	Photons		Neutrons	
	Type	Radiation	Type	Radiation (neutrons/sec)
$^{238}PuO_2$ with 1.2 ppm ^{236}Pu	Decay, (α,γ), spontaneous fission, fission products, (n,γ), and $(n\text{-}n',\gamma)$	2×10^{10} gammas/sec at 0.76 Mev from ^{238}Pu decay for separation time of less than two years; 10^9 to 10^{10} gammas/sec at 2.6 Mev from ^{208}Tl for separation time of more than two years	Spontaneous fission	1.2×10^8
			(α,n)	1.8×10^9 with natural oxygen
			(α,n)	1.0×10^8 with ^{18}O depleted by factor of 20[a]
$^{147}Pm_2O_3$ with 10^{-4} to 10^{-5}% ^{146}Pm	Decay and bremsstrahlung	10^{12} to 10^{13} gammas/sec at 0.75 Mev from ^{146}Pm decay		
$^{244}Cm_2O_3$	Decay, (α,γ), spontaneous fission, fission products, (n,γ), and $(n\text{-}n',\gamma)$	1- to 4-Mev gammas from 4×10^{10} fissions/sec	Spontaneous fission	1.1×10^{11}
			(α,n)	3×10^9

[a]Level of other chemical contaminants assumed insignificant.

with ^{17}O and ^{18}O. There are several proven processes for separating oxygen isotopes, and if the ^{18}O content were depleted by a factor of 20 and the ^{17}O content by a factor of 4, the intensity of neutrons from the (α,n) reaction would be reduced to about the same intensity as that from spontaneous fission provided there were not significant quantities of other contaminants with high (α,n) reaction rates. In this application, the number of neutrons from subcritical multiplication was estimated to be less than 25% of the neutrons from the other processes and was neglected.

Ten-group gamma source strengths for the $^{238}PuO_2$ (Table 6.2) were obtained with the data of Stoddard and Albenesius.[45] The neutron-source energy spectrum (Fig. 6.2) for the $^{238}PuO_2$ product was calculated for the composition of plutonium given by Stoddard and Albenesius,[45] a ^{235}U fission spectrum for the contribution from spontaneous fission, and the ^{210}Po-oxygen-(α,n) spectrum from Russian experiments[46] for the contribution from (α,n) reactions. This (α,n) contribution causes the $^{238}PuO_2$ spectrum to be sharply peaked at approximately 2.5 Mev. If enriched ^{16}O is used the peak is diminished and the $^{238}PuO_2$ spectrum approximates that from thermal fission of ^{235}U.

The efficiency of the (α,n) reaction is assumed to be 80% of theoretical; consequently the yield of neutrons from (α,n) reactions with natural oxygen is 40,000 neutrons/sec per gram of pure ^{238}Pu as compared with 2640 neutrons/sec·g from spontaneous fission.

6.2.2 $^{147}Pm_2O_3$

Promethium-147 is a fission product and the most significant impurity is ^{146}Pm, which is formed primarily by (n,2n) reactions on ^{147}Pm and which has a half-life almost twice as long as that of ^{147}Pm (Sect. 3). Production reactor ^{147}Pm contains approximately 5×10^{-5}% ^{146}Pm on an activity basis. An order-of-magnitude higher concentration is predicted in typical power reactor fuels (Table 3.5, Sect. 3).

The $^{147}Pm_2O_3$ emits bremsstrahlung radiation, as well as gammas that accompany beta decay. The 0.75-Mev gamma ray from decay of the ^{146}Pm impurity is dominant. The assumed yield and spectrum of primary gammas[47] from the production reactor and power reactor $^{147}Pm_2O_3$ products are given in Table 6.3.

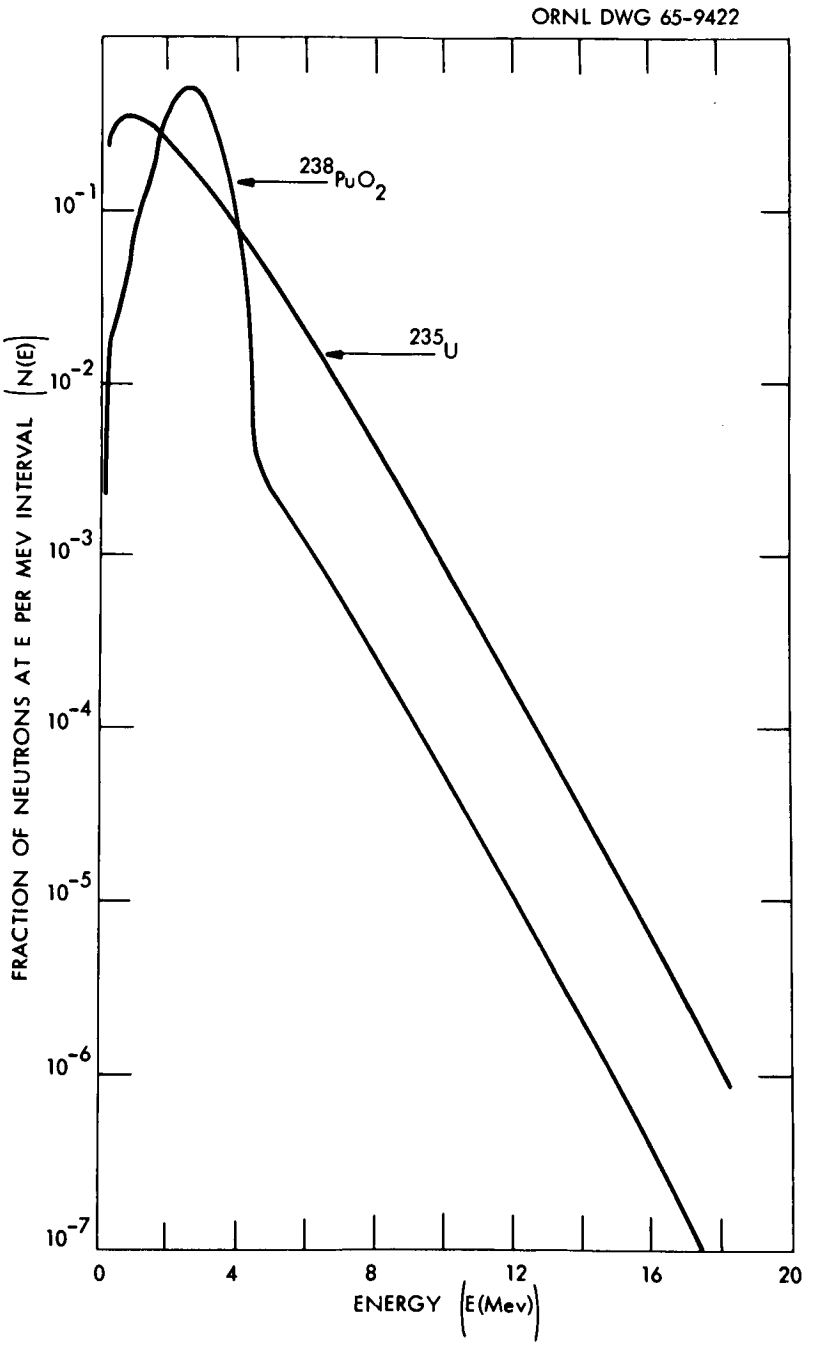

Fig. 6.2. Spectrum of Neutrons from Thermal Fission of ^{235}U and from Spontaneous Fission Plus (α,n) Reactions in $^{238}PuO_2$.

Table 6.2. Effect of Postpurification Time on the Yield and Spectrum of Primary Gammas from ^{238}Pu Product

Product composition:

^{238}Pu – 80.94%	^{241}Pu – 0.79%
^{239}Pu – 15.26%	^{242}Pu – 0.12%
^{240}Pu – 2.88%	^{236}Pu – 1.2 ppm

Photon Energy (Mev)	Photons per Second per 25-kw Heat Source for Postpurification Time of		
	1 Day	1 Year	5 Years
0.3	5.53×10^{11}	5.53×10^{11}	5.54×10^{11}
0.6	3.88×10^{10}	8.29×10^{8}	7.06×10^{9}
0.76	2.05×10^{10}	2.06×10^{10}	2.30×10^{10}
1.0	1.74×10^{8}	1.91×10^{8}	4.38×10^{8}
1.5	2.93×10^{8}	3.04×10^{8}	4.62×10^{8}
2.62	8.56×10^{7}	5.25×10^{8}	6.78×10^{9}
3.5	1.68×10^{7}	1.68×10^{7}	1.68×10^{7}
4.5	5.62×10^{6}	5.62×10^{6}	5.62×10^{6}
5.5	1.43×10^{6}	1.43×10^{6}	1.43×10^{6}
6.5	3.58×10^{5}	3.58×10^{5}	3.58×10^{5}

Table 6.3. Assumed Spectrum and Yield of Primary Gammas from 36.2-kw $^{147}Pm_2O_3$ Heat Source

Source	Photon Energy (Mev)	Yield (photons/sec)
$^{147}Pm_2O_3$ with 5×10^{-5}% ^{146}Pm[a]	0.25	1.4×10^{15}
	0.45	1.1×10^{12}
	0.75	1.1×10^{12}
$^{147}Pm_2O_3$ with 5×10^{-4}% ^{146}Pm[a]	0.25	1.4×10^{15}
	0.45	1.1×10^{13}
	0.75	1.1×10^{13}

[a]Beta activity basis.

6.2.3 $^{244}Cm_2O_3$

Curium-244 is made by neutron irradiations starting with plutonium. Impurities are not very significant in the Savannah River ^{244}Cm product

because the isotopic purity is high, 95% (Table 3.3, Sect. 3), and the penetrating radiation from the ^{244}Cm isotope is abundant.

Photons in the $^{244}Cm_2O_3$ originate in decay processes, alpha interactions, spontaneous fission, fission products from spontaneous fission, and various neutron reactions. The dominant photons are the prompt and delayed gammas from spontaneous fission, which have a broad energy spectrum. In $^{244}Cm_2O_3$ product the neutrons from spontaneous fission are dominant.

The assumed yield and spectrum of primary gammas from the $^{244}Cm_2O_3$ product (Table 6.4) are based on Savannah River data.[10] In the neutron shield calculations the ^{235}U thermal-neutron fission spectrum (Fig. 6.2) was used to approximate the spectrum from spontaneous fission of ^{244}Cm, primarily to make the data more widely applicable. The ^{244}Cm spectrum is known to be intermediate between the ^{235}U fission spectrum and that from spontaneous fission in ^{252}Cf. Based on results of moments-method calculations with these two spectra (Fig. 6.3), we estimate that through three one-tenth-value thicknesses of typical lightweight neutron shields the dose from a ^{244}Cm spectrum is only about 50% higher than that from a ^{235}U spectrum.

Table 6.4. Assumed Spectrum and Yield of Primary Gammas from 26.6-kw $^{244}Cm_2O_3$ Heat Source

Photon Energy (Mev)	Yield (photons/sec)
0.30	3.3×10^{11}
0.60	3.4×10^{11}
1.0	1.5×10^{11}
1.5	1.2×10^{11}
2.5	3.6×10^{10}
3.5	1.3×10^{10}
4.5	4.4×10^{9}
5.5	1.1×10^{9}
6.5	2.8×10^{8}

6.3 Basic Neutron Shield Studies

On a weight and materials compatibility basis, LiH clad with stainless steel was selected as the preferred neutron shield material for phase I designs. These materials are compatible to a temperature of approximately 1200°F, which is well above the predicted shield operating temperature. For isotope sources where few tenth-value thicknesses are required, a simple low-weight shield is obtained by placing a heavy gamma shield near the source and backing it up by a light hydrogenous neutron shield that will also suppress capture gamma radiation from the hydrogen. The ^{6}Li content of natural lithium is sufficient to suppress the capture gammas in the phase I designs. In the phase I designs the maximum capture-gamma dose contributions from the tantalum gamma shield and lithium hydride neutron shield were calculated to be 50% and 2%, respectively, of the transmitted neutron dose.

Water and/or CH_2 are possible alternative materials for use in low-temperature shadow shields or for shadow shields on the gantry. The use in the vehicle may be attractive for a dual-purpose application involving the storage of waste water or hydrocarbon fuel in the shield tank. With these materials, neutron-attenuation factors of approximately 50 may be obtained without introducing an appreciable capture-gamma problem. Additional suppression of capture gammas can be provided by using boron additives. Beryllium is a possible neutron shield material for space applications, but because of its relatively large weight and incompatibility with other materials at elevated temperatures, its use for neutron shields is not attractive.

The fast-neutron attenuation kernel in lithium hydride was calculated by three separate methods. The results are consistent and agree with existing experimental data. The 05R Monte Carlo results, which are believed to be the most accurate, are compared with moments-method and S_nP_n (neutron transport theory) results in Table 6.5. The RENUPAK moments-method code is useful for inexpensive calculation of the relative effect of various dose response functions. The DTF-II code, which uses 27 energy groups and the S_8P_3 approximation, is useful for the inexpensive calculation of sources of secondary gamma rays.

Table 6.5. Fast-Neutron Dose Rate Multiplied by $4\pi r^2$ in Natural Lithium Hydride[a] as a Function of the Distance from a Unit Point Isotropic Source

Lithium hydride density: 0.75 g/cm^3

Source spectrum	^{235}U	^{235}U	^{235}U	^{235}U	^{235}U	$^{238}PuO_2$	$^{238}PuO_2$
Method of calculation	05R[b]	S_8P_3[c]	RENUPAK	RENUPAK[d]	RENUPAK[d]	RENUPAK[d]	RENUPAK[d]
Dose response function	mrad[e]	mrad[e]	mrad[e]	mrad[e]	mrem[f]	mrad[e]	mrem[f]
	Dose Rate Multiplied by $4\pi r^2$ {[(mrad or mrem/hr)/(neutrons/sec)]·cm^2}						
Distance, cm							
0	1.08×10^{-2}			1.0×10^{-2}	1.2×10^{-1}	1.2×10^{-2}	1.4×10^{-1}
10	4.09×10^{-3}	4.2×10^{-3}	4.30×10^{-3}	4.09×10^{-3}	5.12×10^{-2}	5.31×10^{-3}	6.82×10^{-2}
20	9.38×10^{-4}	1.0×10^{-3}	9.47×10^{-4}	9.38×10^{-4}	1.17×10^{-2}	1.24×10^{-3}	1.63×10^{-2}
30	1.92×10^{-4}	2.1×10^{-4}	2.24×10^{-4}	1.92×10^{-4}	2.34×10^{-3}	1.83×10^{-4}	2.48×10^{-3}
40	3.93×10^{-5}	4.7×10^{-5}	5.07×10^{-5}	3.93×10^{-5}	4.69×10^{-4}	2.68×10^{-5}	3.55×10^{-4}
50	8.53×10^{-6}	1.1×10^{-5}	1.12×10^{-5}	8.53×10^{-6}	9.91×10^{-5}	3.93×10^{-6}	5.20×10^{-5}
60	1.90×10^{-6}	2.6×10^{-6}	2.52×10^{-6}	1.90×10^{-6}	2.15×10^{-5}	5.72×10^{-7}	7.51×10^{-6}
70	5.33×10^{-7}	6.4×10^{-7}	6.20×10^{-7}	5.33×10^{-7}	5.90×10^{-6}	1.01×10^{-7}	1.30×10^{-6}
80	1.41×10^{-7}	1.7×10^{-7}	1.77×10^{-7}	1.41×10^{-7}	1.53×10^{-6}	1.74×10^{-8}	2.12×10^{-7}
90	3.69×10^{-8}	4.9×10^{-8}	5.92×10^{-8}	3.69×10^{-8}	3.96×10^{-7}	3.41×10^{-9}	3.83×10^{-8}

[a] Concentrations of hydrogen, ^6Li, and ^7Li are 0.05686, 0.00426, and 0.05260 atoms/barn·cm, respectively.

[b] Unpublished data, F. B. K. Kam, Neutron Physics Division, ORNL.

[c] DTF-II code with 27 energy groups, unpublished data, N. M. Greene, Central Data Processing, ORGDP.

[d] RENUPAK results for mrads and mrems normalized to 05R results in mrads. Results in these columns are assumed to be the most accurate.

[e] Henderson's single-collision mrads (Ref. 49).

[f] Snyder-Neufeld mrems (Ref. 50).

Dose-attenuation kernels for the mrem response function and ^{235}U and $^{238}PuO_2$ spectra were determined (Fig. 6.4) by normalizing the RENUPAK and 05R results for the mrad response function and the ^{235}U spectrum. The $^{238}PuO_2$ (natural oxygen) spectrum causes a slightly higher dose through small LiH shield thicknesses. The crossover point in LiH is at approximately 30 cm.

The RENUPAK code was also used for calculating fast-neutron dose-attenuation kernels for other materials of interest for use in the spacecraft, as supplementary shielding on the gantry, or in shielded cells for fabrication of source capsules or integration of capsules with the reentry body. The results are presented in Figs. 6.5, 6.6, 6.7, 6.8, and 6.9. Results are also presented for gamma- and neutron-attenuation kernels resulting from point ^{235}U fission sources in water in Fig. 6.10, borated CH_2 in Fig. 6.11, and normal concrete in Fig. 6.12. These latter results were calculated[48] with the RENUPAK code for fast neutrons, DTF for thermal neutrons, SDC for primary gammas, and SAGE (Monte Carlo) for secondary gammas.

6.4 Basic Gamma Shield Studies

Tantalum was chosen as the preferred gamma shield material for phase I designs. A material is required that can be fabricated into complex shapes and which has high density to suppress the buildup of scattered gammas. Tungsten and uranium are difficult to fabricate. In addition, uranium becomes badly activated by fission.

Calculations of the effect of shields on the primary gamma dose rate from sources of $^{238}PuO_2$ (Tables 6.6 and 6.7), $^{244}Cm_2O_3$, and $^{147}Pm_2O_3$ (Table 6.8) were made with the SDC code. The SDC code evaluates the semi-analytical shielding formulas for homogeneous shields and a variety of source geometries by using stored attenuation coefficients and buildup factors.

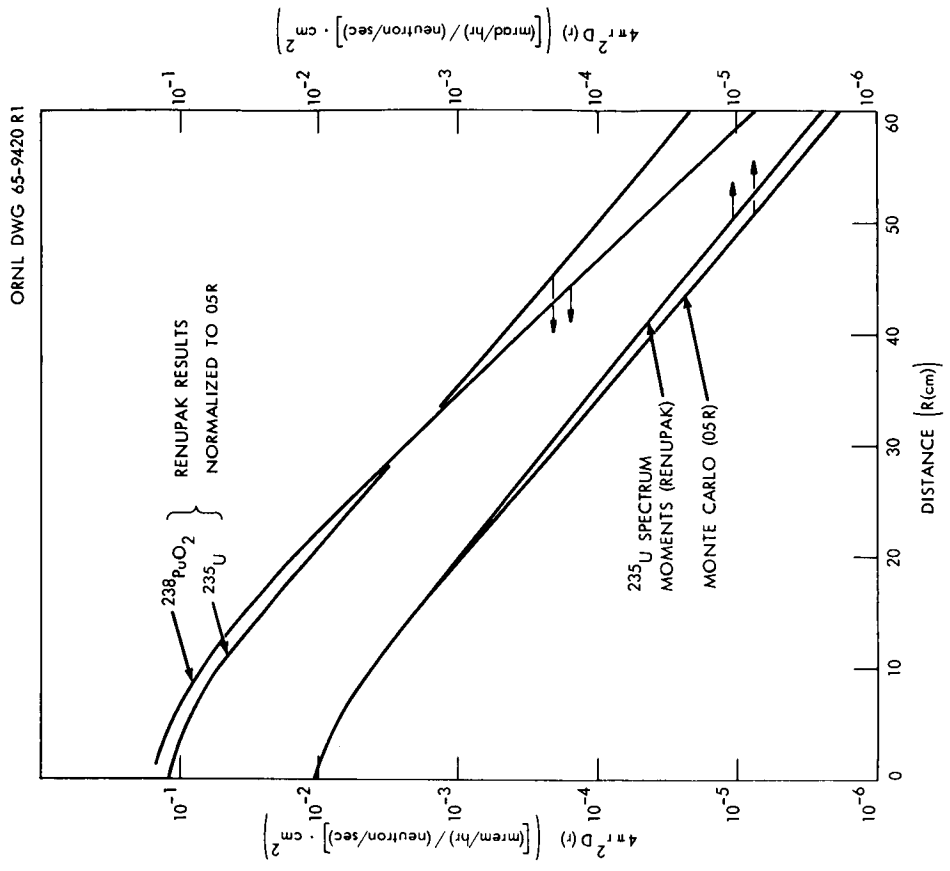

Fig. 6.4. Effect of Spectrum (^{235}U and $^{238}PuO_2$) and Distance from a Unit Point Isotropic Source on the Fast-Neutron Dose Rate in Lithium Hydride of Density 0.75 g/cm^3.

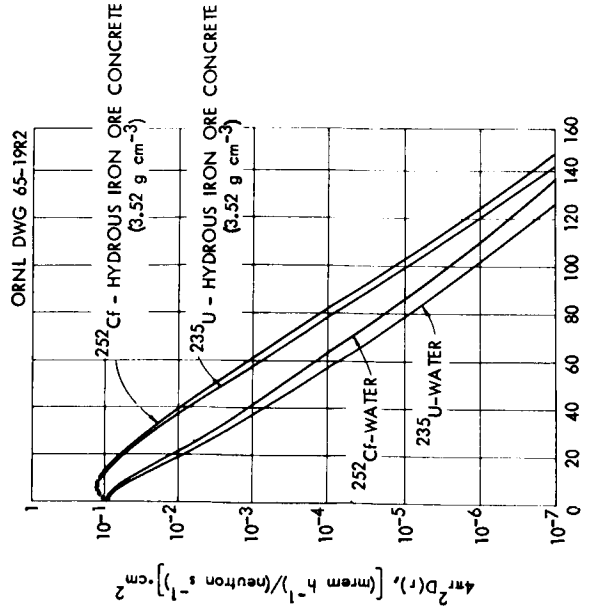

Fig. 6.3. Fast-Neutron Dose Rate in Water and Hydrous Iron Ore Concrete as a Function of the Distance from a Unit Point Isotropic Fission Source of ^{235}U and ^{252}Cf.

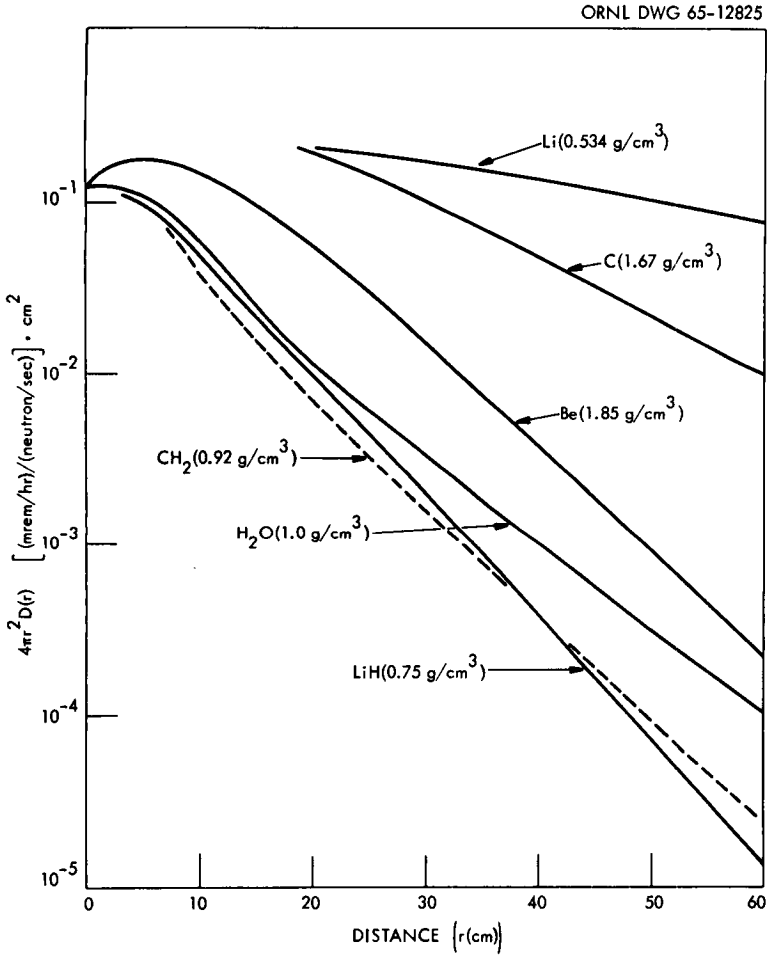

Fig. 6.5. Fast-Neutron Dose Rate in Various Materials as a Function of the Distance from a Unit Point Isotropic Fission Source of ^{235}U.

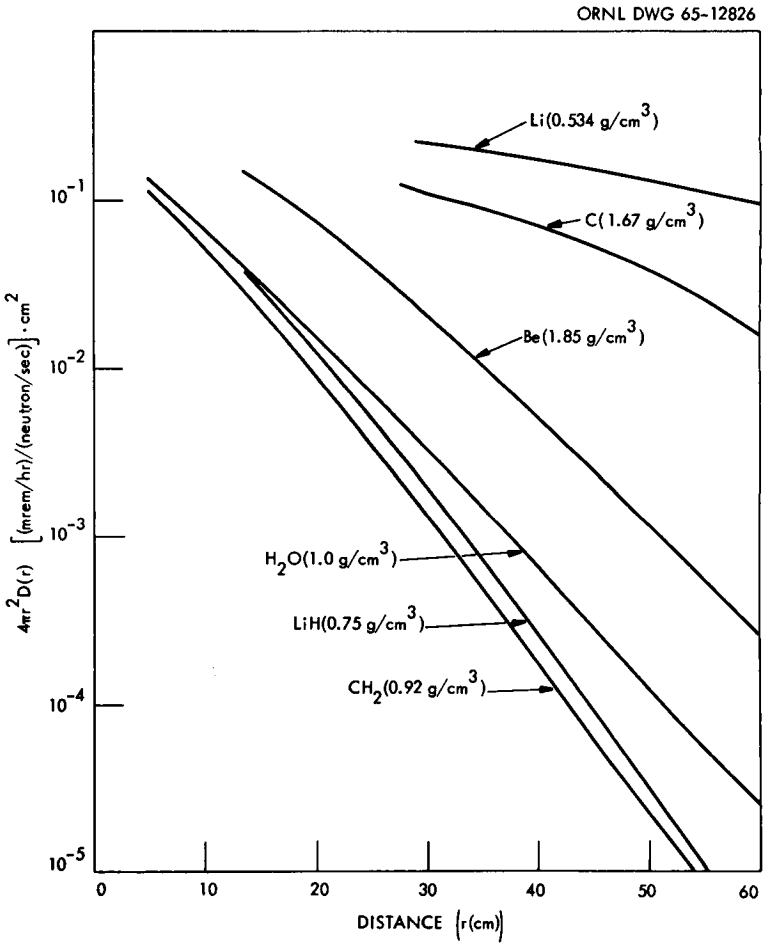

Fig. 6.6. Fast-Neutron Dose Rate in Various Materials as a Function of the Distance from a Unit Point Isotropic Source of Neutrons from $^{238}PuO_2$.

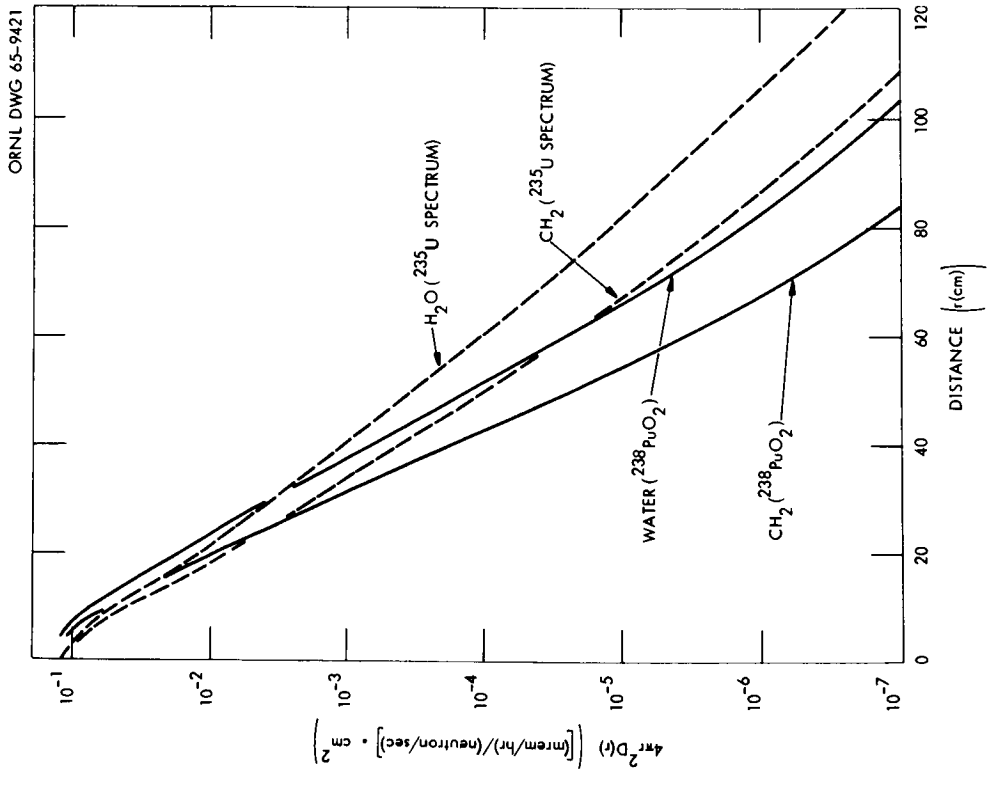

Fig. 6.7. Effect of Spectrum and Distance from a Unit Point Isotropic Source on the Fast-Neutron Dose Rate in Water and CH_2 (Density, 0.92 g/cm³).

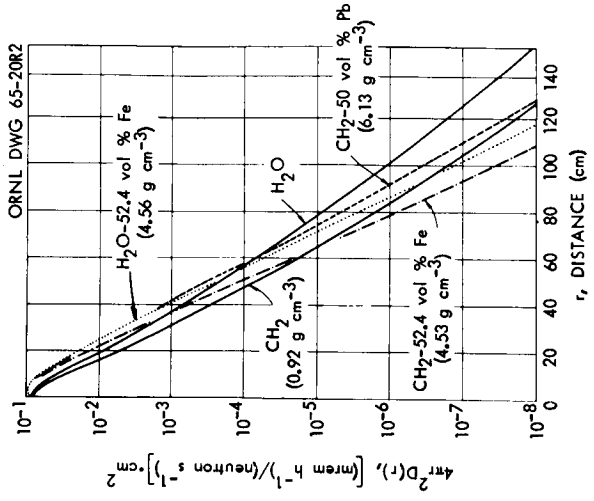

Fig. 6.8. Fast-Neutron Dose Rate in Various Hydrogenous Materials as a Function of the Distance from a Unit Point Isotropic Fission Source of ^{235}U.

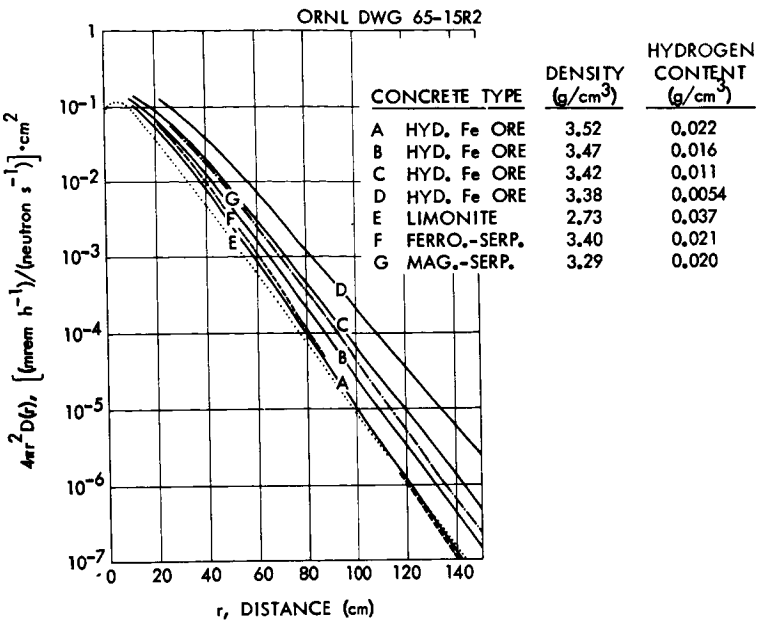

Fig. 6.9. Fast-Neutron Dose Rate in Various Concretes as a Function of Distance from a Unit Point Isotropic Fission Source of ^{235}U.

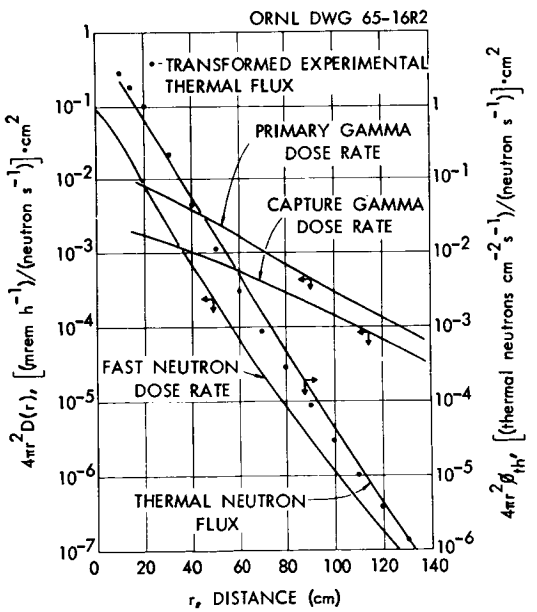

Fig. 6.10. Fast-Neutron, Primary-Gamma, and Capsule-Gamma Dose Rate and Thermal-Neutron Flux in Water as a Function of the Distance from a Unit Point Isotropic Fission Source of ^{235}U.

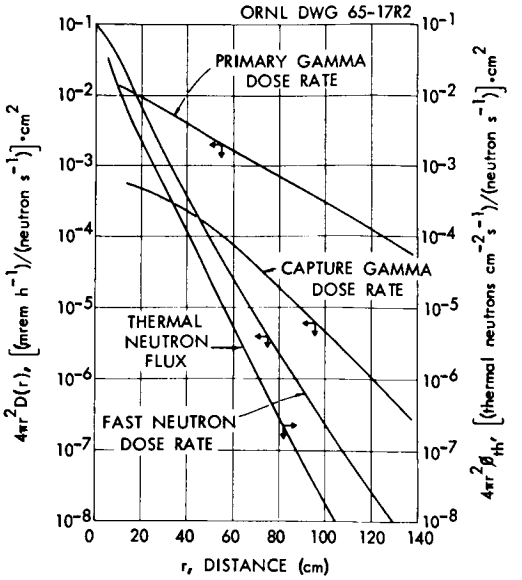

Fig. 6.11. Fast-Neutron, Primary-Gamma, and Capture-Gamma Dose Rate and Thermal-Neutron Flux in CH_2–5 wt % Boron (Density, 1.0 g/ml) as a Function of the Distance from a Unit Point Isotropic Fission Source of ^{235}U.

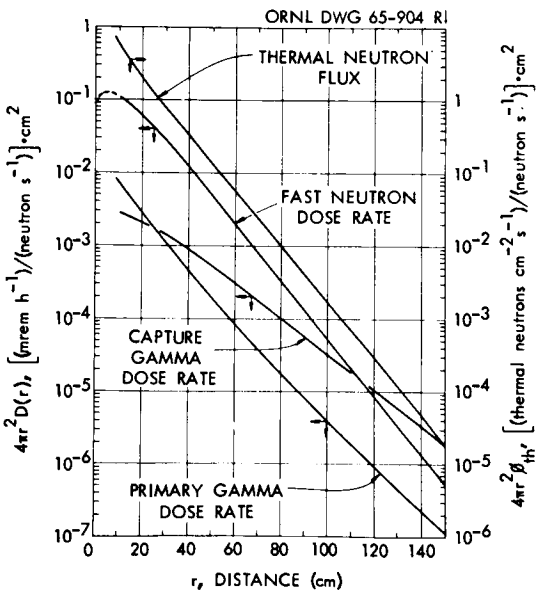

Fig. 6.12. Fast-Neutron, Primary-Gamma, and Capture-Gamma Dose Rate and Thermal-Neutron Flux in Normal Concrete as a Function of the Distance from a Unit Point Isotropic Fission Source of ^{235}U.

Table 6.6. Effect of Source Block Density, Postpurification Time, and Uranium Shield Thickness on Primary Gamma Dose Rate at 3 Meters from the Center of a 1-ft^3 Spherical Source Block Containing a 25-kw $^{238}PuO_2$ Heat Source

Source Block Density (g/cm^3)	Postpurification Time	Dose Rate Through Uranium Shields of Indicated Thickness (mrad/hr)				
		0.5 cm	2 cm	4 cm	6 cm	8 cm
6	1 day	1.03	0.0705	0.00638	0.00116	0.000236
	1 year	1.21	0.131	0.0208	0.00444	0.000948
	5 years	3.82	1.00	0.227	0.0511	0.0111
4	1 day	1.50	0.105	0.00971	0.00178	0.000360
	1 year	1.78	0.198	0.0319	0.00680	0.00145
	5 years	5.74	1.53	0.348	0.0784	0.0170
2	1 day	3.56	0.238	0.0206	0.00370	0.000744
	1 year	4.14	0.431	0.0665	0.0141	0.00300
	5 years	12.5	3.19	0.719	0.162	0.0351
Point source	1 day	11.4	0.666	0.0455	0.00752	0.00147
	1 year	12.6	1.05	0.136	0.0281	0.00594
	5 years	30.3	6.54	1.43	0.321	0.0696

Table 6.7. Effect of Source Block Density, Postpurification Time, and Water Shield Thickness on Primary Gamma Dose Rate at 3 Meters from the Center of a 1-ft^3 Spherical Source Block Containing a 25-kw $^{238}PuO_2$ Heat Source

Source Block Density (g/cm^3)	Postpurification Time	Dose Rate Through Water Shields of Indicated Thickness (mrad/hr)				
		5 cm	20 cm	40 cm	60 cm	80 cm
6	1 day	22.3	16.1	5.18	1.13	0.230
	1 year	22.6	16.3	5.29	1.18	0.258
	5 years	26.4	19.1	6.85	1.99	0.657
4	1 day	29.7	21.4	6.92	1.52	0.316
	1 year	30.1	21.7	7.09	1.61	0.358
	5 years	35.9	25.9	9.45	2.83	0.968
2	1 day	74.1	53.4	17.2	3.76	0.772
	1 year	74.9	54.0	17.6	3.94	0.861
	5 years	87.2	63.0	22.6	6.50	2.13
Point source	1 day	337	244	77.7	16.3	3.19
	1 year	339	245	78.4	16.7	3.37
	5 years	368	266	89.6	22.2	5.99

Table 6.8. Effect of Uranium and Tantalum Shield Thickness on the Primary Gamma Dose Rate at 3 Meters from Nominally 25-kw Point Heat Sources of $^{244}Cm_2O_3$ and $^{147}Pm_2O_3$

Shield Thickness (cm)		Dose Rate (mrad/hr)		
Uranium[a]	Tantalum[b]	$^{244}Cm_2O_3$[c]	$^{147}Pm_2O_3$[d]	$^{147}Pm_2O_3$[e]
0.5	0.57	540	670	4400
0.7	0.80		280	2700
1.0	1.14	310	140	1400
1.5	1.7		47	470
2.0	2.3	120	16	160
3.0	3.4	47	1.7	17
4.0	4.6	20	0.18	1.8
5.0	5.7	8.3	0.019	0.19
6.0	6.8	3.6		
8.0	9.1	0.73		

[a] Density, 18.9 g/cm^3.

[b] Density, 16.6 g/cm^3.

[c] Heat source, 26.6 kw.

[d] Heat source, 36.2 kw; 5×10^{-5}% ^{146}Pm contamination.

[e] Heat source, 36.2 kw; 5×10^{-4}% ^{146}Pm contamination.

6.5 Summary of Relative Shield Thicknesses for Point Isotropic Sources

Figure 6.13 summarizes the effect of shield thickness, tantalum and LiH, on the primary gamma and neutron dose rates at 3 meters from point 25-kw heat sources. The two lower curves show the gamma dose rate from $^{238}PuO_2$ as a function of tantalum thickness and postseparation time. If the $^{238}PuO_2$ contains 1.2 ppm ^{236}Pu, the shield thickness for a postseparation time of one year, which is the average postseparation time in a one-year mission, is little different from that for a postseparation time of one day. About 0.5 in. of tantalum is required for a point source to attain the 3-mrem/hr at 3 meters dose rate. It is shown later that no tantalum shield is required per se for the actual ^{238}Pu source conceptual designs in this study because of the shielding obtained from intervening structures.

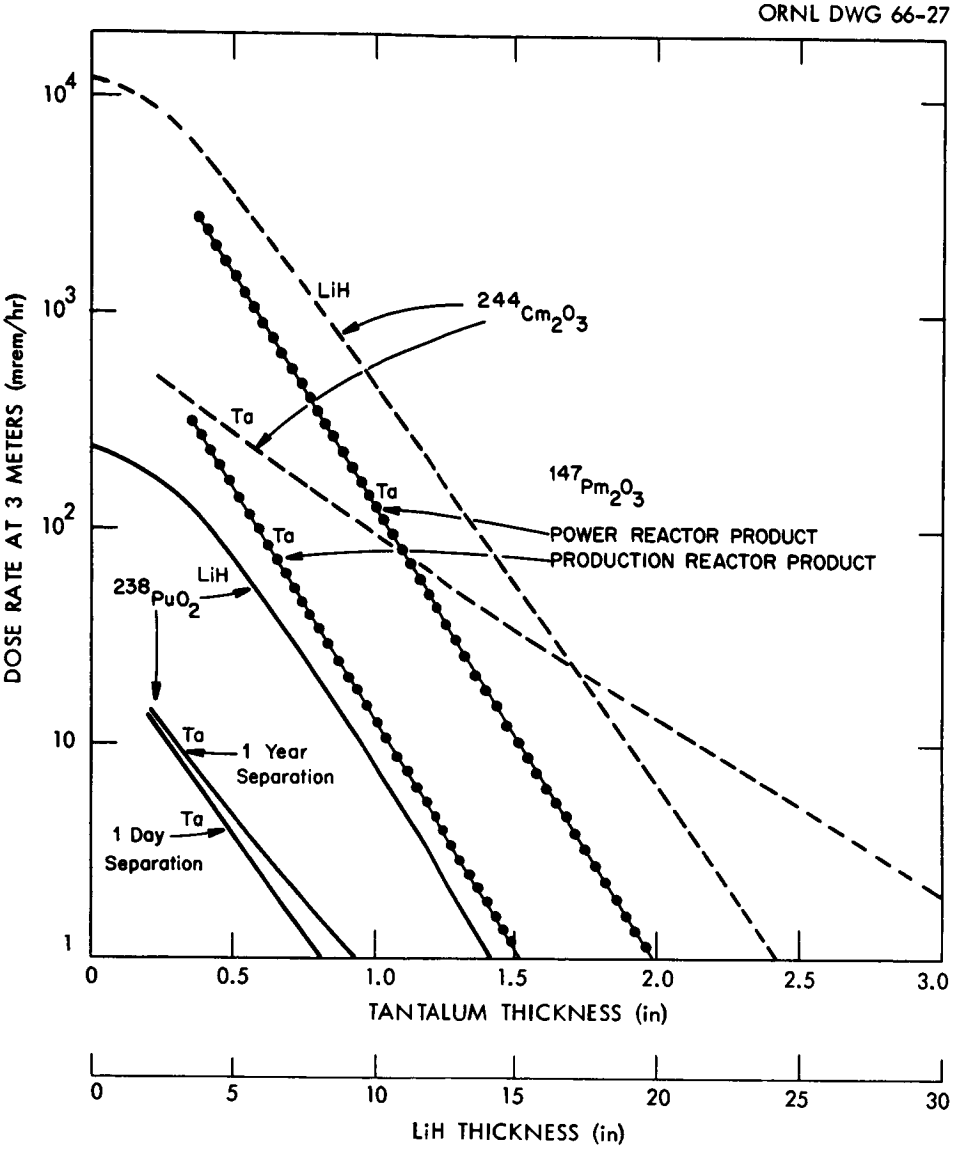

Fig. 6.13. Effect of Tantalum and Lithium Hydride Shield Thickness on the Primary Gamma and Neutron Dose Rate at a Distance of Three Meters from Point 25-kw (End of Life) Heat Sources of $^{238}PuO_2$ (1.2 ppm ^{236}Pu), $^{147}Pm_2O_3$, and $^{244}Cm_2O_3$.

The next higher curve in Fig. 6.13 shows the effect of LiH on the $^{238}PuO_2$ neutron dose rate. About 12 in. is required at the 3-mrem/hr level. The dotted curves are dose rate versus tantalum thickness for ^{147}Pm produced in production and power reactors. Shield thicknesses are in the range 1.5 to 2 in.; the power reactor product requires approximately 0.5 in. more tantalum. The dashed curves are primary gamma and neutron dose rates from ^{244}Cm. At the 3-mrem/hr level, ^{244}Cm requires over 2 in. of tantalum and nearly 30 in. of LiH.

6.6 Conceptual Shield Designs

The shield thicknesses that were selected for phase I designs are listed in Table 6.9. For $^{238}PuO_2$, a 1.2-ppm ^{236}Pu content and one-year separation are assumed. With natural oxygen, 12 in. of LiH is required in the direction of the manned compartment and 6 in. into the equipment compartment to limit the scattered dose. With enriched ^{16}O, only 7 in. of LiH is required in the direction of the manned compartment.

With ^{147}Pm having the expected power reactor composition, 1.7 in. of tantalum is required toward the manned compartment, 1.1 in. toward the equipment compartment, and 0.7 in. toward space. For the production reactor composition the thicknesses are approximately 0.5 in. less.

There is no materials option with ^{244}Cm. Table 6.9 shows the reduction in shield thickness that accrues by providing the same integrated dose for a 90-day mission as for a 1-year mission with the basic dose-rate criteria. With the basic criteria, equivalent to 26 rem in a one-year mission, 2.7 in. of tantalum and 19 in. of LiH are required toward the manned compartment, 1.3 in. of tantalum and 15 in. of LiH into the equipment compartment, and 9 in. of LiH toward space. For a dose of 26 rem in a 90-day mission, 2 in. of tantalum and 16 in. of LiH toward the manned compartment, and 0.7 in. of tantalum and 11.5 in. of LiH into the equipment compartment are required. Nine inches of LiH is still required toward space because the 600 mrem/hr at 3 meters criterion was not relaxed.

The shield thickness in the direction of the equipment compartment, which is heavily dependent on the geometry and type of scattering materials in the compartment, is the least accurate of these shield thickness numbers.

Table 6.9. Phase I Shield Thicknesses

Fuel	Shield					
	Toward Crew Compartment		Toward Equipment Compartment		Toward Space	
	Material	Thickness (in.)	Material	Thickness (in.)	Material	Thickness (in.)
$^{238}PuO_2$ with 1.2 ppm ^{236}Pu after one-year of separation						
Natural oxygen	LiH	12	LiH	6		
Enriched ^{16}O (a)	LiH	7				
$^{147}Pm_2O_3$						
$5 \times 10^{-4}\%$ ^{146}Pm	Ta	1.75	Ta	1.15	Ta	0.7
$5 \times 10^{-5}\%$ ^{146}Pm	Ta	1.3	Ta	0.7	Ta	0.25
$^{244}Cm_2O_3$						
26 rem per year	Ta	2.7	Ta	1.3		
	LiH	19	LiH	15	LiH	9
26 rem in 90 days	Ta	2.0	Ta	0.7		
	LiH	16	LiH	11.5	LiH	9

[a]Assumes (α,n) neutrons reduced by a factor of 18.

To provide for phase I designs it was assumed that 4000 lb of low-atomic-number material is located in the equipment compartment at an average distance of 2 meters from the isotope source. A point source was assumed and only elastic scattering was considered. Shield thicknesses were chosen to allow the neutron dose to be the dominant contribution at the wall of the crew compartment. The use of such a gross model for phase I studies is justified on the basis that the weight of the shields in the direction of the equipment compartment is no more than 25 to 30% of the total shield weight.

7. CRITICALITY HAZARDS

Since two of the fuels considered in this study, ^{244}Cm and ^{238}Pu, could, in sufficient quantity, constitute a chain-reacting critical mass, a criticality hazards evaluation was performed to determine whether the quantities required for a 25-kw heat source constitute criticality problems that would impose design constraints. Previously reported calculations performed at other installations indicated that a 70-kg ^{238}Pu heat source would exceed the minimum critical mass.[51-53] However, the reported calculations disagree as to whether criticality is possible with a 10-kg ^{244}Cm heat source.[52,53] In this evaluation, multigroup nuclear cross-section sets were compiled for ^{238}Pu and ^{244}Cm, and these sets were used to perform a series of multigroup transport-theory calculations to define critical configurations and densities for both the oxides and metals of ^{238}Pu and ^{244}Cm.

7.1 Cross-Section Evaluation

Since the results of criticality calculations depend, in the absence of experimental data, entirely on the assumptions made in the evaluation of the cross sections used, a brief résumé of the high-energy nuclear property data used in this analysis is necessary. The compilation of cross sections for ^{238}Pu and ^{244}Cm is hampered by the paucity of experimental data, and recourse must be made to nuclear systematics and theoretical models.

7.1.1 ^{238}Pu Cross Sections

The fission cross section of ^{238}Pu has been measured in the energy range from 0.1 to 1.7 Mev by Butler and Sjoblom.[54] Their results indicate that this energy range accounts for 70% of the fissions in a bare metallic assembly, and practically all fissions occur at energies above 0.1 Mev. The experimental data were used as reported. At energies above 1.7 Mev the fission cross section was assumed to have the same energy dependence as that of neighboring nuclides. In the kilovolt energy range the fission cross section was assumed to have the same shape as that of ^{240}Pu. No

experimental information is available on the mean number of neutrons emitted per fission for ^{238}Pu. In lieu of experimental data, the empirical correlation of Gordeeva and Smirenkin[55] was used; it indicated that

$$\nu = 2.78 + 0.13E \ .$$

The radiative capture cross section in the high-energy range was calculated by nuclear systematics to be 1.75 times that of ^{238}U, and this relationship was used.

As an experimental check on these assumptions, the set of derived cross sections was used to calculate replacement measurements made at Los Alamos with ^{238}Pu samples in the "dirty Jezebel" assembly.[56] The experimentally measured neutron-production cross section was reported as

$$\sigma_p = 3.76 \pm 0.23 \text{ b} \ ,$$

and the calculated value was

$$\sigma_p = 4.25 \text{ b} \ .$$

This overestimate of the production cross section could lead to a 10 to 25% underestimate of the critical mass of ^{238}Pu.

7.1.2 ^{244}Cm Cross Sections

No experimental data are available for high-energy curium cross sections, and recourse must be made to nuclear systematics and theoretical models. However, the low-energy measurements of Coté, Barnes, and Diamond do provide average strength functions.[57] The fission cross section of ^{244}Cm was assumed to have the same line shape as the even-even isotope ^{238}Pu, and the ratio of the ^{244}Cm to ^{238}Pu fission cross sections was calculated by nuclear systematics to be 0.85. No experimental information is available on the mean number of neutrons emitted per fission, and again the empirical correlation of Gordeeva and Smirenkin[55] was used. This correlation predicts

$$\nu = 3.20 + 0.13E \text{ neutrons/fission} \ .$$

The radiative capture cross section in the high-energy range was calculated by systematics to be 1.2 times that of ^{238}U.

A check of the derived ^{244}Cm cross sections was made by comparing them with experimental replacement measurements made at Los Alamos.[56] The experimental neutron-production cross section was measured to be

$$\sigma_p = 3.32 \pm ? \text{ b} ,$$

in contrast to a calculated value of

$$\sigma_p = 4.46 \text{ b} .$$

The experimental uncertainty in the neutron-production cross section is unknown. This large, possibly 35%, overestimate of the production cross section is unresolved, and point measurements are planned to pinpoint the difficulty. If it is assumed that the 3.32 b is correct, the large calculated production cross section could lead to a 55% underestimate of the critical mass of ^{244}Cm.

7.2 Criticality Calculations

The criticality calculations were performed with the multigroup S_nP_n transport-theory code ADTF.[58] They were performed in a 15-group S_4P_3 approximation. The 15-group constants were obtained from a 99-group B_3 calculation performed with GAM-II.[59]

7.2.1 Bare Assemblies

Calculations were performed to determine the minimum critical masses of bare spheres of the oxides and metals of ^{238}Pu and ^{244}Cm as functions of density. The assumed isotopic compositions were approximately 81% ^{238}Pu and 98% ^{244}Cm. In the calculation of the curium systems all even isotopes were treated as ^{244}Cm and all odd isotopes as ^{241}Pu. Figure 7.1 summarizes the results of these calculations and presents the results of calculations performed elsewhere for comparison. The calculated critical masses of the oxides and the metals differ only slightly and are represented by a single line. Complete tabulations of the calculational results is presented in Table 7.1.

The $^{238}PuO_2$ fuel form used for the Brayton-cycle heat source designs has a density of 9.12 g/cm^3, which corresponds to a calculated critical mass of 29.5 kg in a bare spherical configuration. Calculations reported

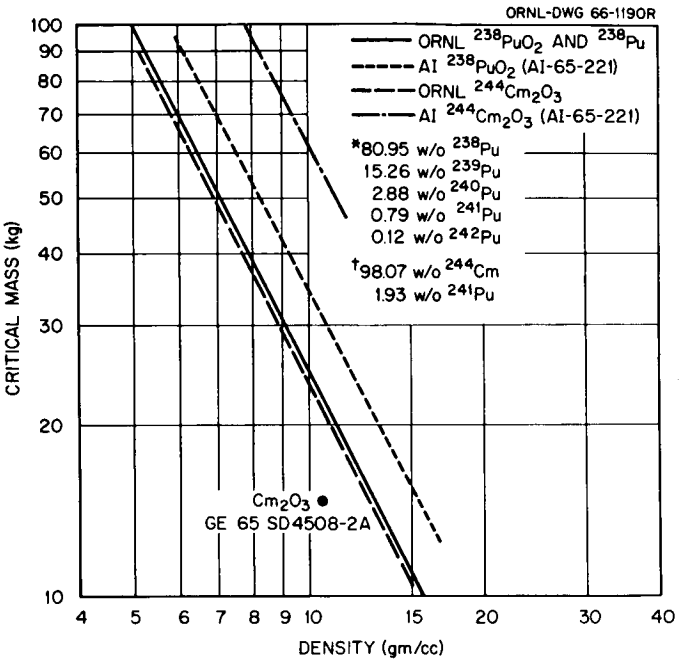

Fig. 7.1. Critical Masses of $^{238}PuO_2$ and $^{244}Cm_2O_3$ as Functions of Density. (Atomics International data from Ref. 53; General Electric Company data from Ref. 52.)

Table 7.1. Results of Critical Mass Calculations

Critical Mass Equations

Pu	$M_c = 2450\ \rho^{-2}$
PuO_2	$M_c = 2460\ \rho^{-2}$
Cm	$M_c = 2450\ \rho^{-2}$
Cm_2O_3	$M_c = 2370\ \rho^{-2}$

Core		Reflector		Critical Mass (kg)	Critical Radius (cm)
Mixture	Density (g/cm^3)	Mixture	Thickness (cm)		
Pu[a]	11.60	Bare		18.2	7.2064
PuO_2[a]	11.40	Bare		18.9	7.3434
PuO_2	9.12	Bare		29.5	9.1776
PuO_2	6.84	Bare		52.6	12.2465
PuO_2	9.12	H_2O	15.0	20.2	8.0846
PuO_2	9.12	H_2O	7.5	20.4	8.1178
PuO_2	9.12	H_2O	2.5	23.5	8.5026
Cm[b]	14.0	Bare		12.5	5.97
Cm_2O_3[b]	10.60	Bare		21.1	7.8031
Cm_2O_3	9.01	Bare		29.2	9.1803
Cm_2O_3	10.60	Au-H_2O	4.0–15.0	11.9	6.4540
Cm_2O_3	10.60	Au-H_2O	2.0–7.5	13.5	6.7188
Cm_2O_3	10.60	Au-H_2O	0.5–2.0	16.5	7.1966

[a] 80.95 wt % ^{238}Pu, 15.26 wt % ^{239}Pu, 2.88 wt % ^{240}Pu, 0.79 wt % ^{241}Pu, and 0.12 wt % ^{242}Pu.

[b] 98.07 wt % ^{244}Cm and 1.93 wt % ^{241}Pu.

by General Electric[52] yield approximately the same value, but calculations reported by Atomics International[53] yield a value 35% greater. As noted previously, the comparison of the cross-section set calculated for this analysis with the Los Alamos experiments indicated that possibly a 25% underestimate of the critical mass might be expected. Hence, the regions of uncertainty in the $^{238}PuO_2$ critical masses as calculated by ORNL and AI overlap, and based on the Los Alamos experiment the ORNL calculation is conservative. On the basis of these calculations a 70-kg $^{238}PuO_2$ mission load for a 25-kw heat source represents between two and three critical masses in the bare spherical configuration.

There are large differences between the calculated critical masses reported for $^{244}Cm_2O_3$ by ORNL, AI, and GE. The value calculated in this study is 21.1 kg at the design density of 10.6 g/cm^3, in contrast to a value 30% lower calculated by GE[52] and 2.6 times greater calculated by AI.[53] The major difference between the ORNL and GE calculations is the value used for the mean number of neutrons per fission, for which no experimental data are available. However, based on the Los Alamos experiments the ORNL data are conservative. The factor of 2.6 difference between the ORNL and AI calculations exceeds the possible 55% conservatism of the ORNL calculation deduced from the Los Alamos experiments. However, in the bare spherical configuration all estimates of the minimum critical mass at the design density of 10.6 g/cm^3 exceed the approximately 12 kg of $^{244}Cm_2O_3$ needed for a 25-kw Brayton-cycle heat source.

7.2.2 Reflected Assemblies

Calculations were performed to determine the reduction in critical mass due to reflection. The results of these calculations are presented in Fig. 7.2. At a density of 9.12 g/cm^3 the critical mass of $^{238}PuO_2$ may be reduced by one-third by reflecting the sphere with water. The critical mass decreases with increasing reflector thickness from 29.5 to 20.2 kg. With a thick water reflector the 25-kw mission load of $^{238}PuO_2$ represents approximately four critical masses.

Because of the rapid decreases in the fission cross sections of ^{238}Pu and ^{244}Cm with decreasing neutron energy, some metals make better reflecting materials than water. At a density of 10.6 g/cm^3 the critical mass of $^{244}Cm_2O_3$ may be reduced 44% by combining an inner reflector of gold with an outer reflector of water. The calculated critical mass decreases from a bare value of 21.1 to 11.9 kg for a 4-cm gold inner reflector and 15-cm water outer reflector, which represents a limiting case. However, even in this idealized situation the conservative critical mass of 11.9 kg just barely equals the 25-kw design start-of-life mission load of 12 kg of $^{244}Cm_2O_3$. On the basis of these calculations and the conservatism indicated by the Los Alamos experiment, it is concluded that no criticality problem exists for a $^{244}Cm_2O_3$ isotopic fuel power source so long as the weight of the radioisotope fuel does not significantly exceed 12 kg.

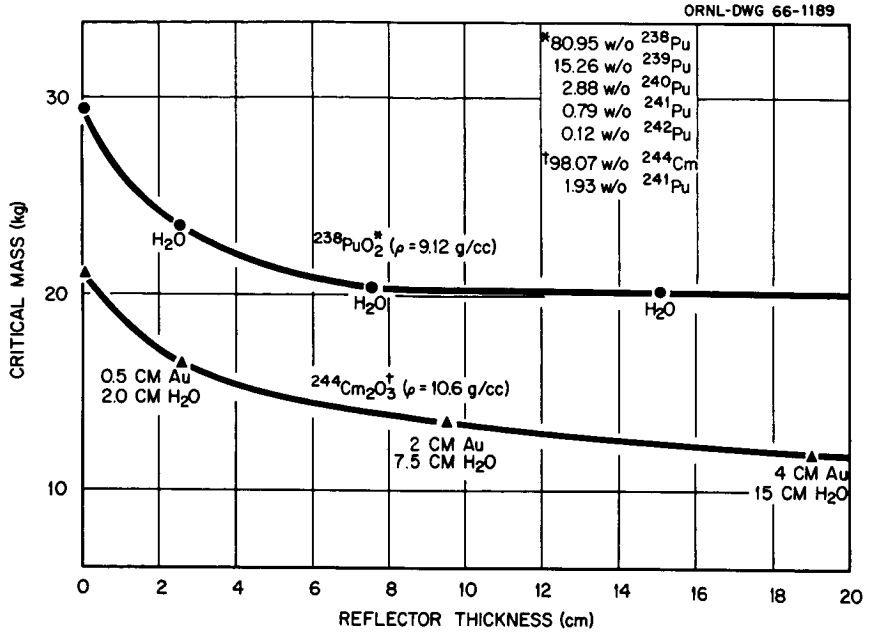

Fig. 7.2. $^{238}PuO_2$ and $^{244}Cm_2O_3$ Reflected Critical Mass.

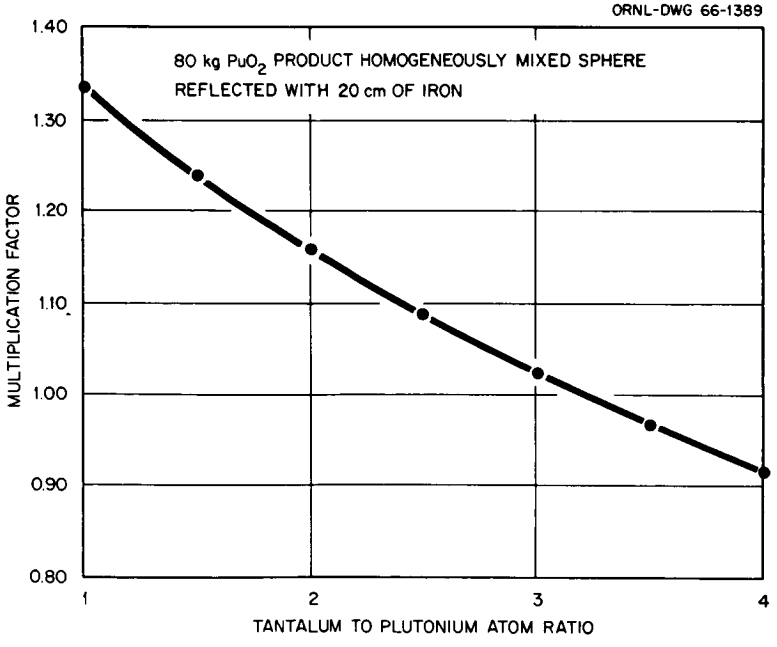

Fig. 7.3. Multiplication Factor as a Function of the Tantalum-to-Plutonium Atom Ratio.

7.2.3 Mixed Tantalum and Plutonium Assemblies

Since the $^{238}PuO_2$ 25-kw design heat source exceeds the minimum critical mass several times over, a series of calculations was performed to determine the type of assembly that could result in criticality. An infinite medium calculation performed for the design capsule shown in Fig. 5.1 (Sect. 5) yielded a multiplication factor of 0.60. This represents an upper limit on the multiplication factor that might be obtained with any possible array of intact capsules.

Calculations were performed to determine the dependence of the multiplication factor on the tantalum-to-plutonium ratio since the alloy used in the conceptual capsule design is largely composed of tantalum. The calculation model assumed 80 kg of $^{238}PuO_2$ fuel uniformly mixed with sufficient tantalum to achieve the desired tantalum-to-plutonium ratio. Spherical geometry was used with a 20-cm iron reflector. Table 7.2 and Fig. 7.3 present the results of these calculations. The critical (k_{eff} = 1) tantalum-to-plutonium ratio was calculated to be approximately 3.2, in contrast to a design value of approximately 9.

Table 7.2. Effective Multiplication Factors for Mixed Tantalum and Plutonium Assemblies

Mixture Composition	k_{eff}
Design PuO_2 capsule (infinite)	0.60
80-kg PuO_2 (20-cm Fe reflector) mixed with tantalum to give the following tantalum-to-plutonium ratio	
1	1.3355
1.5	1.2408
2.0	1.1586
2.5	1.0876
3.0	1.0244
3.5	0.9686
4.0	0.9210
9.5	0.5925

It is highly improbable that mechanical reassembly alone could result in a tantalum-to-plutonium ratio less than the critical value of 3.2. For example, in order to achieve a ratio less than this it would be necessary to assume that 70% of the fuel in every capsule puddled in one of the hemispherical end caps of the capsule and then, selectively, only end caps containing fuel were mechanically compressed into a sphere. This would yield a tantalum-to-plutonium ratio of approximately 3.20 and a marginally critical system if reflected with a reflector equivalent to 20 cm of iron. Any other less favorable mechanical reassembly of the capsules would result in a subcritical system.

It is concluded on the basis of these calculations that the only credible mechanism that could produce criticality in a 25-kw $^{238}PuO_2$ heat source with a capsule design of the type used in this study would be a massive meltdown of the fuel capsules and subsequent reassembly of the fuel in some container such as the reentry body. In that event it is probable that criticality would only introduce another heat-generation mechanism that would increase the rate of fuel vaporization. Since the design criteria require that the fuel be contained in the capsules and that there be no meltdown, criticality problems impose no design constraints.

In summary, on the basis of these calculations, it was concluded that

1. The conceptual designs for the curium heat source pose no criticality problems.

2. No possible array of the intact plutonium capsules used in the conceptual design could achieve criticality.

3. Mechanical deformation of the design mission load of plutonium capsules could not produce criticality.

4. Criticality of the plutonium capsules could be achieved only by massive meltdown and reassembly of about one-fourth the fuel.

8. REENTRY STUDIES

The normal operating procedure for the return of the heat source to the earth at the completion of its required mission life assumes the use of a controlled ferry vehicle. However, in the event of a mission abort, either during the launch phase or after the orbit is established, the radioisotope heat source will enter the earth's atmosphere in an uncontrolled fashion. Because of the large quantity of radioactive material in a 25-kw heat source, the conceptual system designs developed in this study are all based on an intact reentry of the fuel capsules under all normal and accident conditions to insure a maximum degree of safety. There are no prescribed conditions under which this emergency reentry could happen; therefore, the initial conditions were assumed to be random. For study purposes the "worst" conditions were used in selecting the final design criteria. This portion of the study was concerned with the expected range of aerodynamic heating and the necessary protection, impact velocity on the surface, cratering depths at impaction, and a broad view of the aerodynamic stability of the fuel capsules and the reentry body. The analysis presented here is broken into two main parts: the first part is a consideration of an unprotected fuel capsule and its behavior under reentry conditions, and the second part discusses a single reentry body containing and protecting the fuel capsule array.

8.1 Unprotected Fuel Capsule Reentry

The fuel capsule design, described in Section 5, is "unprotected" in the sense of thermal protection for the reentry. Ablative materials, such as graphite, ceramics, and impregnated sponge metals, for protecting individual fuel capsules during reentry may be available in the future, but at this time none of these materials are known to be able to survive a continual temperature of 2000° F (operating temperature of the capsule) in vacuum for a period of one year and maintain their reentry thermal protection properties. For the analysis, therefore, the assumption was made that the bare capsule would undergo the reentry. A schematic diagram of the fuel capsule studied and the nomenclature used in this first portion of the study are shown in Fig. 8.1

ORNL DWG 66-12255

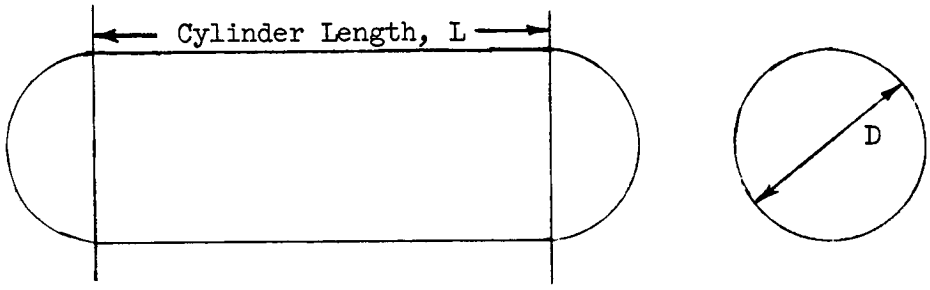

Fig. 8.1. Fuel Capsule Shape.

The impact velocity of a body on the earth's surface is given, in fps, by the relation,

$$V_{IMPACT} = \sqrt{\frac{2g_0}{\rho_0}\left(\frac{W}{C_{D,0}A_D}\right)},$$

when it is assumed that the body strikes perpendicular to the surface. The terms used in this relation are

g_0 = acceleration of gravity at surface, ft/sec^2,

ρ_0 = atmosphere density at surface, lb/ft^3,

W = body weight, lb,

A_D = drag area, ft^2,

$C_{D,0}$ = drag coefficient at surface conditions and impact velocity.

The motion of the fuel capsule could be random tumbling, but the most severe impaction would occur if the capsule descended end-on so that the drag was a minimum for that shape, and thus the ballistic coefficient was a maximum. The drag of the capsule is considered to be comprised of the drag of a sphere of diameter D plus the skin friction drag of a cylinder

of length L and diameter D. Figure 8.2 is a plot of sphere drag coefficient versus sphere Reynolds number at subsonic conditions.[60] From the data shown a minimum value of the subsonic drag coefficient C_D, defined as

$$C_D = \frac{\text{DRAG}}{\frac{1}{2g}\rho V^2 A_D} ,$$

would be a constant, 0.4, for a Reynolds number range of 10^4 to 2.5×10^5. In this expression V is the velocity (fps), g is the acceleration of gravity (ft/sec^2), and ρ is density (lb/ft^3). At a Reynolds number of 2.5×10^5 the drag coefficient drops rapidly. For the purposes of this calculation the drag coefficient for Reynolds numbers (Re) greater than this critical Reynolds number is taken to be given by

$$C_D = \frac{4}{3} \times 10^{-4}\sqrt{Re} = 0.0422\sqrt{Re \times 10^{-5}} ,$$

with

$$Re = \frac{\rho VD}{\mu} ,$$

where μ is the coefficient of viscosity, lb/ft·sec.

The skin-friction drag coefficient for the cylinder is taken to be the relation, for turbulent flow,

$$C_F = 0.074\ (Re_C)^{-0.2} = 0.0074\ (Re_C \times 10^{-5})^{-0.2} ,$$

where the cylinder Reynolds number, Re_C, is given by

$$Re_C = \frac{\rho V}{\mu} L = Re\ (L/D)$$

and satisfies $5 \times 10^5 \leq Re_C$. For $Re_C < 5 \times 10^5$ the laminar resistance relation is

$$C_F = 1.328\ (Re_C)^{-0.5} = 0.00416\ (Re_C \times 10^{-5})^{-0.5} .$$

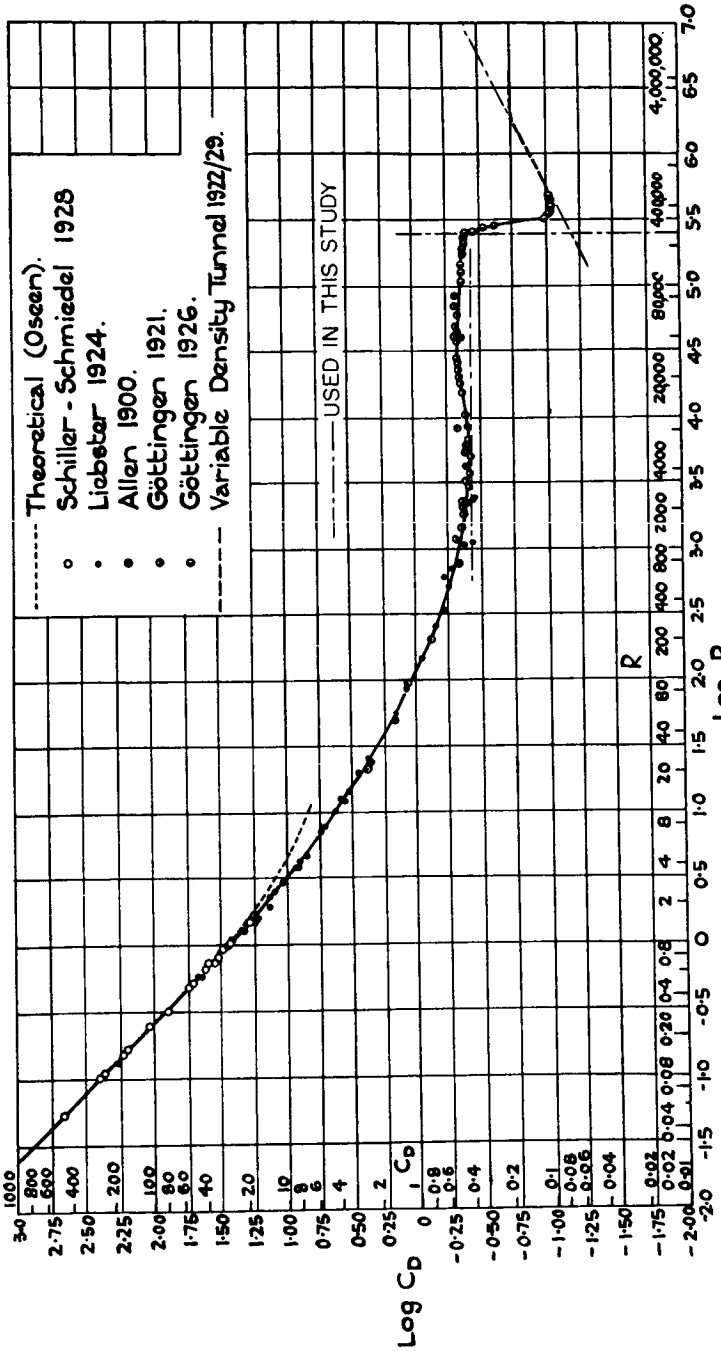

Fig. 8.2. Sphere Drag Coefficient. (From Ref. 60)

The impact velocity was computed for assumed values of the ballistic coefficient. The results of this computation, shown in Fig. 8.3, indicate that the impact velocity can reach rather severe values for nominal values of the ballistic coefficient at sea-level conditions.

Computations of $W/C_{D,o}A_D$ and impact velocity, V_{IMPACT}, were made for a range of diameters, fuel capsule densities, and L/D ratios. The results of this computation are given for a range of parameters in Table 8.1. For some configurations the impact velocity is better than 1000 fps, with a minimum calculated impact velocity of 411 fps, and it seems highly unlikely that the capsules could survive impaction upon rock at these velocities.

The heat transfer to the capsule, based on a constant wall temperature of 2000°F and only convective aerodynamic heating, was determined for the stagnation point by means of approximate relations for cold-wall heating and then corrected by the factor

$$1 - \frac{2gC_pT_w}{V^2},$$

where

T_w = capsule wall temperature, 2460°R,
C_p = heat capacity of air, ft·lb/lb·°R,
V = velocity of reentry, fps.

This correction factor is an approximation to the temperature differential

$$\frac{T_{a,w} - T_w}{T_{a,w}},$$

where $T_{a,w}$ represents the adiabatic wall temperature. At these flight velocities $T_{a,w}$ is nearly equal to the free-stream stagnation temperature, which in turn is approximated by $V^2/2gC_p$.

The cold-wall heating is given in the form of a nomogram for laminar convective heating and is shown in Fig. 8.4. This nomogram was developed from data from Ref. 61.

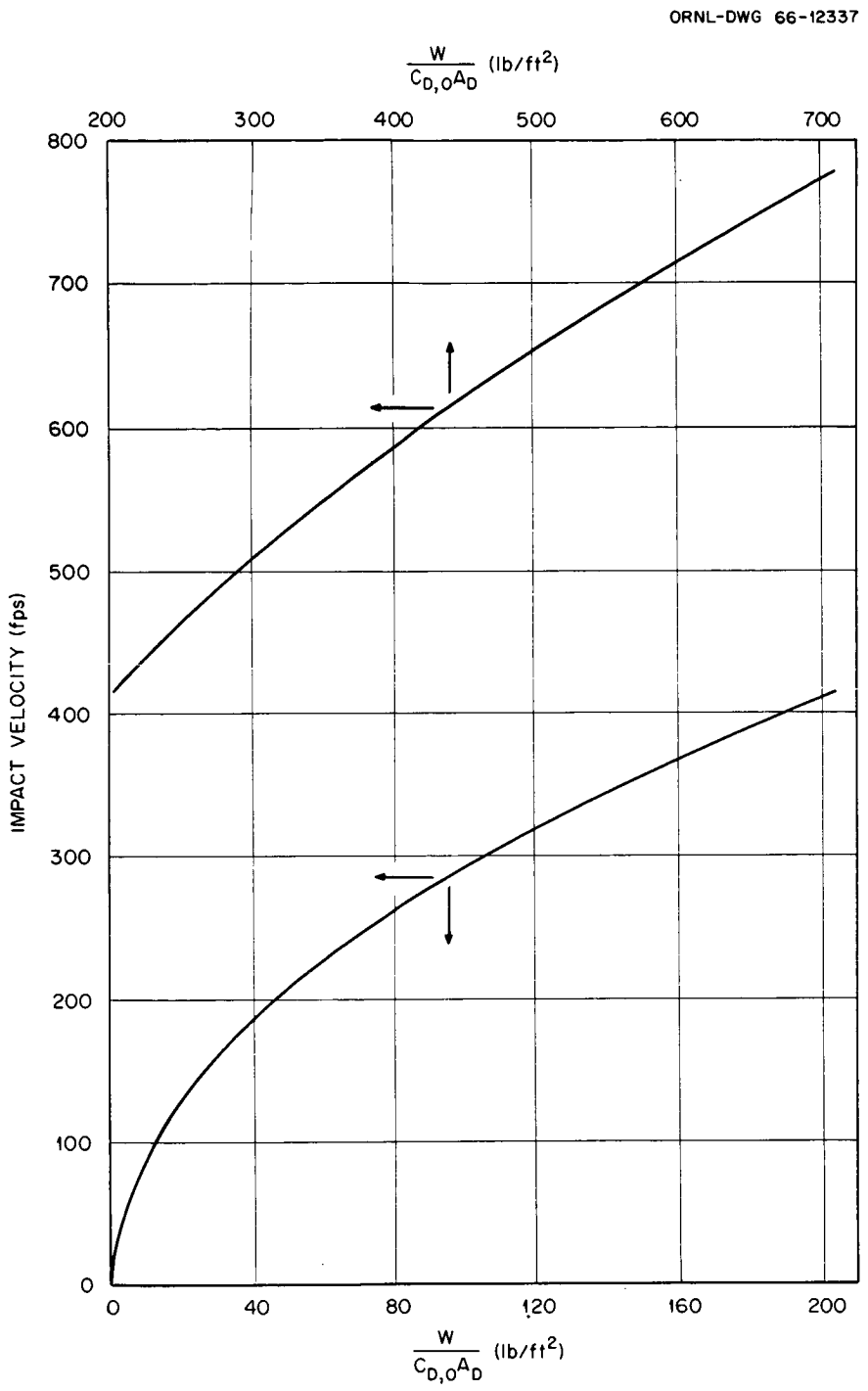

Fig. 8.3. Impact Velocity Versus Subsonic Ballistic Coefficient.

Table 8.1. Fuel Capsule Reentry Conditions

L/D	W/C_DA (lb/ft^2)		V_{IMPACT} (fps)		q_{max} (Btu/sec)		Q (Btu)	
	0.875 in.[a]	1.750 in.[a]	0.875 in.	1.750 in.	0.875 in.	1.750 in.	0.875 in.	1.750 in.
			Fuel Capsule Density = 0.243 lb/in.^{3}					
2.0	196	1040	411	947	11.0	72.3	539	3540
4.0	935	1493	898	1134	24.3	86.6	1190	4240
6.0	1127	1864	985	1267	26.4	95.2	1290	4660
			Fuel Capsule Density = 0.412 lb/in.^{3}					
2.0	333	1628	536	1184	13.4	88.9	655	4430
4.0	1510	2360	1141	1426	30.8	115.0	1520	5610
6.0	1838	2969	1258	1599	33.9	118.0	1660	5760

[a]Fuel capsule diameter, D.

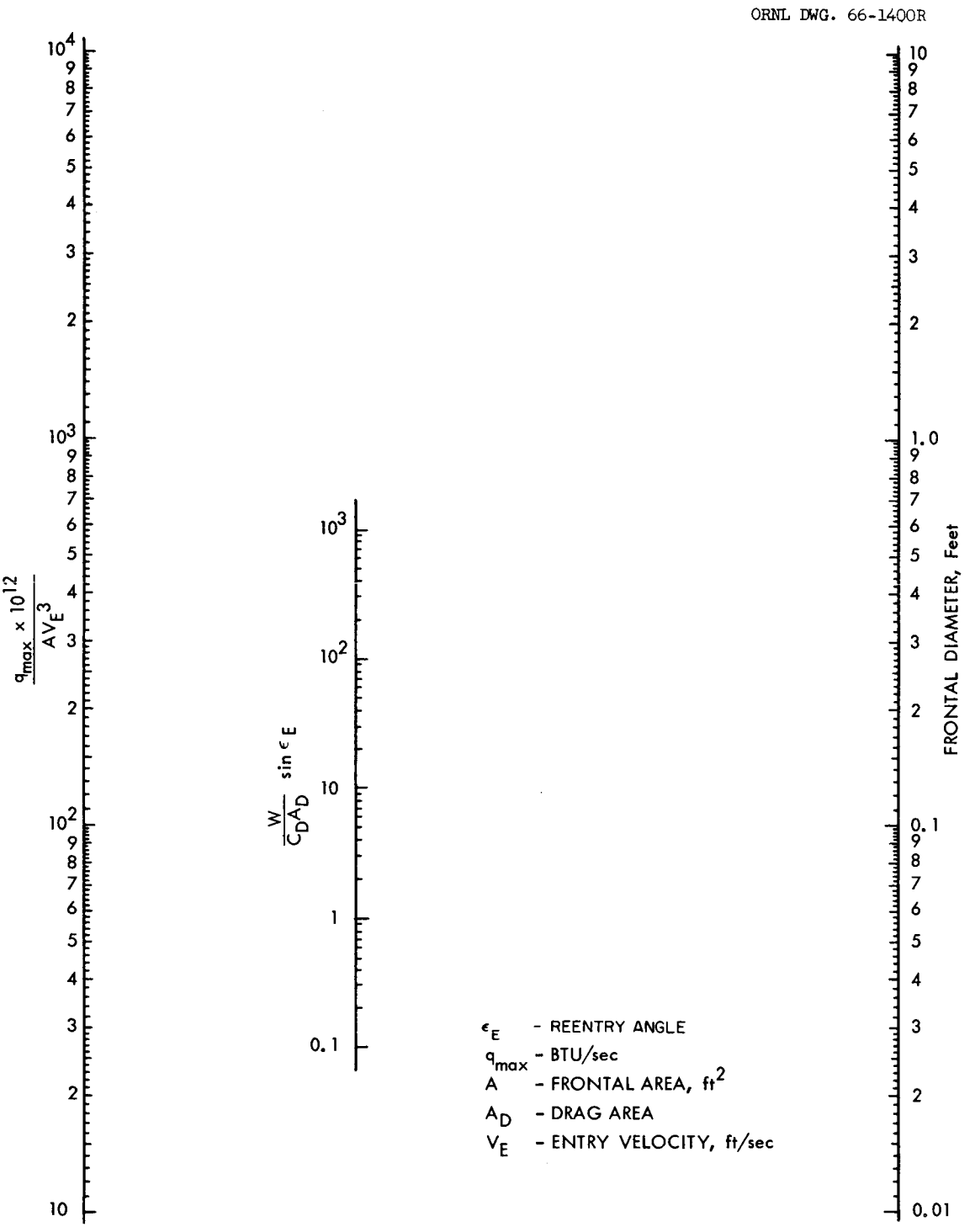

Fig. 8.4. Nomogram for Determining Maximum Heating Rate.

At the time of maximum heating rate, the reentry velocity would not be significantly different (~85%) from the initial velocity; that is, nearly 26,000 fps. For this velocity the correction factor would be 0.95. For the capsule descending end-on (maximum W/C_DA), an estimate of the hypersonic (W/C_DA) of 50% of the subsonic value, and a 0° angle of attack, the maximum heat input is determined from the nomogram. Over the significant heating portion of the trajectory the angle of flight is constant and therefore equal to the initial reentry angle.

It is difficult to picture any accident abort, from an orbit, that would give the fuel element an initial entry angle of more than 4 to 5°, and the angle would probably be less. The maximum heating pulse would not be very large, but the total amount of heat acquired by the capsule would be high. This total amount of heat can be estimated by means of the relation

$$Q = \frac{111{,}000}{V \sin \epsilon_E} \frac{q_{max}}{A} A ,$$

where

Q = total heat input, Btu,
A = frontal area, ft^2,
ϵ_E = reentry angle.

The values of q_{max}/A and Q listed in Table 8.1 are overestimates.

The temperature rise of the capsule, with the internal heat generation and the heat radiation to space ignored (these are in the direction of being compensating factors), is calculated from

$$T_w = 2460 + \frac{Q - Q_L}{W_m C_t} ,$$

where

Q_L = heat lost by conduction, radiation, etc.,
W_m = weight of the metal in the fuel capsule,
C_t = average thermal capacity of capsule materials.

For a particular capsule, with a length of 10.564 in., a diameter of 2.696 in., and a metal weight of 15 lb, the $W_m C_t$ values are approximately 0.57 Btu/°R at 2000°F and 0.84 Btu/°R at 4940°F.

From Table 8.1 at an L/D of 4.0 and a diameter of 1.750 in., the total heat input, Q, is 4240 Btu. If there were no heat losses, an estimate of temperature rise, is given by

$$\Delta T = Q/W_m C_t = 4240/0.84 = 5000°F .$$

However, at 4400°F the heat loss by radiation to space is estimated to be equal to the maximum heating rate of 86.6 Btu/sec (Table 8.1), so the capsule surface temperature cannot rise above about 4400°F.

From the above analysis the conclusion can be drawn that unprotected individual fuel capsules of reasonable design cannot be expected to survive reentry and impaction and remain intact. As noted previously, future developments may provide a protective material that can be applied directly to individual fuel capsules without introducing large weight and temperature-drop penalties and which will maintain its integrity over long periods at high temperature in a space vacuum. However, such materials are not now available, and the use of a single reentry body to contain the entire heat source seems much more attractive at this time from a reliability and safety standpoint.

8.2 Reentry Body Analysis

The reentry body in the final emergency mode must be functionally passive to provide maximum assurance that the fuel block contained in the reentry body will remain intact. No final dependence of safe operation during an anomaly should be placed in an active device such as the opening of a parachute. The normal mode of operation calls for a controlled vehicle to return the heat source to earth, and the following discussion pertains only to an abort condition where the heat sink returns to the surface without active control.

Two main protection features must exist in such a body:

1. It must protect the heat source and itself from the aerodynamic effects of reentry.

2. It must allow the fuel block to survive impaction upon the earth's surface.

It must have, therefore, a low ballistic coefficient, adequate thermal protection, a high degree of inherent aerodynamic stability (any initial body orientation is possible), and sufficient energy absorption and low terminal velocity to alleviate impact conditions. These are also the conditions that any Mars' mission package must satisfy. Of the published studies on a Mars' mission[62] a concensus of results shows that, of the various shapes imaginable for a reentry body, the most promising are the blunted cone,[63] the spherical dish, and the tension shell concept. The spherical dish is a special case of the blunted cone and was not considered separately in this initial study. Exploratory aerodynamic testing of the tension shell[64] has shown that it has a larger total surface heat input than an equivalent blunted cone and that it is subject to erratic shock behavior that leads to instability problems. Thus the blunted cone was chosen as the reentry body shape for the conceptual design study.

For purposes of initial design effort, a cone angle of 60° and a cone nose radius of 15 in. were chosen. These values are to be used in the phase II study as the first step in an iterative design process for the selection of the optimum blunted cone. This parametric study thus provides guidance for the conceptual heat source system designs.

The impact velocity expected can be determined from Fig. 8.3. Initial estimates of the subsonic ballistic coefficient for the reentry body based on the fuel block layout shown in Section 9 place it in the range of 60 to 100; this gives impact velocities in the range of 240 to 300 fps. It is probable that the problem of structural integrity at impaction can be solved for this range of velocities.

The depth of cratering upon impact was analyzed with the empirical Petry formula:[65]

$$P = \frac{K}{144} \frac{W}{A} \log \left(1 + \frac{V^2_{IMPACT}}{215,000}\right) ,$$

where

P = penetration depth, ft,

W = reentry body weight, lb,

A = frontal area, ft^2,

and K is a coefficient dependent upon soil characteristics and missile nose geometry. The usual range is 1.0 to 7.0; the smaller the K value, the harder the surface and the broader the missile nose.

Figure 8.5 is a graph of the cratering depth of the reentry body for a range of ballistic coefficients and cone angle. The effect of the cone angle enters through the variation in subsonic drag coefficient, as shown in Fig. 8.6, and by rearrangement of the Petry formula to the form

$$P = \frac{K}{144} C_D \frac{W}{C_D A} \log \left[1 + 4\left(\frac{W}{C_D A}\right) \times 10^{-3}\right] .$$

In Fig. 8.5 the variations of cratering depth for constant frontal loading at a drag coefficient equivalent to an 80° cone angle are also given. This graph clearly shows that low ballistic coefficients are desired, but even more important is the fact that the penetration depth for a K value of 7.0 and maximum $W/C_D A$ of 100 is less than 1 ft. It was therefore concluded that the reentry body used in the conceptual designs will not bury itself under impaction, and the nonburial criterion for maximum safety is satisfied.

The next portion of the analysis was to determine the amount of ablative material needed to protect the reentry body from thermal heating during a high altitude or orbital altitude abort reentry. This calculation consisted of determining the maximum heating rate per unit area and total heat input per unit area at the stagnation point of the body for various assumed initial entry angles and an initial entry velocity of 26,000 fps. These calculations were performed by NASA-Langley Research Center (P. J. Bobbitt) for a range of hypersonic ballistic coefficients and the 60° blunted cone used in the conceptual system designs. The results are listed in Table 8.2 and shown in Figs. 8.7 and 8.8. A hypersonic drag coefficient, $C_{D,H}$, of 1.50 was used in this investigation.

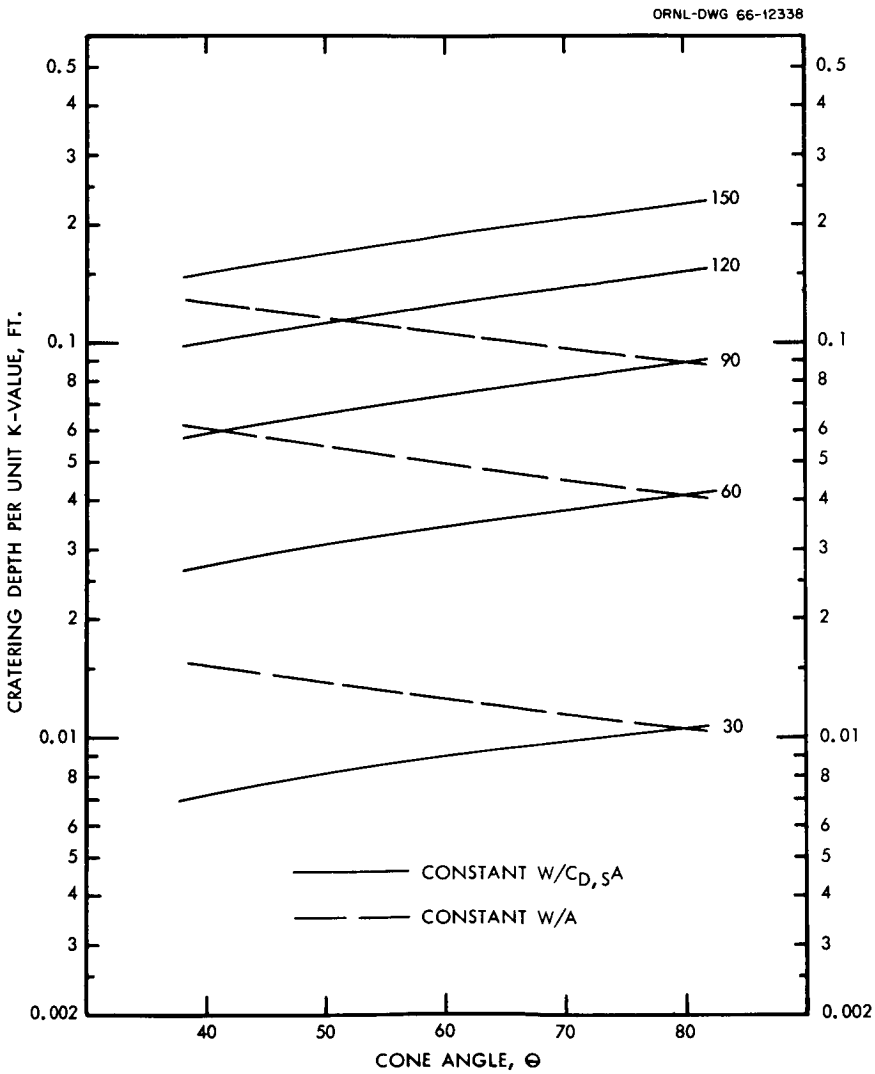

Fig. 8.5. Cratering Depth of a Reentry Body.

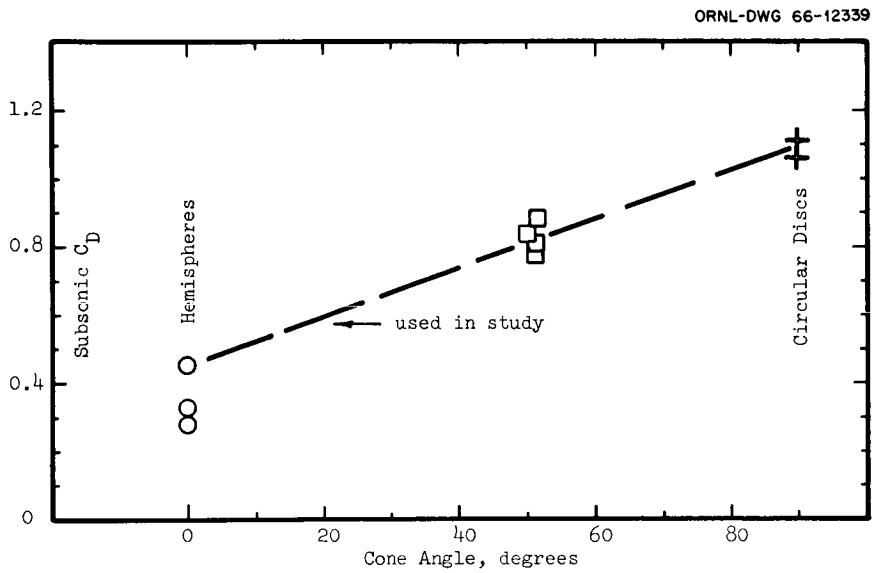

Fig. 8.6. Blunted-Cone Subsonic Drag Variation.

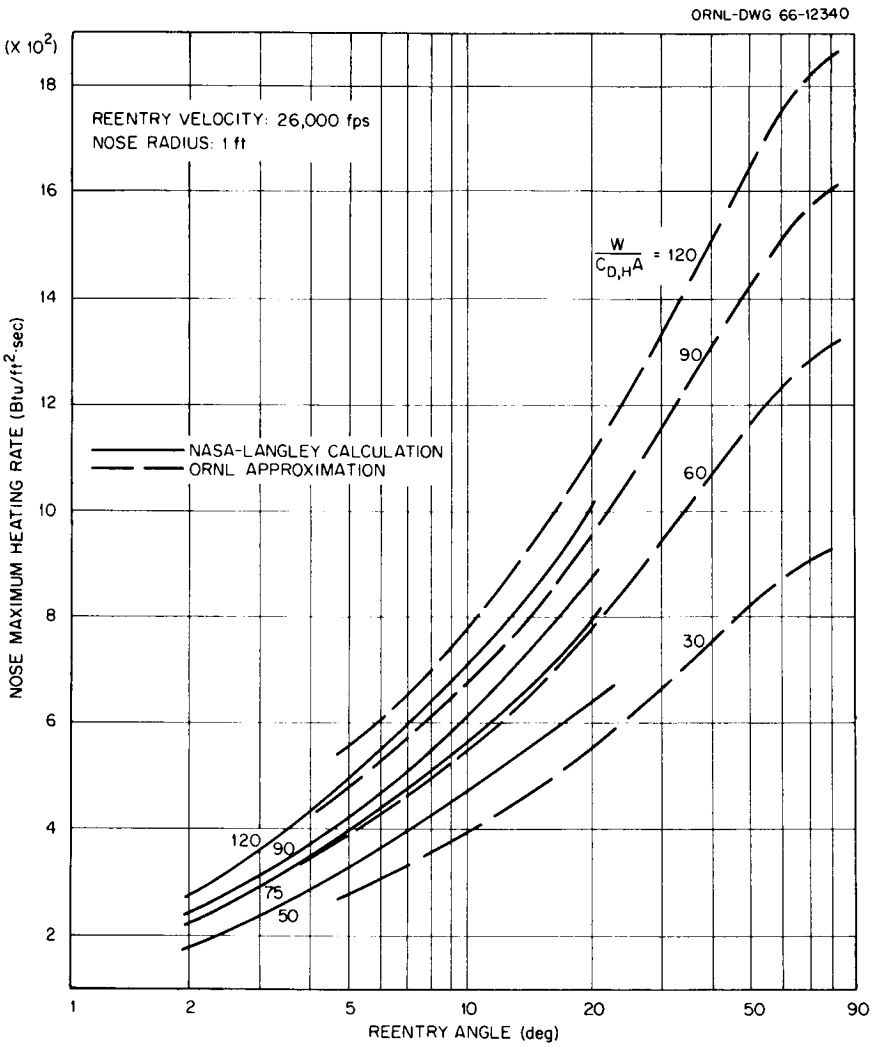

Fig. 8.7. Reentry Body Heating Rates.

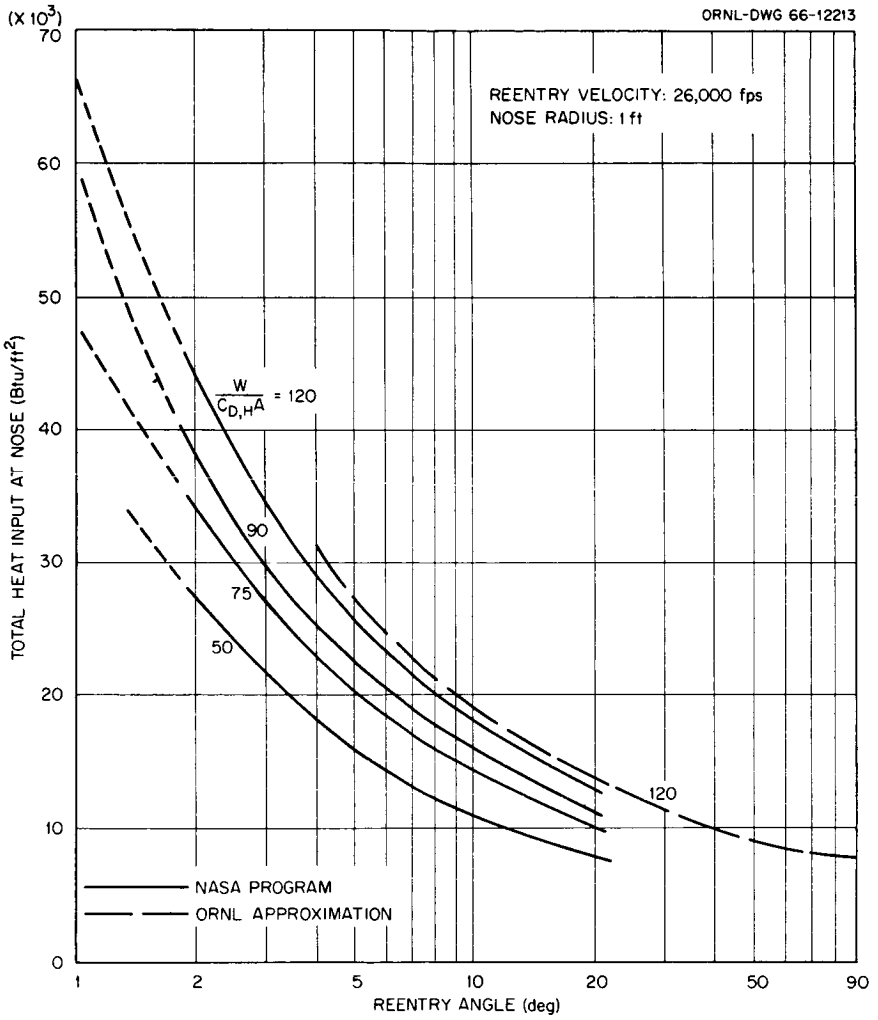

Fig. 8.8. Reentry Body Total Heat Input.

Table 8.2. Trajectory Calculations at Stagnation Point

Nose radius = 1.0 ft

W/C_DA	Initial Angle (deg)	Maximum Heating Rate (Btu/sec.ft^2)	Total Heat Input (Btu/ft^2)	Maximum Deceleration (ft/sec^2)	Maximum Dynamic Pressure (lb/ft^2)
50	20	641	8,305	1950	3027
	15	560	9,545		2292
	10	456	11,656	990	1536
	6	380	13,929		1081
	3	238	21,573	314	497
	2	184	27,264	257	403
	1	156	54,094[a]	264	404
75	20	787	10,191	1950	4550
	10	559	14,310	990	2305
	3	290	26,623	315	741
	2	222	33,952	257	600
	1	192	75,257[a]	264	607
90	20	867	11,177	1950	5470
	10	613	15,696	990	2772
	6	467	20,700	597	1680
	3	318	29,273	315	887
	2	242	37,496	257	722
	1	212	84,654[a]	264	734
120	20	999	12,908	1950	7260
	10	708	18,133	990	3670
	6	543	23,464	597	2225
	3	365	33,950	315	1174
	2	276	43,806	257	956
	1	243	105,794[a]	264	985

[a]Reentry body "skips" at this initial entry angle. Total heat input includes the amount during the skip portion of the trajectory.

At orbital altitudes and velocities it is assumed that there is insufficient fuel to permit an abort impulse that would lead to a reentry angle greater than 4 to 5° (as in the case of the fuel capsule). The maximum heating rate is relatively low at these angles but the total heat input is large. Estimates of thermal protection weight (as supplied by NASA-Langley) are given in Table 8.3.

Table 8.3. Ablative Protection Requirements

Charring ablators assumed

W/C_DA	Total Weight (lb)	Weight of Ablative Protection Required (lb/ft^2)	
		At Nose	At End of Flare
120	145	8.5	4.3
90	118	7.5	3.5
75	105	6.9	3.0
50	83	5.5	2.4

These thermal protection weights can be compared with protection requirements estimated by Swann,[66] as shown in Fig. 8.9 (except for the Langley computed line, this figure is a reproduction from Ref. 66). The rates of heating and total quantities of heat experienced at an entry angle of 1° are shown on Fig. 8.9. The comparison is favorable and indicates that progress has been made in reducing thermal protection weights required for a given mission. It is also clear from the graph that the protection required for the large total heat input can also adequately safeguard the vehicle from the higher heating rates but smaller total heat loads that are obtained at larger entry angles if the ablator can remain intact under the higher dynamic loads.

In summary, for purposes of maximum safety during an emergency abort of the heat source the fuel capsules can be embodied in a reentry shape that provides impaction integrity and protection from the aerodynamic forces and heating of hypersonic reentry.

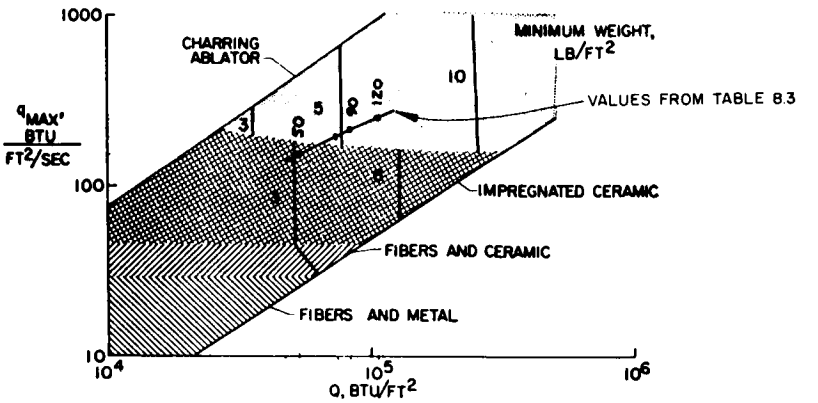

(a) Thermal protection weight requirements; no erosion of char.

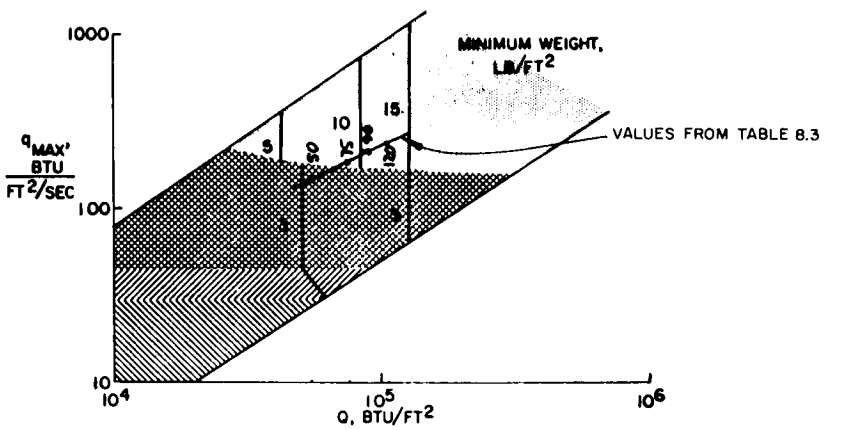

(b) Thermal protection weight requirements; maximum char thickness = 0.10 in.

Fig. 8.9. Thermal Protection Weight Requirements. (From Ref. 66)

9. HEAT TRANSFER

The design approaches to methods for transferring heat from the fuel block to the Brayton-cycle working fluid were largely determined by the following criteria:

1. The fuel capsule surface temperature was not to exceed 2000°F.
2. In the event of a mission abort, the fuel block was to be ejected from the spacecraft and reenter in a package that was separate from the rest of Brayton-cycle power system.
3. In the event the Brayton-cycle power conversion system became inoperative, the fuel block was to be able to dissipate all its heat to space without exceeding the 2000°F capsule temperature limitation.
4. The fuel block and reentry body combination was to have a low enough ballistic coefficient and frontal loading to preclude the possibility of burial upon impact in a medium like dry sand in the event of a random reentry.

The following methods of transferring heat from the fuel to the Brayton-cycle working fluid were considered:

1. liquid metal heat exchange loop,
2. direct cooling with Brayton-cycle working fluid (argon),
3. radiant heat transfer,
4. heat pipe, and
5. conduction by mechanical contact of heat exchanger and fuel block.

Preliminary evaluations for complexity, fabricability, operational simplicity, handling, and reliability led to the general conclusions that

1. Schemes involving liquid metals, except as evaporative material in a heat pipe concept, offered no advantage over simpler methods in the temperature range of interest (1500–2000°F), and the introduction of a secondary heat transfer loop would reduce the overall system reliability.
2. Any method of conduction through mechanical contact would have to be treated as radiant heat transfer because of the difficulty in assessing the amount of area in good thermal contact and guaranteeing that this contact would be maintained throughout the mission.
3. The use of a heat pipe for the normal operating mode offered no large advantage in the way of making a more compact fuel block because

the fuel block area requirements for maintaining a 2000°F or less capsule temperature are dictated by the temperature drop between the back side and front operating side of the capsule, as well as by the temperature drop between the operating surface and the heat exchanger. In addition, the total fuel block and reentry body volume was determined by the need for a ballistic coefficient of 100 or less and not by heat exchanger area requirements.

The concept of using a modified form of the heat pipe for dumping the entire heat load of the source to space in the event the Brayton-cycle power conversion system became inoperative offered system reliability advantages; it is described in Section 10. The above phase I preliminary evaluation and conclusions left direct cooling and radiant heat transfer as the methods of most interest for fuel block–heat exchanger arrangements. Direct cooling would provide a small-volume light-weight system and minimum capsule surface temperatures; however, it might be operationally objectionable because of disconnect problems. Heat transfer calculations were carried out in enough detail to insure that the conceptual system designs developed in the phase I portion of the study would not, upon more rigorous analysis in phase II, result in excessive capsule temperatures or unachievable heat exchanger designs.

9.1 Heat Transfer Calculational Models

A general analysis of heat transfer and fluid flow for the argon coolant was developed for cooling the fuel capsules by direct contact with the fuel block or indirect cooling through an intermediate heat exchanger, as would be the case with radiant heat transfer. Both cooling methods have the same gas-film behavior, and therefore a common solution was generated with the following basic assumptions:

1. Reynolds number greater than 10,000,
2. specific heat constant,
3. Fanning friction inversely proportional to 5th root of the Reynolds number,
4. combined inlet and exit pressure losses 10% of the total allowable pressure drop across the heat exchanger,

5. a mass flow rate of 1080 lb/hr,
6. a mean gas pressure of 1900 lb/ft^2.

The analytical expressions for the Reynolds number, heat transfer coefficient, and gas flow path length were determined to be

$$Re = \frac{4320}{\mu_B \beta},$$

$$h = \frac{0.75\beta^{0.2}\mu_S^{0.2}}{A_c}\left(\frac{T_B}{T_S}\right)^{0.8},$$

$$L = \frac{4.16 \times 10^6 \, A_c^3 \, (\Delta P/P)}{\beta^{1.2}\mu_B^{0.2}},$$

where

Re = Reynolds number,
μ = viscosity, $lb_m/ft \cdot hr$,
β = wetted perimeter of flow area, ft,
h = heat transfer coefficient, $Btu/hr \cdot ft^2 \cdot °F$,
T = absolute temperature, °R,
A = area, ft^2,
L = gas flow path length, ft,
ΔP = allowable pressure drop across component, lb_f/ft^3,
P = mean absolute pressure in component, lb_f/ft^2.

The subscript B indicates bulk temperature properties; subscript S, surface temperature properties; and the subscript c, cross-sectional value.

A calculational model heat exchanger design that was analyzed had a radiantly heated surface and internal gas coolant passages. The total wetted perimeter of the gas passages was utilized to transfer 25 kw of heat to the argon gas with an inlet temperature of approximately 900°F and an outlet temperature of 1500°F. It was assumed that no temperature gradient existed between the heat deposition surface and the internal passage surface area. A parametric examination of possible gas flow passage configurations was made, and the results are given in Table 9.1. The

Table 9.1. Gas-Side Heat Exchanger Arrangement

q = 25 kw
Exit temperature = 1500°F

Type of Coolant Passage	Passage Dimensions (in.)	Number of Parallel Passages	Number of Coolant Passes	Mean Surface Temperature (°R)	Fractional Pressure Loss (ΔP/P)	Flow Passage Pitch (in.)	Heat Exchanger Surface (ft)	
							Width	Length
Rectangular	1 3/4 × 7/8	5	3	2037	0.0484	2.38	3.13	4.99
		5	3	2037	0.0565	1.88	2.50	5.01
Rectangular	7/8 × 1 3/4	5	3	2037	0.0673	1.00	1.66	4.97
Square	7/8 × 7/8	10	3	2037	0.0600	1.19	3.28	3.54
Circular	1/2 (ips)	20	5	2120	0.0573	1.20	10.0	0.97
		20	3	2120	0.0465	1.20	6.00	1.45
		20	1	2120	0.0357	1.00	2.0	4.065
		20	1	2043	0.0600	1.00	2.0	6.83
Circular	3/4 (ips)	16	1	2046	0.03	1.05	1.40	8.95
		16	1	2046	0.03	1.30	1.73	8.95
		15	1	2016	0.04	1.30	1.63	10.63
		10	3	2000	0.0635	1.05	3.15	3.93
Circular	5/8 (BWG-20)	24	1	2080	0.0568	0.625	1.25	5.28
		24	1	2080	0.0568	0.875	1.75	5.28
		24	1	2065	0.0600	0.825	1.25	5.58
		24	1	2065	0.0600	0.875	1.75	5.58
Circular	5/8 (BWG-18)	25	1	2102	0.0600	0.625	1.29	4.68
		25	1	2102	0.0600	0.875	1.81	4.68
Circular	3/4 (BWG-14)	22	1	2057	0.0600	0.750	1.38	6.10
		22	1	2057	0.0600	1.000	1.83	6.10
		22	1	2080	0.0555	0.750	1.38	5.59
		22	1	2080	0.0555	1.000	1.83	5.59
Circular	7/8 (BWG-18)	17	1	2040	0.0347	0.875	1.24	8.72
		17	1	2040	0.0347	1.125	1.59	8.72
		14	1	2024	0.0600	0.875	1.02	10.63
		14	1	2024	0.0600	1.125	1.31	10.63
		17	1	2075	0.0300	0.875	1.24	7.54
		17	1	2075	0.0300	1.125	1.59	7.54
		16	1	2112	0.0300	0.875	1.24	6.76
		16	1	2112	0.0300	1.125	1.59	6.76
Circular	7/8 (BWG-12)	20	1	2092	0.0400	0.875	1.46	6.02
		20	1	2092	0.0400	1.125	1.87	6.02
		20	1	2092	0.0400	1.375	2.29	6.02

mean surface temperatures range from 350 to 500°F above the mean gas temperature of 1200°F. The friction losses as a function of pressure drop vary from 3 to 7%, as specified in the heat exchanger design guidelines (Sect. 1). A compromise between friction loss, mean surface temperature, and gas flow path length governs the selection of the particular heat exchanger configuration. Generally, a heat exchanger of ten parallel passages with three coolant passes was selected as the design. This selection gave 4 ft of tubing per pass, a fractional pressure drop of about 0.06, and a mean surface temperature of approximately 1540°F. The selected heat exchanger combination was integrated with heat block designs to form components of the system designs discussed in Section 10.

Since ^{244}Cm was expected to have the highest temperature drop through the capsule because of its higher power density, it was used in the calculational model to determine the fuel block temperature profile. The model was an infinite-length curium fuel capsule inserted in a tubular capsule holder. The fuel capsule had the standard multiple-layer construction, as described in Section 5, with an outside diameter of 1.598 in. The average heat generation rate was assumed to be 10% greater than the minimum requirements for a beginning-of-life capsule to compensate for expected heat losses, and this rate existed over the entire capsule length. The problem was thus reduced to a two-dimensional heat transfer problem, which was solved by relaxation techniques on an IBM 7090 computer. The tubular capsule holder was assumed to be made of a superalloy with a 1/16-in. wall thickness. The tube radiated from one-half the holder surface, and the remaining surface was insulated. The radiative surface was assumed to see an average receiver temperature of 1350°F, and the surface emissivities and/or absorptivities were assumed to be 0.8, which is consistent with the properties of the iron titanate coating used in the conceptual capsule designs. Average geometry factors were assumed, and no area amplification (finning) was used in the temperature distribution calculation. The results obtained with this model are shown in Fig. 9.1. The radiating surface temperature range was 1740 to 1850°F, whereas the T-222 alloy containment shell maximum temperature was 1924°F. The pressed oxide pellet temperatures were in the neighborhood of 1900 to 1930°F at the metal-oxide interfaces.

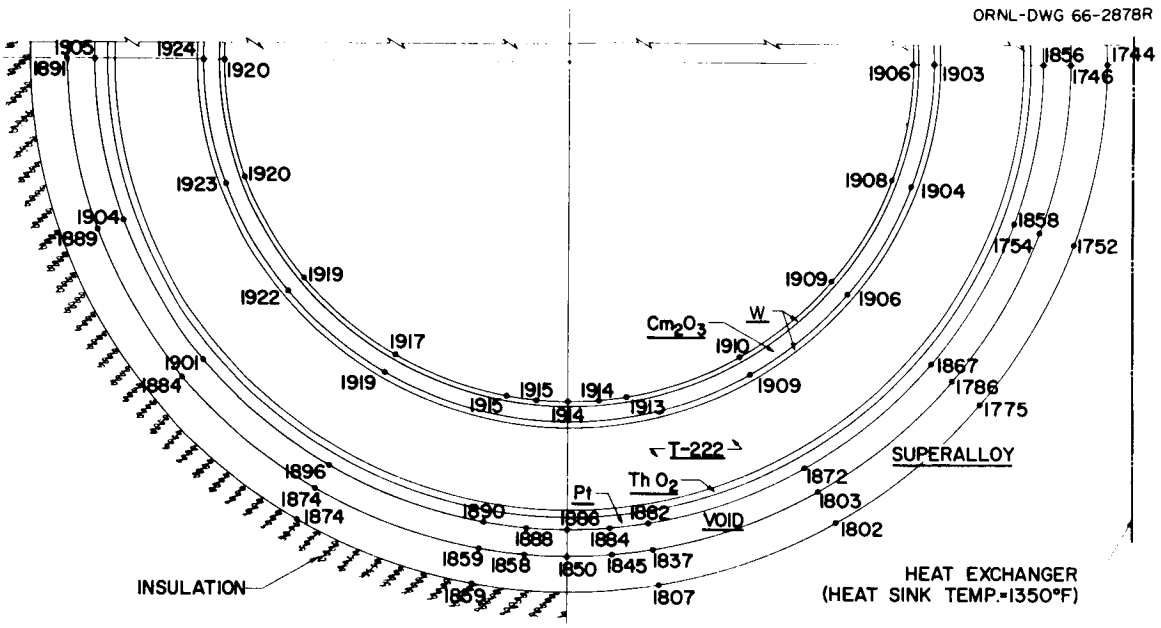

Fig. 9.1. Temperature Profile of Typical Curium Capsule. Temperatures are in °F.

Most of the heat would be transferred by conduction from the vicinity of the capsule opposite the radiating surface. A small fraction of the heat would be radiated across the internal gas storage volume, but it would not be significant. A check was made by filling the void in the model with metal, and the analysis showed approximately 10°F less for the maximum T-222 containment shell temperature.

Radiation heat transfer of 25 kw was first estimated for average black-body radiating and receiver temperatures. Then, an all inclusive interchange efficiency factor was introduced as a combined variable for the geometrical factor, emissivities, absorptivities, reflection, and re-radiation from inactive surfaces. The results are shown in Fig. 9.2 for the mutual influence of the parameters. Based on values determined from the previous models for average gas side and fuel block temperatures, Fig. 9.2 shows that at a receiver (gas side heat exchanger) temperature of 1550°F, a radiator (fuel block) temperature of 1800°F, and an interchange factor of 0.7, approximately 7 ft^2 of fuel block area would be required to transfer 25 kw to the gas heat exchanger. At an average fuel block temperature of 1700°F, approximately 13 ft^2 would be required for the same conditions. This analysis gave assurance that there would be sufficient fuel block heat exchange area because of the large number of capsules involved to stay within the 2000°F capsule temperature limitation without resorting to extended-surface fuel block designs.

9.2 Fuel Block and Capsule Arrangements

The capsule design investigations provided a table of suitable capsule dimensions and number of capsules to fulfill stated criteria. The various combinations of size and number of capsules were made into layout drawings to establish physical dimensions of the fuel block. In the final system concepts (Sect. 10) the fuel block had to be incorporated into a reentry body design so that emergency reentry modes could be accommodated, and this was considered in arriving at acceptable arrangements. It was assumed for the purpose of the layouts that all capsules were to be installed in superalloy tubular holders with a 1/16-in. wall thickness and a 3/32-in. diametrical clearance. It was decided to use tubular holders

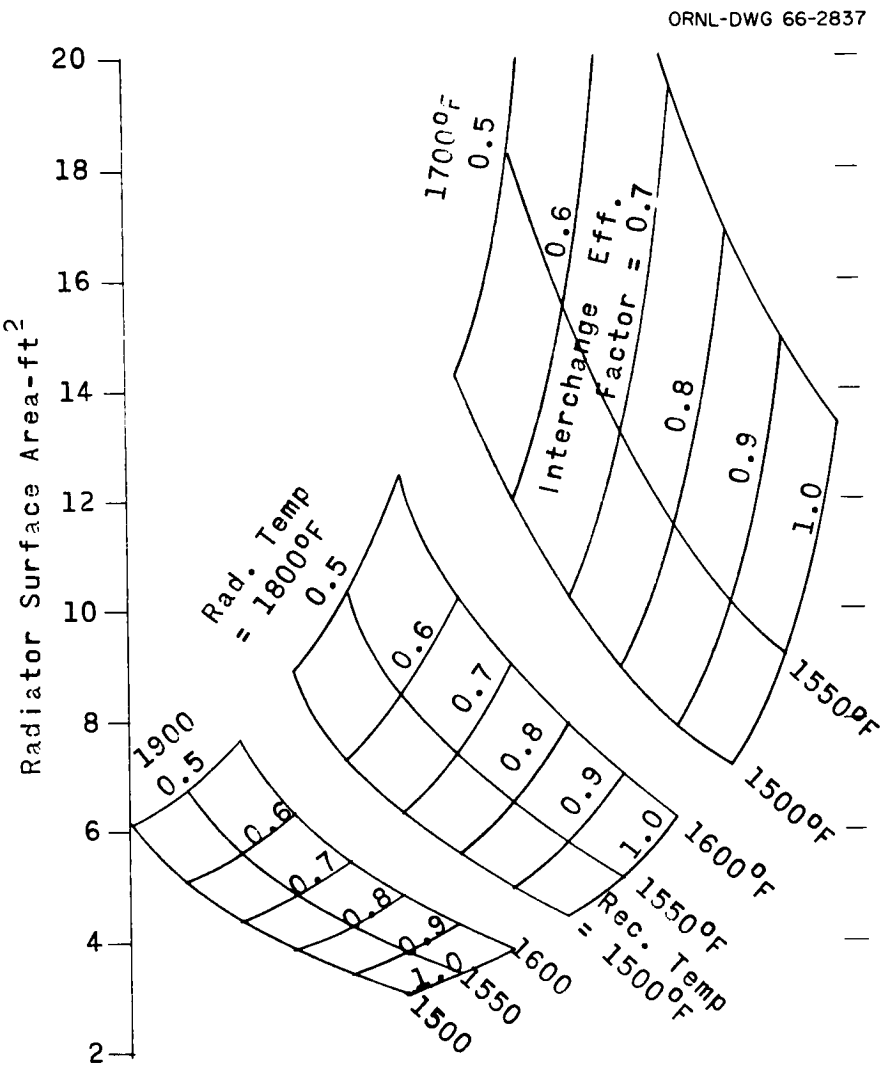

Fig. 9.2. Radiator Surface Area Requirements for a 25-kw Heat Source.

because, at operating temperatures, the outer platinum layer of the capsule would not have sufficient strength to permit a direct clamping arrangement. The holders would also facilitate assembly of the source and would be expected to provide adequate reentry heating protection on the backside of the reentry body where the heating rate is low. The supporting structure for these holders to withstand reentry forces was not included in the layouts or weight summaries discussed later.

The configuration of capsules and holders was incorporated into a reentry body shape of a blunted cone with a spherical nose having a 1-ft radius (Sect. 8). The various layouts obtained for the tubular capsule holder concepts were reviewed, and the vehicles with minimum projected diameter were determined for each fuel form by an iterative process, as indicated in Table 9.2. The minimum diameter reentry bodies were expected to give minimum volume systems for which nuclear radiation shields would have to be provided. Consequently, the total lift-off weight (reentry body plus shield) was anticipated to be a minimum when the reentry body diameter was a minimum.

The minimum reentry body sizes were analyzed, and weights were calculated for the following items:

1. capsule,
2. capsule holder,
3. ablative protection, based on 8 lb/ft^2 (Sect. 8) of frontal surface area,
4. insulation, based on 1 in. of Superinsulation with a density of 20 lb/ft^3 (Sect. 9.3) between the reentry body shell and the capsule tube sheet,
5. reentry body structure, based on 20 lb/ft^2 of projected area (NASA-Langley estimate), and
6. heat sink (100 lb BeO for all reentry bodies).

The corresponding weights and projected diameters were combined with an estimated thermal drag coefficient of 0.89 to obtain the terminal ballistic coefficient (W/C_DA) for the various reentry body designs.

The first capsule configuration that was investigated was a linear array of adjacent rows of capsule holders at the base of the conical section of the reentry body, as shown in Fig. 9.3. A cone angle of 60° was

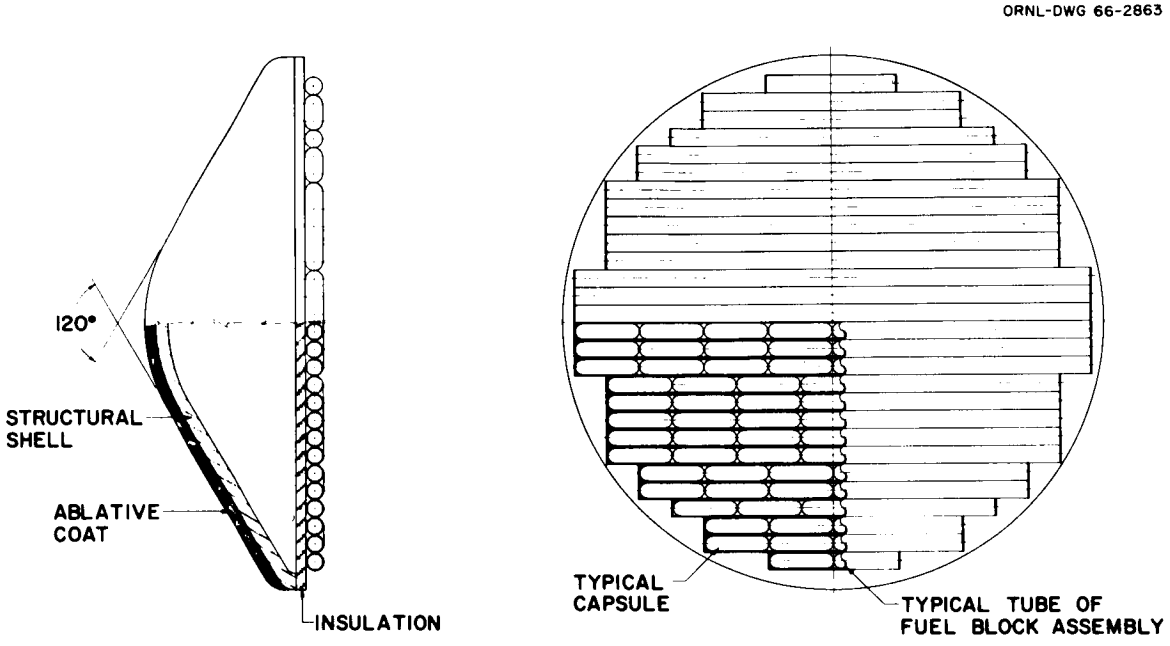

USABLE WITH:
ROTATING REENTRY BODY CONCEPT
INCLINED REENTRY BODY CONCEPT
SURFACE TENSION REFLUXING CONDENSER CONCEPT
FOLDING HEAT EXCHANGER CONCEPT

Fig. 9.3. Reentry Body for a Plane Fuel Array.

tentatively selected (Sect. 8), as indicated in the figure. The essential components are listed as the ablative coating, structural shell, insulation, tubular capsule holders, and fuel capsules. Also included are references to conceptual systems discussed in Section 10.

A summary (Table 9.2) for a $^{238}PuO_2$ capsule stress-rate safety factor of 2.5 illustrates the variations in the diameter, weight, and terminal ballistic coefficient found in these typical investigations. The weight of the fuel capsules would be approximately 1400 lb, which is approximately 60% of the total reentry body weight. The column of remarks in the table refers to Fig. 5.19 in Section 5. Generally, the minimum volume of capsules provided the reentry vehicle with the minimum projected diameter but gave the largest terminal ballistic coefficient for any constant capsule stress-rate safety factor.

Table 9.2. $^{238}PuO_2$ Fuel Reentry Body Design for a Plane Fuel Array

Stress-rate safety factor: 2.5

Capsule Size (in.)		Capsules Required	Reentry Body Projected Diameter (in.)	Reentry Body Weight (lb)	Terminal Ballistic Coefficient	Remarks
Outside Diameter	Length					
2.580	10.13	108	68	2300	105	Minimum volume of capsules
2.934	11.55	88	72	2330	88	
3.580	14.13	70	76	2380	84	Minimum weight of capsules

A similar treatment of the $^{244}Cm_2O_3$ fuel form resulted in the summary given in Table 9.3 for a capsule stress-rate reduction (rupture stress-rate safety factor) of 7. The capsules would weigh approximately 500 lb, which is about 45% of the total weights given. For this particular case, the reentry body of minimum projected diameter had the minimum volume of capsules, like the $^{238}PuO_2$ capsules previously discussed. However, the design selected varied slightly from the minimum volume capsule

Table 9.3. $^{244}Cm_2O_3$ Fuel Reentry Body Design for a Plane Fuel Array

Capsule Size (in.)		Capsules Required	Reentry Body Projected Diameter (in.)	Reentry Body Weight (lb)	Terminal Ballistic Coefficient	Remarks
Outside Diameter	Length					
2.048	8.00	134	58	1170	72	Minimum weight of capsules
1.598	6.20	172	52	1040	79	Selected design
1.416	5.47	212	52	1150	87	Minimum volume of capsules

design to give the minimum reentry body weight. This coincidence of minimum capsule volume and minimum reentry body diameter was not a general rule with the curium fuel form for other safety factors. However, in all cases the minimum reentry body dimension always occurred with a fuel capsule volume that was nearly the minimum value for each stress-rate safety factor.

The same examination of other capsule stress-rate safety factors resulted in Fig. 9.4 for reentry body diameter and Fig. 9.5 for reentry body weight for the curium and plutonium fuel forms. Also included is the $^{147}Pm_2O_3$ fuel form, which has no helium pressure buildup and therefore is not influenced by stress-rate safety factors in the optimized capsule design. The slope of the ^{238}Pu curve is 1.5 times the slope of the ^{244}Cm curve in both figures. Although the ^{147}Pm reentry body diameter is the same as that for one ^{244}Cm design, the weight of the reentry body is 250 lb more than that of the corresponding ^{244}Cm reentry body because the weight of the promethium fuel and capsules is greater.

Another capsule arrangement, shown in Fig. 9.6, has the capsules nested on the inside conical surface of the reentry body. The same general information is supplied on the drawing as in the previous fuel arrangement, except for the reference to use in different system concepts. The slopes of the plutonium and curium weight and diameter curves for the

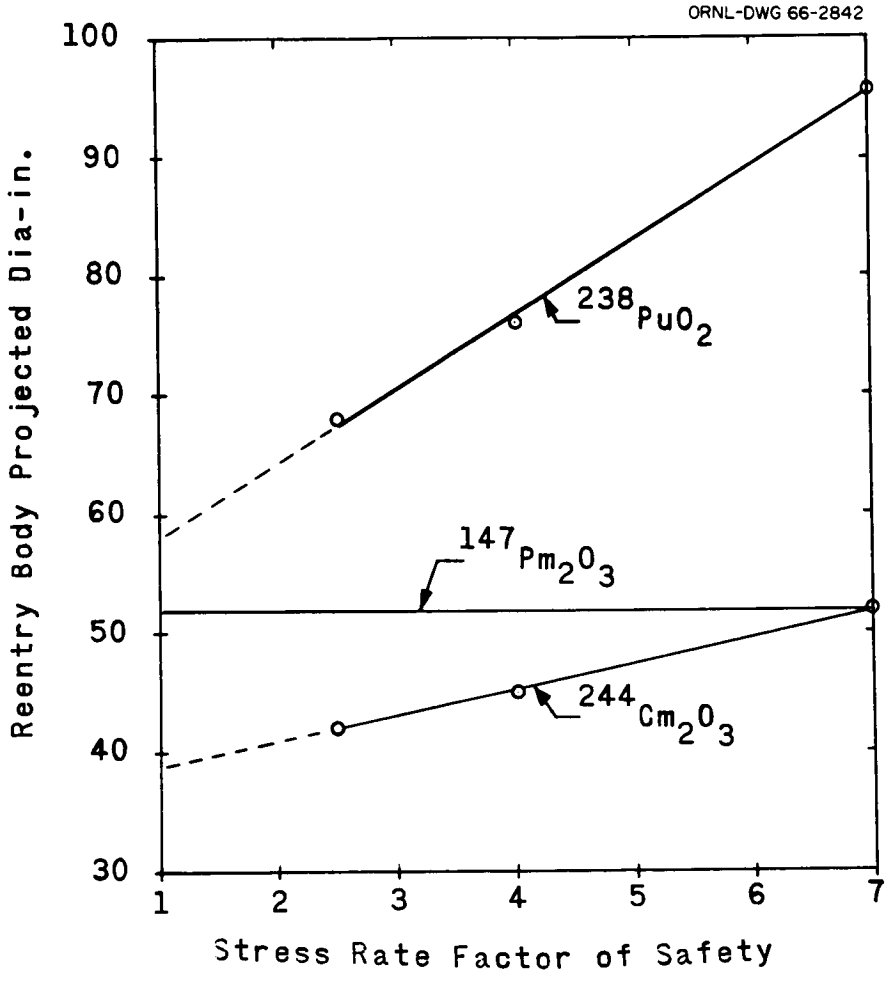

Fig. 9.4. Effect of Capsule Stress-Rate Reduction on Reentry Body Diameter for a Plane Fuel Array.

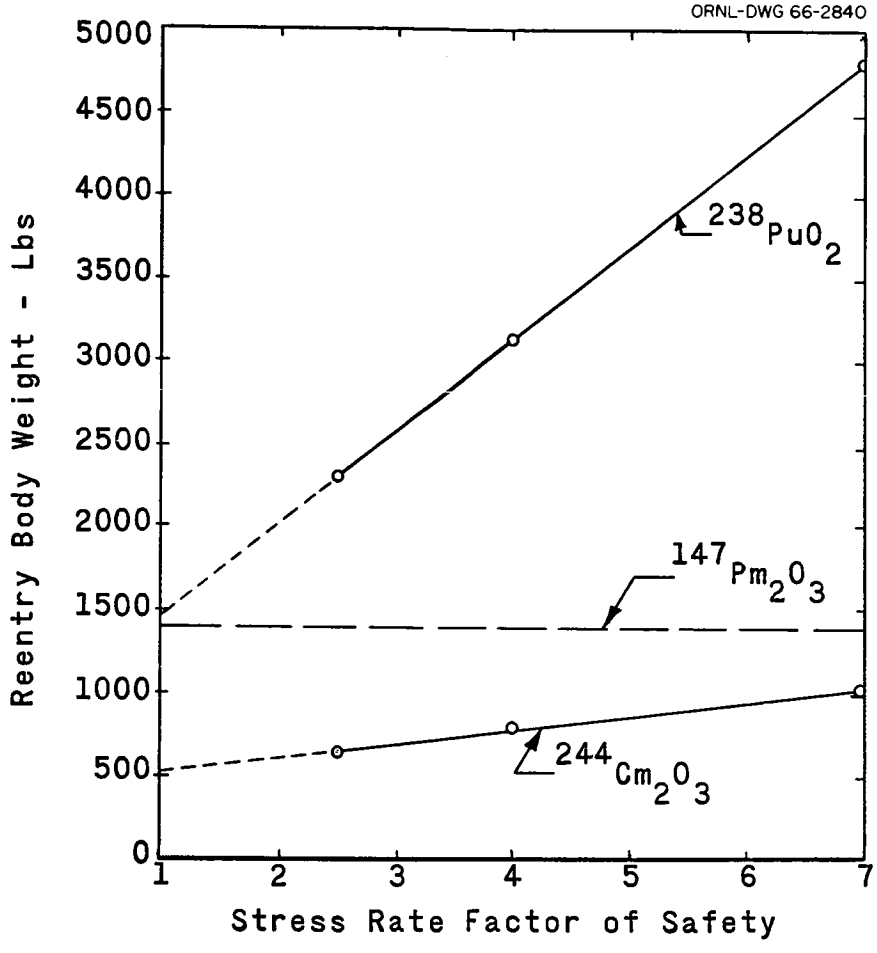

Fig. 9.5. Effect of Capsule Stress Rate-Reduction on Reentry Body Weight for a Plane Fuel Array.

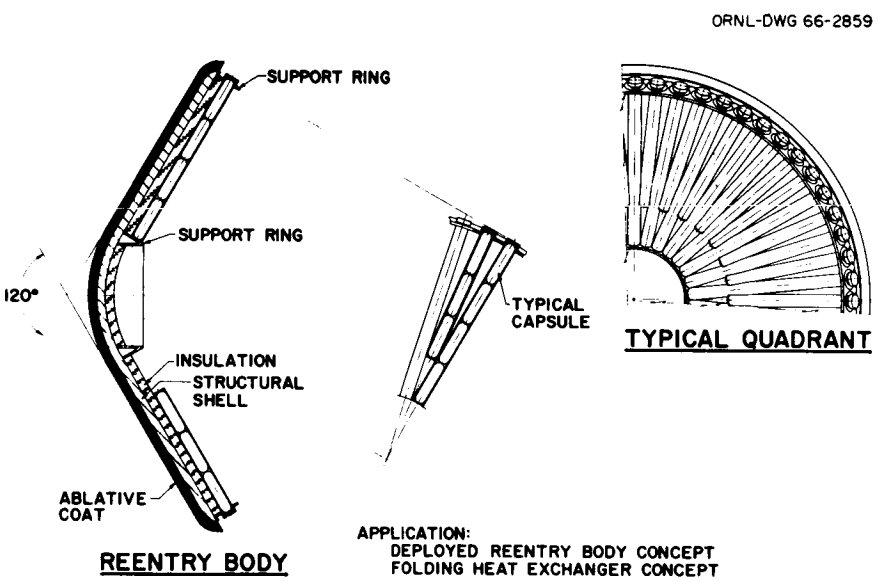

Fig. 9.6. Reentry Body for a 60° Conical Fuel Array.

plane fuel array just discussed were normalized to calculated points for this configuration. The same general trend was expected to prevail for this configuration as for the plane fuel array for changes in the capsule stress-rate safety factor, and it was expected that the extrapolation would be adequate for the conceptual design phase of the study. The results of the extrapolation are shown in Fig. 9.7. As before, the promethium curve is given for reference. A comparison of the conical fuel arrangement with the plane fuel array revealed that the conical array weighs approximately 200 lb more. This weight penalty was a direct result of a larger reentry body diameter. The diameter increase was brought about by the inefficient use of the conical area in contrast to the efficiently used plane area.

An attempt to more effectively utilize the internal volume of the reentry body for capsule placement gave the configuration shown in Fig. 9.8. Although the parallel rows of capsules with the heat exchanger tubes fitting between the rows of fuel slugs provided better heat removal conditions, the reentry body had a projected diameter that fell between those of the plane fuel array and the conical fuel array. Use of this arrangement did not appear to offer any weight savings.

Another conceptual arrangement to accomplish the last objective was tried with the concentric capsule arrangement shown in Fig. 9.9. The fuel slugs were stacked so that a blunted cone with a cylindrical extension would result in a small projected diameter. However, the protrusion of the cylinder behind the blunted cone in all probability would upset the stability of the reentry body during reentry by disturbing the correct relationship between center of gravity and center of pressure for proper orientation. If the sides of the cone are extended to a cone diameter where the fuel is approximately contained within the cone volume, the fuel arrangement falls into the same category as the previously mentioned parallel rows design; that is, it is an in-between design that does not offer any outstanding advantages.

The range of terminal ballistic coefficients for the fuel block and reentry body concepts for the three fuels is given below:

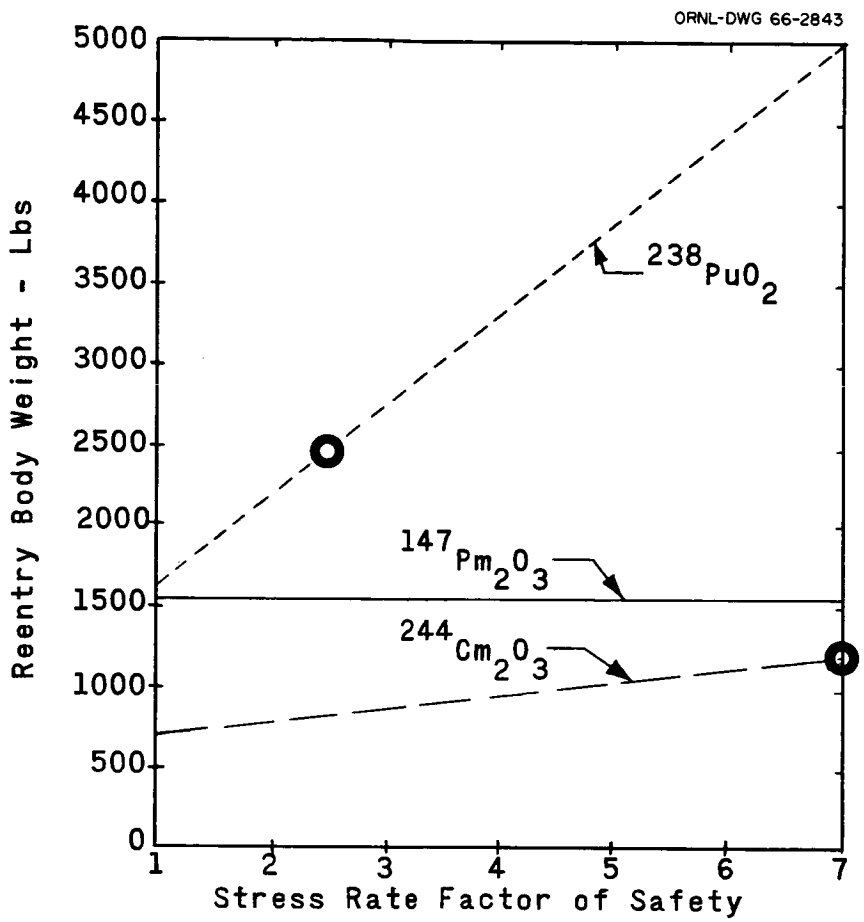

Fig. 9.7. Estimated Effect of Stress-Rate Reduction on Reentry Body Weight for a 60° Conical Fuel Array.

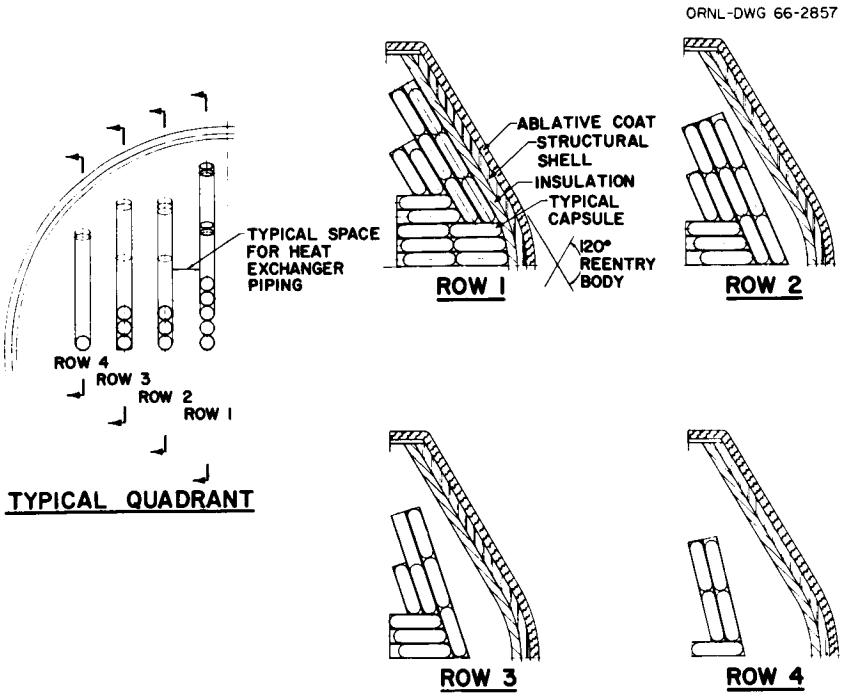

Fig. 9.8. Reentry Body for Fuel in Parallel Rows.

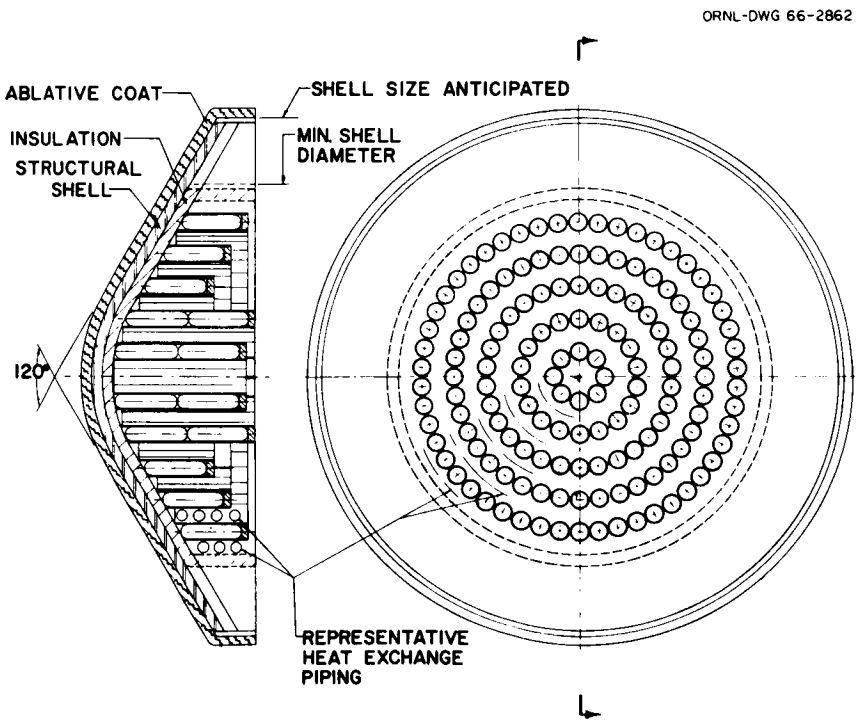

Fig. 9.9. Reentry Body for a Concentric Fuel Array.

Fuel	Terminal Ballistic Coefficient Range
$^{238}PuO_2$	80–110
$^{147}Pm_2O_3$	90–100
$^{244}Cm_2O_3$	70–90

These values show that the desired value of approximately 100 for impact considerations is a reasonable objective for an isotopic heat source in this size range.

9.3 Thermal Insulation

Part of the thermal insulation for the heat source would be contained within the reentry body and should be as light a weight as possible so that it does not add significantly to the reentry body weight. It should also be highly efficient to minimize the amount of excess fuel required in the heat source to compensate for heat losses.

A review of conventional insulation indicated that one of the most promising materials is Superinsulation manufactured by Linde Division of Union Carbide Corporation. Superinsulation, a multiple-layer system consisting of highly reflective shields and low-conductivity fillers in vacuum, has been successfully used for insulating cryogenic liquids in storage. Although the normal materials of construction are not suitable for the high temperatures encountered in the Brayton-cycle isotopic power system, discussions with the Linde Laboratories at Tonawanda, New York, indicated that a new multilayer composite has been designed for long service life in a 2000°F environment. The new composite, a system of 1-mil-thick layers of tantalum and 15-mil-thick quartz spacers, consists of approximately 60 layers of each material per inch of insulation thickness. The estimated thermal conductivity of the composite system was 2.4×10^{-3} Btu-ft/hr·ft^2·°F with one surface at 2000°F and the other surface at 100°F. The use of quartz spacers in intimate contact with tantalum at high temperatures for long periods of time may introduce compatibility problems; however, it is expected that other ceramic spacer materials can be substituted for the quartz if necessary.

A comparison of this estimate was made with data for some other high-temperature Superinsulations currently available at Linde. These materials have the thermal characteristics given in Fig. 9.10. The estimated tantalum-quartz value appeared to be conservative because tantalum has a lower absorptivity and a higher reflectivity for the temperature range of interest when compared with the metals used to generate the data in the figure. The significance of such low-thermal-conductivity insulation was evaluated for the conceptual systems with 1 in. of insulation and a thermal conductivity of 2.4×10^{-3} Btu-ft/hr·ft^2·°F. The inner surface temperatures were assumed to be 2000°F, and the outside skin temperature was calculated to be 67°F with an effective sink temperature of −20°F. The heat flux was determined to be 56 Btu/hr·ft^2, and this heat flux resulted in the heat-loss percentages given in Table 9.4. Figure 9.10 does not include any losses due to conduction along metal supports that might penetrate the insulation for support purposes.

Table 9.4. Estimated Heat Losses for Conceptual Systems

Fuel	Range of Surface Area for Shielded Volume (ft^2)	Range of Heat Loss (%)
$^{238}PuO_2$	90–150	6–9.5
$^{147}Pm_2O_3$	60–90	4–6
$^{244}Cm_2O_3$	50–100	3.5–7.0

Normally, Superinsulation units are maintained at a pressure of 1 to 10 μ Hg. The insulation sections employed on the conceptual systems would not be sealed, so the laminated composite could communicate directly with the space vacuum of 10^{-8} μ (at 380 miles altitude) or less. The value of the space vacuum pressure is immaterial because the insulating quality is essentially unchanged at pressures below 10 μ. The unsealed insulation would lose its superinsulating value when it returned to the earth's atmosphere; this is a desirable feature in helping to prevent excessive fuel

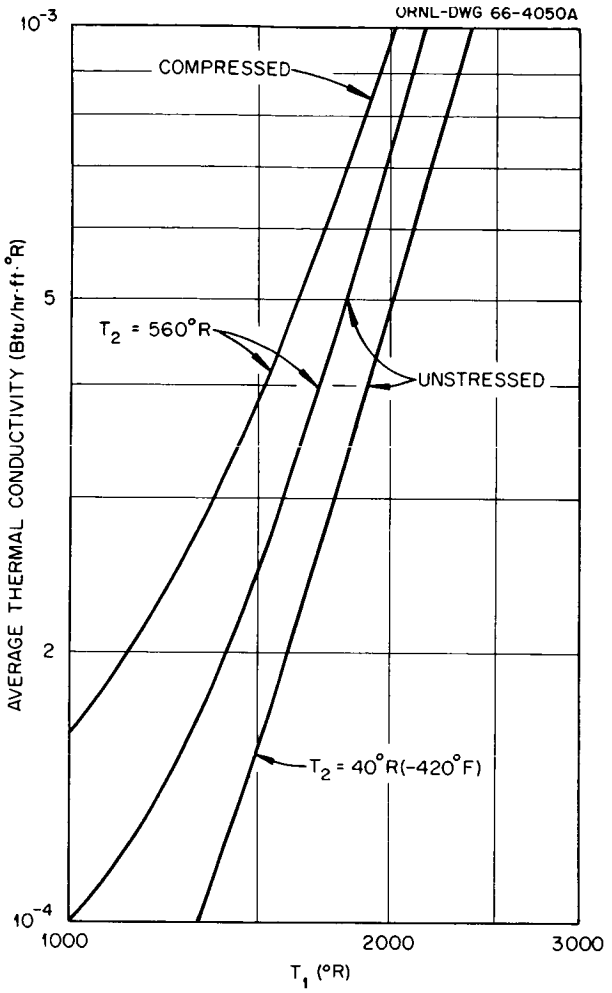

Fig. 9.10. Thermal Conductivity of Superinsulation, Which Consists of Nickel, Copper, or Aluminum Metal Foil and Spacers That Are a Combination of Quartz and Borosilicate Glass. (From Ref. 67)

block temperatures in the event of random reentry. Also, the tantalum would rapidly oxidize and disintegrate after reentry; this is also considered to be beneficial.

10. HEAT SOURCE SYSTEM CONCEPTUAL DESIGNS

Nine heat source concepts were studied, and each was examined for use with two or more of the fuels. The layouts of the components, including the shield configurations are described in the following sections. The capsule design for each fuel is described in Section 5. All the concepts employ a blunted-cone-shaped reentry body, as described in Sections 8 and 9. Each concept is examined for the normal mode of operation and emergency heat rejection. The reentry body diameters for various fuel capsule arrangements are given in Section 9; they range between 40 and 100 in. depending on the concept, fuel form, and stress-rate safety factor employed.

The system conceptual designs were detailed only to the extent necessary to obtain and compare approximate weights and volumes. The calculated weights include the fuel, fuel capsules, fuel capsule mounting structure, reentry body shell, ablative material, neutron shield, and gamma shield. All these weights, except those for the neutron and gamma shields, were combined to give a reentry body weight that is the total weight of that part of the system which would reenter the earth's atmosphere in the event of a mission abort that utilized the passive reentry body. This weight was used to calculate the ballistic coefficient of the reentry portion of the system. Support structure for the reentry body, latches, ejection mechanisms, and similar items were not included in the system weight.

In Section 10.1 the reference shielding model supplied by NASA is used. The weight reduction study in Section 10.2 makes comparisons that result from the use of other dose level criteria and variations in heat source to crew compartment separation distance.

10.1 Conceptual Design Descriptions

10.1.1 Folding Heat Exchanger for a Plane Fuel Reentry Body

The equipment layout for the plane fuel reentry body with a folding heat exchanger is given in Fig. 10.1. The fuel block, a plane fuel array in a blunted-cone reentry body, is located adjacent to the heat exchanger, which was put next to the spacecraft skin. A redundant heat exchanger is included in the equipment layout. The two heat exchangers were

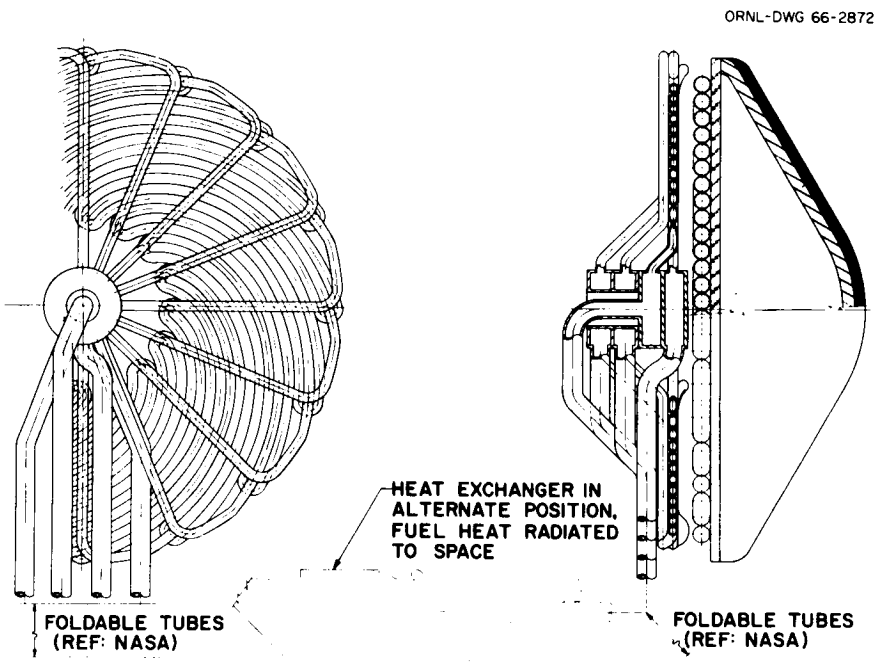

Fig. 10.1. Equipment Arrangement for Plane Fuel Reentry Body with Folding Heat Exchanger.

integrated into a disk array by making the tubes into involutes of a circle. The tubes were then nested together to form a continuous heat receiver plane from which either set of tubes would remove the heat in the normal mode of operation. The emergency mode of operation would be initiated if the Brayton-cycle system failed to operate by opening a door in the spacecraft and folding the heat exchanger disk out of the way. The exposed fuel capsule holders would then be able to radiate to a space environment heat sink. The ability to fold the exchanger out of the way required both the inlet and outlet coolant lines to be flexible. This was accomplished with the foldable tubes developed at Lewis Research Center[68] (shown in Fig. 10.2). The hinging action is obtained by first collapsing the tube and then bending it around a pivot point. Tests at Lewis have shown that the foldable tube can withstand repeated flexing action without failure.

The thermal path in normal operation would be radiation from the fuel capsules to the capsule holder tubes, conduction in the tubular walls, and then radiation to the active heat exchanger. The emergency mode is essentially the same except that the tube holders are exposed to the space heat sink when the heat exchangers are folded out of the thermal path.

The shielding configuration for the foldable heat exchanger concept is shown in Fig. 10.3. The shield was designed as a 4π solid angle unit. The figure is an expanded view of the shield for the $^{244}Cm_2O_3$ fuel form. There are three distinct thicknesses of shield, with the thinnest section corresponding to an enveloping shield that provides for a radiation dose rate of 600 mrem/hr at 3 meters. The intermediate thickness was needed to reduce the scattered radiation dose rate at the crew-compartment bulkhead to the design level of 3 mrem/hr. Scattering collisions can occur at any point in the equipment module; and consequently a large solid angle had to be shielded to protect against this contribution to the dose rate in the crew compartment. The additional thin layer over part of the scattered-radiation shield was added to bring the uncollided dose rate down to a level that was acceptable in the crew compartment.

A breakdown of shield weights for this concept follows the general outline of the solid angle that the shield protects. The scattered,

PHOTO 73128

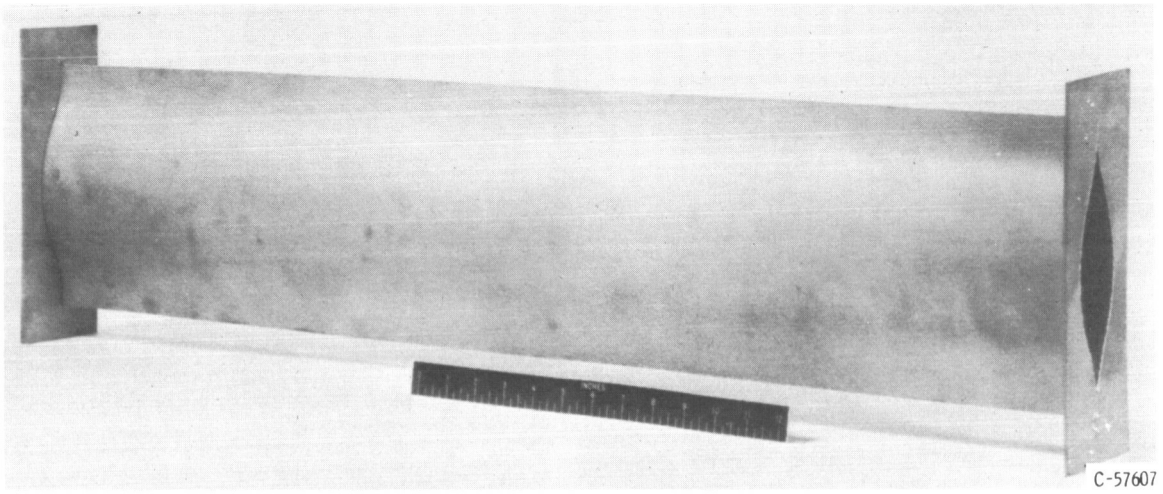

C-57607

(a) Side view.

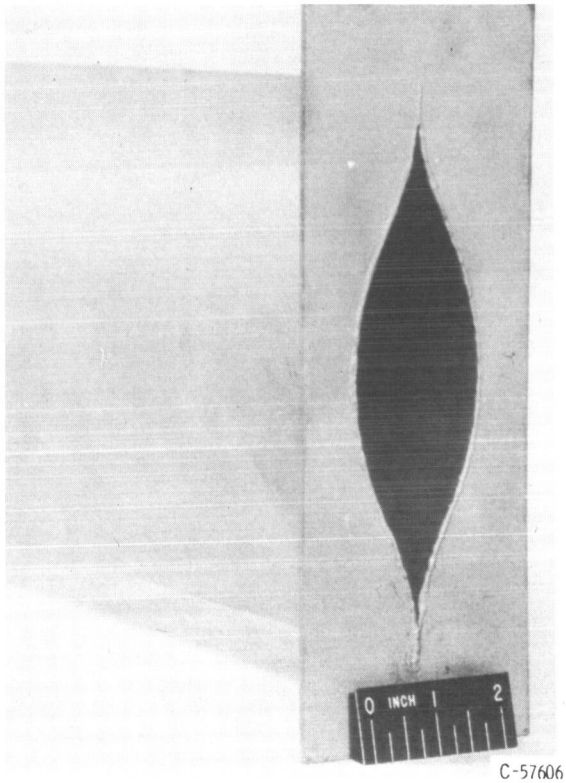

C-57606

(b) Oblique view of end showing closeup of cross section.

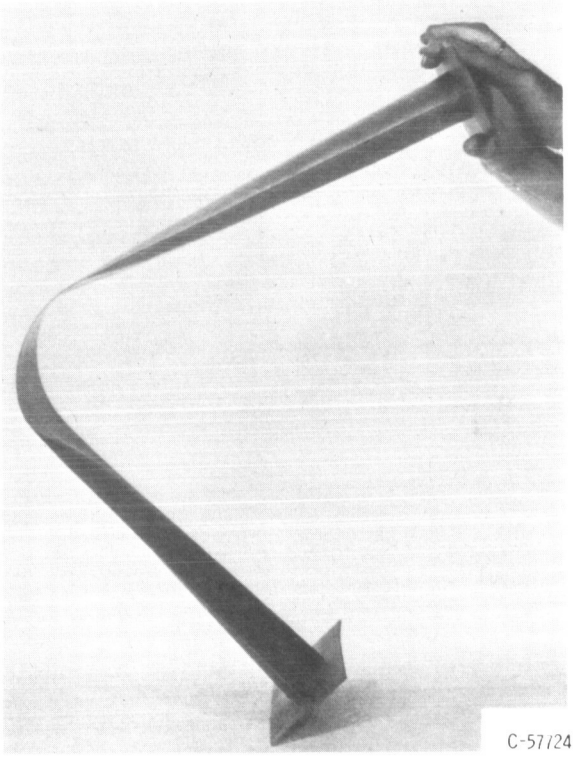

C-57724

(c) Specimen in collapsed and bent position.

Fig. 10.2. Foldable-Tube Specimen Equivalent to 3-in.-ID Tube.

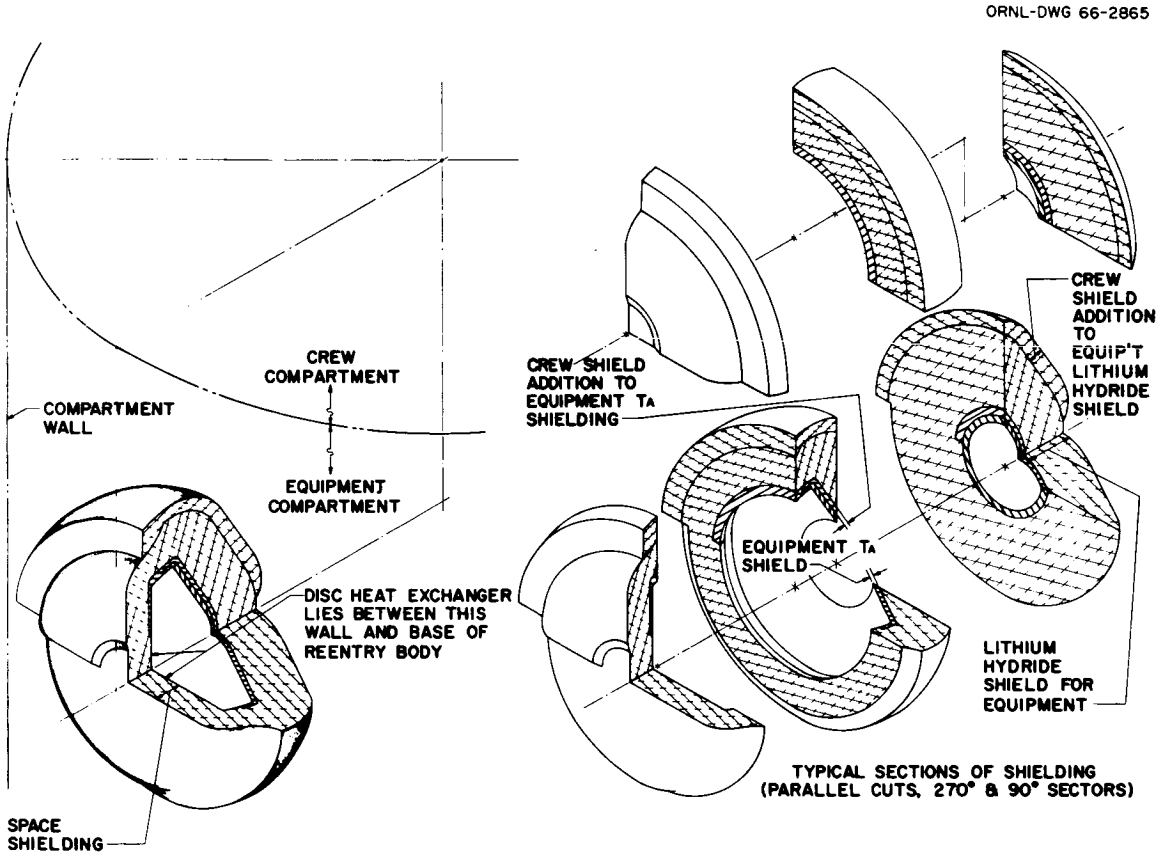

Fig. 10.3. Shielding Configuration for Plane Fuel Reentry Body with Folding Heat Exchanger.

uncollided, and 4π solid angle contributions are included with the fuel forms, shield materials, and total shield weights in Table 10.1.

Table 10.1. Shield Weights for One-Year Occupancy of a System with a Plane Fuel Array and a Folding Heat Exchanger

Stress-rate safety factor: 2.5

Fuel	Shielding Material	Crew Shield Weight (lb)		4π Solid Angle Shield Weight (lb)	Total Shield Weight (lb)
		For Scattered Radiation	For Direct Radiation		
$^{238}PuO_2$[a]	LiH	0	950	0	950
$^{238}PuO_2$[b]	LiH	300	1810	0	2110
$^{147}Pm_2O_3$[c,d]	Tantalum	550	2620	380	3550
$^{147}Pm_2O_3$[d,e]	Tantalum	900	3530	1070	5500
$^{244}Cm_2O_3$	LiH	700	1960	420	3080
	Tantalum	430	3340	0	3770
	Total	1130	5300	420	6850

[a] Oxygen-18 depleted by a factor of 20 in fuel compound.

[b] Natural oxygen in fuel compound.

[c] $5 \times 10^{-5}\%$ ^{146}Pm contamination.

[d] $^{147}Pm_2O_3$ capsules independent of stress-rate reduction.

[e] $5 \times 10^{-4}\%$ ^{146}Pm contamination.

The breakdown has two $^{238}PuO_2$ entries. The first corresponds to the fuel compound depleted in ^{18}O and the second is for fuel containing natural oxygen if it is assumed that (α,n) neutrons from other impurities are insignificant. Isotopic purification of the oxygen to deplete ^{18}O by a factor of 20 reduced the nuclear radiation source intensity by a factor of 10 below that associated with the use of natural oxygen in the fuel compound. Neither of the plutonium fuel forms required a 4π shield, and only a shadow shield is required when depleted oxygen is used in the fuel compound.

Two cases are also considered for the $^{147}Pm_2O_3$ fuel form. Promethium-147 obtained from production reactor fuel reprocessing typically has approximately $10^{-5}\%$ ^{146}Pm, while ^{147}Pm from power reactor fuels is expected to have approximately $10^{-4}\%$ ^{146}Pm. The effect on the shield weight of this factor of 10 in ^{146}Pm concentration is significant even at these very low contamination levels.

The $^{244}Cm_2O_3$ fuel has both tantalum and LiH shielding requirements in contrast to only LiH for the plutonium fuels and tantalum for the promethium fuels. As a result the curium concepts are the heaviest, irrespective of the stress-rate safety factor used in the capsule design. This is shown in Fig. 10.4, where the lift-off weights (reentry body plus fuel and total shield weight) for the plutonium and curium fuels are plotted against the stress-rate safety factor. When the stress-rate safety factor is varied from 2.5 to 7, the plutonium fuels exhibit a factor of approximately 2 change in weights, whereas the curium fuels have a factor of approximately 1.5. The promethium fuel designs that have a plane fuel array have a lift-off weight of 5000 lb for production reactor material and 7000 lb if power reactor material is used.

10.1.2 Folding Heat Exchanger for a 60° Conical Fuel Reentry Body

The plane fuel array concept was next modified to a conical fuel array in the reentry body. The modification permitted the heat exchangers to nest within the reentry body, as shown in Fig. 10.5. There are both an active heat exchanger and an inactive one. The energy transmission encounters consecutive radiation, conduction, and radiation resistances in the thermal path. The heat exchanger complex folds out of the thermal path so that the capsule holders are exposed to space through a door when emergency or passive heat rejection is required. The heat exchangers must have hinged joints in the coolant lines like those of the foldable tube that was described for the previous concept (Sect. 10.1.1).

The shielding configuration, shown in Fig. 10.6, is only slightly different from that for the previous concept. The shield weights, shown in Table 10.2, reflect an increase in reentry body diameter for the conical fuel array over the plane fuel array. The weights are greater than for

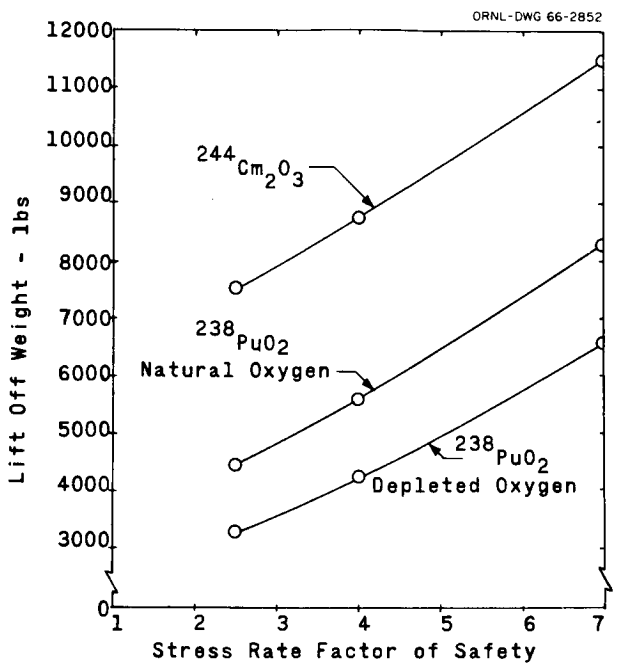

Fig. 10.4. Effect of Capsule Stress-Rate Reduction on Lift-off Weight for a Plane Fuel Array.

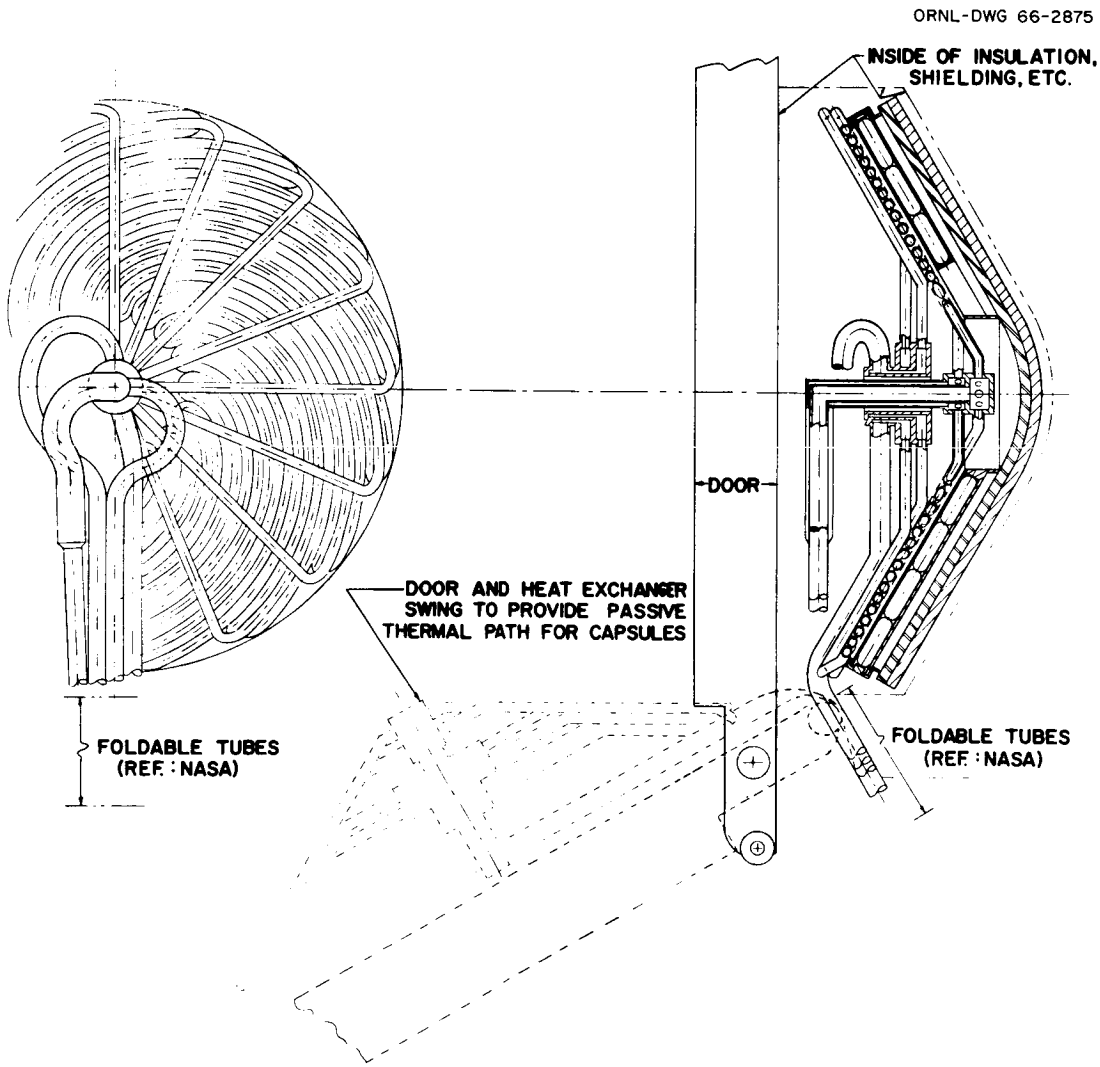

Fig. 10.5. Equipment Arrangement for a 60° Conical Fuel Reentry Body with a Folding Heat Exchanger.

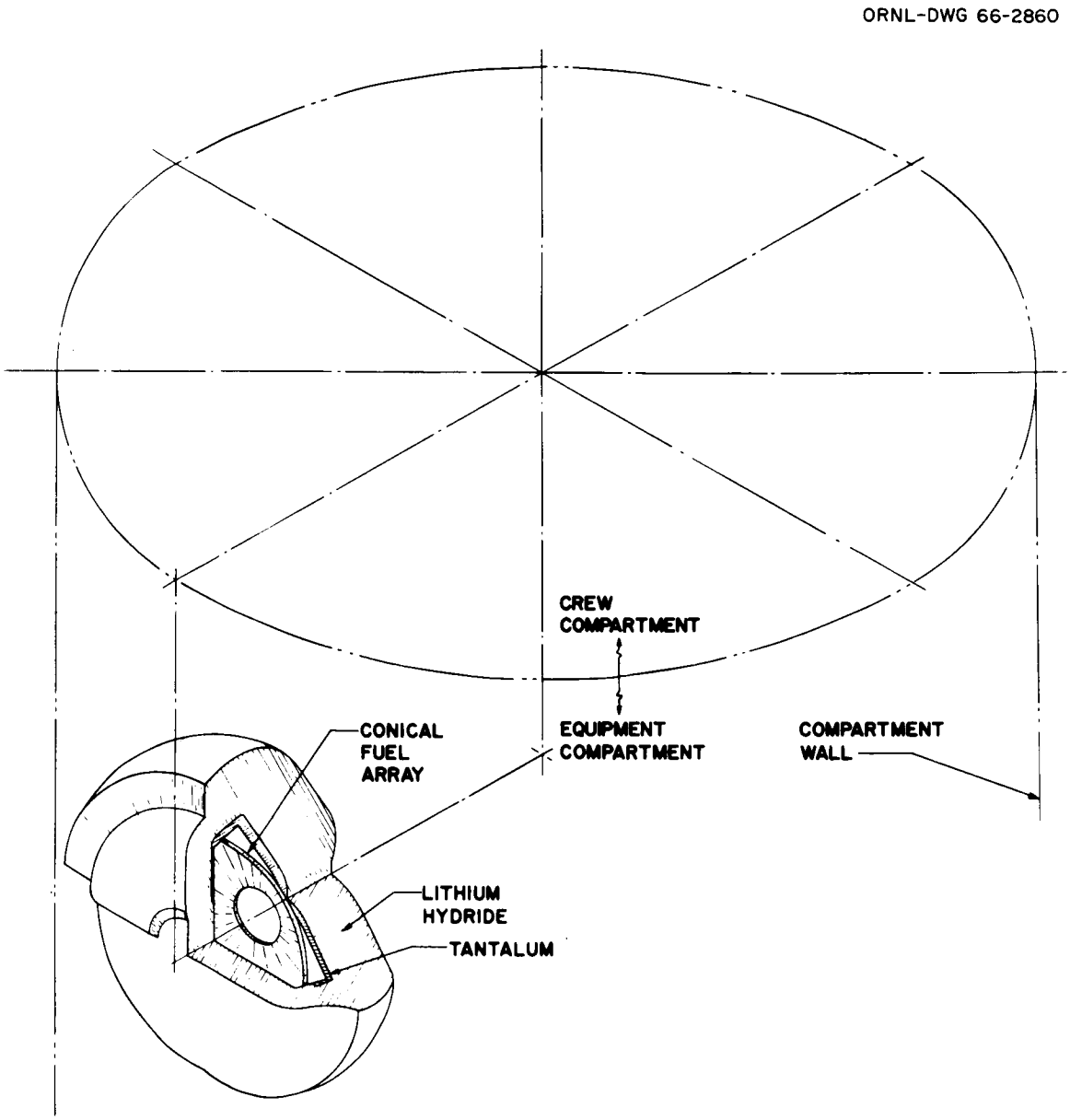

Fig. 10.6. Shielding Configuration for a 60° Conical Fuel Reentry Body with a Folding Heat Exchanger.

Table 10.2. Shield Weights for One-Year Occupancy of a System With a 60° Conical Fuel Array and a Folding Heat Exchanger

Fuel	Shielding Material	Crew Shield Weight (lb)		4π Solid Angle Shield Weight (lb)	Total Shield Weight (lb)
		For Scattered Radiation	For Direct Radiation		
$^{244}Cm_2O_3$[a]	LiH	1480	3230	1140	5,850
	Tantalum	1100	6190	0	7,290
	Total	2580	9420	1140	13,140
$^{238}PuO_2$[b,c]	LiH	490	2930	0	3,420
$^{238}PuO_2$[c,d]	LiH	0	1150	0	1,150
$^{147}Pm_2O_3$[e]	Tantalum	1720	3740	750	6,210
$^{147}Pm_2O_3$[f]	Tantalum	500	3050	700	4,250

[a] Stress-rate safety factor of 7.

[b] Natural oxygen in fuel compound.

[c] Stress-rate safety factor of 2.5.

[d] Oxygen-18 depleted by a factor of 20 in fuel compound.

[e] $5 \times 10^{-4}\%$ ^{146}Pm contamination.

[f] $5 \times 10^{-5}\%$ ^{146}Pm contamination

the previous concept, as would be expected because of the larger shielded volume.

10.1.3 Deployed 60° Conical Fuel Reentry Body

Equipment identical with that for the previous concept was used for the deployed reentry body, but the roles of the heat exchangers and reentry body were inverted in the passive heat rejection mode. The emergency mode would consist of deploying the reentry body through a door in the spacecraft by a translation and rotation to expose the fuel capsule holders to the heat sink. The equipment shown in Fig. 10.7 presents the slightly different shielding configuration shown in Fig. 10.8. The shield weights in Table 10.3 show that there is not a significant weight advantage

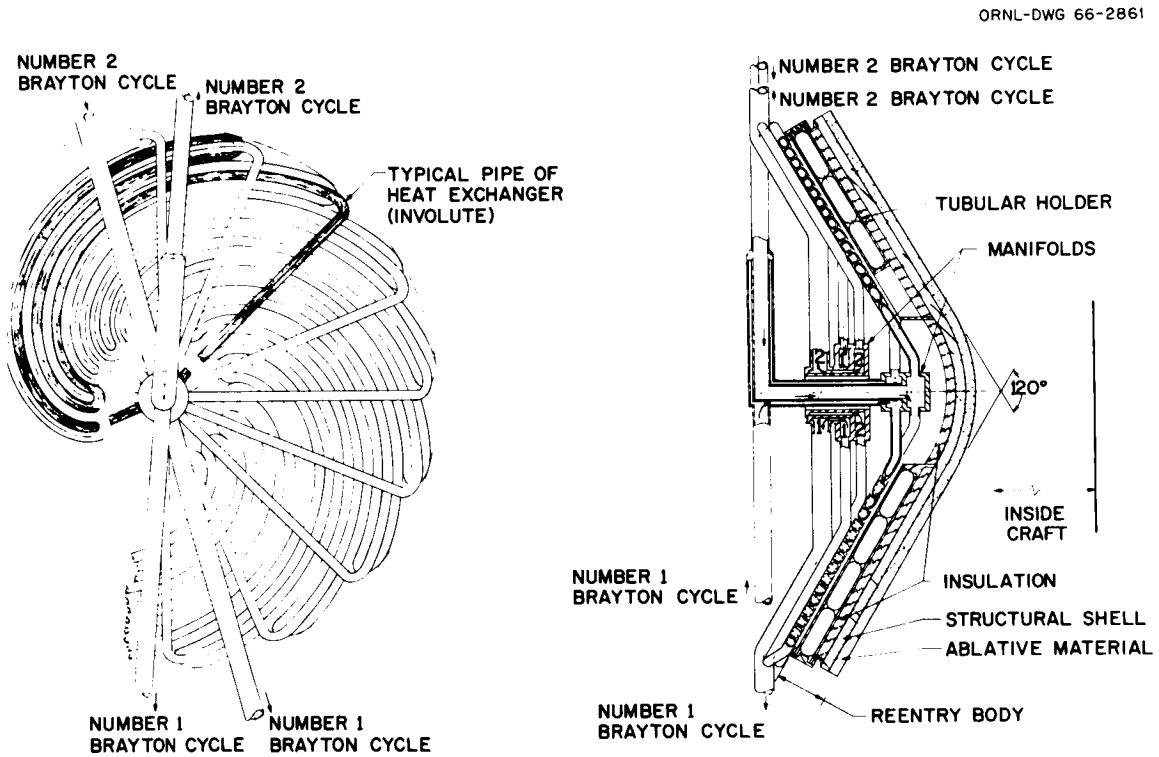

Fig. 10.7. Equipment Arrangement for a Deployed 60° Conical Fuel Reentry Body with a Conical Heat Exchanger.

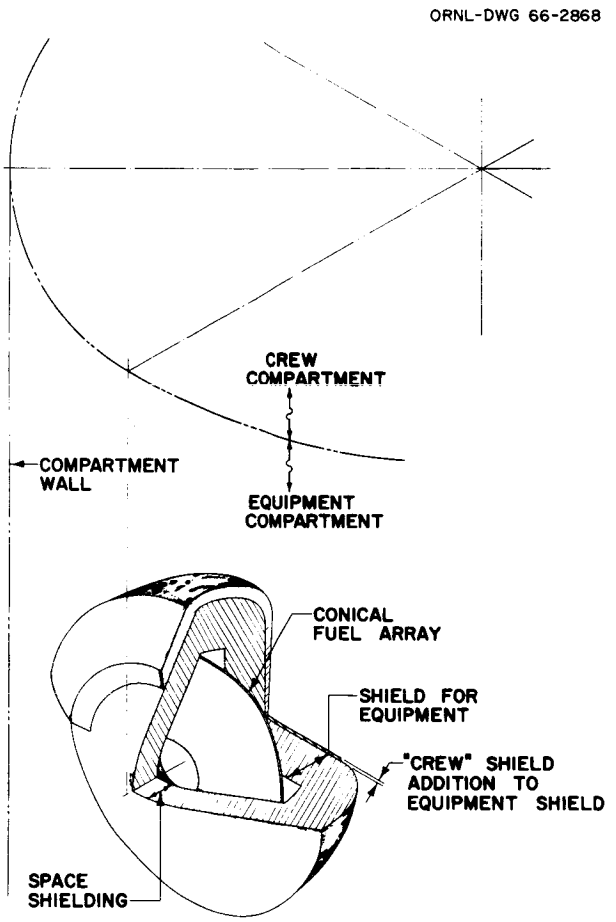

Fig. 10.8. Shielding Configuration for a Deployed 60° Conical Fuel Reentry Body with a Conical Heat Exchanger.

Table 10.3. Shield Weights for One-Year Occupancy of a System With a 60° Conical Fuel Array and a Deployed Reentry Body

Fuel	Shielding Material	Crew Shield Weight (lb)		4π Solid Angle Shield Weight (lb)	Total Shield Weight (lb)
		For Scattered Radiation	For Direct Radiation		
$^{244}Cm_2O_3$[a]	LiH	1690	3,770	670	6,130
	Tantalum	1780	7,180	0	8,960
	Total	3470	10,950	670	15,090
$^{238}PuO_2$[b,c]	LiH	690	2,980	0	3,670
$^{238}PuO_2$[c,d]	LiH	0	1,590	0	1,590
$^{147}Pm_2O_3$[e]	Tantalum	1980	4,060	270	6,310
$^{147}Pm_2O_3$[f]	Tantalum	1200	3,010	100	4,310

[a] Stress-rate safety factor of 7.

[b] Natural oxygen in fuel compound.

[c] Stress-rate safety factor of 2.5.

[d] Oxygen-18 depleted by a factor of 20 in fuel compound.

[e] $5 \times 10^{-4}\%$ ^{146}Pm contamination.

[f] $5 \times 10^{-5}\%$ ^{146}Pm contamination.

between this and the previous concept. The advantage of either concept would be in the reliability of the devices required to produce the necessary motion for emergency heat rejection.

10.1.4 Inclined Plane Fuel Reentry Body

An arrangement of the disk-shaped heat exchangers and the plane fuel array reentry body so that the plane surfaces are inclined to each other is shown in Fig. 10.9. The normal mode of operation provides a direct view of the active heat exchanger tubes by the fuel holders for direct radiant energy transfer. Also heat transmission occurs by reflection and radiation from the inactive walls surrounding the system. Consecutive

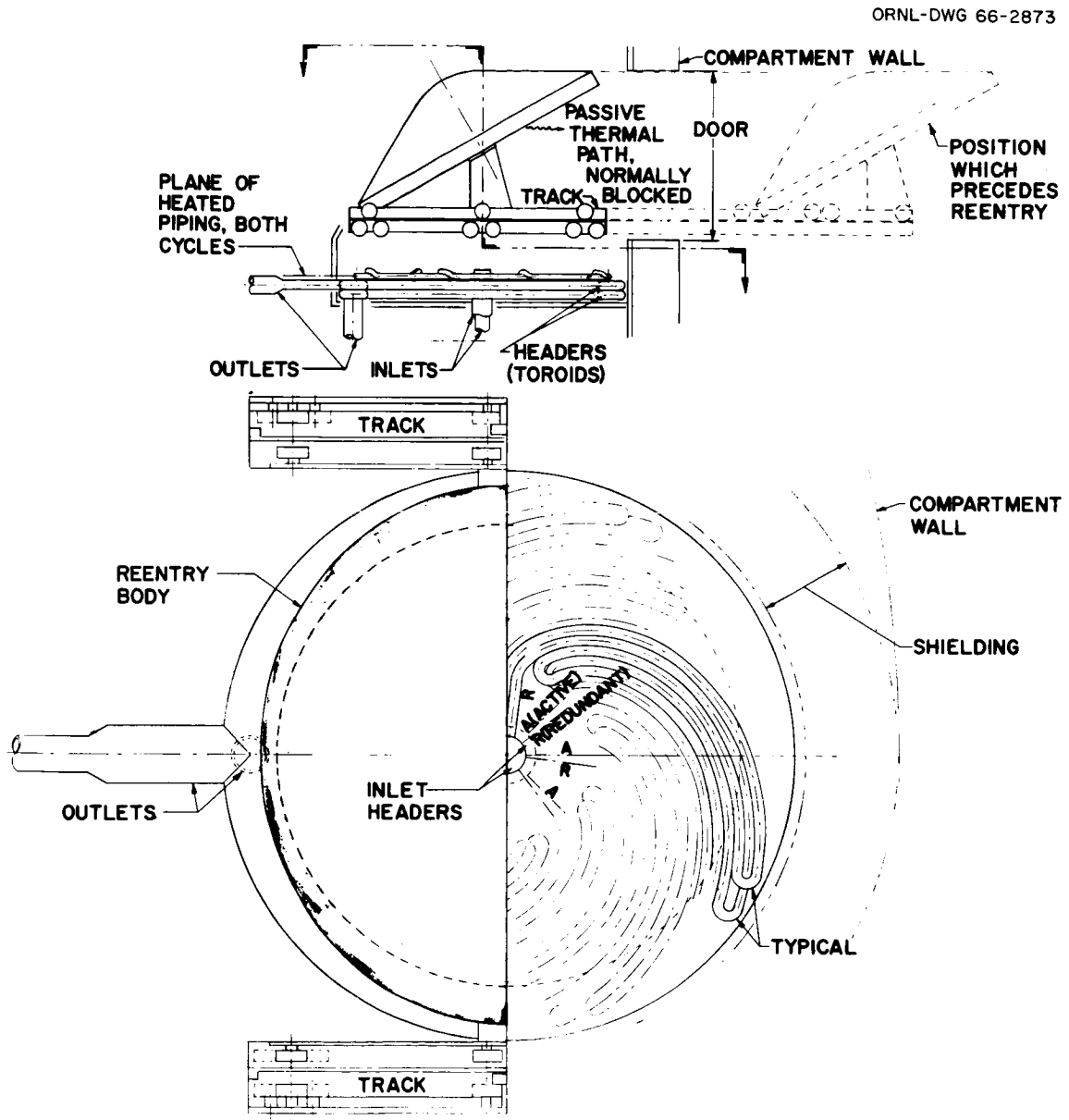

Fig. 10.9. Equipment Arrangement for Inclined Plane Fuel Reentry Body with a Disk Heat Exchanger.

radiation, conduction, and radiation is the manner in which the energy travels from the fuel capsules to the heat exchanger.

The passive heat rejection mode is initiated when a door in the spacecraft opens to allow the fuel holders to have a direct view toward space. The view angle toward space is sufficient to cool the fuel capsules without exceeding the temperature limitation.

The shielding arrangement is given in Fig. 10.10 for the inclined reentry body concept. The isometric is distorted by the inclination of the surfaces, but the breakdown in Table 10.4 establishes that these weights are essentially the same as those for the deployed reentry body concept.

Table 10.4. Shield Weights for One-Year Occupancy of a System With an Inclined Plane Fuel Reentry Body

Stress-rate safety factor: 7

Fuel	Shielding Material	Crew Shield Weight (lb)		4π Solid Angle Shield Weight (lb)	Total Shield Weight (lb)
		For Scattered Radiation	For Direct Radiation		
$^{244}Cm_2O_3$	LiH	3050	2360	1710	7,120
	Tantalum	3980	3910	0	7,890
	Total	7030	6270	1710	15,010

10.1.5 Directly Cooled Plane Fuel Reentry Body

A directly cooled body is shown in Fig. 10.11. The fuel capsules are inserted in holes with separate internal coolant passages near each line of capsules. One set of coolant passages is the active heat exchanger, whereas the other set provides the redundant coolant system. The thermal path is by radiation from the capsules to the tubesheet and then by conduction to the coolant passages.

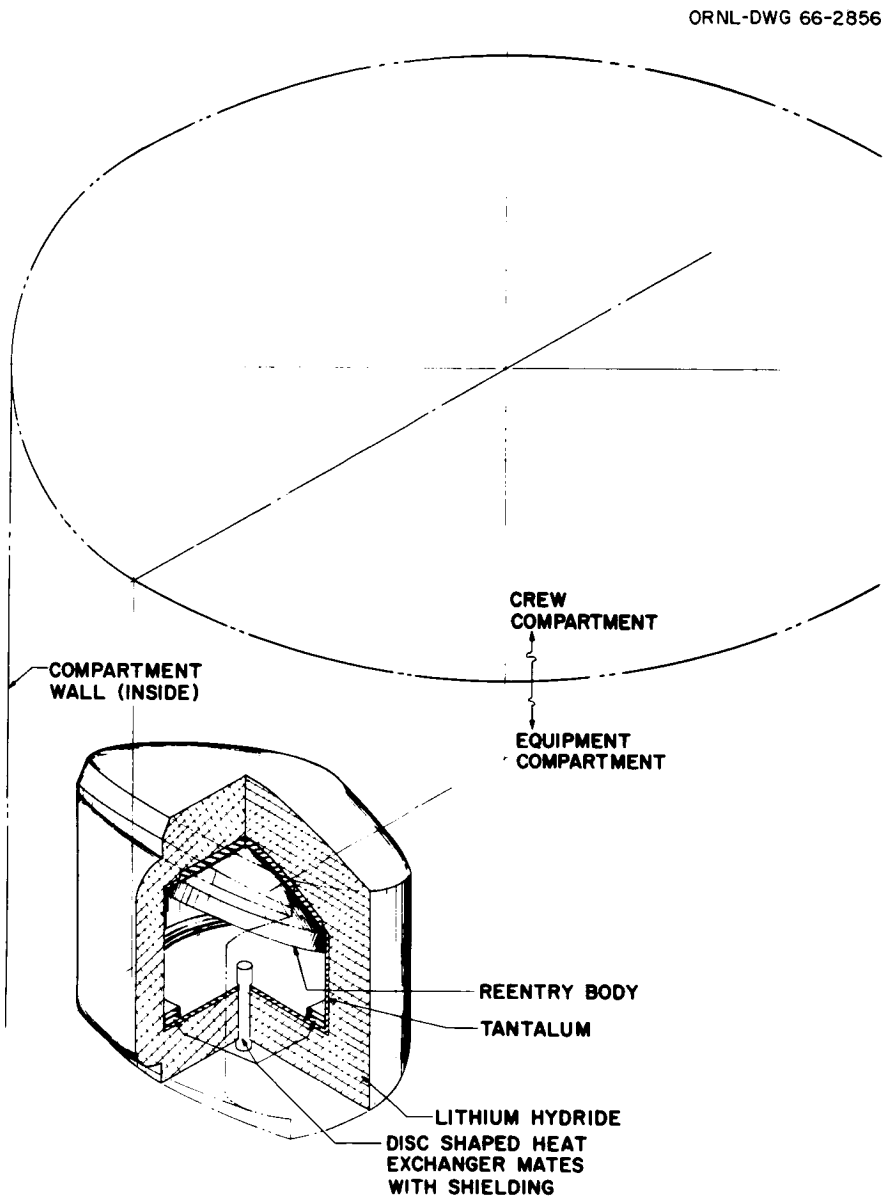

Fig. 10.10. Shielding Configuration for Inclined Plane Fuel Reentry Body with a Disk Heat Exchanger.

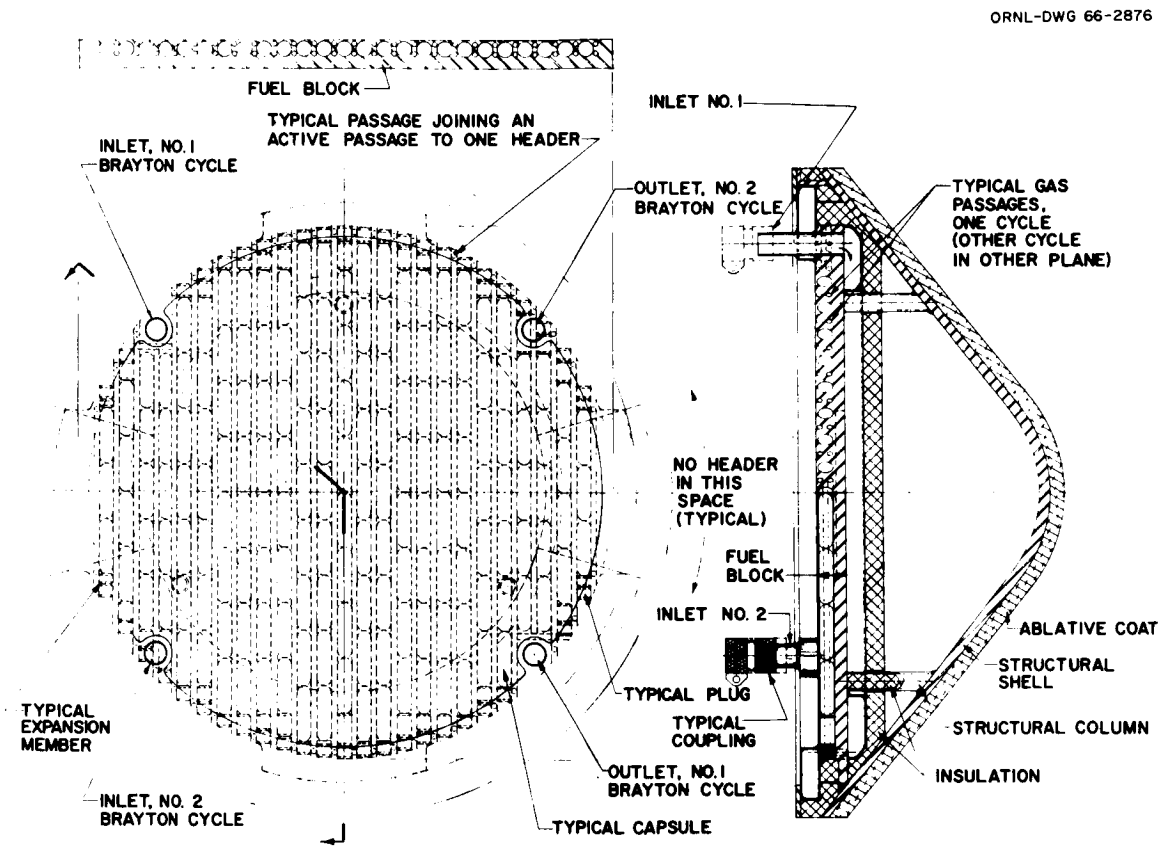

Fig. 10.11. Equipment Arrangement for a Directly Cooled Plane Fuel Reentry Body.

The placement of the reentry body has the tubesheet adjacent to the spacecraft wall. This location permits a door in the craft to open for heat rejection to space if coolant flow stops.

Emergency ejection of the reentry body for return to the earth's atmosphere is hampered by the coolant lines. These connections would have to be severed before the body could be separated from the craft. Quick disconnects would present problems in coolant leakage, in addition to the delay needed to break the connentions during a sudden abort situation.

The shielding configuration is much the same as for the previous concepts. The shield shown in Fig. 10.12 has the weight breakdown given in Table 10.5.

Table 10.5. Shield Weights for One-Year Occupancy of a System With a Directly Cooled Plane Fuel Reentry Body

Stress-rate safety factor: 7

Fuel	Shielding Material	Crew Shield Weight (lb)		4π Solid Angle Shield Weight (lb)	Total Shield Weight (lb)
		For Scattered Radiation	For Direct Radiation		
$^{244}Cm_2O_3$	LiH	1610	3,820	870	6,300
	Tantalum	920	6,410	0	7,330
	Total	2530	10,230	870	13,630

10.1.6 Rotating Plane Fuel Reentry Body

The equipment layout (Fig. 10.13) for a rotating plane fuel reentry body includes a mechanism with which the reentry body could be rotated to see space through a door in the spacecraft for passive heat rejection. Normal heat removal would be quite similar to that previously discussed, but the separation distance between the heat exchanger disk and the reentry body would have to be increased to provide clearance for the reentry

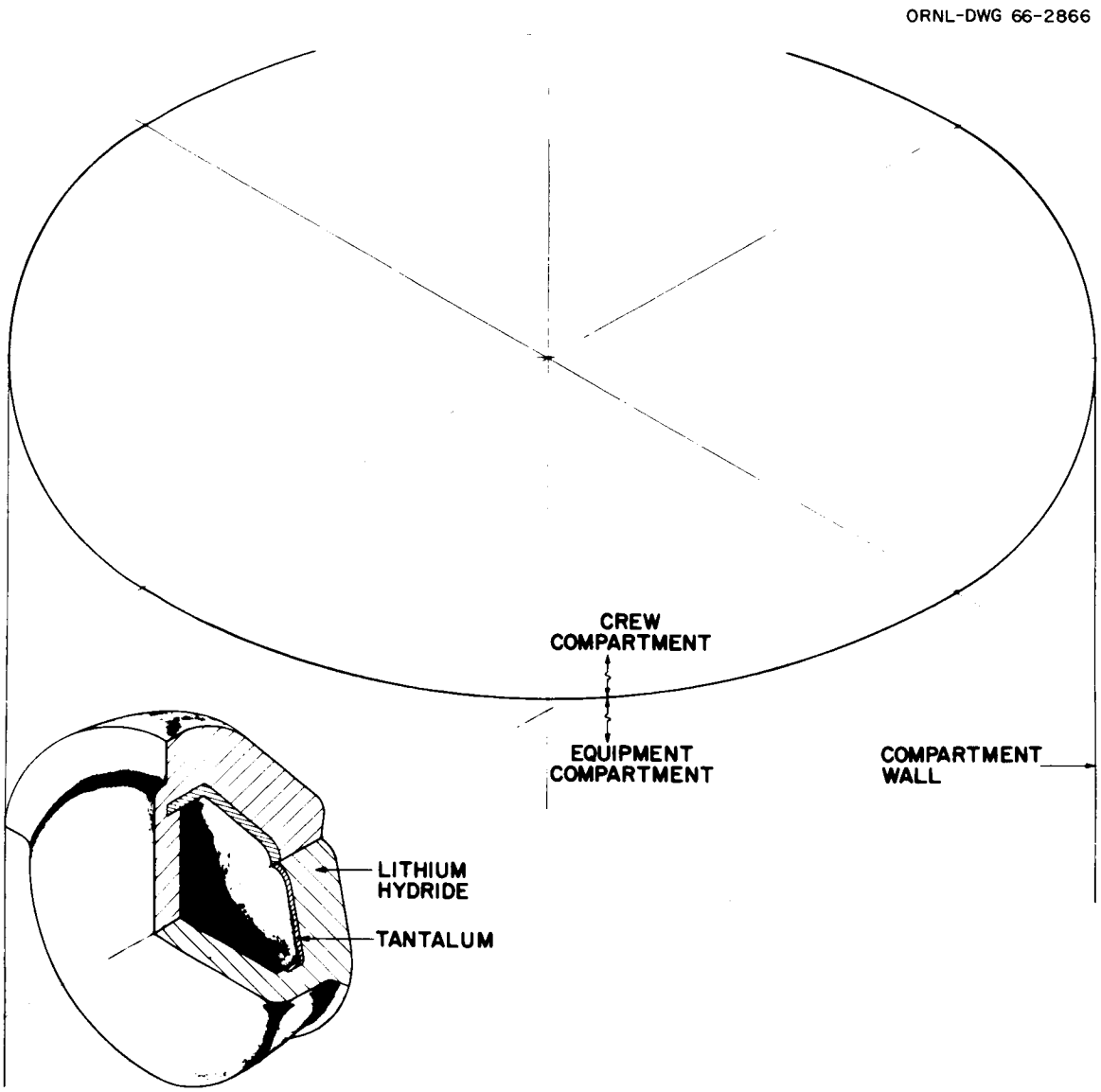

Fig. 10.12. Shielding Configuration for a Directly Cooled Plane Fuel Reentry Body.

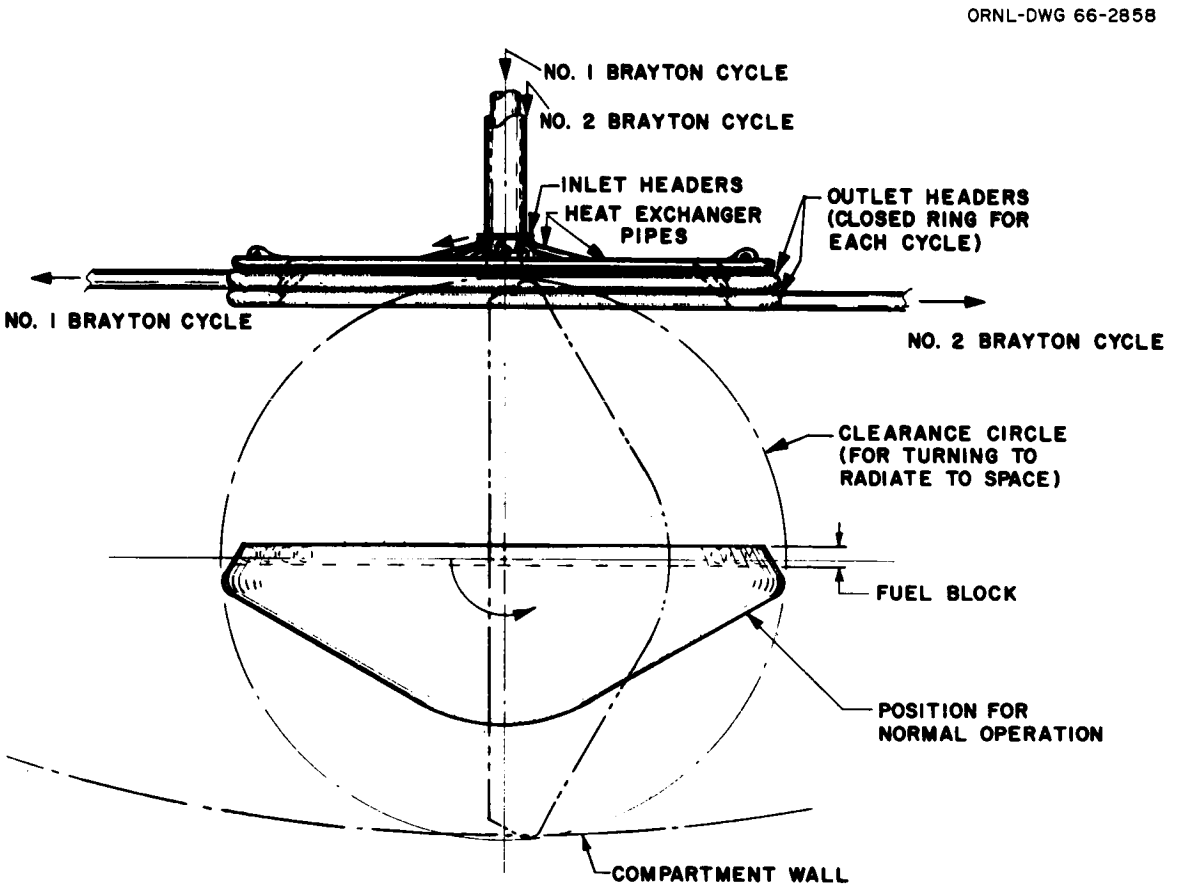

Fig. 10.13. Equipment Arrangement for a Rotating Plane Fuel Reentry Body with a Disk Heat Exchanger.

body during its rotation to see space. The added volume for the clearance space is reflected in the shield configuration given in Fig. 10.14. The shield is elongated and distorted due to the turning mechanism and these perturbations are reflected in the shield weights given in Table 10.6. The table also shows the drastically increased shield weights due to added system volume.

Table 10.6. Shield Weights for One-Year Occupancy of a System With a Rotating Plane Fuel Reentry Body

Fuel	Shielding Material	Crew Shield Weight (lb)		4π Solid Angle Shield Weight (lb)	Total Shield Weight (lb)
		For Scattered Radiation	For Direct Radiation		
$^{244}Cm_2O_3$[a]	LiH	2110	6,290	1410	9,810
	Tantalum	770	12,320	0	13,090
	Total	2880	18,610	1410	22,900
$^{238}PuO_2$[b,c]	LiH	1700	4,180	0	5,880
$^{238}PuO_2$[c,d]	LiH	0	2,190	0	2,190
$^{147}Pm_2O_3$[e]	Tantalum	3470	7,660	750	11,880
$^{147}Pm_2O_3$[f]	Tantalum	2110	5,830	270	8,210

[a] Stress-rate safety factor of 7.

[b] Natural oxygen in fuel compound.

[c] Stress-rate safety factor of 2.5.

[d] Oxygen-18 depleted by a factor of 20 in fuel compound.

[e] $5 \times 10^{-4}\%$ ^{146}Pm contamination.

[f] $5 \times 10^{-5}\%$ ^{146}Pm contamination.

10.1.7 Refluxing Condenser With Surface Tension Forces

A heat pipe concept to eliminate doors, mechanism, and flow-sensing elements led to the equipment arrangement shown in Fig. 10.15. For normal operation the disk heat exchangers and plane fuel reentry body function in the scheme as similar concepts already discussed. The basic

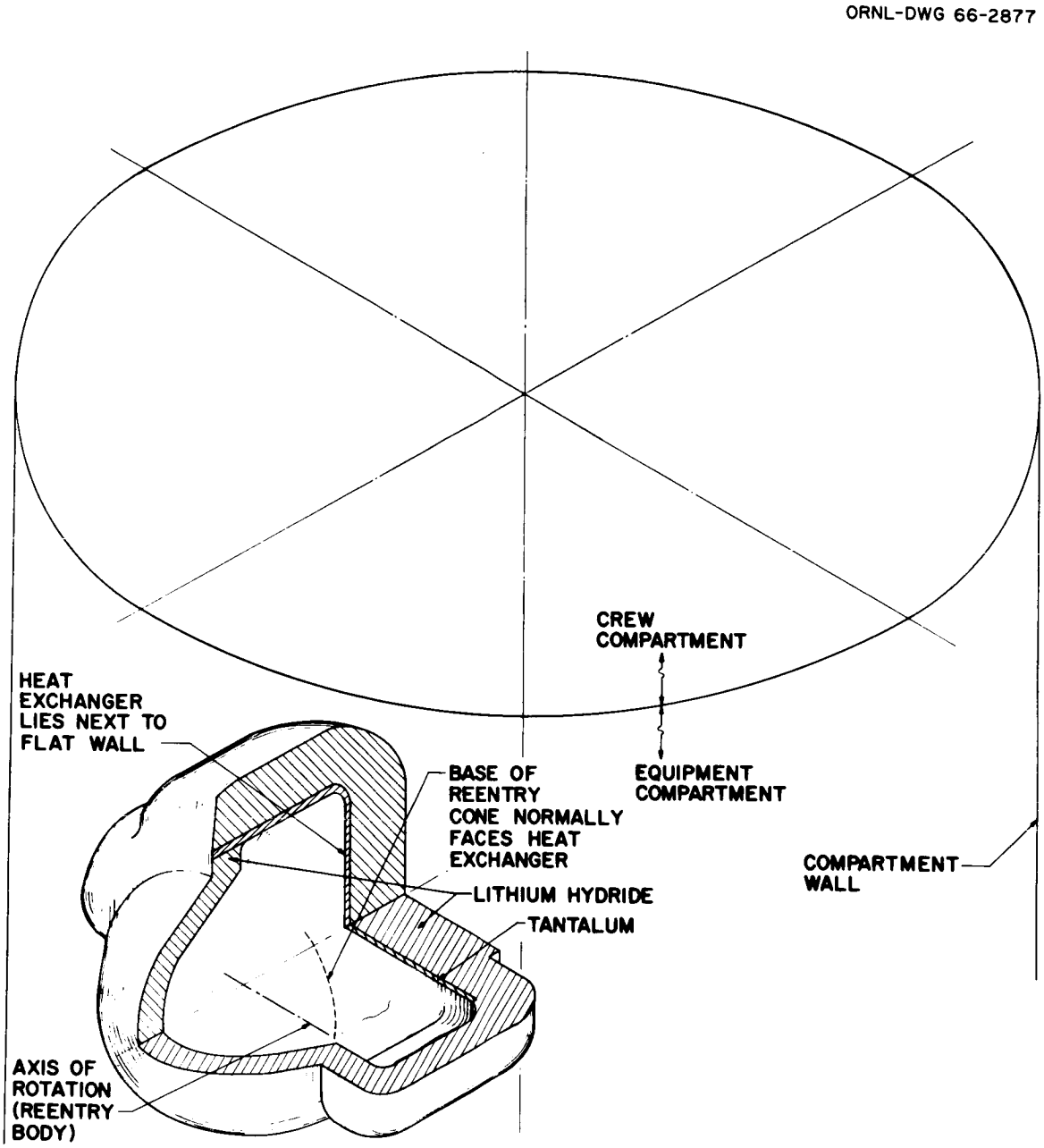

Fig. 10.14. Shielding Configuration for a Rotating Plane Fuel Reentry Body with a Disk Heat Exchanger.

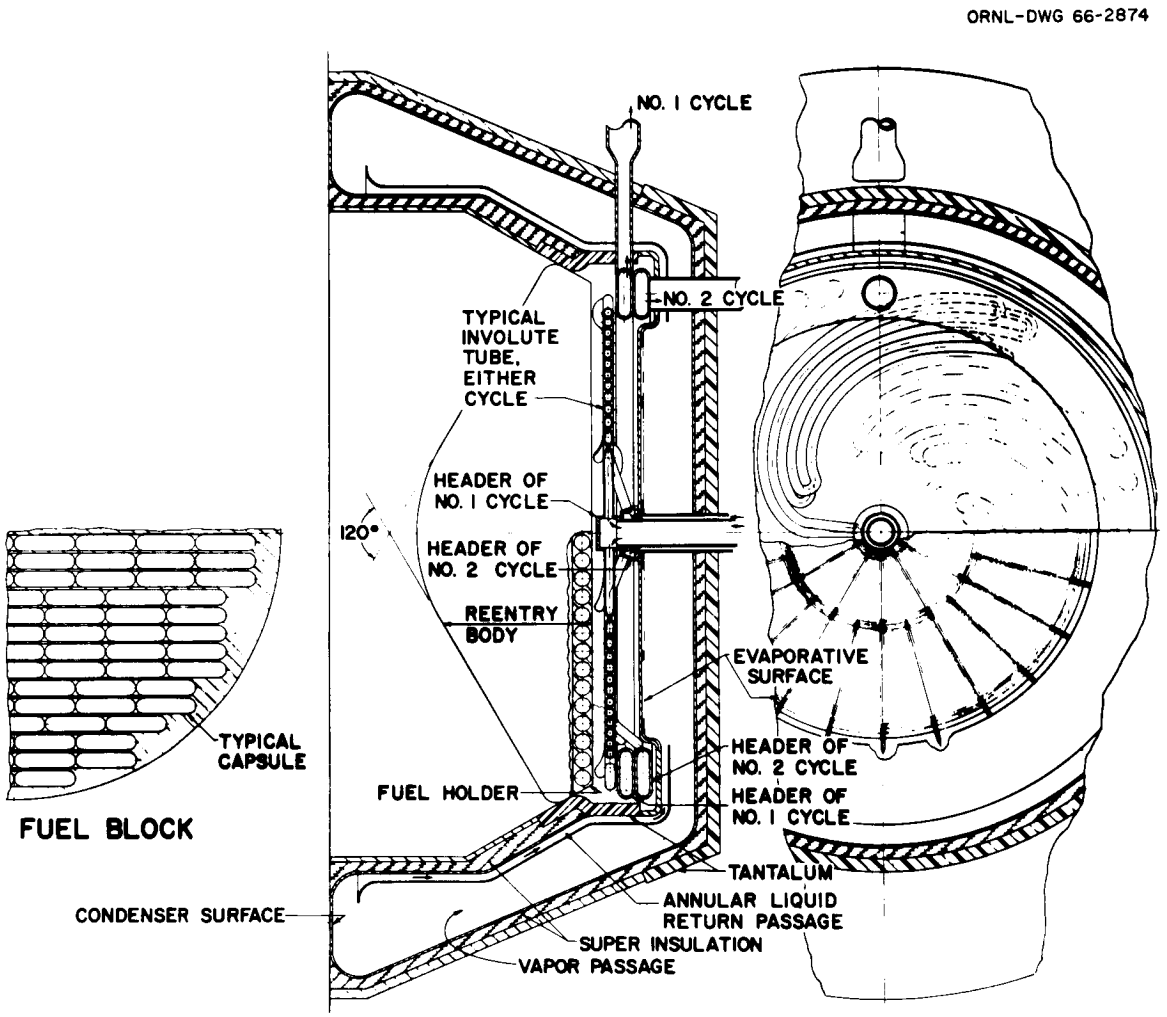

Fig. 10.15. Equipment Arrangement for a Plane Fuel Reentry Body and a Refluxing Condenser with Surface Tension Forces.

difference from the other concepts lies in the passive heat rejection mode.

The passive condition would be activated upon failure of the normal mode by the temperature increasing on the grooved surface located above the heat exchanger tubes. Liquid lithium would begin to evaporate from the surface, and the driving force developed because of differential vapor pressure would force the vapor to the cooler condensing surface. The vapor would condense and the surface tension forces, in the absence of effective gravitational forces, would draw the liquid through the annular return passage and back to the evaporative surface. This is analogous to a simple reflux condenser in which gravity, instead of surface tension, is used to return the liquid to the hot surface, and vapor pressure is used to move the vapor from the hot surface to the condensing section. Both systems have limiting heat fluxes that are determined by vapor binding of the heated surface. In the case of the industrial reflux condenser, buoyancy is used to move the vapor bubbles away from the hot surface to the surface of the liquid. Since in a space application the necessary buoyant forces are absent, surface tension forces would be used to prevent vapor blanketing of the hot surface. The use of the triangular grooves for the capillary distribution system in this heat pipe concept enhances vapor movement from the apex of the grooves to the surface of the liquid. Directional movement results from unequal vapor bubble curvatures that drive the bubble toward the enlarged section of the groove because of the unequal surface tension force. The average heat flux in this heat pipe concept is approximately 5000 $Btu/hr \cdot ft^2$, and it is expected that this is low enough to avoid vapor blanketing problems. With lithium as the heat transfer fluid, a rise in temperature of approximately 300°F above the normal operating temperature would be sufficient to remove the entire heat output of the radioisotope source.

The passive heat rejection would be stopped and normal operation reestablished by starting the argon coolant flow to reduce the temperature on the vaporizing surface. Even at the reduced normal operating temperature at this surface (~1500°F) and the correspondingly low (~2 mm Hg) vapor pressure at the evaporative surface, there would be a small continuous mass transport that would be a disadvantage in this design. However,

it is a completely passive temperature control method that operates independently of controls and orientation, and the intrinsic value of such a self-regulating temperature control circuit could outweigh the disadvantage of the additional builtin energy losses. The development of alloys with a steeper vapor pressure–temperature curve in the range of interest would reduce the heat loss.

The system has a larger volume to be shielded, as shown in Fig. 10.16. Also, the shield must overlap to form a 4π shield arrangement, which further increases the shield weight over that needed for just a large volume. The shield weights shown in Table 10.7 reflect both of these weight increases. The size and location of the flow passages would have a large effect on the shield weight, and it might be possible to reduce their effect on the system weight in a more detailed design study.

Table 10.7. Shield Weights for One-Year Occupancy of a System With a Plane Fuel Reentry Body and a Refluxing Condenser With Surface Tension Forces

Fuel	Shielding Material	Crew Shield Weight (lb)		4π Solid Angle Shield Weight (lb)	Total Shield Weight (lb)
		For Scattered Radiation	For Direct Radiation		
$^{244}Cm_2O_3$[a]	LiH	1240	5,180	1550	7,970
	Tantalum	2470	14,580	0	17,050
	Total	3710	19,760	1550	25,020
$^{238}PuO_2$[b,c]	LiH	870	2,560	0	3,430
$^{238}PuO_2$[c,d]	LiH	0	1,070	0	1,070
$^{147}Pm_2O_3$[e]	Tantalum	990	7,210	2630	10,830
$^{147}Pm_2O_3$[f]	Tantalum	600	5,300	940	6,840

[a] Stress-rate safety factor of 7.

[b] Natural oxygen in fuel compound.

[c] Stress-rate safety factor of 2.5.

[d] Oxygen-18 depleted by a factor of 20 in fuel compound.

[e] $5 \times 10^{-4}\%$ ^{146}Pm contamination.

[f] $5 \times 10^{-5}\%$ ^{146}Pm contamination.

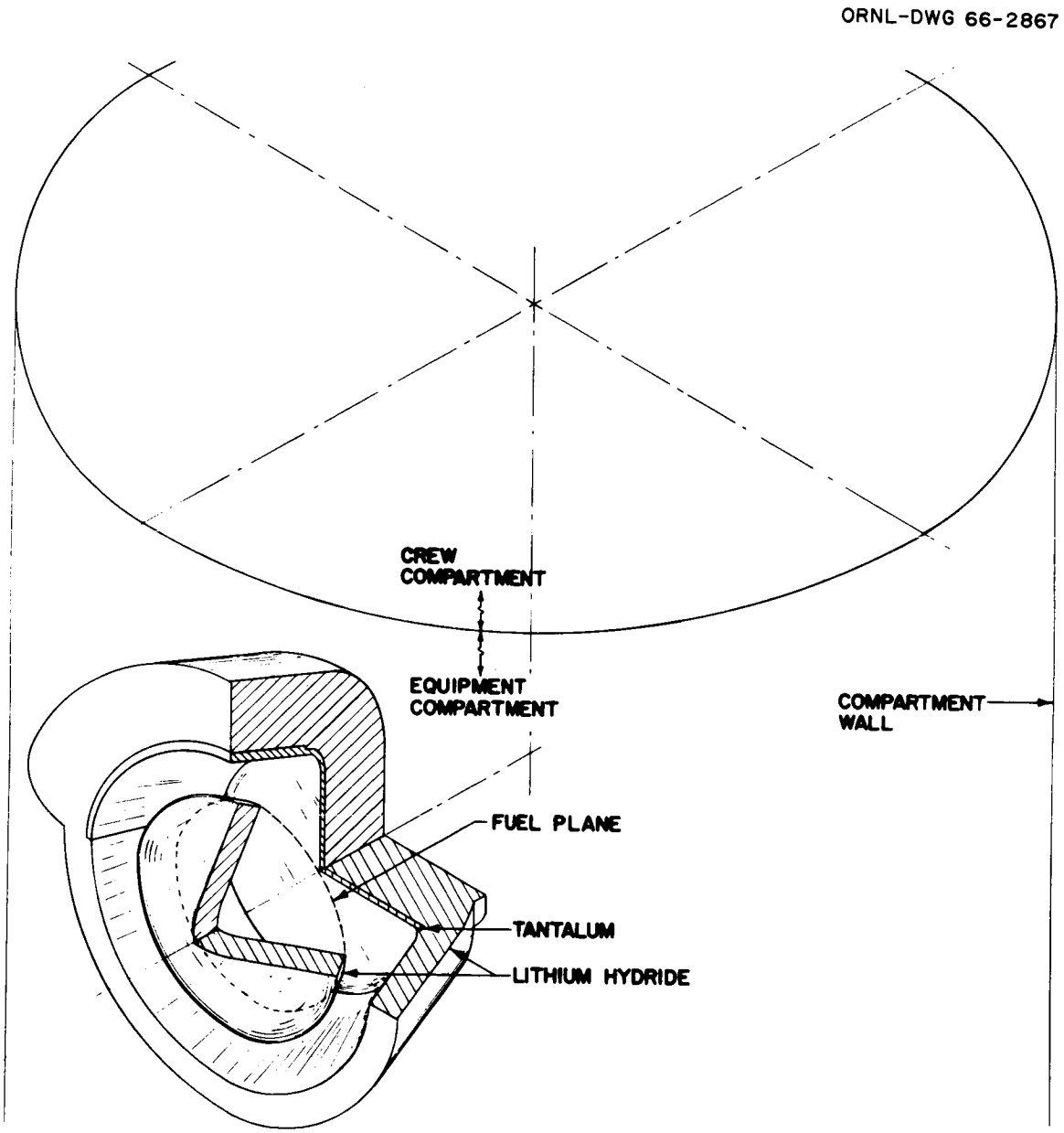

Fig. 10.16. Shielding Configuration for a Plane Fuel Reentry Body and a Refluxing Condenser with Surface Tension Forces.

10.1.8 Fuel in Parallel Rows

An attempt to minimize the shielded volume led to the concept of stacking the fuel capsules in rows, as shown in Fig. 10.17. The entire surface area of the fuel holders would radiate to either active heat exchanger of the redundant pair that penetrate into the heat block. The thermal path would encounter radiation, conduction, and radiation resistances as the heat traveled from the fuel capsules to the working heat exchanger.

The emergency mode of operation would require a door to open, the exchanger to fold out of the way, and radiative heat rejection to space. The capsule holders and heat exchanger tubes are arranged so that the tubes would easily swing out and expose the holders to space. The capsules and holders located the deepest in the fuel block would have high temperatures that would have to be investigated further. It might be necessary to use capsules with a lower heat generation rate per unit surface area toward the center of the array.

Another drawback to this arrangement of fuel and coolant tubes involves the number of heat exchanger tubes in the area of abundant capsules. Although it would be possible to adequately place the required number of tubes in the region of closely spaced capsules, there would be surplus heat exchanger area where the capsules were sparse.

The shielding configuration is shown in Fig. 10.18. The weights would be essentially the same as for some of the previous concepts, as indicated in Table 10.8. This concept has a relatively light weight when compared with the two large-volume concepts (rotating reentry body and reflux condenser with surface tension effects).

10.1.9 Concentric Fuel Array

The concentric stacking of fuel capsules in Fig. 10.19 is another arrangement for a minimum volume system. The comments in Section 10.1.8 about fuel in parallel rows apply equally to this concept. The only change is the method of emergency heat rejection. The roles of the reentry body and heat exchangers would be inverted so that the reentry body

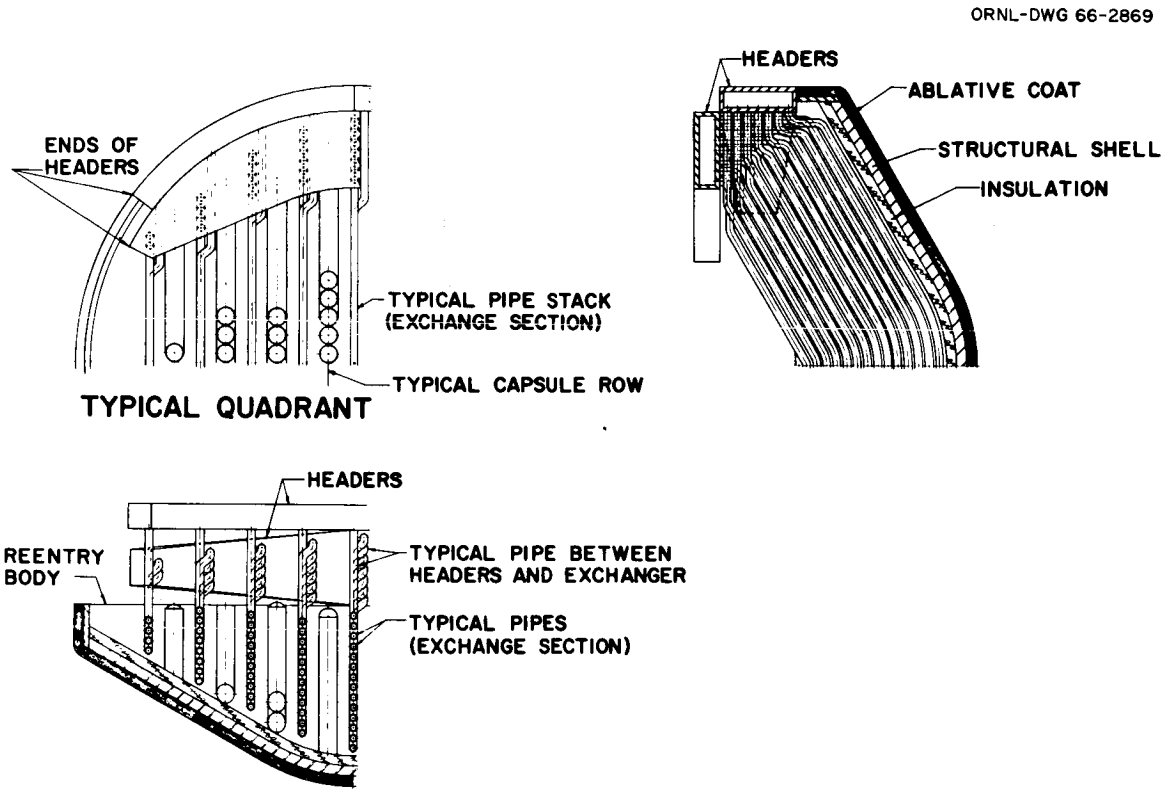

Fig. 10.17. Equipment Arrangement for Fuel in Parallel Rows.

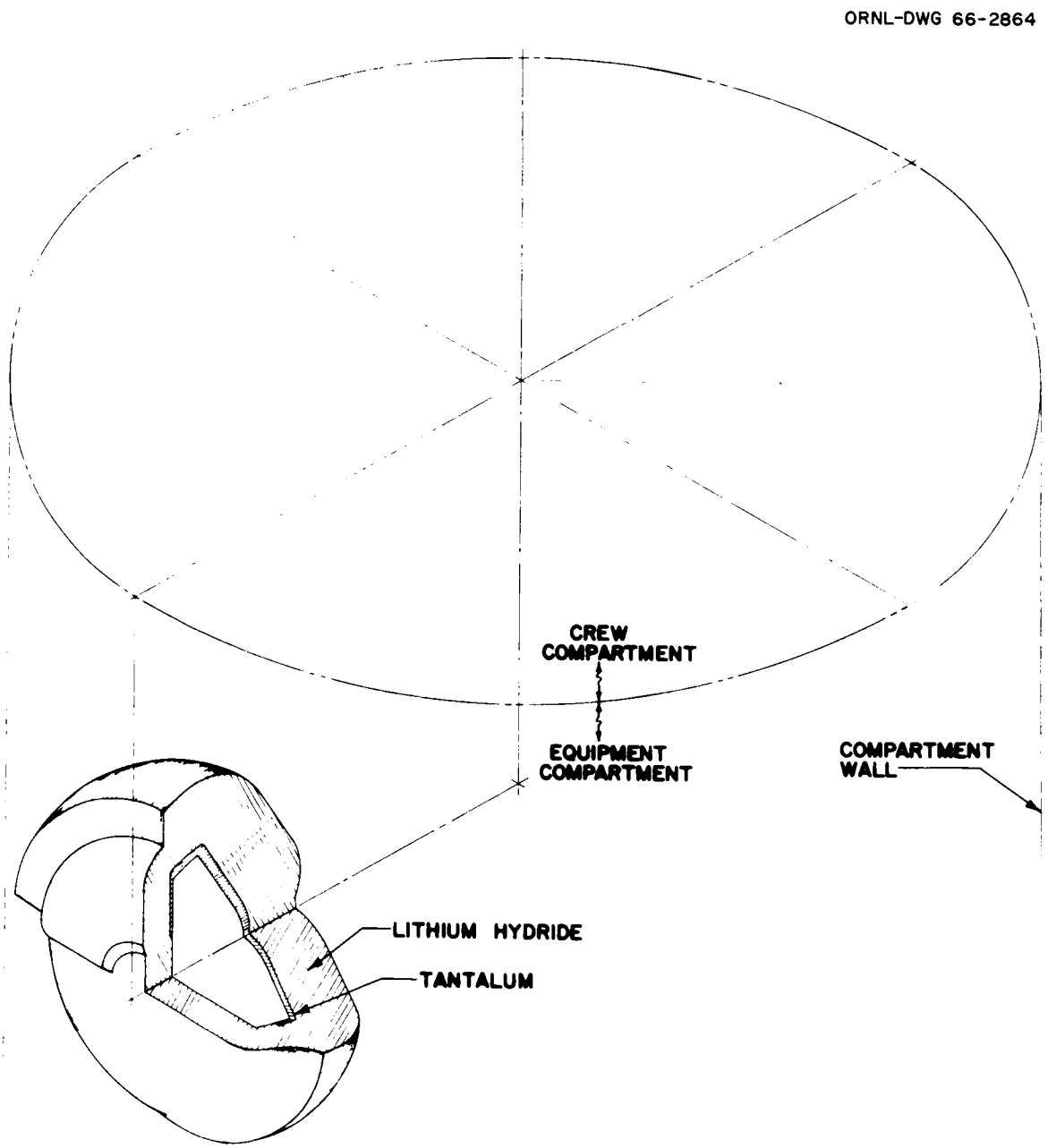

Fig. 10.18. Shielding Configuration for Fuel in Parallel Rows.

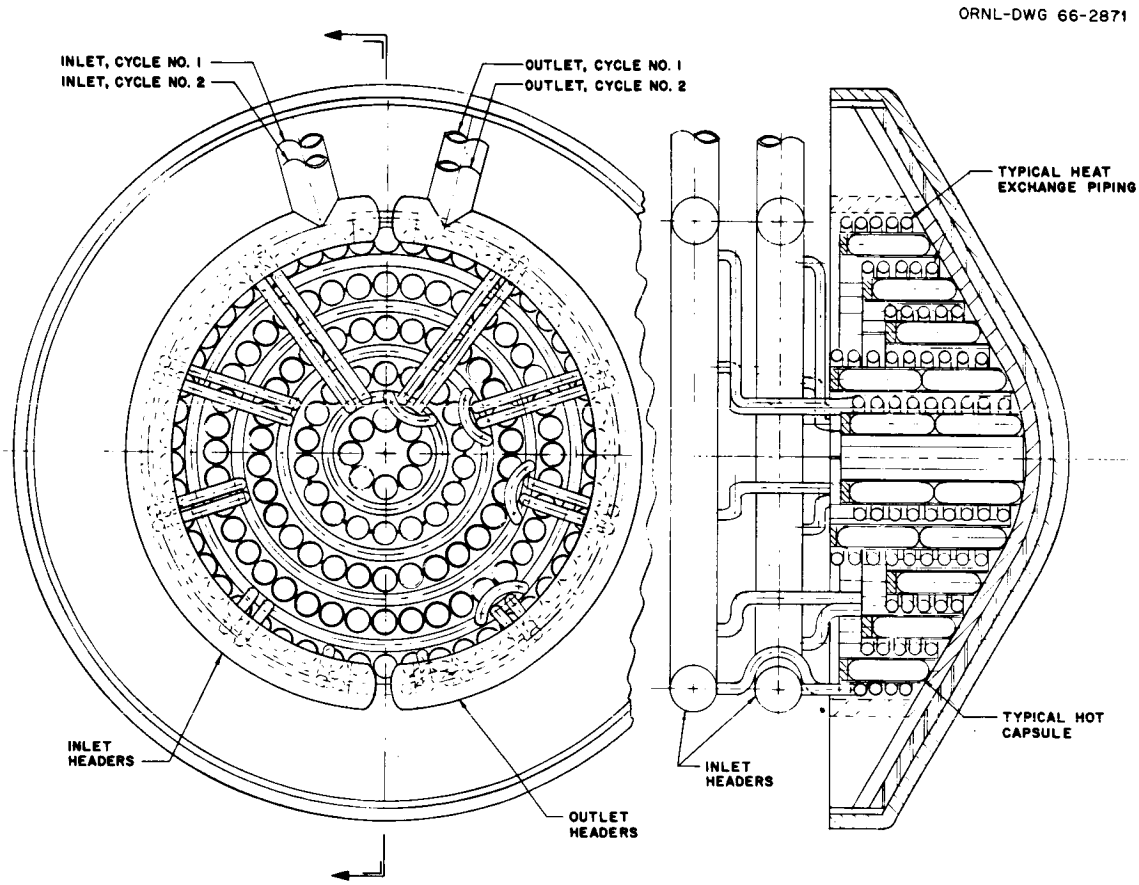

Fig. 10.19. Equipment Arrangement for a Concentric Fuel Array.

Table 10.8. Shield Weights for One-Year Occupancy of a System With Fuel in Parallel Rows

Fuel	Shielding Material	Crew Shield Weight (lb)		4π Solid Angle Shield Weight (lb)	Total Shield Weight (lb)
		For Scattered Radiation	For Direct Radiation		
$^{244}Cm_2O_3$[a]	LiH	1480	3230	1140	5,850
	Tantalum	1100	6190	0	7,290
	Total	2580	9420	1140	13,140
$^{147}Pm_2O_3$[b]	Tantalum	1720	3740	750	6,210
$^{147}Pm_2O_3$[c]	Tantalum	700	3050	500	4,250

[a] Stress-rate safety factor of 7.

[b] $5 \times 10^{-4}\%$ ^{146}Pm contamination.

[c] $5 \times 10^{-5}\%$ ^{146}Pm contamination.

would translate and rotate through a door in the spacecraft. The movement would position the fuel capsules for heat rejection to a space environment.

The shield configuration and shield weights are given in Fig. 10.20 and Table 10.9, respectively, for the concentric fuel array. These weights are in the same range as those for some of the previous concepts.

10.1.10 Summary of Weight Estimates for Conceptual Designs

The system weights for the three fuels are summarized in Tables 10.10 through 10.14 for the concepts that were investigated. The tables give the shield weight, reentry body weight, including fuel capsules, and the sum of these, which is called the lift-off weight. Each table permits a fuel form to be compared for all the concepts for which it was studied.

The summary for the $^{238}PuO_2$ compound depleted in ^{18}O is given in Table 10.10 and the effects of the stress-rate safety factor on system weight are shown for the lightest lift-off weight concept. The weight of this system increased from 3250 to 6550 lb, a factor of 2, as the

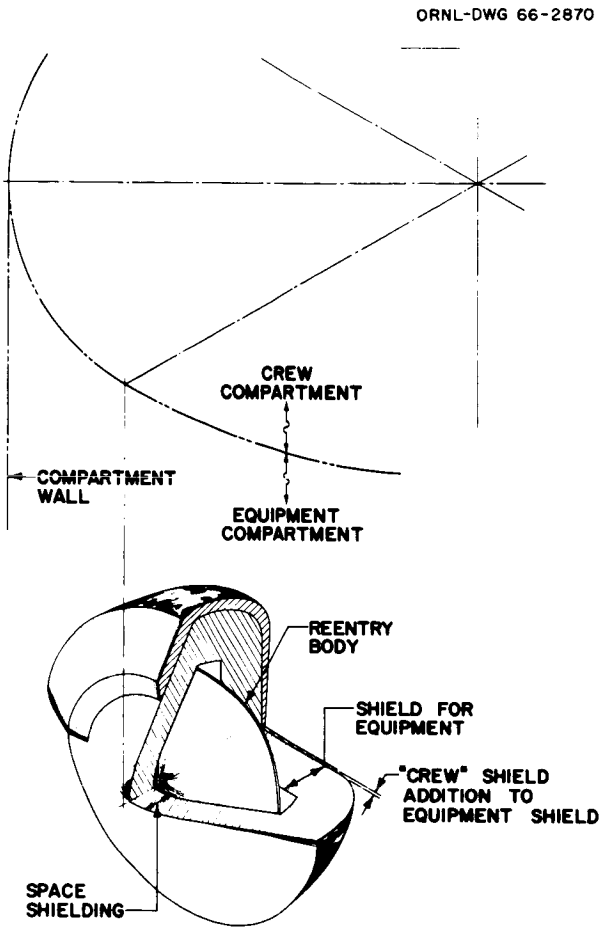

Fig. 10.20. Shielding Configuration for Concentric Fuel Array.

Table 10.9. Shield Weights for One-Year Occupancy of a System With a Concentric Fuel Array

Fuel	Shielding Material	Crew Shield Weight (lb)		4π Solid Angle Shield Weight (lb)	Total Shield Weight (lb)
		For Scattered Radiation	For Direct Radiation		
$^{244}Cm_2O_3$[a]	LiH	1690	3,770	670	6,130
	Tantalum	1780	7,180	0	8,960
	Total	3470	10,950	670	15,090
$^{147}Pm_2O_3$[b]	Tantalum	1980	4,060	270	6,310
$^{147}Pm_2O_3$[c]	Tantalum	1200	3,010	100	4,310

[a] Stress-rate safety factor of 7.

[b] $5 \times 10^{-4}\%$ ^{146}Pm contamination.

[c] $5 \times 10^{-5}\%$ ^{146}Pm contamination.

Table 10.10 Weight Summary for System With $^{238}PuO_2$ Fuel Designed for One-Year Occupancy

^{18}O depleted by a factor of 20 in fuel compound

Concept	Stress-Rate Safety Factor	Shield Weight (lb)	Reentry Body Weight (lb)	Lift-Off Weight (lb)
Plane fuel reentry body with folding heat exchanger	2.5	950	2300	3250
	4.0	1100	3150	4250
	7.0	1750	4800	6550
60° conical fuel reentry body with folding heat exchanger	2.5	1150	2500	3650
Plane fuel reentry body and refluxing condenser with surface tension forces	2.5	1070	2300	3370
Deployed 60° conical fuel reentry body	2.5	1590	2500	4090
Rotating plane fuel reentry body with disk heat exchanger	2.5	2190	2300	4490

Table 10.11. Weight Summary for System with $^{238}PuO_2$ Fuel Designed for One-Year Occupancy

Natural oxygen in fuel compound

Concept	Stress-Rate Safety Factor	Shield Weight (lb)	Reentry Body Weight (lb)	Lift-Off Weight (lb)
Plane fuel reentry body with folding heat exchanger	2.5	2110	2300	4410
	4.0	2450	3150	5600
	7.0	3500	4800	8300
60° conical fuel reentry body with folding heat exchanger	2.5	3420	2500	5920
Plane fuel reentry body and refluxing condenser with surface tension forces	2.5	3430	2300	5730
Deployed 60° conical fuel reentry body	2.5	3670	2500	6170
Rotating plane fuel reentry body with disk heat exchanger	2.5	5880	2300	8180

safety factor changed from 2.5 to 7. The weight variation between concepts, at a constant safety factor, is only approximately 40% from the lightest to the heaviest.

Natural oxygen in the $^{238}PuO_2$ fuel compound is considered in Table 10.11. The weights show almost a factor of 2 in the effect of the stress-rate safety factor and in comparison of concepts.

Weights for systems with $^{147}Pm_2O_3$ fuel are summarized in Table 10.12 for production reactor feed material and in Table 10.13 for power reactor feed material. Both tables indicate that the choice of concept can change the lift-off weight by a factor of approximately 2 from the lightest weight to the heaviest weight systems.

The weight summary for systems with $^{244}Cm_2O_3$ fuel is given in Table 10.14. A stress-rate safety factor change from 2.5 to 7 for the lightest weight concept (folding heat exchanger) caused a 50% increase in weight. The conceptual choices have over a factor of 2 variation in lift-off weight. The curium fuel with the reference shielding model exhibits an

Table 10.12. Weight Summary for System with $^{147}Pm_2O_3$ Fuel Designed for One-Year Occupancy

$5 \times 10^{-5}\%$ $^{146}Pm_2O_3$ contamination

Concept	Shield Weight (lb)	Reentry Body Weight (lb)	Lift-Off Weight (lb)
Plane fuel reentry body with folding heat exchanger	3550	1390	4940
Fuel in parallel rows	4250	1460	5710
Concentric fuel	4310	1460	5770
60° conical fuel reentry body with folding heat exchanger	4250	1550	5800
Deployed 60° conical fuel reentry body with conical heat exchanger	4310	1550	5860
Plane fuel reentry body and refluxing condenser with surface tension forces	6840	1390	8230
Rotating plane fuel reentry body with disk heat exchanger	8210	1390	9600

obvious weight disadvantage that is directly related to the double shielding (gamma and neutron) requirement, which is not fully compensated by the smaller volume of fuel required for curium concepts.

10.2 Weight Reduction Program

A brief investigation was made to indicate the conditions under which $^{244}Cm_2O_3$ would become competitive with $^{238}PuO_2$ on a system weight basis. Since the shield is the system component that makes the $^{244}Cm_2O_3$ fuel concepts heavier than the $^{238}PuO_2$, varying the location of the heat source with respect to the manned compartment and changing the dose criteria were considered.

Table 10.13. Weight Summary for System with $^{147}Pm_2O_3$ Fuel Designed for One-Year Occupancy

$5 \times 10^{-4}\%$ $^{146}Pm_2O_3$ contamination

Concept	Shield Weight (lb)	Reentry Body Weight (lb)	Lift-Off Weight (lb)
Plane fuel reentry body with folding heat exchanger	5,500	1390	6,890
Fuel in parallel rows	6,210	1460	7,670
60° conical fuel reentry body with folding heat exchanger	6,210	1550	7,760
Concentric fuel	6,310	1460	7,770
Deployed 60° conical fuel reentry body with conical heat exchanger	6,310	1550	7,860
Plane fuel reentry body and refluxing condenser with surface tension forces	10,830	1390	12,220
Rotating plane fuel reentry body with disk heat exchanger	11,880	1390	13,270

10.2.1 Dose Rate Increase

The allowable dose rate was increased by a factor of 4 while retaining the same total accumulated dose by assuming a mission duration for the crew of 90 days rather than one year. The effect of making this assumption on the total system weight for the lightest weight concept (plane fuel array with folding heat exchanger and stress-rate safety factor of 2.5) is shown in Table 10.15. Comparing these weights with those given in Tables 10.10 through 10.14, which are for one-year occupancy, shows that the total system lift-off weight reduction varies from approximately 12% in the case of $^{238}PuO_2$ fuel depleted in ^{18}O to 40% in the case of $^{244}Cm_2O_3$ fuel.

The curium fuel form received the greatest benefit from a dose rate increase because of the relatively heavy shield and light-weight reentry body. Systems with ^{147}Pm show the same trend but to a lesser degree

Table 10.14. Weight Summary for System with $^{244}Cm_2O_3$ Fuel Designed for One-Year Occupancy

Concept	Stress-Rate Safety Factor	Shield Weight (lb)	Reentry Body Weight (lb)	Lift-Off Weight (lb)
Plane fuel reentry body with folding heat exchanger	2.5	6,850	650	7,500
	4.0	7,900	800	8,700
	7.0	10,100	1040	11,140
Fuel in parallel rows	7.0	13,140	1120	14,260
60° conical fuel reentry body with folding heat exchanger	7.0	13,140	1210	14,350
Directly cooled plane fuel reentry body	7.0	13,630	2050	15,680
Inclined plane fuel reentry body with disk heat exchanger	7.0	15,010	1040	16,050
Concentric fuel	7.0	15,090	1120	16,210
Deployed 60° conical fuel reentry body	7.0	15,090	1210	16,300
Rotating plane fuel reentry body with disk heat exchanger	7.0	22,900	1040	23,940
Plane fuel reentry body and refluxing condenser with surface tension forces	7.0	25,020	1040	26,060

Table 10.15. Extimated Weight Summary for 90-Day Occupancy of System with Plane Fuel Array and Folding Heat Exchanger

Stress-rate safety factor: 2.5

Fuel	Shield Weight (lb)	Reentry Body Weight (lb)	Lift-Off Weight (lb)
$^{238}PuO_2$[a]	540	2300	2840
$^{238}PuO_2$[b]	1360	2300	3660
$^{147}Pm_2O_3$[c]	2230	1390	3620
$^{244}Cm_2O_3$	4000	650	4650

[a] Oxygen-18 depleted by a factor of 20 in fuel compound.

[b] Natural oxygen in fuel compound.

[c] $5 \times 10^{-5}\%$ $^{146}Pm_2O_3$ contamination.

because the reentry body weight is greater than that for the curium fuel.

The fuel with the heaviest lift-off weight, $^{244}Cm_2O_3$, was examined for the effect of variations in the heat source concept on shield weights and lift-off weights under this higher dose rate. A stress-rate safety factor of 7 was chosen for the comparison. The shield weight breakdowns given in Table 10.16 show total shield weight decreases of approximately 30% for all concepts. The smaller reduction, 30% for these heat source concept variations compared with 40% for the plane fuel array previously discussed, is caused by the different stress-rate safety factor. The trend follows expectation; that is, the fractional savings in shield weight are reduced as the stress-rate safety factor increases. The lift-off weights in Table 10.17 show the reduction to be approximately 27%, as would be anticipated.

10.2.2 Location

The shadow shield model shown in Fig. 10.21 was used to give a preliminary indication of the effect of location on lift-off weight. The effect of heat source to manned compartment separation distance on lift-off weight is given in Figs. 10.22, 10.23, and 10.24 for stress-rate safety factors of 2.5, 4, and 7, respectively, for $^{244}Cm_2O_3$ and ^{18}O-depleted $^{238}PuO_2$.

The shadow shield model does not include the contribution from scattering collisions or the 4π shield requirement, which were included in the original shield model. In the case of ^{18}O-depleted $^{238}PuO_2$, a 4π shield was not required in the original conceptual design model to meet the dose rate criteria, so the shadow shield model approximates the actual model. This is not true in the case of ^{244}Cm, and therefore a 4π shield model for the folding heat exchanger concept with $^{244}Cm_2O_3$ as the fuel was evaluated for different separation distances. The results are plotted along with those for the shadow shield model in the figures to compare with the shadow shield model results. The plots show that the curium system weights decrease very rapidly with heat source to manned compartment separation distance and that points will be reached where the ^{238}Pu and ^{244}Cm system weights will be equal. Figures 10.22

Table 10.16. Shield Weight Breakdown for a System with $^{244}Cm_2O_3$ Fuel Designed for 90-Day Occupancy

Stress rate safety factor: 7

Concept	Shielding Material	Crew Shield Weight (lb)		4π Solid Angle Shield Weight (lb)	Total Shield Weight (lb)
		For Scattered Radiation	For Direct Radiation		
Plane fuel array with folding heat exchanger	LiH	1020	2,150	1000	4,170
	Tantalum	300	3,430	0	3,730
	Total	1320	5,580	1000	7,900
60° conical fuel reentry body with folding heat exchanger	LiH	830	2,060	1140	4,030
	Tantalum	590	4,590	0	5,180
	Total	1420	6,650	1140	9,210
Fuel in parallel rows	LiH	830	2,060	1140	4,030
	Tantalum	590	4,590	0	5,180
	Total	1420	6,650	1140	9,210
Directly cooled plane fuel reentry body	LiH	990	2,150	870	4,010
	Tantalum	490	4,750	0	5,240
	Total	1480	6,900	870	9,250
Inclined plane fuel reentry body with disk heat exchanger	LiH	1790	1,600	1710	5,100
	Tantalum	2600	2,400	0	5,000
	Total	4390	4,000	1710	10,100
Concentric fuel	LiH	1080	2,670	670	4,420
	Tantalum	920	4,950	0	5,870
	Total	2000	7,620	670	10,290
Deployed 60° conical fuel reentry body	LiH	1080	2,670	670	4,420
	Tantalum	920	4,950	0	5,870
	Total	2000	7,620	670	10,290
Rotating plane fuel reentry body with disk heat exchanger	LiH	1460	4,740	1410	7,610
	Tantalum	410	9,150	0	9,560
	Total	1870	13,890	1410	17,170
Plane fuel reentry body and refluxing condenser with surface tension forces	LiH	980	3,450	1550	5,980
	Tantalum	1330	10,800	0	12,130
	Total	2310	14,250	1550	18,110

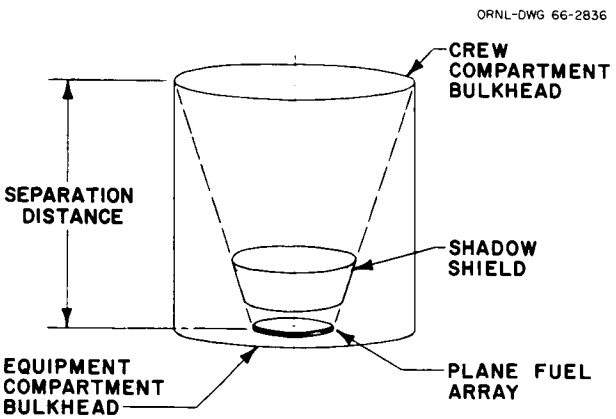

Fig. 10.21. Shadow Shield Analytical Model.

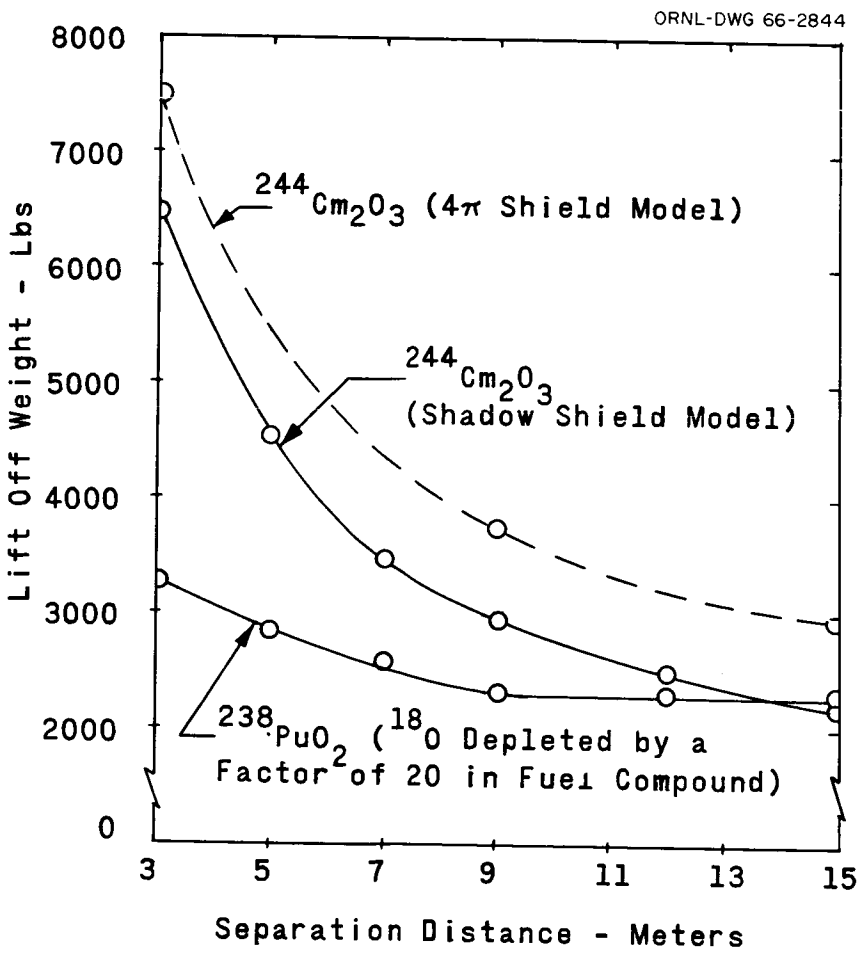

Fig. 10.22. Effect of Reentry Body Location on Lift-off Weight for Stress-Rate Safety Factor of 2.5.

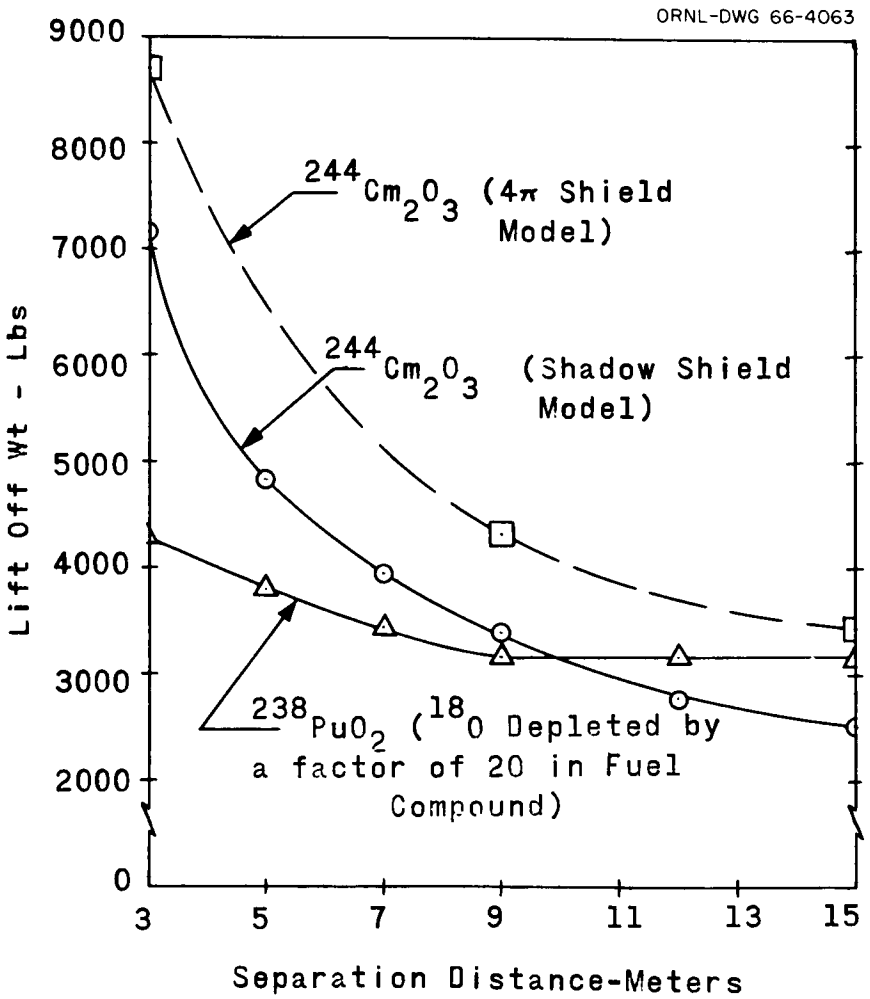

Fig. 10.23. Effect of Reentry Body Location on Lift-off Weight for Stress-Rate Safety Factor of 4.

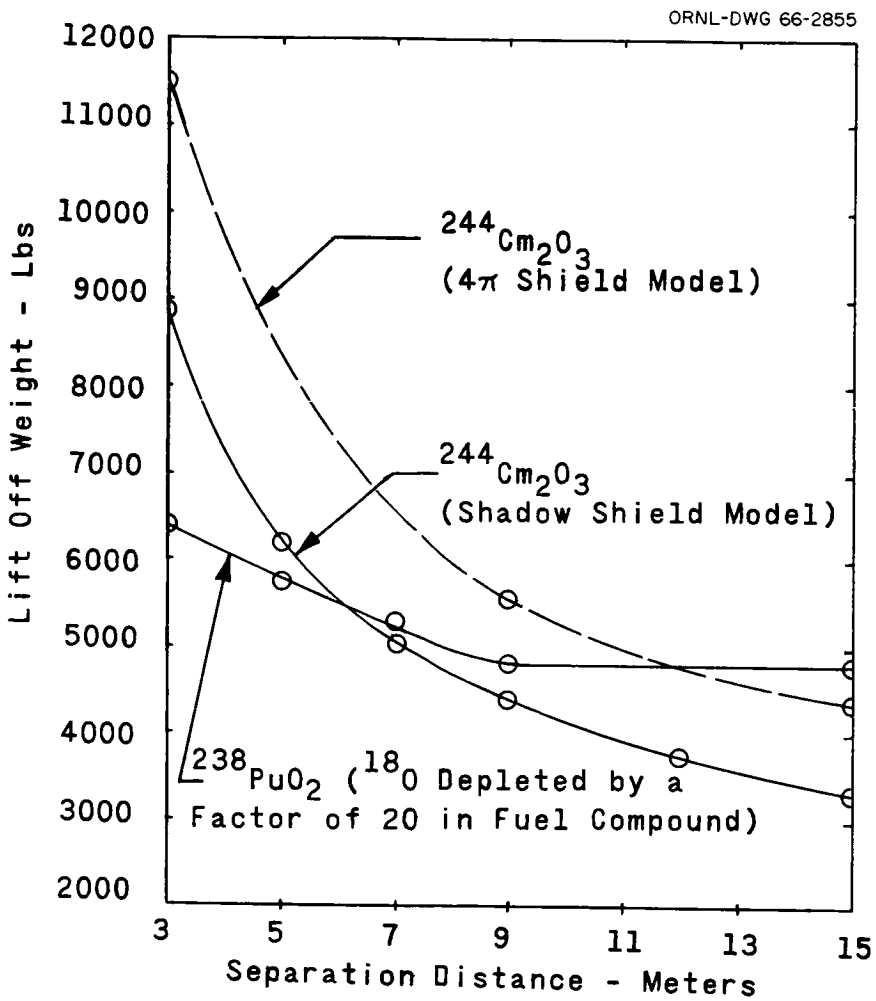

Fig. 10.24. Effect of Reentry Body Location on Lift-off Weight for Stress-Rate Safety Factor of 7.

Table 10.17. Weight Summary for System with $^{244}Cm_2O_3$ Fuel Designed for 90-Day Occupancy

Stress-rate safety factor: 7

Concept	Shield Weight (lb)	Reentry Body Weight (lb)	Lift-Off Weight (lb)
Plane fuel array with folding heat exchanger	7,900	1040	8,940
Fuel in parallel rows	9,210	1120	10,330
60° conical fuel reentry body with folding heat exchanger	9,210	1210	10,420
Inclined plane fuel reentry body with disk heat exchanger	10,100	1040	11,140
Directly cooled plane fuel reentry body	9,250	2050	11,300
Concentric fuel	10,290	1120	11,410
Deployed 60° conical fuel reentry body	10,290	1210	11,500
Rotating plane fuel reentry body with disk heat exchanger	17,170	1040	18,210
Plane fuel reentry body and refluxing condenser with surface tension forces	18,110	1040	19,150

through 10.24 indicate these locations for both the 4π shield model and the shadow shield model for stress-rate safety factors from 2.5 to 7. The locations for the 4π shield model have separation distances that exceed reasonable values, except possibly in the case of a concept with a deployable power generation system. However, as the distance increases, the weight penalty for using $^{244}Cm_2O_3$ rather than PuO_2 with depleted oxygen becomes less significant and may be justifiable on the basis of the fuel availability or safety considerations. A comparison is given in Fig. 10.25 for separation distances of 3 and 9 meters so that the penalty assessment can be evaluated for different capsule stress-rate safety factors. The PuO_2 lift-off weight is included in the figure for reference.

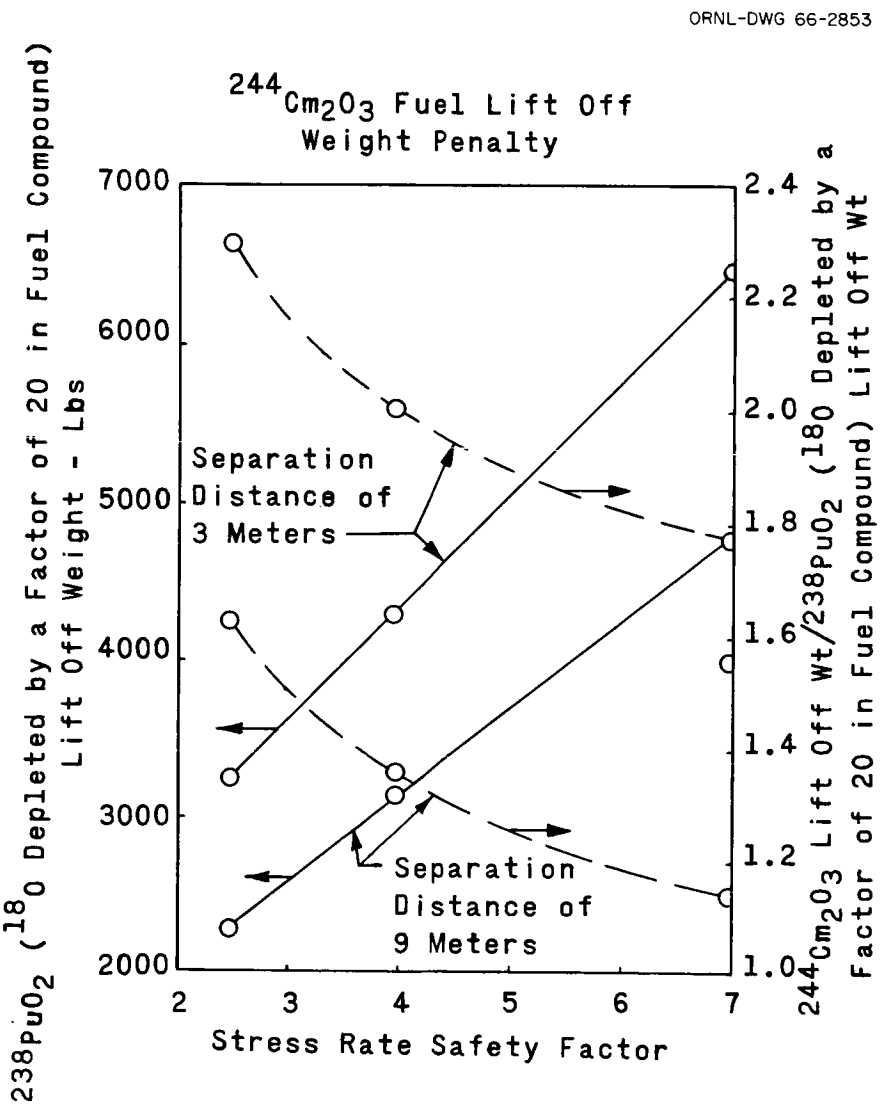

Fig. 10.25. Comparison of Lift-Off Weights for $^{238}PuO_2$ and $^{244}Cm_2O_3$ Fuels as Functions of Separation Distance and Stress-Rate Safety Factor.

ACKNOWLEDGMENT

In addition to the assistance, previously noted, given by L. I. Shure of the NASA-Lewis Research Center, and P. J. Bobbitt of the NASA-Langley Research Center, the authors are also indebted for the assistance given by Mrs. Susan C. Keith of the ORNL Isotopes Development Center who prepared the draft of this report and who offered many valuable suggestions on the arrangement of figures, references, and sections in the report.

REFERENCES

1. G. R. Grove et al., Plutonium-238 Isotopic Power Sources: A Summary Report, USAEC Report MLM-1270, Monsanto Research Corporation, Mound Laboratory, Aug. 19, 1965.
2. Monsanto Research Corporation, Mound Laboratory, Plutonium-238 Fuel Data Sheets, Nov. 15, 1965. Classified
3. L. M. Atlas, G. J. Schlehman, Katharometric and Resistivity Studies of PuO_{2-x} Equilibria, USAEC Report ANL-6960, Argonne National Laboratory, March 1965.
4. A. D. Feith, Thermal Conductivities of Several Ceramic Materials to 2500°C, USAEC Report TM-64-10-4, General Electric Company, NMPO, October 1964.
5. R. M. Dell and M. Allbutt, The Nitrides and Sulphides of Uranium, Thorium, and Plutonium: A Review of Present Knowledge, British Report AERE-R-4253, March 1963.
6. T. Vasilos and W. D. Kingery, Thermal Conductivity: XI, Conductivity of Some Refractory Carbides and Nitrides, J. Amer. Ceram. Soc., 37(9): 409–414 (September 1965).
7. D. L. McElroy, unpublished data, Oak Ridge National Laboratory.
8. J. C. Posey et al., The Influence of Temperature and Oxygen Pressure on the Composition of Curium Oxide, Paper presented at 150th Meeting of the American Chemical Society, Atlantic City, Sept. 13–17, 1965, Abstract 26R-64.
9. H. S. Hilborn, SRL Isotopic Power and Heat Sources Monthly Progress Report, USAEC Report DPST-66-102-9, Savannah River Laboratory, September 1966.
10. D. H. Stoddard (Comp.), Radiation Properties of ^{244}Cm Produced for Isotopic Power Generators, USAEC Report DP-939, Savannah River Laboratory, 1964.
11. R. E. McHenry et al., unpublished data, Oak Ridge National Laboratory.
12. T. A. Butler and R. E. McHenry (Comps.), Curium-244 Status Report, USAEC Report ORNL-TM-1036, Oak Ridge National Laboratory, February 1965. Classified
13. H. H. Van Tuyl (Comp.), Promethium Isotopic Power Data Sheets, USAEC Report NNWC-45, Battelle-Northwest, Mar. 15, 1965.

14. R. K. Williams and D. L. McElroy, Estimated Thermal Conductivity Values for Solid and Liquid Promethium, USAEC Report ORNL-TM-1424, Oak Ridge National Laboratory, March 1966.

15. Isotopic Power Fuels Data, Division of Isotopes Development, U.S. Atomic Energy Commission, March 1966.

16. E. J. Hennelly and R. R. Hood, Radioisotope Production Capabilities of U.S. Power Reactors, USAEC Report DP-1015, Savannah River Laboratory, November 1965.

17. W. Luoma and R. C. Emanuelson, Semi-Annual Progress Report on Determination of the Emissivity of Materials, Report NASA-CR-54891, Pratt & Whitney, December 1965.

18. J. S. Hill and H. J. Albert, Loss of Weight of Plutonium, Rhodium, and Palladium at High Temperatures, Englehardt Industires, Inc., Technical Bulletin No. 2, Vol. IV, pp 59–63, September 1963.

19. C. A. Krier and R. I. Jaffee, Oxidation of the Platium Group Metals, J. Less Common Metals, 5: 411–431 (1963).

20. E. D. Zysk, Effect of Environment on Bare Platinum vs 90 Pt–10 Rh and Platinum vs 87 Pt–13 Rh Thermocouples, Englehardt Industries, Inc., memorandum dated April 12, 1960.

21. H. H. Uhlig, The Corrosion Handbook, p. 449, Wiley, 1948.

22. D. B. Ander, International Nickel Company, personal communication to R. J. Beaver, letter dated December 13, 1965, with attachment.

23. Union Carbide Corporation, Stellite Division, Compilation of Seawater Corrosion Data for Hastelloy C, Report F-30,322, December 1965.

24. D. B. Anderson and R. F. Vines, Anodic Corrosion of Platinum in Seawater, paper presented at Second International Congress on Metallic Corrosion, New York, March 11–15, 1963.

25. R. E. Seebold and L. S. Birks, Elevated Temperature Diffusion in the Systems Nb-Pt, Nb-Se, Nb-Zn, Nb-Co, Ni-Ta, and Fe-Mo, Report NRL-5520, Naval Research Laboratory, Sept. 19, 1960.

26. J. J. English, Binary and Ternary Phase Diagrams of Columbium, Molybdenum, Tantalum, and Tungsten, DMIC Report 183, Battelle Memorial Institute Defense Metals Information Center, Feb. 7, 1963.

27. E. M. Passmore et al., Diffusion Barriers for Tantalum and Columbium, ASM Trans., 57: 760–765 (1964).

28. G. G. Lessman and D. R. Stoner, Welding Refractory Metal Alloys for Space Power System Application, Report WANL-SP-009, Westinghouse Electric Corporation, Astronuclear Laboratory, Nov. 15, 1965.

29. G. G. Lessman and D. R. Stoner, Determination of the Weldability and Elevated Temperature Stability of Refractory Metal Alloys, Ninth Quarterly Report, Report NASA-CR-54923, Westinghouse Electric Corporation, Astronuclear Laboratory, September 1965.

30. Oak Ridge National Laboratory, Metals and Ceramics Division Annual Progress Report for Period Ending May 31, 1962, USAEC Report ORNL-3313, Aug. 16, 1962.

31. Unpublished ORNL data.

32. J. C. Sawyer and E. A. Steigerwald, Generation of Long Time Creep Data of Refractory Alloys at Elevated Temperatures, Eleventh Quarterly Progress Report, Report NASA-CR-54973, TRW Inc., April 1966.

33. R. W. Buckman and R. C. Goodspeed, Development of Dispersion Strengthened Tantalum Base Alloy, Eighth Quarterly Progress Report, Report NASA-CR-54935, Westinghouse Electric Corporation, Astronuclear Laboratory, November 1965.

34. Bureau of Mines Bulletin 542.

35. A. Glassner, The Thermochemical Properties of the Oxides, Fluorides, and Chlorides to 2500°K, USAEC Report ANL-5750, Argonne National Laboratory, 1957.

36. T. D. Chikalla, Plutonium Refractory Compounds, Chapter 6 of an unpublished book.

37. L. E. Russell et al., Pervoskite Type Compounds Based on Plutonium, British Report AERE-R-3044, 1959.

38. J. J. Granger et al., Uranium Dioxide Compatibility with Refractory Metals, Carbides, Borides, Nitrides, and Oxides Between 3500°F and 5000°F, Report NASA-TN-D-262, National Aeronautical and Space Administration, February 1960.

39. Reference 39 deleted.

40. R. G. Gilliland, Brazing Alloy Development, in Metals and Ceramics Division Annual Progress Report for Period Ending June 30, 1965, USAEC Report ORNL-3870, Oak Ridge National Laboratory, November 1965.

41. General Electric Company, Advanced Technology Services, High Temperature Materials and Reactor Component Development Programs, Fourth Annual Report, Vol. I, Materials, Report GEMP-334A, Feb. 26, 1965.

42. C. W. Yound, C. E. Stoneking, and J. L. Colp, Containment Capsule Impact Safety Study, Phase A, Progress Report, Report SC-RR-65-9, Sandia Corporation, July 1965.

43. H. Laurens, The Physiological Effects of Radiant Energy, p. 104, The Chemical Catalog Company, Inc., 1933.

44. B. Manowitz and L. Epel, Brookhaven National Laboratory, personal communication, January 1966.

45. D. H. Stoddard and E. L. Albenesius, Radiation Properties of ^{238}Pu Produced for Isotopic Power Generators, USAEC Report DP-984, Savannah River Laboratory, July 1965.

46. A. G. Khabakhpashev, The Neutron Spectrum of a Po-α-O Source, Atomnaya Energiya, 7: 71 (1959).

47. E. D. Arnold, Handbook of Shielding Requirements and Radiation Characteristics of Isotopic Power Sources for Terrestrial, Marine, and Space Applications, USAEC Report ORNL-3576, Oak Ridge National Laboratory, April 1964.

48. J. P. Nichols, Calculations of Concrete Shields for Fission Sources, USAEC Report ORNL-TM-1167, Oak Ridge National Laboratory, June 1965.

49. B. J. Henderson, Conversion of Neutron or Gamma-Ray Flux to Absorbed Dose Rate, USAEC Report XDC-59-8-179, General Electric Company, Aircraft Nuclear Propulsion Department, Aug. 14, 1959.

50. U.S. National Committee on Radiation Protection and Measurements, Protection Against Neutron Radiation up to 30 Million Electron Volts, NBS Handbook 63, National Bureau of Standards, 1957.

51. L. L. Carter, Unreflected Critical Mass of ^{238}Pu Metal, p. 53 in Physics Research Quarterly Report, July–September 1964, USAEC Report HW-84369, General Electric Company, Hanford Atomic Products Operation, Oct. 15, 1964.

52. General Electric Company, Missile and Space Division, Preliminary Design and Safety Studies of Large Radioisotope Heat Sources for Space Power, Report GE-65SD4508-2A, App. B, 1966.

53. Atomics International, Large Radioisotope Heat Source Study – Final Report, Report AI-65-221, Vol. II, 1965.

54. D. K. Butler and R. K. Sjoblom, Fission Cross Section of Pu^{238}, Bull. Amer. Phys. Soc., 8: 369 (1963).

55. L. D. Gordeeva and G. N. Smirenkin, An Empirical Formula for the Mean Number of Fission Neutrons, AERE Trans., 956 (1962).

56. D. M. Barton, Los Alamos Scientific Laboratory, personal communication to C. W. Craven, Jr., Oak Ridge National Laboratory, 1966.

57. R. E. Cote´ et al., Total Neutron Cross Section of ^{244}Cm, Phys. Rev., 135B: 1281 (1964).

58. C. W. Craven, Jr., Inscattering Approximations in Discrete Variable Transport Theory, USAEC ORNL Report to be issued.

59. G. D. Joanou and J. S. Dudek, GAM-II: A B_3 Code for the Calculation of Fast-Neutron Spectra and Associated Multigroup Constants, USAEC Report GA-4265, General Atomic, 1963.

60. S. Goldstein (Ed.), Modern Developments in Fluid Dynamics, 1st ed., Oxford, 1938.

61. H. H. Koelle (Ed.), Handbook of Astronautical Engineering, 1st ed., McGraw-Hill, New York, 1961.

62. P. Levine, T. R. Ellis, and S. Georgiev, Factors Influencing the Design and Performance of Mars Entry Vehicles, J. Spacecraft, 2(2): 130–146 (1965).

63. F. J. Centolanzi, Heat Transfer to Blunt Conical Bodies Having Cavities to Promote Separation, Report NASA-TN-D-1975, National Aeronautics and Space Administration, July 1963.

64. J. C. Robinson and A. W. Jordan, Exploratory Experimental Aerodynamic Investigation of Tension Shell Shapes at Mach 7, Report NASA-TN-D-2994, September 1965.

65. Letter on Petry Formula, Sandia Corporation to T. G. Chapman, Oak Ridge National Laboratory, dated Nov. 2, 1965.

66. R. T. Swann, Composite Thermal Protection Systems for Manned Re-Entry Vehicles, J. Amer. Rocket Soc., 221–226 (February 1962).

67. D. I.-J. Wang, Multiple Layer Instulations, in Aerodynamically Heated Structures, edited by P. E. Glaser, Prentice Hall, 1962.

68. L. W. Gertsma, J. H. Dunn, and E. E. Kempke, Jr., Evaluation of One Type of Foldable Tube, Report NASA-TM-X-1187, Lewis Research Center, December 1965.

69. Fansteel Metallurgical Corporation, A Tantalum-Base Alloy – Fansteel 222 Metal, Data Sheet.

70. W. H. McAdams, Heat Transmission, p. 25, 3rd ed., McGraw-Hill, New York, 1954.

71. F. D. Kite et al., Launch Hazards Assessment Program. Report on Atlas/Centaur Abort, Report SC-RR-65-333, Sandia Corporation, October 1965.

72. Op. cit. Ref. 70, pp. 165–183.

APPENDICES

Appendix A

FUEL CAPSULE BURIAL-TEMPERATURE CALCULATION

At the completion of a normal mission, it is anticipated that the heat source would be ferried back to earth in order that the valuable radioisotope fuel could be recovered and reprocessed. In the event of a mission abort that resulted in random reentry, the heat source would be protected inside a reentry body with a shape and ballistic coefficient that would limit the terminal velocity and prevent earth burial of the entire source on impact. Earth burial of individual capsules would be a possibility in the event of a mission abort if the reentry body broke up on impact and scattered individual fuel capsules, which could then become covered, over a period of time, by drifting sand. The primary fuel capsule design is based on the criterion that the temperature of the capsule material (T-222 alloy[69]) not exceed 2000°F in the case of ^{238}Pu and ^{244}Cm fuels and 2500°F in the case of ^{147}Pm fuel in the event of random reentry from space. Calculations were made to determine the allowable thermal power and dimensions of capsules consistent with this requirement.

The effect of submergence below an air-earth interface on a heat transfer parameter[70] for various isothermal surfaces that approximate capsules or blocks of capsules is shown in Fig. A.1. These data lead to two pertinent conclusions:

1. The maximum allowable thermal power, which is determined by infinitely deep burial, is closely approached if the source is only about two diameters below the earth-air interface. Therefore, it is not unduly conservative to assume infinitely deep burial in designing capsules.

2. If the parameter is evaluated for the assumed conductivity of dry sand of 0.2 Btu/hr·ft·°F and an allowable surface temperature of 2000°F, it is found that a disk source 50 ft in diameter is required to dissipate 25 kw of heat. Similarly, if 25 kw is proportioned in 200 buried capsules, several feet of separation between capsules is required to assure that individual capsule temperatures will not exceed 2000°F.

These numbers reveal that it is practically impossible to provide for limited-temperature burial of a compact, integrated 25-kw heat source,

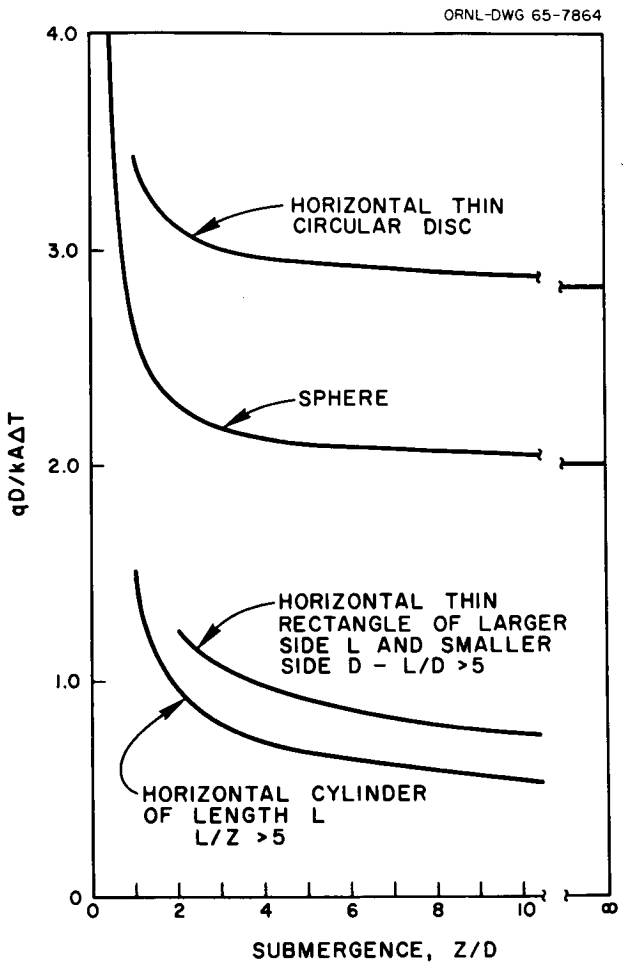

Fig. A.1. Effect of Submergence Below an Air-Earth Interface on the Parameter qD/kA ΔT for Various Isothermal Heat Source Configurations. The parameter qD/kA ΔT is the product of the heat transfer rate and diameter divided by the product of the thermal conductivity of the earth, the total surface area of the source, and the source-to-ambient temperature difference. Z is the distance of the center of the source below the air-earth interface.

but designs can be provided for the burial of separated individual capsules.

Figure A.2 shows the effect of negative submergence. The average heat flux at the surface of spheres 2200°F above ambient temperature is shown as a function of position both above and below the air-earth interface. This shows that for the range of parameters of interest it is possible to transfer more heat in air than in sand.

The unsteady-state condition was evaluated for cylinders deeply buried in dry sand by using the CDC 1604-A program, ONE LINE, which was written by R. L. Bradshaw and J. J. Perona of ORNL. If the thermal diffusivity of sand is assumed to be 0.01 ft^2/hr, the time in days to attain 90% of the steady-state capsule surface temperature is found to be approximately 100 D^2, where D is the capsule diameter in feet. For capsules of diameter less than 1 ft, the steady-state temperatures are attained in a time that is short compared with the half-lives of interest.

An equation was derived for determining the allowable thermal power of a cylindrical capsule with constant heat generation per unit of length as a function of the maximum surface temperature and configuration after deep burial:

$$q = \frac{2\pi kL(T_s - T_a)}{\sinh^{-1}(L/D)} ,$$

where

q = thermal power, Btu/hr,
k = thermal conductivity of the earth and capsule, Btu/hr·ft·°F,
L = length of capsule, ft,
D = diameter of capsule, ft,
T_s = maximum capsule surface temperature, °F,
T_a = ambient earth temperature, °F.

A parametric plot of this equation is shown in Fig. A.3. Data for spheres are shown for comparison. For a given diameter of the fueled capsule the allowable power increases with increasing length-to-diameter ratio, but in a diminishing way.

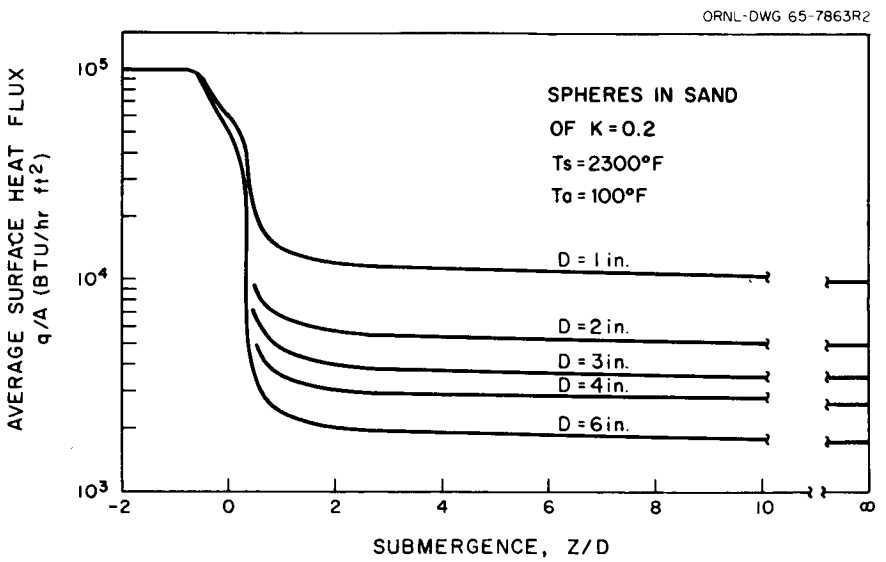

Fig. A.2. Effect of Submergence in Dry Sand (Conductivity of 0.2 Btu/hr·ft·°F) on the Average Heat Flux at the Surface of Spheres of Diameter D Maintained at 2200°F Above Ambient Temperature of 100°F. Z is the distance of the center of the sphere below the air-sand interface.

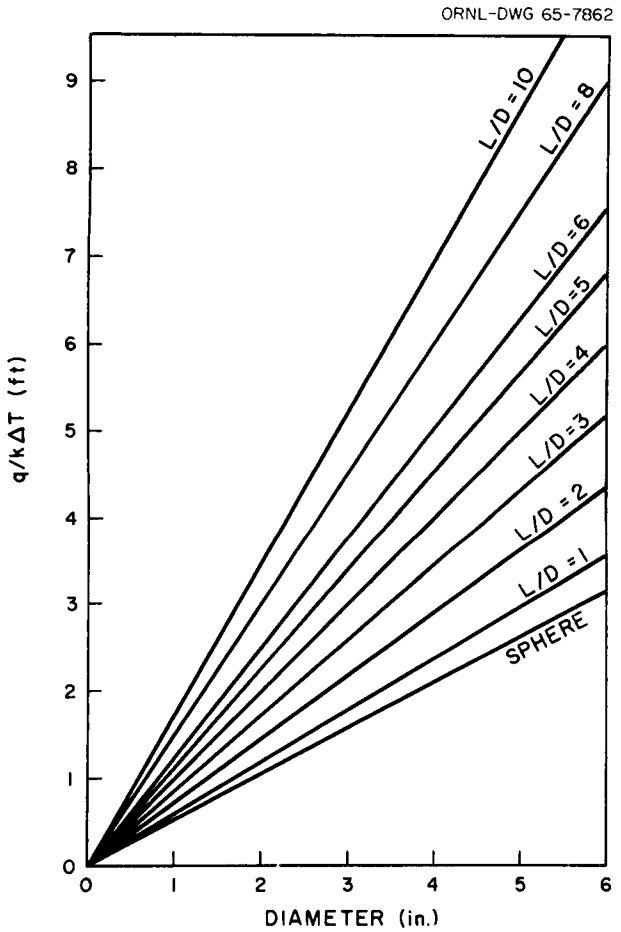

Fig. A.3. Effect of Diameter on the Parameter $q/k\ \Delta T$ for a Sphere and Cylinders of Varying Length-to-Diameter Ratio Enclosed by an Infinite Medium of Conductivity k. The heat production rate is q and ΔT is the maximum difference between the surface temperature and the ambient temperature of the medium at steady state.

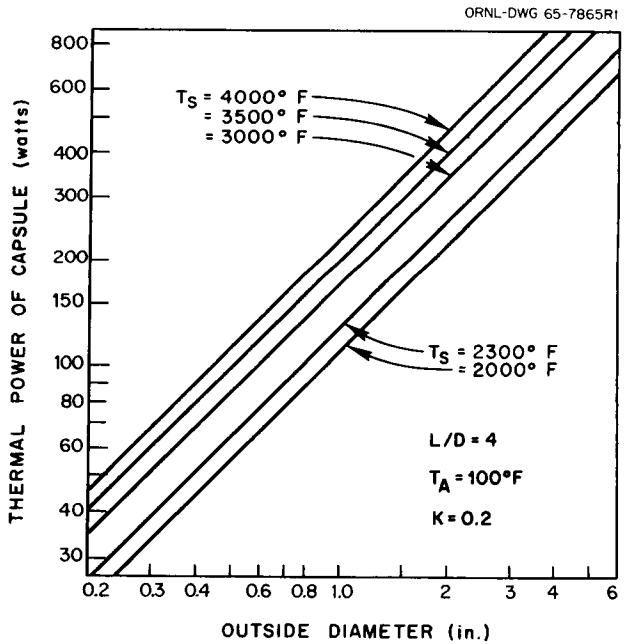

Fig. A.4. Allowable Steady-State Thermal Power of a Fuel Capsule Buried in Dry Sand as a Function of the Outside Diameter and Maximum Surface Temperature, T_S. The length-to-diameter ratio is 4; ambient sand temperature is 100°F; and thermal conductivity of sand is 0.2 Btu/hr·ft·°F.

Figure A.4 is a typical plot of the allowable power in a buried cylindrical capsule as a function of diameter and temperature. The L/D is 4, which is the ratio that is assumed in the conceptual capsule designs for impact resistance. An ambient temperature of 100°F and the conductivity of dry sand were assumed. Corresponding to an outside diameter of 1.5 in., the allowable power in a capsule is in the range of 150 to 200 w for allowable surface temperatures in the range of 2000 to 2500°F.

Heat Storage Requirements

In phase I designs, two criteria were applied in studying methods for storing heat in the isotope source reentry body during the launch phase or in the event of a launch-pad fire:

1. During the launch phase it is necessary to maintain capsule surface temperatures below the normal operating temperature of 2000°F. It is assumed that this requires heat storage for a period of 20 min between disconnection of the launch-pad refrigeration system and active operation of the Brayton cycle in orbit.

2. In the event of a launch-pad fire it is necessary to maintain capsule integrity for 1 hr, based on the assumption that remedial measures can be instituted in that time. A capsule surface temperature of 3000°F is consistent with this requirement because of the low helium pressure at lift-off time.

It was assumed that the launch pad conflagration would consist of prompt H_2/LOX explosions that would tend to crush, eject, or bury the reentry body in debris, and this would be followed by a long-term RP-1/LOX deflagration that would maintain a high-temperature environment. It was assumed that the long-term fire temperature would be 2000°F (apparently the characteristic reaction temperature) after the initial high-temperature spike, which was observed in the RP-1/LOX fire following the Atlas-Centaur abort.[71]

The relatively minimal effect of these constraints on phase I designs can be appreciated by assuming one of the smallest low-heat-capacity reentry bodies. A typical ^{244}Cm design has 480 lb of Cm_2O_3, tantalum, and platinum in the capsules, 120 lb of Nb-1% Zr in the capsule holder or

source block, 375 lb of Haynes-25 or Nb-1% Zr for structure, and 150 lb of insulation and ablative material. For such a device the launch phase and launch-pad fire heat storage criteria are satisfied by placing approximately 100 lb of BeO in the reentry body and cooling the entire heat source approximately 200°F below the normal steady-state heat source operating temperature before launch by means of an active, recirculating gas-cooling system. The connection to the reentry body compartment would be broken and plugged a few minutes before launch.

The BeO was chosen for its high sensible heat capacity and relative chemical inertness at high temperatures. Silicon and beryllium were considered because they have large heats of fusion between the fire temperature and the allowable temperature of a capsule in a fire. They were rejected because they are not compatible with the capsule materials for long periods at high temperature, and in the present design concepts the heat sink cannot be located in a position that would permit it to be jettisoned after orbit was achieved.

In the event of a launch-pad fire it is probable that capsule integrity could be maintained for 1 hr if the BeO and the structure of the reentry body remained in proximity with the capsules, even if the enclosed volume became insulated after attaining the fire temperature. If capsules were separated from the reentry body they would not attain excessively high temperatures if they could radiate directly to the fire.

Fuel Block Temperature in Water and Air

The temperature of the heat source submerged in water is of importance because the heat source would very likely impact in water in the event of a mission abort during the launch phase and might impact in water if there were a random reentry from orbit. In the case of water submersion, the predicted containment life time of the primary capsule would be greatly increased because the capsule temperature would be much lower than that used in the design; however, the outer platinum cladding would have to remain intact to prevent corrosion of the primary capsule. With natural convection alone as the mechanism of heat transfer between the fuel block and the water, the calculated heat transfer coefficient[72] is approximately

50 Btu/hr·ft^2·°F. The fuel block heat flux varies among the various design concepts but does not exceed 5000 Btu/hr·ft^2, which gives a temperature difference of 100°F between the bulk water temperature and the surface of the fuel capsules. As noted in Section 4, seawater corrosion data on platinum were obtained at essentially ambient temperature; however, it is not expected that the rates will change very significantly with only a 100°F increase in temperature. The long-term effect of the gradual growth of scale and plant life on the corrosion resistance of the platinum cladding is not known. Qualitative information suggests that such growths may be helpful from a corrosion standpoint, since there are numerous instances in which brass, copper, and gold artifacts protected by thick encrustations of animal and plant organisms have been recovered essentially intact after 300 years or more in the sea. The temperature at the surface of the platinum would increase as scale built up on the capsule; however, in no case would it approach the design temperature, which is based on earth burial.

The calculated heat transfer coefficient for the case where the fuel block is on the surface of the ground is approximately 5 Btu/hr·ft^2·°F for both natural convection and radiant heat transfer. This gives a temperature drop of 1000°F between the capsule surface and the air for a heat flux of 5000 Btu/hr·ft^2. The oxidation-rate data for platinum given in Section 4 show that the 20-mil platinum capsule cladding is more than adequate for this temperature in air.

Appendix B

CALCULATION OF THE TEMPERATURE-COMPENSATED STRESS-RATE CURVE

The basis and use of a temperature-compensated stress-rate curve to determine capsule wall thickness requirements are described in Section 4.2. The following example illustrates the calculations required to obtain one point on the curve. This particular example uses stress-rupture data for the T-111 alloy; however, the same method is equally applicable for stress to some percent creep. The basis for calculation is

Material data	Stress-rupture data for T-111 alloy
Isotope	$^{244}Cm_2O_3$
Half-life ($\tau_{1/2}$)	18.1 y
Initial capsule temperature	2000°F (1093°C)
Base (ambient) temperature	212°F (100°C)

Step 1

Pick a value of time in the region of interest and calculate the capsule temperature at this time. For this example choose 1297 hr (0.14796 year), and let

$$T = (T_0 - T_a) \exp(-0.693t/\tau_{1/2}) + T_a ,$$

where

t = time,
T = capsule temperature at time t,
T_0 = initial capsule temperature,
T_a = base temperature,
$\tau_{1/2}$ = half-life of fuel.

When evaluated,

$$T = (1093 - 100) \exp[-(0.693)(0.14796)/18.1] + 100$$
$$= 1087°C.$$

Thus the temperature of the capsule after 1297 hr is 1087°C.

Step 2

With the temperature calculated in step 1, calculate the Larson-Miller parameters for two arbitrary times. In this example the times are 10 and 1000 hr, and

$$P_t = (T + 273)(C + \log t) ,$$

where

P_t = Larson-Miller parameter for time t,
T = temperature, °C,
t = time, hr,
C = constant of the Larson-Miller equation based on material and temperature range.

For 10 hr,

$$P_{10} = (1087 + 273)(12.5 + \log 10)$$
$$= 18,360.$$

For 1000 hr,

$$P_{1000} = (1087 + 273)(12.5 + \log 1000)$$
$$= 21,080.$$

Step 3

From the Larson-Miller stress rupture plot for T-111 alloy (Fig. B.1) pick off the stress values corresponding to the two parameter values calculated in step 2:

$$\sigma_{10} = 50,000 \text{ psi},$$
$$\sigma_{1000} = 25,850 \text{ psi},$$

where σ_{10} and σ_{1000} are the stresses to cause rupture in 10 and 1000 hr, respectively. The two stresses with their respective times are the coordinates of two points on a stress-rupture curve for T-111 alloy at 1087°C.

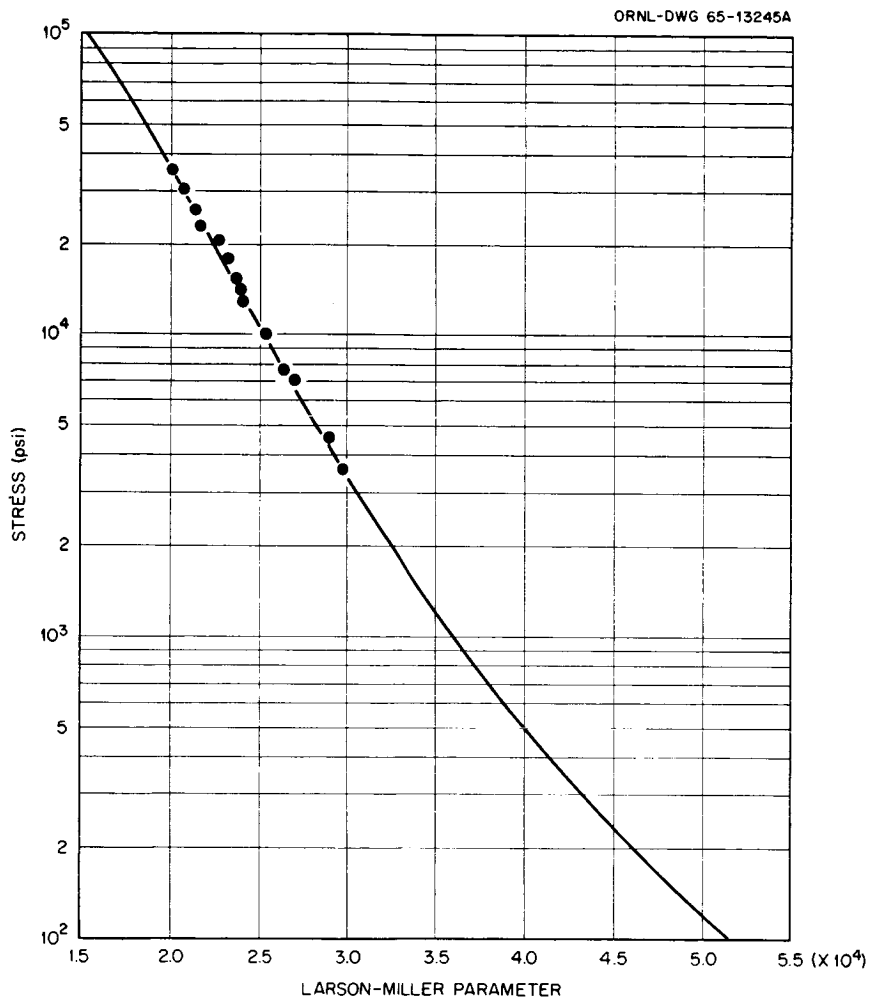

Fig. B.1. Larson-Miller Plot for Rupture of T-111 Alloy.

Step 4

With the two coordinates obtained in step 3, determine the values of the constants in the general equation of a stress-rupture curve:

$$t = (A/\sigma_t)^n ,$$

where

t = time, hr,

A, n = constants,

σ_t = stress to cause rupture at time t, psi.

Rearranging gives

$$\log t = n \log A - n \log \sigma_t ,$$

and solving simultaneously gives

$$1 = n \log A - 4.69897\, n ,$$

$$3 = n \log A - 4.41322\, n ,$$

$$n = 6.9991 ,$$

$$A = 69{,}450 .$$

Step 5

With the values of the constants determined in step 4, determine the rate of stress increase that will cause rupture in the originally assumed time (1297 hr) from the stress-rate equation

$$A^n = \dot{\sigma}^n \left[\frac{t^{(n+1)}}{n+1}\right] ,$$

where $\dot{\sigma}$ is the stress rate that will result in rupture at time t. Rearranging gives

$$\log \dot{\sigma} = \frac{n \log A - [(n+1) \log t - \log (n+1)]}{n}$$

$$= \frac{(6.9991)(4.8418) - [7.9991(3.1129) - 0.9031]}{6.9991}$$

$$= 1.4265$$

and

$$\dot{\sigma} = 25.8 \text{ psi/hr.}$$

This value of stress rate, 25.8 psi/hr, and the corresponding time, 1297 hr, are the coordinates of one point on the temperature-compensated stress-rate curve for a T-111 alloy capsule containing $^{244}Cm_2O_3$. The process is repeated for a range of times to define the entire curve.

Appendix C

BASIS FOR COMPUTER PROGRAM FOR CALCULATION OF STRESS-RATE-LIMITED CAPSULE DESIGN

Calculations for Determining Capsule Design

A computer program was developed for the capsule design study to be used with the CDC 1604-A computer at ORNL. The program made it possible to select capsule designs for minimum capsule weight and for minimum capsule volume. By using known properties for both the radioisotope fuel and the encapsulating material, along with several basic formulas, a range of sizes and number of capsules that meet the strength requirements was determined for several stress-rate safety factors. To reduce the large number of variables, several initial assumptions were made:

1. The temperature at the outer surface of the fuel was assumed to be 2150°F, which allows a conservative 150°F temperature drop across the various capsule layers between the fuel and the capsule outer surface.

2. The outer platinum capsule was assumed to provide no additional strength for internal pressure buildup, and the thickness of the platinum was assumed to be 0.020 in. in all cases.

3. The maximum allowable hoop stress was selected as the limiting allowable stress in the capsule wall for internal pressure buildup.

4. The maximum allowable rate at which pressure would increase in the capsule was based on the rate that would occur during the first 1 hr after encapsulation if the capsule were at the maximum normal operating temperature (2000°F surface). This assumption is conservative because the pressure rate would decrease with time due to the continual decrease of the amount of the radioisotope fuel in the capsule.

5. The temperature of the helium generated was assumed to be uniform and equal to 2150°F plus one half the temperature drop across the fuel compound.

6. The value of thermal conductivity at 2192°F was used for each fuel because the calculated value is approximately a minimum at this temperature. The thermal conductivity was assumed to be constant regardless of temperature.

7. No provision was made in the computer code to analyze capsule irregularities, such as the screw-type joint inside the capsule. For the computer code it was assumed that the capsule shape was a smooth cylinder with perfect hemispherical end caps. To compensate for the irregularities the following allowances were provided in the input data: (a) The allowable stress rate for each safety factor was reduced by 10% to compensate for an assumed reduction of 10% in the void volume available because of spacers, screw-type joints, etc. (b) An additional 10% was added to the total weight of each capsule to compensate for the weight of the internal spacers and thickened section at the screw joint.

Calculations were made only for capsules having inside diameters between the values of 0.5 and 4.0 in., and the length-to-diameter ratio (L/D) of the primary capsule was kept constant for all capsule diameters in each series of calculations. As discussed in Section 5, an L/D of 4 was used in the final conceptual designs. The allowable stress rate for each fuel was obtained from the temperature-compensated stress-rate curves (Section 4), and after applying stress-rate safety factors of 2.5, 4, and 7, the pressure rate inside the capsule was varied to determine its effect on void volume, primary capsule wall thickness, and capsule weight for capsules in the 0.5- to 4.0-in.-ID range.

The first step in the computer program was to determine the primary capsule wall thickness required for a specified allowable pressure rate, allowable stress rate, and capsule inside diameter. This was determined with the following equation for thick cylindrical shells:

$$X_c = r_2(Z^{1/2} - 1) , \qquad (1)$$

where

X_c = minimum required thickness of primary capsule, in.,

r_2 = inside radius of capsule, in.,

$$Z = \frac{SE + \dot{P}}{SE - \dot{P}} ,$$

and

S = allowable stress rate value, psi/hr,

E = joint efficiency,

$\dot{P}$ = allowable design pressure rate, psi/hr, based on the first hour after encapsulation.

In the computer program P was varied for each selected capsule diameter to provide a series of acceptable wall thickness values.

The total length of the primary capsule was then determined from the L/D ratio. The inner radius of the platinum outer capsule was determined by adding 0.012 in. to the outer radius of the primary capsule to allow for a 0.010-in. layer of ThO_2 and a 0.002-in. gas gap. The outer platinum capsule thickness was maintained a constant 0.020 in. throughout the program. The total volume inside the capsule was determined from the equation

$$V_T = \pi r_2^2(L_{cyl} + 1.33r_2) , \qquad (2)$$

where V_T is the total volume inside the capsule, $in.^3$, and L_{cyl} is the length of the cylindrical section of capsule, in.

The maximum allowable amount of fuel in each capsule for each value of pressure rate ($\dot{P}$) used to determine wall thickness was then determined by differentiating the ideal gas law with respect to time at constant temperature and volume:

$$\dot{P}(V_T - V_f) = \dot{N}RT , \qquad (3)$$

where

V_f = fuel volume, $in.^3$,

$\dot{N}$ = rate of helium generation, moles/hr,

R = universal gas constant,

T = average temperature of the helium, °R.

Equation 3 was solved for the same series of pressure rate values ($\dot{P}$) that were used in obtaining the capsule wall thickness values and the values of V_T as determined by Eq. (2). The remaining variables in Eq. (3), V_f, $\dot{N}$, and T, were all expressed in terms of the quantity of fuel in the capsule (C). The fuel volume was determined from

$$V_f = C/16.39\rho_f ,$$

where C is the weight of fuel compound in each capsule, g, and ρ_f is the density of fuel compound, g/cm^3. The rate of helium generation was then

$$\dot{N} = \frac{HC}{M} \lambda e^{-\lambda t} ,$$

where

H = fractional part of fuel compound that is the active alpha emitter,

M = atomic weight of the alpha emitters,

λ = decay constant of the alpha emitters,

t = elapsed time.

As noted previously the elapsed time, t, was set at 1 hr to obtain the helium generation rate at the beginning of life. The average temperature of the helium was obtained from

$$T = T_1 + (qX_f/2kA_m) ,$$

where

T_1 = temperature at the outer surface of the fuel compound, °R,

k = thermal conductivity of fuel compound, Btu/hr·in.·°R,

q = heat flow rate, Btu/hr,

= 3.415BC, where B is power density of fuel compound, w/g, and C is weight of fuel compound, g,

X_f = thickness of fuel, in.

= $r_2 - r_1$, where

$$r_1 = [r_2^2 - (V_f/\pi L_{cyl})]^{1/2}$$

$$V_f = C/16.39\rho_f$$

A_m = log mean fuel area, $in.^2$

$$= \frac{2\pi(r_2 L_{cyl} - r_1 L_{cyl})}{ln\ (r_2/r_1)} .$$

Making the appropriate substitutions for $\dot{N}$, V_f, and T in Eq. (3) and rearranging then gave

$$0.136BC\left[\ln\left(1-\frac{0.0194C}{\rho_f L_{cyl} r_2^2}\right)\right] = T_1 + \frac{\dot{P}M}{HR(1-e^{-\lambda t})}\left(\frac{0.0611}{\rho_f}-\frac{V_T}{C}\right). \quad (4)$$

Equation (4) was solved for C (total allowable weight of fuel compound per capsule) by using the same series of pressure-rate values ($\dot{P}$) and capsule inside diameters as was used to obtain the capsule wall thickness values in Eq. (1). The total number of capsules required was determined by dividing the total weight of fuel compound required for a 25-kw heat source at the end of a one-year mission by the weight of fuel compound allowed per capsule. The total weights of the inner and outer capsules, including fuel, were then determined, multiplied by the number of capsules, and divided into the total initial power (w) required for the heat source to obtain the specific power in w/lb. Typical results of these calculations for several stress-rate safety factors, capsule diameters ranging from 0.5 to 4.0 in. ID, and variable allowable pressure rates for each safety factor are given in Section 5. As may be seen from the typical curves shown in Section 5 (Figs. 5.19 through 5.24), there is one combination of wall thickness, fuel volume, and void volume that gives the minimum weight of capsules for a particular allowable stress rate. Likewise, there is another combination that gives the minimum volume of capsules for the heat source.

Calculation for Checking Capsule Integrity in Elastic Range

The capsule design study described above was based on the assumption that the limiting factor in the capsule design was that the maximum allowable stress rate would not exceed the creep-rupture strength of the capsule. However, the creep mode of failure ceases to be a dominant factor after approximately 0.7 times the half-life for each fuel for an initial surface temperature of 2000°F, but the pressure inside the capsule keeps increasing until it reaches a peak pressure at approximately 1.5 times the fuel half-life. This region between 0.7 and 1.5 times the half-life

was therefore checked on an elastic strength basis to insure that there were adequate safety factors for yield strength (factor of 3) and for ultimate strength (factor of 4).

The first step was to determine the maximum pressure that the capsule would be subjected to during a ten half-life period. Since the rate at which helium would be generated and the average temperature of the helium would be constantly decreasing due to the decay of the radioisotope fuel, this point of maximum pressure would be reached relatively early in the ten half-life period. The pressure at any time, t, after encapsulation of the fuel is given by

$$P = R \left\{ \frac{H\rho_f (1 - e^{-\lambda t}) \left[T_A + (T_H - T_A)\, e^{-\lambda t} \right]}{V_r M} \right\}, \qquad (5)$$

where

P = pressure, in atm,
t = elapsed time since encapsulation of the fuel, hr,
ρ_f = density of fuel compound, g/cm^3,
T_A = ambient temperature, °K,
T_H = initial temperature of helium, °K,
V_r = void volume-to-fuel volume ratio,
M = atomic weight of active alpha emitter, g.

This equation was solved for various times in the ten half-life period, and the results were plotted to give a curve of the equation. The temperature of the helium at any time during the period was also determined and plotted in the same program. A typical set of curves is shown in Fig. C.1. Since the available mechanical strength properties of the T-222 alloy being used as the encapsulating material are of a preliminary nature, a conservative approach was taken in obtaining the allowable stress in the elastic range by using ultimate and yield strength values based on the capsule temperature at the time creep stength stops being a significant factor (1425°F) rather than at the temperature at which the maximum capsule pressure occurs (~800°F). The maximum allowable capsule pressure, calculated according to the ASME Unfired Pressure Vessel Code, was

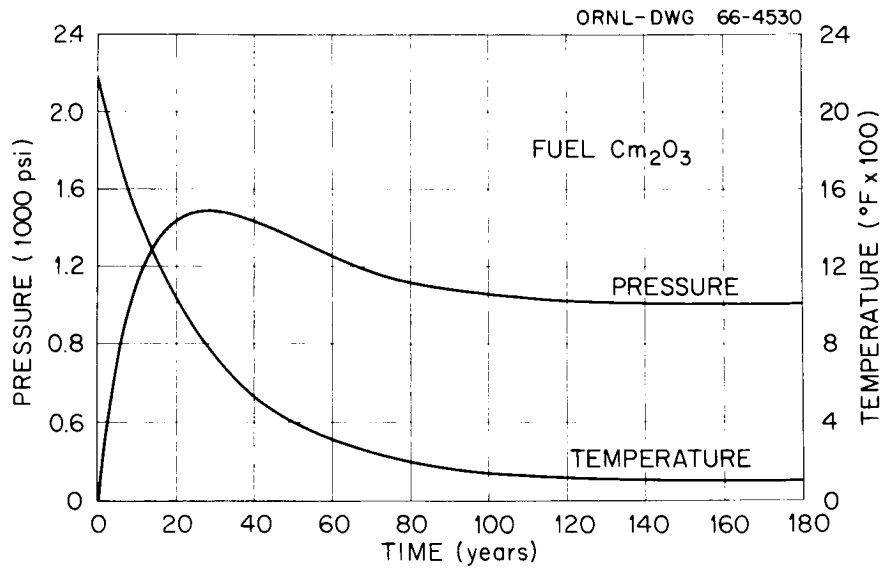

Fig. C.1. Cm_2O_3 Fuel Capsule Pressure-Temperature Curves.

determined by using an allowable stress value that corresponded to this higher capsule temperature. The allowable pressure was then divided by the actual peak pressure obtained from Eq. (5) to give the design safety factor. A typical example of this calculation follows.

In the case of the selected $^{244}Cm_2O_3$ capsule design with an allowable stress-rate safety factor of 7, there would be a total of 170 w in a 1.25-in.-ID capsule with a void volume-to-fuel volume ratio of 14. By applying Eq. (5) to this conceptual design, the pressure-temperature-time history was determined, as shown in Fig. C.1.

As shown in the figure, the maximum pressure attained is 1482 psi at slightly over 27 years. The temperature of the helium at approximately 0.6 times the half-life (~11 y) is 1425°F. At this temperature the tensile strength of T-222 alloy in a recrystallized condition (1 hr at 3000°F) is, as follows:[69]

Ultimate tensile strength at 1425°F, psi	~80,000
Yield strength at 1425°F, psi	~50,000

Based on these data the maximum allowable capsule pressure (P) for each case, as determined by the ASME Unfired Pressure Vessel Code, was the following:

Ultimate Strength Basis

$$P = SE\left(\frac{Z-1}{Z+1}\right),$$

where

S = ultimate strength
= 80,000 psi,

E = joint efficiency
= 0.85,

$Z = \left(\frac{r_2 + X_c}{r_2}\right)^2$, where

r_2 = capsule inside radius
= 0.625 in.,

X_c = capsule wall thickness
= 0.142 in.,

$$= \left(\frac{0.625 + 0.142}{0.625}\right)^2 = 1.5.$$

Thus

$$P = (80,000)(0.85)\left(\frac{1.5 - 1}{1.5 + 1}\right)$$

$$= 13,600 \text{ psi.}$$

Yield Strength Basis

With the same equation but the yield strength of T-222 alloy at 1425°F substituted in place of the ultimate strength, the allowable capsule pressure is

$$P = (50,000)(0.85)(0.5/2.5)$$

$$= 8,500 \text{ psi.}$$

The safety factors in each case are

Ultimate-strength safety factor = 13,600/1482 = 9.17

Yield-strength safety factor = 8,500/1482 = 5.73.

Thus it is evident that in both cases the actual safety factors are well above the required safety factors of 4 and 3, respectively, for the region.

These calculations were repeated for all conceptual capsule designs. In all cases the required safety factors for the elastic strength region were met or exceeded.